



THE HONG KONG  
POLYTECHNIC UNIVERSITY

香港理工大學

Pao Yue-kong Library

包玉剛圖書館

---

## Copyright Undertaking

This thesis is protected by copyright, with all rights reserved.

**By reading and using the thesis, the reader understands and agrees to the following terms:**

1. The reader will abide by the rules and legal ordinances governing copyright regarding the use of the thesis.
2. The reader will use the thesis for the purpose of research or private study only and not for distribution or further reproduction or any other purpose.
3. The reader agrees to indemnify and hold the University harmless from and against any loss, damage, cost, liability or expenses arising from copyright infringement or unauthorized usage.

### IMPORTANT

If you have reasons to believe that any materials in this thesis are deemed not suitable to be distributed in this form, or a copyright owner having difficulty with the material being included in our database, please contact [lbsys@polyu.edu.hk](mailto:lbsys@polyu.edu.hk) providing details. The Library will look into your claim and consider taking remedial action upon receipt of the written requests.

The Hong Kong Polytechnic University

Department of Building Services Engineering

**Study on Renewable Energy Systems with  
Different Energy Storage Solutions for  
Power Supply in Remote Areas**

**Ma Tao**

A thesis submitted in partial fulfillment of the requirements for  
the Degree of Doctor of Philosophy

November, 2014

## **CERTIFICATE OF ORIGINALITY**

I hereby declare that this thesis is my own work and that, to the best of my knowledge and belief, it reproduces no material previously published or written, nor material that has been accepted for the award of any other degree or diploma, except where due acknowledgement has been made in the text.

\_\_\_\_\_ (Signed)

\_\_\_\_\_ Ma Tao \_\_\_\_\_ (Name of student)

Department of Building Services Engineering

The Hong Kong Polytechnic University

Hong Kong SAR, China

November, 2014

## **ABSTRACT**

Abstract of thesis entitled: Study on renewable energy systems with different energy storage solutions for power supply in remote areas

Submitted by: Ma Tao

For the degree of: Doctor of Philosophy

At The Hong Kong Polytechnic University in November 2014

At present, more than 1.3 billion inhabitants worldwide still lack access to grid electricity. Most of the people live in remote areas, such as islands, mountain areas and isolated villages, all some distance from the utility grid. Grid extension to such remote communities is both uneconomical and technically difficult owing to dispersed population or rugged terrain. As a result, their electrical demand is normally met by use of diesel power or there is no power supply at all. Fortunately, such areas, although remote, are usually rich in renewable energy (RE) resources, thus making it worthwhile to explore such local RE resources with the objective of producing much needed electricity. In recent years, the unpredictability of diesel costs, falling RE generation costs as well as technological improvements have encouraged a wider adoption of renewable energies in such areas.

Stand-alone renewable energy power generation systems have been the target of substantial research over the past decades. However, the focus on comprehensive

renewable energy power supply solutions for remote areas, together with the identification of effective and low-cost technologies is limited. In addition, one significant technical challenge for those stand-alone RE systems, such as solar and wind energy, is the fluctuation of their output. This feature prevents the RE from being fully reliable for remote areas. In this context, the development of some effective energy storage solutions, to keep energy in excess for use in time of need, is an essential requirement. Currently battery must be a front-runner for use in remote RE systems. However, it has well known limitations, such as high cost, short lifespan, possibility of environmental damage and explosion, and difficulties for maintenance in isolated areas. Pumped hydro storage (PHS), usually used for conventional power plants, shows a great potential to replace batteries in standalone application, but to date few studies have reported the micro PHS for remote RE systems.

The aim of this thesis is to study the options of power supply and energy storage for remote areas. One remote inhabited island 20 km off the coast of Hong Kong is taken to act as a test site for the proposed RE systems and storage technologies.

To achieve the objectives of the study, a detailed study of different energy technologies for remote electrification was conducted, including system development, mathematical modeling, simulation, optimization, techno-economic evaluation, and sensitivity analysis. Different energy storage technologies, i.e. batteries, PHS, super-capacitors and their hybrids, are investigated via theoretical analysis, numerical simulation and experimental validation. The operational performance of a real PV-battery system on this example island was evaluated.

Firstly, the RE potential and load demand of the selected island were assessed. Mathematical models for each RE technology were developed, and system evaluation

criteria discussed. In particular, a novel simulation model for PV devices, offering a good compromise between accuracy and simplicity, was developed in Matlab to fit the I-V curves and predict PV power output. The model was solved using an integrated analytical and numerical method, then validated through field measurements in a real grid-connected and a standalone PV system.

A detailed study on the use of a traditional energy storage technology, battery, to support a remote area power generation system has been conducted. System configurations of possible combinations of solar energy, wind energy, diesel generator and battery bank were developed. Hourly simulations for a wide variety of configurations were performed to achieve an optimal one based on techno-economic analysis. Two representative systems, the 100% RE and hybrid RE-diesel, were selected for deeper analysis. Emphasis was also placed on examinations of the effects of the PV, wind turbine, diesel generator, and battery bank capacity on the system's reliability and economic performance. The results demonstrated that the island could be powered by a 100% RE system, although it is possible that the energy cost provision will be quite high. The addition of a back-up diesel generator would make the hybrid system, i.e. solar-wind-diesel-battery, a more economically viable option.

The problems which were observed concerning batteries limit a wider and future application of the battery-based RE systems. Thus as an alternative, a small PHS unit was proposed to support the remote area RE power supply systems at a few hundred kW scale. Of interest is the development in this study of a novel operating principle and design process for PHS-based RE systems. With the simulation program developed in this study, the system was simulated for a whole year. The genetic algorithm, along with the Pareto optimality concept, was then employed for system optimization, i.e. to identify the maximization of power supply reliability and

minimization of system cost. The optimized system configuration under zero loss of power supply probability (LPSP) was then investigated. In addition, the system performance of hybrid solar-wind, solar-alone and wind-alone systems with pumped storage under LPSPs from 0 to 5% were compared. Sensitivity analysis on several key parameters was also performed to examine their effects on system performance.

This study proposed a new concept of energy storage to compensate the intermittent nature of renewable energy applications. Even though the overall efficiency of the micro-scaled pumped storage system is not high, a sustainable and environmentally friendly power supply solution is able to be provided, indicating that the pumped storage is one future ideal partner for remote area RE power supply systems.

Further investigation of the battery-based and PHS-based RE system indicates that the use of more than one storage technology will give a better performance as regards complementing fluctuating RE outputs and dynamic power demands. Therefore, a new hybrid energy storage system (HESS), which combines battery for long-term energy management and supercapacitor for fast dynamic power regulation, was proposed. The mathematical models of the passive connected HESS were developed, and then implemented in Matlab/Simulink for numerical simulations. An electric inductance was further introduced to improve the performance of the HESS. In addition, an experimental test bench was developed to validate simulation results. It was demonstrated that the HESS can stabilize energy provision, not only for intermittent RE, but also for other fluctuating load applications. Finally, the benefit of another kind HESS, a combination of pumped storage and battery energy storage system, was analyzed and the system was experimentally studied, as an illustration of the operation states of such hybrid energy storage technology.

The operating data of a 19.8kWp solar PV-battery system on the island was collected and evaluated for the following aspects: the PV array, inverters, the battery bank and overall system. This evaluation enables a detailed understanding of the operating performance of the existing PV system from the technical point of view. It also provides useful reference data for further system extension.

A comprehensive study of stand-alone RE power supply system using different energy storage solutions for remote areas with useful research outputs has been outlined above. The results provide researchers, engineers and policy makers with choices regarding the use of local RE resource, which could be aligned with the characteristics of individual remote area of interest. It is believed that the findings have provided a good reference for the selection of suitable RE and energy storage technologies, and the methodology presented can also be viewed as a starting point for planning and designing RE systems for remote communities around the world.

## PUBLICATIONS DURING PHD STUDY

### Journal papers:

- [1] T. Ma, H. Yang, L. Lu, Performance evaluation of a stand-alone photovoltaic system on an isolated island in Hong Kong, *Applied Energy*, 112 (2013) 663-672.
- [2] T. Ma, H. Yang, L. Lu, Development of a model to simulate the performance characteristics of crystalline silicon photovoltaic modules/strings/arrays, *Solar Energy*, 100 (2014) 31-41.
- [3] T. Ma, H. Yang, L. Lu, Feasibility study and economic analysis of pumped hydro storage and battery storage for a renewable energy powered island, *Energy Conversion and Management*, 79 (2014) 387-397.
- [4] T. Ma, H. Yang, L. Lu, A feasibility study of a stand-alone hybrid solar–wind–battery system for a remote island, *Applied Energy*, 121 (2014) 149-158.
- [5] T. Ma, P.A. Østergaard, H. Lund, H. Yang, L. Lu, An energy system model for Hong Kong in 2020, *Energy*, 68 (2014) 301-310.
- [6] T. Ma, H. Yang, L. Lu, J. Peng, Technical feasibility study on a standalone hybrid solar-wind system with pumped hydro storage for a remote island in Hong Kong, *Renewable Energy*, 69 (2014) 7-15.
- [7] T. Ma, H. Yang, L. Lu, Solar photovoltaic system modeling and performance prediction, *Renewable and Sustainable Energy Reviews*, 36 (2014) 304-315.

- [8] T. Ma, H. Yang, L. Lu, Study on stand-alone power supply options for an isolated community, *International Journal of Electrical Power & Energy Systems*, 65 (2015) 1-11.
- [9] T. Ma, H. Yang, L. Lu, J. Peng, Pumped storage-based standalone photovoltaic power generation system: Modeling and techno-economic optimization, *Applied Energy*, 137 (2015) 649-659.
- [10] T. Ma, H. Yang, L. Lu, J. Peng, Optimal design of an autonomous solar-wind-pumped storage power supply system. *Applied Energy* (2014) In Press ([doi:10.1016/j.apenergy.2014.11.026](https://doi.org/10.1016/j.apenergy.2014.11.026))
- [11] T. Ma, H. Yang, L. Lu, Y. Zhang and X. Wang. Using phase change materials in photovoltaic systems for thermal regulation and electrical efficiency improvement: a review and outlook. *Renewable and Sustainable Energy Reviews* 43 (2015) 1273–1284.
- [12] T. Ma, H. Yang, L. Lu, Development of hybrid battery-supercapacitor energy storage for remote area renewable energy systems, *Applied Energy* (2014) In Press ([doi:10.1016/j.apenergy.2014.12.008](https://doi.org/10.1016/j.apenergy.2014.12.008))
- [13] T. Ma, H. Yang, L. Lu, J. Peng, An Optimization Sizing Model for Solar Photovoltaic Power Generation System with Pumped Storage. *Energy Procedia* 61 (2014) 5-8.

## **Monograph:**

- [1] H. Yang, L. Lu, T. Ma. *Application of Hybrid Solar-Wind Power Generation Technologies*. Beijing: China Architecture & Building Press. 2014. (in Chinese)
- [2] H. Yang, X. Gao, T. Ma, X. Guo, D. Liu. *Wind energy conversion systems, Handbook of Clean Energy System*. New York: Wiley, 2015 (In Press, Corrected Proof).

## **Conference papers:**

- [1] T. Ma, H. Yang, L. Lu. Performance evaluation of a stand-alone photovoltaic system on an isolated island in Hong Kong, *Proceeding of International Conference on Applied Energy (ICAE2012)*, Suzhou, China, Jul 5-8, 2012
- [2] T. Ma, C. Lou, L. Lu, H. Yang. Study on stand-alone hybrid solar pumped storage systems. *Proceeding of 11<sup>th</sup> International Conference on Sustainable Energy technologies (SET-2012)*, Vancouver, Canada, Sep 2-5, 2012
- [3] T. Ma, H. Yang, L. Lu, J. Peng. Simulation study of a standalone hybrid solar-wind system with pumped storage. *Proceeding of APEC Conference on Low-carbon Towns and Physical Energy Storage*, Changsha, China, May 25-26, 2013
- [4] T. Ma, H. Yang, L. Lu. Modelling and case study of a standalone photovoltaic system with pumped hydro storage. *Proceeding of International Conference on Applied Energy (ICAE2013)*, Pretoria, South Africa, Jul 1-4, 2013
- [5] T. Ma, H. Yang, L. Lu. Feasibility study of a stand-alone solar-wind-battery system on a remote island in Hong Kong. *Proceeding of 12<sup>th</sup> International*

*Conference on Sustainable Energy technologies (SET-2013)*, Hong Kong, China,  
Aug 26-29, 2013

[6] T. Ma, H. Yang, L. Lu, J. Peng. An optimization sizing model for solar photovoltaic power generation system with pumped storage. *Proceeding of International Conference on Applied Energy (ICAE2014)*, Taipei, Taiwan, May 29- Jun 2, 2014

[7] T. Ma, H. Yang, L. Lu, R. Qi. Developing a zero-carbon-emission green deck using renewable energy. *Proceeding of 2<sup>nd</sup> International Conference on Sustainable Urbanization*. Hong Kong, China, Jan 7-9, 2015

## ACKNOWLEDGEMENTS

This thesis is the result of four-years of work whereby I have been accompanied and supported by many people.

First and foremost, I would like to express my deepest appreciation to my chief supervisor, Prof. Yang Hongxing, for his excellent guidance, endless encouragement, full support and providing me with an excellent research atmosphere. His optimism and friendly nature has taught me much not only about research but also about life.

My sincere gratitude is also given to my co-supervisor, Dr. Lu Lin, for her insightful views and great help in my research and life. Appreciation is also offered to Prof. Zhang Yinping of Tsinghua University for his recommendation of my PhD study in Hong Kong and his constructive suggestions throughout the study.

My appreciation is also given to Prof. Henrik Lund and Dr. Poul Alberg Østergaard, for their great support and valuable instruction when I studied at Aalborg University, Denmark as a visiting PhD student.

I would like to acknowledge Prof. Wang Shengwei, Prof. Henrik Lund and Prof. Denis Y.C. Leung for their constructive comments for improving the thesis and encouraging discussions during oral examination.

I would also thanks to all the members in the Renewable Energy Research Group for their help, company and advice during my PhD study. My colleagues and friends at this university deserve my appreciation as well.

Grateful acknowledgements should be given to Mrs. Elaine Anson for her care and encouragement, particularly for her effort in improving my English. My appreciation is also extended to Mr. C.C. Ngan of China Light & Power (CLP) Holding Limited (Hong Kong) for his valuable suggestions on my work.

Last, but not least, I would like to thank my family including my parents and parents-in-law for their considerable support, understanding and deep love. In particular, I am indebted to my darling wife, Ms. Liu Si, for her loving support and understanding. These past several years have not been an easy ride, both academically and personally. I truly thank my wife for sticking by my side, even when I was irritable and depressed during tough times in the PhD pursuit. The lovely smile of my baby son, Toby Ma, has also given me great strength to continually step up my efforts, especially during the writing of this thesis.

# TABLE OF CONTENTS

CERTIFICATE OF ORIGINALITY .....	I
ABSTRACT .....	II
PUBLICATIONS DURING PHD STUDY .....	VII
ACKNOWLEDGEMENTS .....	XI
TABLE OF CONTENTS .....	XIII
LIST OF FIGURES .....	XX
LIST OF TABLES .....	XXVII
ABBREVIATION.....	XXIX
CHAPTER 1 INTRODUCTION .....	1
1.1 The need for power supply in remote areas .....	1
1.2 Diesel generator power supply and its problems .....	4
1.3 Using renewable energy for RAPS .....	5
1.4 Energy storage for the RE-based RAPS systems.....	6
1.5 Motivation and objective of this thesis .....	8
1.5.1 Motivation.....	8
1.5.2 Aims & Objectives.....	9
1.6 Organization of this thesis.....	11
CHAPTER 2 LITERATURE REVIEW.....	13
2.1 Standalone renewable energy systems for RAPS .....	13
2.2 Modeling of PV system and parameter-determination methods.....	16
2.2.1 Equivalent circuit and mathematical models for PV devices.....	17
2.2.2 Determination methods for solving model parameters .....	23

2.3	System sizing and optimization techniques .....	25
2.3.1	Probabilistic approach .....	27
2.3.2	Analytical approach .....	27
2.3.3	Iterative approach.....	27
2.3.4	Artificial intelligence (AI) approach.....	28
2.3.5	Multi-objective optimization approach .....	30
2.3.6	Design space based approach.....	31
2.3.7	Hybrid approaches .....	31
2.3.8	Other optimization techniques .....	32
2.3.9	Simulation and optimization software tools for hybrid RE systems.....	32
2.4	Energy storage for renewable energy supply systems .....	33
2.4.1	The role of energy storage.....	34
2.4.2	Classification of ESS .....	35
2.4.3	Battery energy storage.....	37
2.4.4	Pumped hydro storage.....	39
CHAPTER 3 SYSTEM MODELING AND EVALUATION METHODS.....		48
3.1	Mathematical modeling of photovoltaic system .....	48
3.1.1	Physical configuration of PV cell, module, string, array and plant .....	49
3.1.2	Simulation model and determination method developed in this study ..	50
3.1.3	Model validation through field measurements.....	63
3.1.4	Solar PV system modeling and performance evaluation .....	72
3.2	Mathematical modeling of wind energy system .....	83
3.2.1	Power output characteristics of a wind turbine .....	83
3.2.2	The probability for WT operation .....	84
3.3	Mathematical modeling of battery energy storage.....	85

3.4	Mathematical modeling of pumped storage system.....	89
3.4.1	Pump/motor unit .....	89
3.4.2	Turbine/generator unit.....	91
3.4.3	Upper reservoir (UR) .....	92
3.5	Energy balance model for generation and consumption .....	93
3.6	Other components .....	94
3.6.1	Diesel generator (DG).....	94
3.6.2	Converters .....	97
3.7	System performance evaluation methods.....	98
3.7.1	Technical reliability evaluation.....	98
3.7.2	Economic cost evaluation .....	99
3.7.3	Payback time .....	102
3.7.4	Environmental effect evaluation .....	102
3.8	Summary .....	103
CHAPTER 4 ASSESSMENT OF RENEWABLE ENERGY POTENTIAL AND		
LOAD DEMAND .....		104
4.1	Background of Town Island.....	104
4.2	Solar energy potential .....	106
4.3	Wind energy potential .....	109
4.3.1	Assessment procedure .....	109
4.3.2	Analysis of the collected data .....	112
4.3.3	Analysis of wind power potential .....	114
4.3.4	Analysis of wind power at different hub heights .....	116
4.3.5	Predicted performance of the turbine at the hub height of 15m.....	118
4.4	Solar and wind energy complementary characteristic .....	119

4.5	Island load demand profile.....	120
<b>CHAPTER 5 DEVELOPMENT OF BATTERY-BASED RENEWABLE</b>		
<b>ENERGY SYSTEMS .....</b>		
5.1	System configuration of battery based power generation systems .....	125
5.1.1	100% renewable energy system.....	126
5.1.2	Renewable energy system with backup diesel.....	127
5.2	System modeling and constraints.....	130
5.2.1	System modeling and components information.....	130
5.2.2	Constraints .....	131
5.3	Overall results of the battery based power generation options .....	132
5.3.1	Overall results of the eight options .....	132
5.3.2	Sensitivity analysis of the load demand.....	136
5.3.3	Sensitivity analysis of renewable energy resources.....	137
5.3.4	Payback time .....	138
5.4	Simulation performance of a 100% RE system .....	139
5.4.1	Simulation performance of system components .....	139
5.4.2	Total cost break-down.....	142
5.4.3	Hourly simulation results .....	142
5.4.4	The effects of PV, wind turbine, battery capacity on simulation results	144
5.5	Simulation performance of a RE system with backup DG .....	145
5.5.1	Simulation performance of system components .....	146
5.5.2	Total cost break-down.....	149
5.5.3	Energy flow or energy balance analysis.....	149
5.5.4	Hourly simulation results .....	150

5.5.5	Renewable fraction.....	151
5.5.6	Dispatch strategy .....	151
5.5.7	The effect of diesel price.....	153
5.5.8	The effect of PV, number of WT and battery capacities on the result of Option 1.....	154
5.6	Summary of this chapter .....	156
CHAPTER 6 DEVELOPMENT OF PUMPED STORAGE BASED- RENEWABLE ENERGY SYSTEMS .....		158
6.1	System configuration and operation principle .....	159
6.1.1	Pumped storage based renewable energy systems .....	159
6.1.2	Operation principle.....	161
6.2	System modeling, simulation and optimization .....	162
6.2.1	Mathematical modeling.....	162
6.2.2	Initial design.....	162
6.2.3	Simulation and optimization .....	165
6.3	Technical feasibility study .....	168
6.3.1	Sizing curve.....	169
6.3.2	Wind turbine alone system.....	171
6.4	Techno-economic optimization of PV-PHS.....	172
6.4.1	Single-objective and two-objective optimization.....	172
6.4.2	The optimal configuration assuming zero LPSP.....	176
6.5	Techno-economic optimization of PV-wind-PHS systems .....	181
6.5.1	Performance analysis of the optimized, oversized and undersized systems .....	181
6.5.2	The optimal configuration assuming zero LPSP.....	182

6.5.3	Comparison with solar-pumped storage and solar-wind-PHS .....	188
6.6	Summary of this chapter .....	191
CHAPTER 7    DEVELOPMENT OF HYBRID ENERGY STORAGE		
TECHNOLOGIES .....		
7.1	Introduction .....	193
7.2	System description of the passive hybrid .....	196
7.3	Mathematical models .....	197
7.3.1	Numerical analytic of the HESS .....	197
7.3.2	Currents under steady state conditions .....	200
7.3.3	Performance of HESS in peak power enhancement .....	201
7.4	Numerical simulation .....	202
7.4.1	Numerical simulation using Matlab/Simulink .....	202
7.4.2	Performance enhancement through an inductor .....	205
7.4.3	Comparison between hybrid energy storage and battery alone system .....	206
7.5	Experimental validation .....	207
7.5.1	Experiment tests of the passive connected system .....	207
7.5.2	Experimental results and data analysis .....	208
7.5.3	Experiment tests of the improved passive HESS .....	208
7.6	Experimental study on the hybrid PHS-battery energy storage system .....	210
7.6.1	The benefit of a battery bank for the pumped energy storage system .....	210
7.6.2	Experimental test system .....	213
7.6.3	Experimental results and analysis .....	215
7.7	Summary of this chapter .....	218
CHAPTER 8    PERFORMANCE EVALUATION OF A REMOTE		
RENEWABLE ENERGY SYSTEM .....		
		219

8.1	System description .....	220
8.2	System performance evaluation methods.....	222
8.3	Performance evaluation results and analysis.....	224
8.3.1	PV array performance analysis .....	224
8.3.2	SMC inverter performance analysis.....	228
8.3.3	SI inverter performance analysis.....	229
8.3.4	Battery bank performance analysis .....	230
8.3.5	Entire system performance analysis.....	234
8.4	Summary of this chapter .....	239
CHAPTER 9 SUMMARY AND SUGGESTIONS FOR FUTURE STUDY ...		241
9.1	Summary of research findings/contribution.....	241
9.1.1	System modeling and evaluation .....	241
9.1.2	Development of the battery-based RE systems.....	242
9.1.3	Development of the PHS-based RE systems .....	243
9.1.4	Development of hybrid energy storage system.....	244
9.1.5	Performance evaluation of a RE system .....	245
9.2	Recommendations for future research .....	246
REFERENCES.....		249

## LIST OF FIGURES

Fig. 1.1 Composite nighttime photograph of the Earth from space [2] .....	3
Fig. 2.1 Equivalent PV cell electrical circuits: (a) ideal model; (b) one-diode only with $R_s$ (4-p model); (c) one-diode with $R_s$ and $R_p$ (5-p model) and (d) two-diode models (7-p model).....	17
Fig. 2.2 PV module I–V characteristic curve with three characteristic points.....	18
Fig. 2.3 Number of articles using optimization algorithms in the study of RE over the last 20 years.....	26
Fig. 2.4 Sizing and optimization methods.....	26
Fig. 2.5 Load profile of an electricity storage system. (a) EES in Peak Shaving; (b) EES in load levelling [252] .....	34
Fig. 2.6 Classification of energy storage systems .....	35
Fig. 2.7 Pumped hydroelectric storage plant.....	39
Fig. 2.8 Typical arrangement of Wind–PSP system [297].....	41
Fig. 2.9 Configuration of the proposed hybrid power plant PV-PHS [353] .....	43
Fig. 3.1 Physical configuration of a photovoltaic cell (a), a cell series string (b), a module (c) and a PV array (d).....	50
Fig. 3.2 Equivalent circuit for a solar cell (five-parameter model).....	50
Fig. 3.3 The relationship between I-V curve, $R_s$ and $R_p$ .....	53
Fig. 3.4 I-V curves and P-V curves under different solar radiation levels (cell temperature=25 °C) .....	61
Fig. 3.5 I-V curves and P-V curves under different PV cell temperature levels (irradiance=1000W/m <sup>2</sup> ) .....	62

Fig. 3.6 Field measurement instruments and test rig of the 22kWp PV system .....	63
Fig. 3.7 PV system configuration and test items including PV modules (M1, M2, M3, M4), strings (S1, S2, S3) and arrays (A1, A2, A3).....	64
Fig. 3.8 The measured and calculated I-V curves of PV module M1 .....	65
Fig. 3.9 Distribution of the converted $I_{sc}$ , $I_m$ , $V_{oc}$ and $V_m$ values to STC on 21 <sup>st</sup> Dec 2012.....	66
Fig. 3.10 Comparison between measured and calculated I-V curves, P-V curves and MPPs of PV module #M1 .....	68
Fig. 3.11 I-V curves and MPP comparison of the four PV modules .....	70
Fig. 3.12 Comparison between measured and calculated I-V curves, P-V curves and MPPs of PV string #S1 .....	70
Fig. 3.13 Comparison between measured and calculated I-V curves, P-V curves and MPPs of PV array #A1, # A2, #A3.....	71
Fig. 3.14 PV module's I-V curves and P-V curves under different solar radiation intensity ( $T_c=25\text{ }^\circ\text{C}$ ).....	73
Fig. 3.15 PV module's I-V curves and P-V curves under different PV cell temperature (irradiance= $1000\text{W/m}^2$ ) .....	74
Fig. 3.16 Measurement and simulation results of PV module string A.....	75
Fig. 3.17 Measurement and simulation results of PV module string F.....	75
Fig. 3.18 Predicted and measured power-output profile of PV array #1 on 12 <sup>th</sup> Oct 2010 (sunny day).....	76
Fig. 3.19 Predicted and measured power-output profiles of PV array #1 on 12 <sup>th</sup> Feb 2012 (semi-cloudy day).....	77
Fig. 3.20 Predicted and measured power-output profiles of PV array #1 on 16 <sup>th</sup> May 2011 (cloudy day) .....	78

Fig. 3.21 Predicted and measured power-output of PV array #1 on 30 <sup>th</sup> May 2011 with SOC and charging voltage profile.....	81
Fig. 3.22 Wind turbine power output characteristic curve of Proven 11 .....	84
Fig. 3.23 Lifetime cycles-to-failure and throughput of the battery.....	88
Fig. 3.24 Generator fuel curve and efficiency curve.....	96
Fig. 4.1 Kau Sai Chau solar radiation station .....	106
Fig. 4.2 Frequency distribution of daily average irradiation less than specified amounts (kWh/m <sup>2</sup> /day).....	107
Fig. 4.3 Hourly distribution of solar radiation (a) monthly average (b) yearly average .....	107
Fig. 4.4 The monthly solar radiation and the clearness index in 2009.....	108
Fig. 4.5 Wind speed collected in 2010.....	112
Fig. 4.6 Diurnal wind speed profile in different months (10 years mean).....	113
Fig. 4.7 Wind direction frequency rose during 10 years.....	114
Fig. 4.8 Wind speed Weibull distribution (10 years data) .....	114
Fig. 4.9 Wind speed Weibull distribution in August and December .....	115
Fig. 4.10 Monthly (and yearly) average wind power density and average wind speed .....	116
Fig. 4.11 The solar and wind energy resource on the island (a) monthly energy density in 2009 (b) Daily solar radiation and wind speed distribution on 1 <sup>st</sup> -2 <sup>nd</sup> January 2009 .....	119
Fig. 4.12 A sample daily load profile for this island.....	121
Fig. 4.13 Yearly load profile on this island.....	123
Fig. 5.1 Eenergy flow diagram of the hybrid solar–wind system with battery storage .....	126

Fig. 5.2 Operating strategy of this hybrid solar -wind system employing a battery bank .....	127
Fig. 5.3 Control strategy of dispatchable system components.....	129
Fig. 5.4 Cost of energy of five power supply options versus load consumption .....	136
Fig. 5.5 Optimal system type against with solar radiation and wind speed .....	137
Fig. 5.6 Cumulative cash flow savings for the Option1 and Option 3 compared to diesel-only system.....	138
Fig. 5.7 Daily mean power generated by PV and wind in different months .....	141
Fig. 5.8 rainbow profile of battery bank SOC during the simulated year .....	141
Fig. 5.9 Cash flow break-down by components and cost type.....	142
Fig. 5.10 Hourly sample simulation results for four consecutive days (1 <sup>st</sup> to 4 <sup>th</sup> March) .....	143
Fig. 5.11 The effect of PV capacity and battery string number on total NPC .....	144
Fig. 5.12 PV, battery, NPV and excess power versus WT number .....	145
Fig. 5.13 System diagram of the hybrid solar-wind-diesel-battery system developed in HOMER .....	145
Fig. 5.14 Hourly mean power generated by PV, wind and diesel by month .....	148
Fig. 5.15 Coarse rainbow profile of battery bank state of charge during the simulated year .....	148
Fig. 5.16 Cash flow break-down by components and cost type.....	149
Fig. 5.17 Summary of the energy flow during the simulated year.....	150
Fig. 5.18 Hourly sample simulation results on 6 <sup>th</sup> March.....	150
Fig. 5.19 Cost comparisons of battery and diesel generator for different fuel prices .....	152
Fig. 5.20 COE of two systems types against with diesel price .....	153

Fig. 5.21 The optimal system configuration versus PV size and WT number in Option 1: (a) optimal string of batteries; (b) COE values and (c) diesel consumption.....	154
Fig. 5.22 The optimal system configuration versus PV size and battery strings in Option 1: (a) optimal WT number; (b) COE values; (c) diesel consumption.....	155
Fig. 5.23 The optimal system configuration versus WT number and battery strings in Option 1: (a) optimal PV size; (b) COE values; (c) diesel consumption.....	155
Fig. 6.1 System schematic of a hybrid solar-wind system with pumped storage system .....	159
Fig. 6.2 System schematic of a pumped storage-based PV power generation system .....	160
Fig. 6.3 Flowchart to determine initial values of components ( $N_{PV}$ , $N_{WT}$ , $V_{UR}$ ).....	162
Fig. 6.4 Flowchart of the system optimization process using GA .....	167
Fig. 6.5 Overall simulation results .....	169
Fig. 6.6 sizing curve for pumped storage-based renewable energy system.....	170
Fig. 6.7 LPSP and excess energy percentage of the wind-alone system .....	171
Fig. 6.8 Progress chart (variations of COE during GA optimization process) .....	172
Fig. 6.9 COE vs. system configuration when LPSP is fixed at 0% under single-objective optimization.....	173
Fig. 6.10 Pareto front in the double-objective optimization .....	174
Fig. 6.11 Break-down of NPC by components .....	177
Fig. 6.12 Breakdown of PV output after the PV inverter.....	178
Fig. 6.13 Hourly load shared by PV direct output and turbine .....	179
Fig. 6.14 Frequency distribution of UR's SOC.....	179
Fig. 6.15 Hourly simulation results on a sample day .....	180

Fig. 6.16 SOC of the energy storage system under different system configurations .....	181
Fig. 6.17 Daily mean renewable energy power production and load demand.....	183
Fig. 6.18 Summary of daily average electricity flow and water flow .....	184
Fig. 6.19 Rainbow profile of UR's state of charge during the simulated year .....	184
Fig. 6.20 Annual duration curves of power surplus and deficit.....	185
Fig. 6.21 Energy distributions for a typical day.....	186
Fig. 6.22 Sensitivity analysis results on several key parameters .....	187
Fig. 6.23 System COE under various LPSP.....	188
Fig. 7.1 Ragone Plot of energy storage technologies.....	195
Fig. 7.2 Standalone RE system with passive hybrid energy storage system .....	196
Fig. 7.3 Equivalent circuit of a supercapacitor in parallel connection with a battery .....	197
Fig. 7.4 Simulation model formatted in Matlab/Simulink .....	203
Fig. 7.5 Currents of battery and SC in reaction to a pulsed charging source or load .....	203
Fig. 7.6 Semi-active connection of the hybrid system.....	205
Fig. 7.7 Currents profile of semi-active connected hybrid energy storage system..	206
Fig. 7.8 Voltage profiles of the HESS and battery-alone system.....	206
Fig. 7.9 Experimental layout of the hybrid battery-supercapacitor storage system.	207
Fig. 7.10 System experimental currents for the hybrid energy storage system .....	208
Fig. 7.11 Circuit diagram of the experimental semi-active connected system .....	209
Fig. 7.12 Experimental currents for the passive HESS with inductor .....	209
Fig. 7.13 Schematic of a micro PV system with hybrid PHS and battery energy storage .....	213

Fig. 7.14 Laboratory implementation of the hybrid energy storage system for PV [361] .....	214
Fig. 8.1 The installed PV system on a remote island in Hong Kong (19.8kWp).....	220
Fig. 8.2 Schematic diagram of the standalone PV system .....	221
Fig. 8.3 Relationship between these normalized parameters .....	224
Fig. 8.4 The PV array DC output power versus solar irradiance (1 <sup>st</sup> to 10 <sup>th</sup> May 2011) .....	225
Fig. 8.5 The output power per peak watt versus solar irradiance on 10 <sup>th</sup> May 2011 .....	225
Fig. 8.6 Electricity generation profile in 2011 .....	226
Fig. 8.7 Daily average AC power output ratio of PV module during 2011 .....	227
Fig. 8.8 Daily average temperatures of ambient, battery and PV module .....	228
Fig. 8.9 SMC inverter efficiency from 1 <sup>st</sup> to 10 <sup>th</sup> May 2011 .....	228
Fig. 8.10 Sunny Island bi-directional inverter efficiency from 1st to 10th May 2011 .....	229
Fig. 8.11 The status of battery bank from 1 <sup>st</sup> to 10 <sup>th</sup> May 2011 .....	230
Fig. 8.12 Monthly battery SOC profile during 2011.....	231
Fig. 8.13 Battery SOC hourly variation (time interval: 5 minutes) .....	232
Fig. 8.14 Frequency distribution of battery bank's state of charge (SOC) during 2011 .....	233
Fig. 8.15 Daily electricity generation and load consumption in May 2011 .....	234
Fig. 8.16 Monthly Normalized parameters .....	237

## LIST OF TABLES

Table 1.1 Number of people without access to electricity in 2011 and projection for 2030 (million) [1] .....	2
Table 2.1 Comparison of technical, economic and environmental characteristics of different ESSs [259] .....	36
Table 3.1 The key specifications of the Shell Solar SQ175-PC PV module .....	52
Table 3.2 Calculated parameters of PV cell/module.....	57
Table 3.3 Summary of parameter results .....	60
Table 3.4 Comparisons between specifications under STC and corrected values with derating factor .....	67
Table 3.5 Calculated parameter values with corrected values for PV cell/module model .....	67
Table 3.6 The characteristic points (Isc, Voc and Pmmp) comparisons between PV module #M1's measured data and calculated data.....	69
Table 3.7 The key specifications of the Suntech STP200-18/Ub-1 PV panel .....	72
Table 3.8 The weather conditions of the three cases .....	76
Table 3.9 performance statistic of the proposed model .....	79
Table 3.10 Measured and predicted energy production on the three example days ..	80
Table 3.11 Details of wind turbine.....	85
Table 3.12 Details of the selected battery .....	86
Table 3.13 Specification of diesel generator set .....	95
Table 3.14 Details of converter SI5048 .....	97
Table 3.15 Emission factor from diesel power generation .....	103

Table 4.1 Wind distribution results for different hub heights .....	117
Table 4.2 Turbine operating performance results at different hub heights .....	117
Table 4.3 Monthly wind turbine operating performance (for hub height at 15m)...	118
Table 4.4 Average daily power demands of major components in Town Island....	121
Table 4.5 Monthly load coefficient and total electricity demand .....	122
Table 5.1 Categorized options with lowest net present cost .....	135
Table 5.2 Components operating performances of solar-wind-battery during the simulated year .....	140
Table 5.3 Components of operating performance for the solar-wind-diesel-battery system (option 1).....	147
Table 6.1 Optimal system configurations under different LPSP values .....	175
Table 6.2 System configuration and resultant performance index.....	182
Table 6.3 Optimal system configurations of different system types.....	189
Table 7.1 Experimental data collected under charging status.....	215
Table 7.2 Experimental data collected under discharging status .....	216
Table 7.3 Energy balance of the hybrid energy storage system under three cases ..	217
Table 8.1 Summary of the entire system energy performance.....	235

## ABBREVIATION

SAPS	stand-alone power system
PV	photovoltaic
AI	artificial intelligence
ANN	artificial neural networks
BBO	Biogeography based optimization
CAES	compressed air energy storage
CC	cycle-charging
COE	cost of energy
DG	diesel generator
DOD	depth of discharge
EENS	expected energy not supplied
EIR	energy index of reliability
ESS	energy storage system
GA	genetic algorithm
HESS	hybrid energy storage system
HT	hydro turbine

IC	initial cost
IEA	International Energy Agency
LA	level of autonomy
LCC	life cycle cost
LF	load-following
LM	Levenberg-Marquardt
LPSP	loss of load probability
MBE	mean bias error
NF	Neuro-fuzzy
NPC	net present cost
O&M	operation and maintenance
PBT	payback time
PDF	probability distribution function
PHS	pumped hydro storage
PSO	particle swarm optimization
PV	photovoltaic
RAPS	remote area power supply
RE	renewable energy
RF	renewable fraction

RMSE	root mean square error
SA	simulated annealing
SC	supercapacitor
SI	Sunny Island
SMC	Sunny Mini Center
SOC	state of charge
STC	standard tests conditions
UR	upper reservoir
WT	wind turbine



# CHAPTER 1 INTRODUCTION

Energy is an active force which stimulates both social activities and the provision of services to enable comfortable and efficient living. In terms of services, at present, the world is mainly powered by conventional fossil fuels, some of which are destined to be exhausted in several decades, based on the current rate of exploration and subsequent consumption. However, together with these fears, in recent years, the rising price of fossil fuels, the wide concerns about global warming and harmful emissions from carbon fuels have resulted in an emerging interest in the development of renewable energy (RE) applications. A particular recent stimulator, in this respect, has been the Fukushima nuclear accident, which added to the concerns outlined above, can be considered a turning point or motivator in the call for a transition from the risky nuclear and CO<sub>2</sub> intensive fossil fuels to a power supply provided by sustainable and environmental-friendly renewable energy, such as solar photovoltaic (PV), wind and hydro. In this context, a global movement to explore the possibility of further developing RE is accelerating, to help meet increased energy needs and carbon reduction targets.

## 1.1 The need for power supply in remote areas

Over the last two decades, almost every inhabitant of the industrialized world has access to a degree of constant electricity. This is not the case, however, for the planet's entire population. According to a recent report [1], approximately 1.3 billion people worldwide, that is close to one-fifth of the total global population do not have access to an electricity supply (Table 1.1). In China, the number of people without electricity

has been greatly reduced due to the rapid economic development, but currently, 3 million people still lack access to electricity.

Table 1.1 Number of people without access to electricity in 2011 and projection for 2030 (million) [1]

Region	2011		2030 (projection)
	Population	Share of population	Population
Developing Countries	1257	23%	969
Africa	600	57%	645
<i>Sub-Saharan Africa</i>	599	68%	645
Developing Asia	615	17%	324
<i>China</i>	3	0.2%	0
<i>India</i>	306	25%	147
Latin America	24	5%	0
Middle East	19	9%	0
	1258	18%	969 (12%)

A composite satellite photograph of the Earth from space is presented in Fig. 1.1, showing the areas of the world with and without electricity (the dark areas have no power). Significantly, only about 30% of households in Sub-Sahara Africa and northern India have electricity and outages are frequent. The International Energy Agency (IEA) report projected that close to 1 billion people, approximately 60% of which are located in Sub-Saharan Africa, will still be without grid electricity in 2030. Lack of electricity is the major barrier to global poverty alleviation, living standard improvement, economic development and urbanization in those developing countries.



Fig. 1.1 Composite nighttime photograph of the Earth from space [2]

Inhabited areas without access to electricity are likely to be remote and sparsely populated areas such as deserts, islands and mountain areas remote from the utility grid. Grid extension to such communities is often impractical, technically difficult and uneconomical [3-8]:

- 1) Owing to their physical separation in terms of distance from those societies with such technology in situ resulting in lack of electricity distribution system to each isolated area;
- 2) The high cost of constructing long distribution lines and maintaining large-scale electrification networks, owing to such as harsh and inhospitable terrain coupled with highly sparse population;
- 3) Difficulties in maintenance and hence poor quality and unreliability, even if the power grids have been established;
- 4) Upgrading and grid extension can often be beyond the financial capacity of such remote areas.

Hence remote communities beyond the reach of electricity and facing an inappropriate infrastructure are usually or have to be abandoned by attempts to be connected to the grid. In such a context, remote area power supply (RAPS) systems [9] offer a sensible and effective solution. Generally, RAPS systems are defined as electrical power-supply systems for remote and isolated homes and farms, rural business enterprises and isolated villages and towns, where a stand-alone power system is more cost-effective than grid extension. In the literature, different variants of RAPS system are described include ‘stand-alone power systems’, ‘off-grid power system’, ‘isolated power systems’, ‘remote power systems’, ‘autonomous power systems’, ‘household power systems’, ‘microgrids or minigrids’ [10]. The development of such systems are highly promoted by United Nations Foundation to improve universal access to modern energy service and therefore have been proceeding at an accelerated rate over the past ten years [11]. Such systems are powered by diesel fuel.

## **1.2 Diesel generator power supply and its problems**

Currently, diesel generators (DG) normally meet the electrical demand in remote areas, such as those described above [12, 13]. DG-based RAPS systems are simple and have good reliability. However, currently further development has received a negative response because:

- (i) The cost of power supply is exaggerated and could reach the point of being financially unacceptable, due to significant rise in diesel price and extra costs of shipment [14, 15].
- (ii) The efficiency of diesel generators can be low when operated under partial load. Usually, the load in a RAPS system is subject to frequent fluctuations

and thus the corresponding power factor of DG is low. Using generators of different capacities to operate under different load conditions increases the loading level, but does not reduce high generation costs [10];

- (iii) Diesel usage damages the local ecological system, causing noise, water, soil and air pollution [16];
- (iv) Maintenance of DGs is expensive and time consuming in terms of travel to remote inhospitable locations. [17].

The above is responsible for extensive public attention being drawn to finding alternatives for DG-based RAPS system.

### **1.3 Using renewable energy for RAPS**

Fortunately, those areas as described above, although remote, are usually rich in RE resources, thus diesel replacement and the production of cheaper electricity is not beyond the realms of possibility [16]. The environmentally friendly and inexhaustible RE systems, such as photovoltaics (PV) power, wind power, micro hydro and their hybrids, is most likely to be most promising solution for RAPS [15, 18].

In recent years, standalone RE systems, when compared with conventional resources, have become cost-competitive because of the rise in diesel cost and the rapid decline in RE cost. Additionally, RE systems, if in general use, could contribute to future energy sustainability and also offer a contribution to restraining environmental pollution. The above factors, the advances in RE technologies plus some inter-related initiatives to promote RE utilization both by the government and power supply companies have encouraged a dramatic expansion in the use of RE as an alternative to expensive grid extension or diesel-based electrification in remote areas. For example, Ref. [19-21] have demonstrated that a stand-alone RE system can provide a cost-

effective alternative to DG, offering important opportunities for remote communities to avoid environment problems, improve power supply quality and living conditions. Further examples are given below in Chapter 5.

#### **1.4 Energy storage for the RE-based RAPS systems**

As indicated above, technological improvement and the rapid development of RE technologies make high initial cost no longer the key barrier to the use of RE systems. One significant technical challenge of RE power supply systems, however, is unpredictable output and weather-dependent characteristics. Their electricity production is likely to experience great fluctuations, making it difficult for them to self-adjust to suit the load demand. Hence, the intermittency characteristic prevents such systems from being fully reliable. In this regard, a feasible energy storage system is indispensable and must be employed as an integral part of the RE-based RAPS systems to compensate for the above problem. Unfortunately the energy storage device has proved to be one of the most expensive components of a standalone RE system [22]. Therefore, how to store the electricity harnessed from the RE sources at a reasonable cost becomes a crucial issue, but also a necessary challenge if RE systems are to be successfully promoted in remote areas.

Given the problem of intermittency, a reliable energy storage system (ESS) is critical in negating this problem and hence enabling RE production to be a viable concern. The user needs to be safely assured that energy can be supplied when needed. Ideally the ESS should act as an energy buffer and backup, storing the generated electricity when power generation exceeds demand and subsequently enabling dispatch when required. Thus the ESS will provide the means whereby the imbalance between

generation and load demand can be significantly mitigated and thereby dramatically improve system reliability.

The growing academic interest in energy storage technologies is accompanied by an ongoing world-wide utilization of RE in remote areas. Currently various energy storage technologies have been used in stand-alone RE systems, such as batteries, flywheels, compressed air, fuel cells, supercapacitors, and pumped hydro storage. Among these technologies, rechargeable lead-acid batteries, particularly those with deep discharge rates and high cycling stability, are commonly employed because of their technical maturity and wide availability [23-26]. RE outputs, however, are not ideal for battery charging as the output fluctuates greatly depending on weather conditions. It is unlikely that batteries will recover from rapid power fluctuations without a dramatic reduction in their lifetime. In addition, batteries have well known limitations, such as high initial investment, relatively short lifespan, possibility of environmental damage and explosion due to lead and sulfuric acid content, and maintenance difficulties in isolated areas.

Some potential alternatives to batteries for RAPS systems have been extensively studied by researchers in recent years, and from these studies PHS is considered to be the most promising candidate. PHS, is highly respected worldwide and has been utilized in association with conventional power plants and nuclear power plants for the past hundred years due to its low cost and maturity, and remains the most commonly used and commercially viable electricity storage technology. The PHS system, based on two vertically-separated water reservoirs, stores potential energy by using low-cost off-peak electricity to pump water from the lower reservoir to an upper reservoir. During the periods of peak load demand, stored water is released to flow downhill through a turbine to redeliver power.

## **1.5 Motivations and objectives of this thesis**

### **1.5.1 Motivations**

Aligned with the rapid growth of solar PV application, a better understanding of PV system operating performance has become an essential research area. Accurate prediction of PV system power output under real weather conditions is of importance for system designers and engineers to make a sound decision on the selection of PV modules and the prediction of PV module energy production. The development of a reliable and accurate PV power prediction model is indispensable for deep evaluation and any subsequent further developments. Over the past decades, a substantial amount of work has been conducted to specifically develop simulation models for PV devices. However, poor accuracy or high complexity of these models and software packages has not proved suitable for practical application. Therefore in-depth research is required to develop an efficient PV performance simulation model, with a good compromise between accuracy and simplicity.

Effective energy storage technology is an ongoing problem which has not yet been solved sufficiently to produce an effective system. Many reports on the use of batteries are given in the literature and, in theory, appear to be front-runners in RAPS systems. As indicated in Section 1.4, barriers, such as high cost and short lifetime continue to limit applications. With these shortcomings in mind, PHS appears worthy of further scrutiny as regards its suitability and potential for battery replacement in standalone RE systems.

Current PHS literature appears to have focused almost exclusively on the theory of PHS or the development of the technology itself for the large scale grid-connected

systems. A few studies have reported on the suitability of micro PHS for island wind power generation systems. Detailed practical studies have not yet been included. From the available literature, it appears that the technical issues arising from integrating PHS into hybrid RE systems for remote areas is in need of further investigation, as regards the following: the physical model, mathematical model, operation principle, simulation, optimization and techno-economic evaluation of the PHS-based standalone RE systems. These areas do not appear to be widely documented. Therefore, more in-depth research on feasibility studies, model development, system simulation, optimization, experiments and demonstrations is required and would be of complementary value for RE applications in remote areas.

In addition, usually a single energy storage technology is difficult to response fluctuating RE output and dynamic power demand. In order to make ESS more reliable, a reasonable solution is to use the hybrid energy storage system (HESS), such as the combination of battery and supercapacitor, and the combination of PHS and battery, to leverage their complementary characteristics. Actually, the hybrid lithium battery and supercapacitor have been widely used for the electric vehicle. However, in literature, little has been done on the two hybrid energy storage systems for the standalone RE systems.

### **1.5.2 Aims & Objectives**

The aim of this thesis is to study the stand-alone power supply options together with different energy storage technologies for remote areas. The solar PV, WT and backup DG are considered as the major power generators. Battery, pumped storage and supercapacitor and their hybrids are proposed as the energy storage subsystem. A

remote inhabited island off the coast of Hong Kong, Town Island, is taken as a test centre for installing and testing the proposed RE systems and storage technologies.

The specific objectives of this thesis are summarized as follows:

- (i) To develop a novel simulation model for fitting the I-V curves and predicting the PV power output. Field measurements are carried out for real PV systems to validate the proposed model. To develop the mathematical models for other power generators (wind turbine and diesel generator) and models for energy storage technologies (battery and PHS).
- (ii) To simulate the dynamic performance of battery-based RAPS systems based on time-series, and to determine an optimal system configuration of various combinations of four technologies, i.e. PV, WT, DG, and battery, through simulation and techno-economic optimization.
- (iii) To propose an alternative, PHS, to support the standalone RE systems for remote areas. To develop a novel operating principle, design process, simulation and optimization program for the proposed system. To conduct a sensitivity analysis in relation to several key parameters.
- (iv) To propose a hybrid battery-supercapacitor energy storage system for RE-based RAPS systems. To develop mathematical models of the HESS for theoretical analysis and numerical simulation. To devise an experimental test bench to validate the simulation model.
- (v) To experientially investigate the hybrid PHS-battery energy storage for a PV system, and to conduct a long term testing campaign to evaluate the operation performance of a PV-battery system on the island.

## **1.6 Organization of this thesis**

The rest of this thesis is structured as follows:

A comprehensive Literature Review on standalone RE power supply systems and energy storage technologies is presented in Chapter 2, to introduce the previous research methods/outputs and identify the research gap/limitations in this field.

The mathematical models of power generators (PV, WT, DG) and energy storage technologies (battery, pumped hydro storage) in RAPS systems are developed in Chapter 3. The purpose of this chapter is to explore the maths and theory behind the modeling of RAPS systems. In particular, a novel simulation model for PV devices, offering a good compromise between accuracy and simplicity, is developed in Matlab to simulate the I-V curves and predict PV power output. The RE potential and load demand of the selected island are then assessed in Chapter 4.

In Chapter 5, a study of the traditional energy storage technology, battery, to support the microgrid RE power generation system, is carried out. System configurations of possible combinations of PV, WT, DG and battery banks are developed. Hourly simulations for a wide variety of configurations are performed to achieve the optimal example based on techno-economic analysis. Two representative systems, the 100% RE and hybrid RE-diesel, are selected for deeper analysis. The effects of the generator and storage capacities on the system's reliability and cost are also examined.

The barriers affecting battery storage limit a wider and future application of the battery-based RE systems. Therefore, an alternative, a small PHS unit, is proposed and described in Chapter 6. The aim is to support the remote area RE power supply systems at a few hundred kW scale. A novel operating principle and design process are

developed. The proposed system is to be simulated for a year and then optimized using a genetic algorithm based on techno-economic results. The dynamic behaviour of a case study based on the involved island is analyzed. A sensitivity analysis, in relation to several key parameters, is also performed.

The investigation of the battery-based and PHS-based RE systems in the above two chapters indicate that the use of more than one storage technology will give a better performance as regards complementing fluctuating RE outputs and dynamic power demands. Therefore, a HESS is proposed in Chapter 7. The mathematical models of the HESS are developed for numerical simulations. An electric inductance is further introduced to improve the performance of the HESS. In addition, an experimental test bench is developed to validate simulation results. Another type of HESS, the combination of PHS and battery, is also analyzed and a physical representation of the system is studied experimentally.

Chapter 8 presents the long term performance evaluation results of a 19.8kWp solar PV-battery system on the involved island, covering the following aspects: PV array, inverter, the battery bank and overall system.

The major conclusions and achievements are drawn in Chapter 9. Recommendations for the future research, based on the limitations described in this thesis, are also presented.

## **CHAPTER 2 LITERATURE REVIEW**

A comprehensive overview of the current-state-of-knowledge concerning the topics in this thesis and limitations in literature is presented in this chapter. The focus of Section 2.1 is the current research on RE systems for RAPS. Section 2.2 gives an overview of PV system modeling and simulation, and Section 2.3 provides a review of sizing and optimization methods for the RE-based RAPS systems, while energy storage system, as a core part of the standalone RE systems, is discussed in Section 2.4.

### **2.1 Standalone renewable energy systems for RAPS**

Further application of diesel-based RAPS systems has become hindered by high operating cost and negative environmental problems. Focus has thus turned to the utilization of RE as an alternative of diesel. RE has a reputation for being clean, inexhaustible, environmentally friendly and cost-effective [5, 20, 21]. For islands, remote regions and national borders where the national grid is not available or too costly to be implemented, the most practical and cost-effective energy future is standalone RE power supply systems. The reasons include, such as shortage of electric power supply [27], expensive grid connection or diesel fuel cost [28], preference for a clean system [29], desire for energy independence and avoidance of overhead lines or undersea cables in environmentally sensitive areas [29]. Not surprisingly, the remote areas around the world are at the forefront of the transition towards a more sustainable energy future. A RE-based RAPS system, therefore, can be viewed as a sustainable solution stimulated by the social, economic and environmental benefits described below.

- i) Direct and indirect social benefits of electricity generation by renewable sources in rural areas include electrification, irrigation, food preservation, crop processing, cooling, and small-scale industries. As a result, the remote residents can achieve improved health and living standards, greater self-reliance, more work opportunities and the basic means of technological advances [30]. Renewable energies also avoid the safety problems derived from such as atomic power [31, 32].
- ii) The use of RE provides a wide variety of economic benefits. It enables RAPS could be cost-effective, in that money is saved by reduced diesel use or grid extensions. A transition to RE-based energy systems currently appears more likely, as the costs of solar and wind power system have dropped substantially over the past 30 years, while the diesel price is high and fluctuates greatly. Additionally, the use of RE can stimulate economic growth in impoverished areas and the corresponding better living conditions [33].
- iii) From an environmental point of view, RE resources are based on unlimited, inexhaustible, environment friendly and sustainable sources, all of which contribute to less air and water pollution, thereby lowering greenhouse gas emissions, and maintaining natural resources for the long term [34, 35].

An awareness of the above has caused the last decade to witness a dramatic expansion in the use of RE as replacements for fossil-based energy. As RE costs decrease worldwide, the transition from fossil fuels to a greater reliance on local and sustainable sources of energy is increasingly compelling [36].

RE-based RAPS systems usually incorporate a combination of photovoltaic (PV) systems, wind turbines (WT), diesel generators (DG), power conditioning units, and energy storage devices [37]. Sometime they are accompanied by hydro turbines [38].

The system configurations to integrate different generation and storage systems can be divided into three categories: DC coupled configuration, AC coupled configuration, and hybrid DC-AC coupled configuration [39]. In areas where people live close together in a village, one large system can power the entire village via a mini-grid. Where homes are further apart, individual micro-scale systems are often employed.

Substantial studies show that the RE resources have attracted energy sectors to generate power on a large scale [40]. A common drawback to wind and solar energy is their unpredictable nature as well as dependence on weather and climatic changes. It is evident that neither a single PV nor a single wind energy system is able to provide a continuous power supply because of seasonal and periodical fluctuations [41]. The independent use of any single technology usually leads to a considerably oversized generation system and energy storage subsystem for a reliable power supply, which in turn requires higher operating and life cycle costs [14, 21, 42, 43].

The problem of variability of RE output, fortunately, can be partially overcome by 1) installing individual large renewable power plants, or 2) adding energy storage facilities, or 3) developing hybrid energy systems in a proper combination [30]. A hybrid renewable energy system is composed of two or more renewable power generation technologies to achieve better performance and higher efficiency [44]. A substantial number of studies have indicated that a hybrid solar and wind system, which can leverage the strengths of each technology to provide a more reliable and less costly power supply in remote areas [29, 35, 36, 45, 46]. The hybrid solar–wind power generation systems can effectively improve the system energy usage factor, advance energy supply reliability, and reduce the energy storage requirements [14, 47], due to the complementary nature exhibited from solar and wind energy supply in daily

and seasonal patterns [48, 49]. Such is the interest and belief in hybrid solar and wind system that much research has been reported and commonly demonstrates that such hybrid system with energy storage is techno-economically viable for rural electrification in remote areas [50-55].

Additionally, the combination of RE and DG is also used in some RAPS systems, for example hybrid PV-wind-diesel-battery systems [56-58], and wind-diesel system [45, 59], and PV-diesel system [13, 34, 60] and PV-wind-hydro-diesel system [61]. The hybrid system takes its primary energy from RE generator and the balance from DG, and has an energy storage system as well to balance out-of-phase supply and demand. In such a system, the DG can only be run for a few hours per day, but, importantly, at its optimum efficiency, thus minimizing fuel consumption and exhaust emissions [9]. In this way, the system cost will be reduced greatly and power supply reliability will be improved.

## **2.2 Modeling of PV system and parameter-determination methods**

Because of the rapid growth of and interest in the use of solar PV application in the world, understanding the PV operating performance is an essential topic of research. Accurate prediction of PV module power output under real weather conditions is of great importance for system designers in system configuration and product selection. It is also crucial for engineers to evaluate PV systems' operation performance [62-64]. However, it has been found that the specifications of a PV module given by manufacturers does not or cannot accurately predict PV performance under general conditions. Therefore, an accurate and reliable solar PV power prediction model is of vital importance [65, 66]. Below a comprehensive Literature Review on simulation models for PV devices and determination methods is presented.

### 2.2.1 Equivalent circuit and mathematical models for PV devices

The ability to model PV device output is key to the analysis of PV system performance. A PV cell is traditionally represented by an equivalent circuit composed of a current source, one or two anti-parallel diodes (D), with or without an internal series resistance ( $R_s$ ) and a shunt/parallel resistance ( $R_p$ ). The equivalent PV cell electrical circuits based on the ideal model, a one-diode model and a two-diode model are presented in Fig. 2.1. These PV cell electrical power models are widely described in the literature [67-70]. The literature also reveals that the circuit in Fig. 2.1c is the more commonly used [71], as it can be represented by a simple and accurate simulation model.

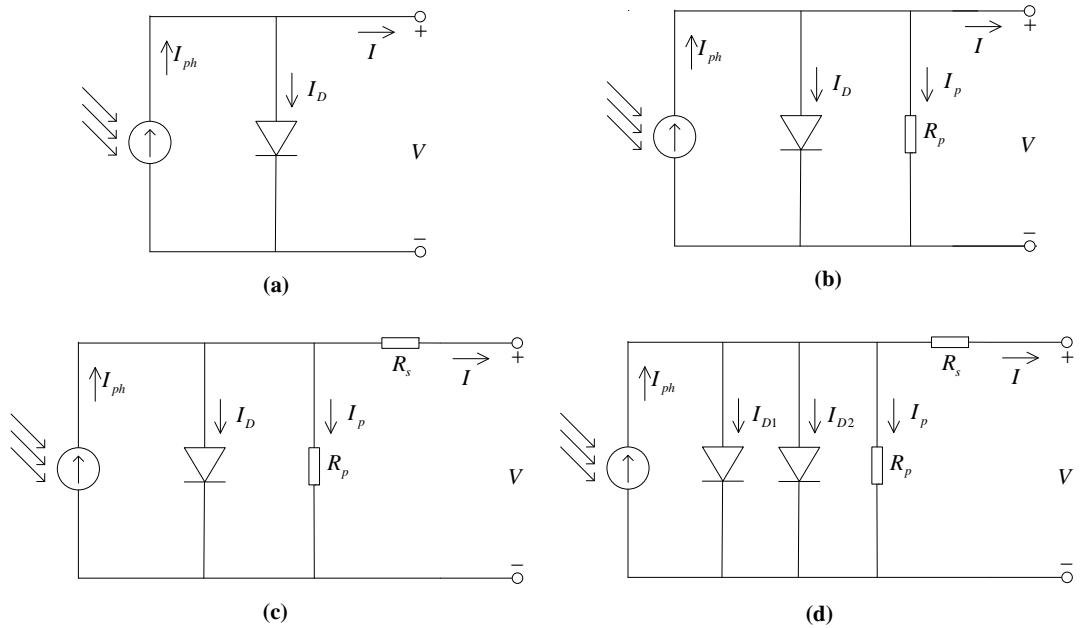


Fig. 2.1 Equivalent PV cell electrical circuits: (a) ideal model; (b) one-diode only with  $R_s$  (4-p model); (c) one-diode with  $R_s$  and  $R_p$  (5-p model) and (d) two-diode models (7-p model)

The outputs from these models are the current and voltage data points, which can be connected to produce the I-V curve (Fig. 2.2). One primary objective of PV device modeling revealed in the literature, is to fit the predicted I-V curves to the

experimental curves of the practical system, particularly at the three characteristic points: short circuit (0,  $I_{sc}$ ), MPP ( $V_m$ ,  $I_m$ ), and open circuit ( $V_{oc}$ , 0). Relevant research related to PV mathematical and simulation models is as follows.

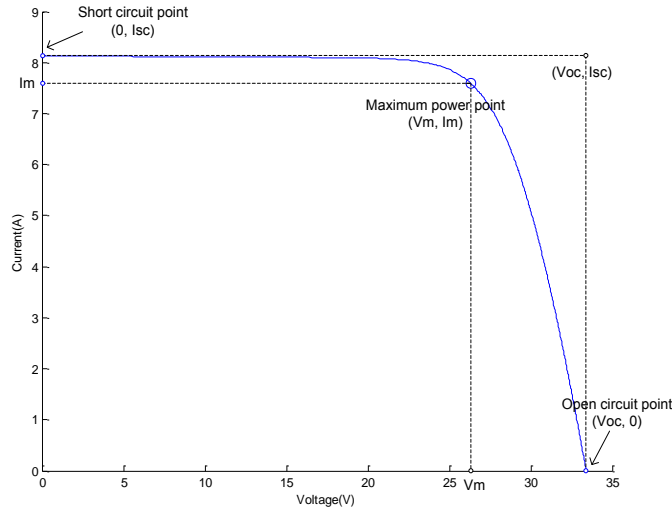


Fig. 2.2 PV module I–V characteristic curve with three characteristic points

### 2.2.1.1 Ideal model

As presented in Fig. 2.1a, the ideal PV cell model has the simplest form, since it takes no account of the effect of internal electrical series resistance and parallel resistance. Based on the Shockley theory, recombination in the space-charge zone, it can be neglected and the second diode term can therefore be omitted. [72]. It is acknowledged that the PV cell is neither a constant voltage source nor a constant current source. The externally measured current can be related to voltage and the relationship between them has been investigated [73, 74]. Based on the Shockley and Queisser (SQ) diode equation, the ideal mathematical model for an individual PV cell is expressed as [75, 76]:

$$I = I_{ph} - I_D = I_{ph} - I_0(e^{V/V_t} - 1) \quad (2.1)$$

where  $I_{ph}$  is the photo current (A), assumed constant along the I-V curve and proportional to the irradiance, with only a weak temperature dependency;  $I_0$  is the diode saturation current (A);  $V_t$  is the diode thermal voltage;  $n$  is the diode ideality factor;  $k$  is Boltzmann's constant ( $1.381 \times 10^{-23}$  J/K);  $q$  is the absolute value of the charge on an electron ( $-1.602 \times 10^{-19}$  C) and  $T$  is the cell temperature (K), assumed equal to the temperature of the P-N junction [77].

Some studies have been carried out using simple models involving a linear independent current source parallel to a diode [78]. However, it is demonstrated in the literature that the ideal cell model, in the absence of recognition of internal resistance effects, is not suitable for modeling the actual PV cell current and voltage relationship [73].

#### 2.2.1.2 One-diode model taking account only of $R_s$ (4-p model)

Fig. 2.1b illustrates the equivalent PV cell electrical circuit for the series resistance case. This is the so-called four-parameter (4-p) model [79-86], in which the parallel resistance is considered as infinite, and thus its effect is not taken into account. Its mathematical model is presented as:

$$I = I_{ph} - I_D = I_{ph} - I_0 \left( e^{\frac{V + IR_s}{V_t}} - 1 \right) \quad (2.2)$$

In Ref. [87], the 4-p PV model was proposed, and incorporated into the transient simulation program TRNSYS. This model was used to estimate and optimize the performance of a pumping system PV installation [81, 88]. The model, based on four parameters, was used to simulate three types of PV panels, each differently constructed,

one with thin film, another with polycrystalline silicon, and the third with monocrystalline silicon materials [89].

Recent research studies [63], however, show that the 4-p model, which ignores the effects of shunt resistance, is inadequate to fit experimental I-V and P-V data into the current-source operation. [90, 91] also demonstrated that the simplified 4-p model does not satisfactorily reflect the effect of high temperature on the current, and leads to a less accurate current prediction than the 5-p model.

### 2.2.1.3 One-diode model considering $R_s$ and $R_p$ (5-p model)

To improve the accuracy of the simulation model, parallel resistance is thus introduced in the one-diode model. This is the well-known five-parameter (5-p) model, shown in Fig. 2.1c and represented by Eq. (2.3).

$$I = I_{ph} - I_D - I_p = I_{ph} - I_0 \left( e^{\frac{V+IR_s}{V_t}} - 1 \right) - \frac{V + IR_s}{R_p} \quad (2.3)$$

It is widely acknowledged that both series resistance  $R_s$  and parallel resistance  $R_p$  can affect the I–V characteristics of a PV device. In general, the parallel resistance reduces the available electrical current, and the series resistance affects the output voltage.

Recently, a new method to extract the five parameters has been developed by Ma et al. [92] and Bai et al. [93]. The dynamic behaviour of a 3.2kWp photovoltaic system was evaluated in real conditions using the 5-p model [94], and the output of a partially shaded PV module was also modelled based on the 5-p model [95]. Five of the recent and most cited articles concerning the 5-p model [62, 66, 77, 96, 97] have been discussed [98], in relation to the mathematical models themselves, the parameter extraction procedures, and the major hypotheses and simplifications involved. The

literature shows that much research has been carried out in developing the 5-p model, and also provides some directions for improvement and/or simplification to obtain the five parameters ( $I_L$ ,  $I_0$ ,  $V_t$ ,  $R_s$ ,  $R_p$ ). Results from those studies demonstrate acceptable levels of accuracy [40, 90, 99-105].

#### 2.2.1.4 Two-diode model

The commonly used one-diode model can achieve acceptable accuracy, but the reality is that the saturation current of the PV cell is the result of a linear superposition of charge diffusion and recombination in the space-charge layer [106]. This means that two Shockley terms, i.e. two diodes contribute to the saturation current. Therefore the two-diode model, also called the double-diode model, was proposed [106-113]. The schematic diagram of the equivalent electrical circuit is illustrated in Fig. 2.1d and the mathematical model is expressed as:

$$I = I_{ph} - I_{D1} - I_{D2} - I_p = I_{ph} - I_{01} \left( e^{\frac{V+IR_s}{V_{t1}}} - 1 \right) - I_{02} \left( e^{\frac{V+IR_s}{V_{t2}}} - 1 \right) - \frac{V + IR_s}{R_p} \quad (2.4)$$

where  $I_{D1}$  and  $I_{D2}$  are the currents passing through the corresponding diodes. As for the single-diode model with  $R_p$  and  $R_s$  (five-parameter model), the internal series and shunt resistances affect the output voltage and current, respectively.

The two-diode model can achieve greater accuracy, particularly at low irradiance level and during partial shading conditions [114]. The inclusion of an additional diode, however, increases the number of computed parameters. Eq. (2.4) indicates that this model is quite complex, being a nonlinear and implicit equation with two exponential terms and up to seven unknown parameters. The computational time is, therefore,

relatively long [68, 70]. In addition, other new coefficients are introduced into the equations, further increasing the computing burden.

Many attempts have been made to reduce the computational complexity of the two-diode model, but they appear to be unsatisfactory [70]. Some researchers assumed the diode ideality factors to be  $n_1=1$  and  $n_2=2$  to simplify the model. The latter is an approximation of Schokley-Read-Hall recombination in the space charge layer in the photodiode [115]. This assumption is widely used, even though it does not always hold true [116]. [70] developed an improved two-diode model and simplified the current equation, resulting in a requirement for only four parameters. The reverse saturation currents  $I_{D1}$ ,  $I_{D2}$ , however, are then forced to be equal in magnitude. Such simplification may result in some inaccuracy although computation time is reduced.

The two-diode model provides higher PV cell modeling accuracy, however it was not selected for this study for the following two reasons. One concerns the fact that the recombination incurred by the second diode dominates at low voltage and low irradiance [96, 117], conditions seldom selected for simulation studies. The other reason is that the parameter determination would be very complicated if another diode is added.

#### *2.2.1.5 Other models*

In addition to the above models, the three-diode model [118] has been studied, but not to a great extent, because of the calculation complexity. Thermal models to simulate PV performance, such as one based on overall heat loss coefficient has also been investigated [119, 120]. These models are usually not suitable for wide use because of insufficient information supplied by the module manufacturer. Mathematical modeling of PV module output taking account of solar cell mismatching and the

interconnection ribbon was proposed in [121]. An empirical general PV device model was studied by [78], and a method called APTIV, which fits the I-V curve in two different zones was used to extract the solar cell physical parameters [122]. Accuracy, however, focuses only on the three characteristic points, rather than the complete characteristic curves.

### **2.2.2 Determination methods for solving model parameters**

Following the development of the simulation model, the determination of the unknown model parameters is challenging, as the simultaneous equations are usually non-linear and include exponential terms. Mathematical techniques, are therefore, usually employed to extract the unknown parameters. Many studies have been conducted attempting to solve the above equations using the analytical and numerical methods.

#### *2.2.2.1 Available analytical solutions*

The traditional analytical approach introduces a series of simplifications and approximations, to obtain simpler solutions and avoid bringing obvious errors to the model [90, 96]. Analytical methods have been reported and discussed in many publications [81, 90, 97, 123-127]. A data-based approach has also been presented in an attempt to avoid modeling complexity [89]. It is worthy of note that errors in the unknown parameters, can be significant if the key points on the I-V curves are not correctly specified [68].

#### *2.2.2.2 Available numerical solutions*

Numerical solutions, also known as algebraic solutions, employ powerful mathematical tools and iterative methods to solve the implicit non-linear equations

associated with PV simulation models. Numerical solutions are widely used in systems engineering because they offer a reasonable compromise between simplicity and accuracy [128].

Various numerical techniques, such as resistive-companion methods [129], non-linear least squares optimization [130] the Newton-Raphson method [77], the bisection method [100], and the equation solver EES [62], have been proposed for the simultaneous solution of these non-linear equations. An iterative programming method was introduced by [84, 131] which estimated the parameters associated with PV simulation models. This method was also improved using interpolation techniques [132]. Most of those approaches, however, demand much computing effort. Another numerical iterative method, the Levenberg–Marquardt (LM) algorithm, was employed by [90, 96, 106, 109] to solve the implicit non-linear equations, proving to be a robust method possessing sufficiently rapid convergence characteristics. However this technique requires good initial estimation of parameter values to attain convergence, particularly in the case of the two-diode model [98]. In some cases heuristic solutions need to be sought [70]. A simulation model has also been implemented using Microsoft Excel VBA macros [66].

The performance simulation models of PV devices are also available in some existing software, such as PVWATTS, PVMOD, PVFORM, INSEL, PVWATTS, PHANTASM, TRNSYS, P-Spice, PV-DesignPro, SolarPro, PVcad, and PVsyst [65, 92, 98, 114, 133, 134]. In addition, the PV model has been solved using the LSODI FORTRAN Livermore solver [135], the FORTRAN computer code was also programed in [136, 137] and added to the standard TRNSYS library with sub-programs, to solve the I–V equation numerically. A PV simulation model was written in the C language and run on a PC using a Borland C++ compiler [104]. An intricate

PSpice software-based simulation was presented by [138]. Furthermore, many studies solving PV simulation models in the Matlab/Simulink environment have been reported [91, 94, 103, 112, 114, 139-142], as this tool provides a graphical interface for models constructed as block diagrams. Such models can easily be connected so as to simulate a particular specific system [143]. These software/tools, however, are either quite sophisticated and intended for advanced users[98], or too general with results that are not so accurate [92]. Usually new coefficients are introduced into the equations, thereby increasing the computational loading [114]. They are also relatively expensive and unnecessarily complex [144].

Recently, various evolutionary algorithms have been utilized for the parameter extraction of PV device simulation models, such as the genetic algorithm [145, 146], differential evolution [69, 147], and particle swarm optimization [148]. Some studies have been made on PV device I-V curves using artificial intelligence [69, 70], such as fuzzy logic [149, 150] and artificial neural networks (ANN) [80, 91, 101, 128, 151-153]. Despite the more accurate results, artificial intelligence techniques require extensive computation, and ANN requires a large amount of data for network training purposes.

### **2.3 System sizing and optimization techniques**

The performance of a hybrid RE system depends on proper sizing of the system. In recent years, many attempts have been made to size and optimize system configuration through different techniques. Based on the Scopus database, various sizing and optimization methodologies have been reported in the literature. Fig. 2.3 shows an exponential evolution in the number of research papers that use optimization

algorithms applied to RE systems, indicating that many researchers are continuously proposing and applying new methods in the field of RE. The aim of this section is to review the state-of-art of sizing and optimization approaches that are applied to the RE-based RAPS systems. Various approaches for unit sizing of hybrid RE systems are given in Fig. 2.4.

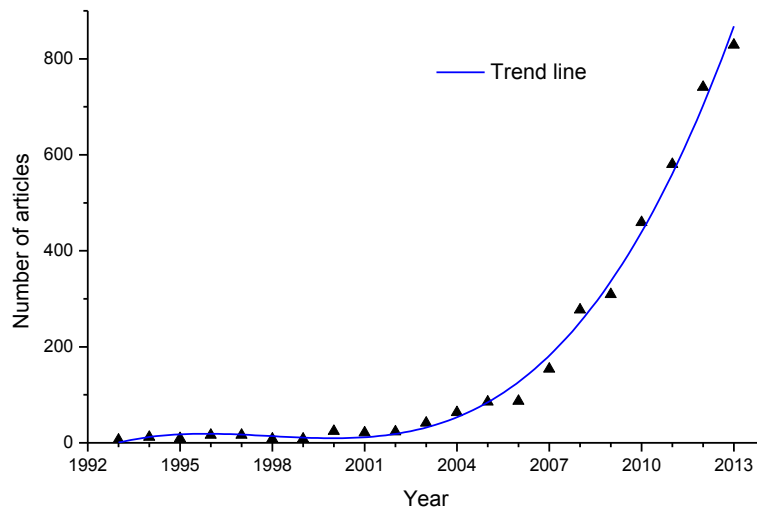


Fig. 2.3 Number of articles using optimization algorithms in the study of RE over the last 20 years

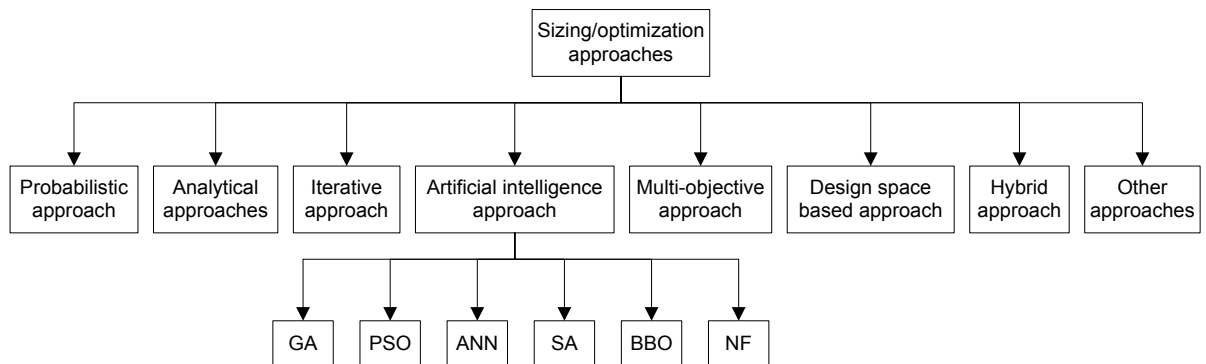


Fig. 2.4 Sizing and optimization methods

### **2.3.1 Probabilistic approach**

The probabilistic approach may be simplest method. Considered is the effect of RE resources and load demand during sizing, but not the dynamic changing performance. Thus it is not the most suitable for finding the best solution [37]. Many papers are available in the literature presenting optimized hybrid system sizing using probabilistic approaches. A probabilistic approach using a typical meteorological year is proposed by [55], to assess the performance of a hybrid solar-wind system. An updated probabilistic approach which considers the probability density function is suggested by [154, 155] to optimize the long-term performance of hybrid solar-wind power systems. In addition, a three-event probability density approximation was employed by [43], based on the two state process proposed by [156].

### **2.3.2 Analytical approach**

In the analytical approaches, the components of the hybrid RE systems are represented by mathematical models, which describe hybrid system size in terms of the function of its feasibility [157]. Consequently, the performance of the hybrid system can be assessed for a set of possible configurations, the best is then selected based on one or some evaluation criteria. Such a method requires a lengthy period, usually one year, of weather data for the simulations. In recent years, many studies have employed this approach to design and optimize system configuration [158-161].

### **2.3.3 Iterative approach**

A typical feature of the iterative method is that evaluation of system performance is completed by a recursive process which continues until the best configuration with design specifications is reached [157]. System reliability and cost, i.e. techno-

economic index, is usually evaluated in the iterative approach based optimization. An iterative process is introduced by [162] to achieve an optimal hybrid RE system configuration based on techno-economic evaluation results. [45] reported an iterative method to size a hybrid wind-diesel system based on economic cost, the same method was also applied in a hybrid PV-wind based RAPS system [163]. A new iterative method based on adaptive feedback learning, for fast convergence, was also proposed by [164] to obtain the optimal combination for a PV-battery system.

#### **2.3.4 Artificial intelligence (AI) approach**

AI is a term meaning the ability of a machine or artifact to perform similar kinds of functions that characterize human thought. The bio-inspired AI method has been widely reported, including genetic algorithms, artificial neural networks, particle swarm optimization, biogeography based optimization, simulated annealing, or a hybrid of such techniques [165]. An overview of the AI techniques for sizing PV systems is presented by [166], indicating that the major benefit of this approach is that it can deal with the non-linear behavior of system components and stochastic variability of RE sources, while its disadvantage is that it requires considerable computing time. Various studies based on AI approaches available in literature are briefly reviewed below.

The concept of genetic algorithm (GA), inspired by the evolutionist theory explaining the origin of the species, was proposed by [167] and then widely utilized in various applications. A good overview was presented by [168] to describe the GA developed specifically for problems with multiple objectives. Due to its presented advantages, substantial publications have been reported using GA for system sizing, optimization, and operational control of hybrid RE systems, including PV-diesel system [5, 60, 169,

170], PV-wind-diesel system [171], PV-wind system [50, 53, 171-173], PV-battery-full cell system [174] and PV-wind-diesel-battery system [175]. GA is also used to obtain the maximum power point based of PV devices based on I-V curves [176].

A review of the optimization methods for hybrid renewable energy systems demonstrated that the most popular applied methods were GA and Particle swarm optimization (PSO) [177]. PSO is an optimization technique based on the movement and intelligence of swarms. The basic idea of the algorithm was to seek the optimal solution through collaboration and information sharing among individuals in groups. Similar to the GA approach, PSO is also used widely in hybrid RE system sizing. For example, PSO was applied to solve the PV-WT capacity coordination by [178, 179], to optimize the PV-WT-DG system for fulfilling techno-socio-economic criterion [180], to optimize sizing of a hybrid wind-PV-fuel cell generation system [181, 182], to process economic dispatch problems by [183]. A study [184] also presented a fuzzy adaptive PSO algorithm to solve the optimal operation management of distribution networks including fuel cells power plants.

Artificial neural networks (ANNs) are based on our present understanding of the brain and its associated nervous systems. They use processing elements connected by links of variable weights to form a black box representation of systems [166]. The optimization based on ANN has been employed for sizing PV system by [80, 185, 186]. Both ANN and GA were used to maximize the economic benefits of a solar system [187].

The Simulated annealing (SA), introduced by [188], is a general optimization technique for solving combinatorial optimization problems that. A novel discrete

chaotic harmony search-based SA algorithm for optimal sizing of PV-wind-battery was developed by [189, 190].

Biogeography based optimization (BBO), a new optimization concept, is a population-based evolutionary algorithm. Similar to GA and PSO, BBO is the study of the geographical natural distribution of biological organisms. The developed BBO algorithm has been applied for optimal sizing a standalone wind/PV system by [191].

Neuro-fuzzy (NF) theory is used to simulate the aspect of human cognition that can be called approximate reasoning. It has many applications in the field of engineering. Daily management of the household PV power generation without using storage equipment was optimized by [192] by a NF algorithm. The NF logic for a wind–diesel system sizing optimization was also developed by [193].

### **2.3.5 Multi-objective optimization approach**

Most popular computational optimization methods have focused only on solving single-objective problems [194]. However, in reality, many real engineering problems have two or even multiple objectives, such as cost, system performance, reliability, which are generally in conflict and should be simultaneous optimized. Generally there are two approaches for the multi-objective optimization, i.e. aggregate weight functions [195] and Pareto optimal set based method [196].

With the aim of achieving optimal economic and environmental performance, 120 Pareto optimal sets for hybrid PV-wind system were developed by [197]. A multi-objective algorithm was also introduced to simultaneously minimize the cost of the system and total greenhouse gas emissions [198]. In addition, two algorithms for multi-objective optimization in wind-PV-DG based system was studied by [199]. A multi-objective optimization of load dispatch of power systems including RE and CO<sub>2</sub>

capture/storage technologies was conducted by [200]. More similar works using multi-objective optimization approach can be found in studies by [201-203].

### **2.3.6 Design space based approach**

The design space based approach, which can generate the sizing curve for hybrid RE systems, has also been widely employed in the academic field. The set of feasible configurations that can meet the load requirements determines the feasible design space for the entire system [49]. The concept of design space was introduced for optimized sizing of solar thermal systems by [204]. For standalone power supply systems, the design space approach was used for diesel-battery systems [205], PV-battery systems [206-208], wind-battery systems [209, 210] and hybrid PV-wind systems [211-214], hybrid systems [215].

### **2.3.7 Hybrid approaches**

For improvement, hybrid optimization methods are combined with two or more methodologies, to increase convergence time in the optimization process. These methodologies are characterized by their flexibility and dynamism in the sizing process and are hence considered the most powerful sizing methodologies. They have been widely used in the literature dealing with hybrid system sizing problems, for example, an optimal solution was obtained through the combined artificial bee colony algorithm and the Pareto front [216]. A hybrid simulated annealing and tabu search method was introduced by [217], demonstrating that the obtained solution was better than that provided by an individual method, in terms of quality and convergence. Additionally, a combination of neural network and wavelet transform was proposed by [218] to size a standalone PV system. Both GA and PSO were also implemented

for solving a planning problem for thermal units integrated with wind and solar energy systems [219].

### **2.3.8 Other optimization techniques**

Apart from the above optimization techniques, other approaches such as linear programming [30, 220, 221], simplex algorithm [174, 222], dynamic programming [223], response surface methodology [224, 225], matrix approach [226], quasi-Newton algorithm [162], and “Energy hub” concept [227] have been utilized by researchers to design hybrid RE systems in a cost effective way. The contribution of these algorithms offers an enriching promise to that literature dedicated to sizing hybrid RE systems.

### **2.3.9 Simulation and optimization software tools for hybrid RE systems**

In recent years computer-based simulation and optimization programs have received growing attention, and are becoming important tools for sizing hybrid RE systems. An overview of different simulation and optimization tools for hybrid RE systems has been presented by [228-231]. The reviews demonstrate that, for the purpose of hybrid systems optimization, HOMER is considered as the most famous and widely-used [29]. HOMER is a computer model originally developed by the U.S. National Renewable Energy Laboratory, to assist in the design of micropower generation systems across a wide range of applications [232]. HOMER has been extensively used by scholars in the field of RE supply case studies, simulation and optimization, for example, HOMER is employed to investigate the PV-diesel system in remote areas in Malaysia [13], Saudi Arabia [34, 233, 234], Cameroon [235], Brazil [236], and Jordan [237]. HOMER is also used to simulate a standalone PV system to power a health clinic in southern Iraq [238], a homestead in West Australia [239]. HOMER has been used

extensively in feasibility studies of stand-alone wind-diesel systems in Saudi Arabia [59, 240], Algeria [35] and Alaska [241], a hybrid solar-wind system in Bangladesh [242], a small Hydro/PV/Wind hybrid system in Ethiopia [12], and a hybrid microhydro-PV system in Africa [243].

Several more software tools are available for simulation and optimization of hybrid RE systems. Examples included HYBRID2 for long term performance and economic analysis [244, 245]; RETScreen for evaluating technical and financial viability of RE, energy efficiency and cogeneration projects [246, 247]; GRHYSO for grid-connected renewable hybrid systems optimization [160]; H<sub>2</sub>RES for balancing the integration of RE into energy-systems [248] and HOGA for design hybrid RE systems using genetic algorithm [60].

## **2.4 Energy storage for renewable energy supply systems**

RE sources are usually intermittent, unpredictable and time/weather dependent. Therefore, a continuous and reliable power supply is hardly possible without energy storage. By employing an energy storage system (ESS), the surplus energy can be stored when power generation exceeds demand and then be released to cover the periods when net load exists, providing a robust back-up to intermittent RE [249]. The ESS is thus a critical component and powerful partner to ensure sustainable supply of RE [250]. The European Commission finds that the ESS will play a key role in enabling the world to develop a low-carbon power supply system.

The growing academic interest in energy storage technologies is accompanied by the world-widely ongoing utilization of RE in remote areas. Current energy storage is a well-established technology but it is still relatively unexplored [251]. At present, it is

one of the greatest technical and commercial barriers to the wide integration of renewable energy applications, especially for those standalone systems completely powered by intermittent solar or wind energy, because they are available or strong only at certain times of the day.

#### 2.4.1 The role of energy storage

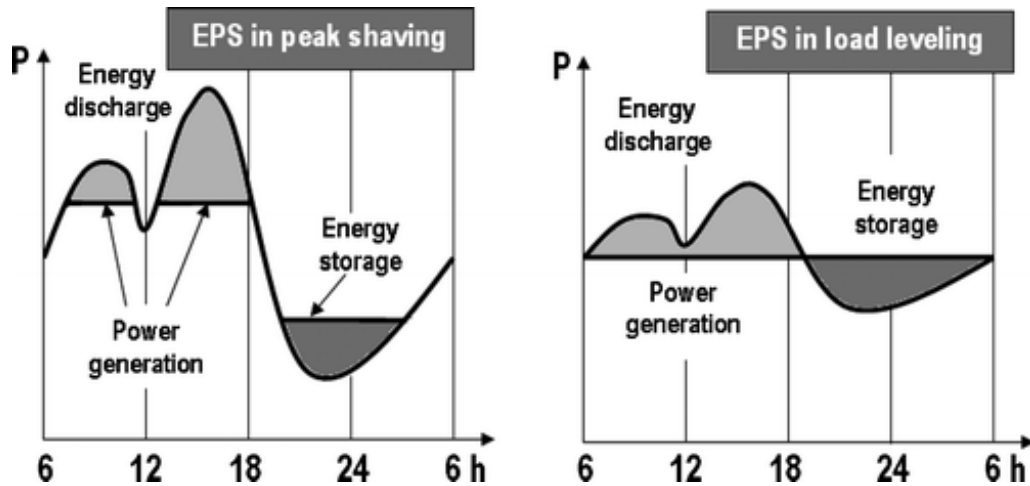


Fig. 2.5 Load profile of an electricity storage system. (a) EES in Peak Shaving; (b) EES in load levelling [252]

Energy storage is a topic of great importance in the deployment of RE, since it appears to be the only solution to the problem of intermittency and lack of controllability of its production [253, 254]. The basic roles of the EES for standalone RE are summarized as follows:

- ESS can ramp the fluctuating output from RE, and ensure that power produced by renewables can be released and dispatched reliably to better fit demand.
- It acts as an energy buffer, allowing energy produced to be held when demand is low, ready for discharge when demand is high, i.e. the function of load leveling and peak shaving as shown in Fig. 2.5 [252]. In this way, the

imbalance between generation and load demand can be significantly mitigated and system reliability can be improved dramatically [10].

- It can stabilize the power grid with a high penetration level of RE.

To facilitate the RE becoming completely reliable as a primary energy source, an economical ESS is therefore a crucial challenge that must be overcome.

### 2.4.2 Classification of ESS

Generally energy storage technologies are classified into four main categories: mechanical, electrochemical, electromagnetic, and thermal processes (Fig. 2.6). The energy storage systems in use for electrical energy usually include the first three classification types. Ref. [255] has given an overview of energy storage technologies used for electric power applications. For distributed renewable energy integration, a review of energy storage technologies was carried out by [256-258].

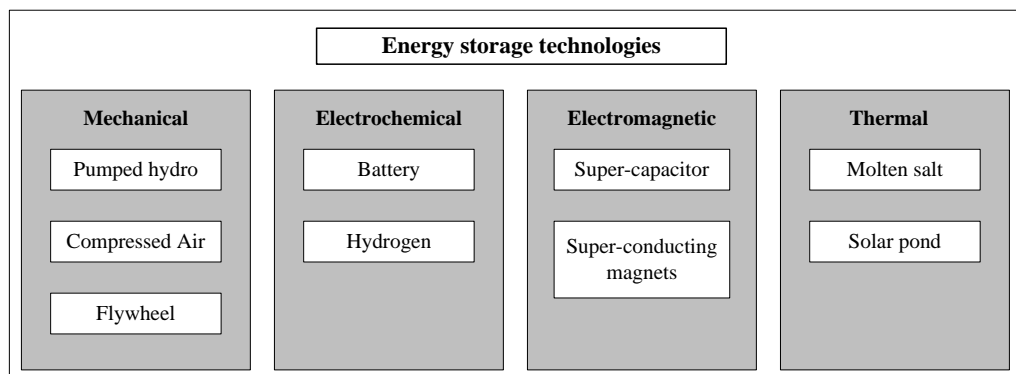


Fig. 2.6 Classification of energy storage systems

Table 2.1 Comparison of technical, economic and environmental characteristics of different ESSs [259]

ESS	Efficiency (%)	Capacity (MW)	Energy density (Wh/kg)	Capital (\$/kW)	Capital (\$/kWh)	Response time	Lifetime (years)	Maturity	Environmental impact
TES	30–60	0–300	80–250	200–300	3–50	–	5–40	Developed	Small
PHS	75–85	100–5000	0.5–1.5	600–2000	5–100	Fast (ms)	40–60	Mature	Negative
CAES	50–89	3–400	30–60	400–2000	2–100	Fast	20–60	Developed	Negative
Flywheel	93–95	0.25	10–30	350	5000	Very fast (<ms)	~15	Demonstration	Almost
Pb–acid battery	70–90	0–40	30–50	300	400	Fast	5–15	Mature	Negative
Ni–Cd battery	60–65	0–40	50–75	500–1500	800–1500	Fast	10–20	Commercial	Negative
Na–S battery	80–90	0.05–8	150–240	1000–3000	300–500	Fast	10–15	Commercial	Negative
Li-ion battery	85–90	0.1	75–200	4000	2500	Fast	5–15	Demonstration	Negative
Fuel cells	20–50	0–50	800–10,000	500–1500	10–20	Good (<1 s)	5–15	Developing	Small
Flow battery	75–85	0.3–15	10–50	600–1500	150–1000	Very fast	5–15	Developing	Negative
Capacitors	60–65	0.05	0.05–5	400	1000	Very fast	~5	Developed	Small
Supercapacitors	90–95	0.3	2.5–15	300	2000	Very fast	20+	Developed	Small
SMES	95–98	0.1–10	0.5–5	300	10,000	Very fast	20+	Demonstration	Benign

Various energy storage technologies are currently in use for distributed renewable energy integration, including battery, flywheel [260, 261], compressed air energy storage (CAES) [262], fuel cell [263, 264], Supercapacitor [265, 266], and pumped hydro storage. A good review of energy storage technologies was presented by [256–258]. The technical, economic and environmental characteristics of different energy storage technologies are summarized in Table 2.1 [259]. It can be observed that capital cost per kWh of PHS is lower than other energy storage technologies. Flywheels and supercapacitors show the highest maximum efficiency, and fastest response times, while fuel cells have a lower efficiency due to large losses. The cycle lives of the EES systems based on the electrical technologies, such as supercapacitor, are very high. The cycle abilities of batteries and fuel cells are not as high as other technologies owing to chemical deterioration with the operating time [259]. However, according to

a study by [267], these technologies are limited in some way specifically for RE. For example, with only 66% efficiency and the use of natural gas firings during operations, the amount of energy lost and the taint of fossil fuels find a CAES system lacking. A flywheel system is clean, renewable, and efficient but it is only capable of storing energy over an interval of minutes, if not seconds, the same for supercapacitors.

### **2.4.3 Battery energy storage**

Usually, standalone renewable energy systems employ rechargeable batteries to store excess electricity [23]. A good review of battery energy storage for standalone renewable energy systems has been presented by [268] and 8 types of battery technologies for PV systems have been evaluated by [269, 270]. The characteristics of different battery technologies are summarized in Table 2.1. Among those batteries, the nickel-cadmium batteries have been employed in relatively few systems due to the higher cost, lower cell voltage, lower energy efficiency and limited upper operating temperature [271, 272]. Nickel metal hydride (NiMH) batteries also suffer from severe self-discharge, making them inefficient for long-term energy storage in RAPS systems, even though NiMH is environmentally friendly in comparison to lead-acid batteries due to the lack of toxic substances such as cadmium, lead or mercury. The lithium-ion battery appears well-suited for the intermittency of RE systems [273], while it is still plausible in the not-so-distant future although such batteries are predominant in the small portable electronics market [25]. Sodium-sulfur (NaS) batteries, with the benefit in higher power and energy density, have already been employed in power systems for more than 20 projects worldwide [274]. NaS battery has potential for microgrid RE systems for power regulations. However the disadvantages of its usage are high cost and high self-discharge per day [275] .

The lead-acid battery is the oldest and most mature technology used for electrical energy storage and is currently a front-runner for use in distributed generation application, particularly those with deep discharge rate and high cycling stability. Deep-cycle lead-acid batteries are ideal for small-scale renewable energy applications; these batteries can be discharged repeatedly by as much as 80% of their capacity and hence are suited for the RE integration applications [25, 26]. However, the lead-acid batteries have well-known limitations [38, 255, 259, 273, 276-279]:

- The initial investment is high, especially for large-scale and high capacity systems;
- They have a relatively low lifespan due to the intense charging/discharging in an RE based power system (usually 1 - 8 years). Frequent replacement imposes an additional financial burden.
- They are unattractive owing to the toxic remains/wastes such as lead, which can cause environmental problems during shipment, installation, and particularly in ultimate disposal.
- They tend to be dangerous with sulfuric acid and in the possibility of explosion;
- They may have maintenance and replacement difficulties in isolated and remote areas.
- They have poor performance at low and high ambient temperatures

Such factors are barriers as regards to more wide and future application. As a result, in recent years, effort has been put into finding alternatives.

#### 2.4.4 Pumped hydro storage

Numerous energy storage technologies are currently known about, but to date none, in terms of ratings, can be compared to pumped hydro storage (PHS), which has the characteristics of being simple, mature and well-developed [280-282].

Hydropower is not only a renewable and sustainable energy source, but its potential as a flexible energy storage solution also makes it desirable to improve power supply quality and to support the deployment of intermittent RE sources such as wind and solar power. As a result, a renewed interest in PHS is globally emerging, together with the growing utilization of RE sources. This following section presents an overview of PHS, enlarging on its technological advances and challenges for RE systems.

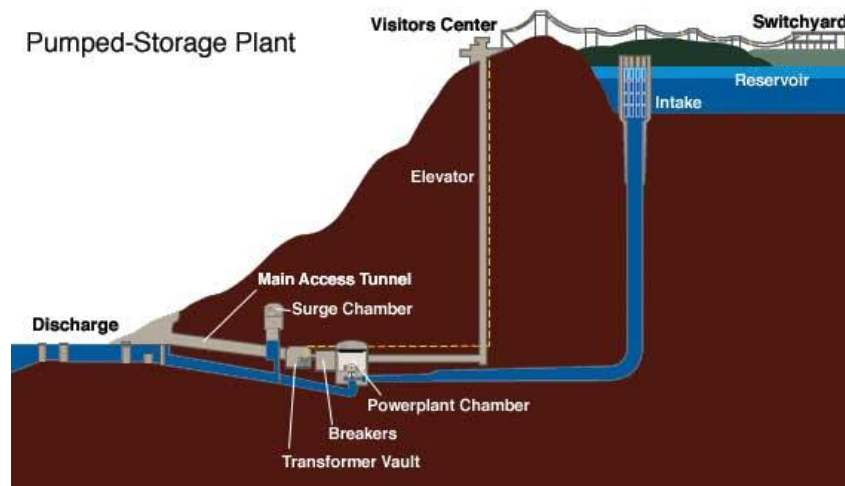


Fig. 2.7 Pumped hydroelectric storage plant

Pumped hydro energy storage, as a leading energy storage technology, has been utilized for the past hundred years and was first used in Italy and Switzerland in the 1890s [103]. It remains the most commonly used and most commercially viable electricity storage technology in the world, with an efficiency range of 75–85% and competitive costs (1500-4300 \$/kW, 250-430 \$/kWh) [255, 283, 284]. Reversible

pump-turbines and adjustable speed machines are now widely used to improve efficiency [180]. Due to low cost and maturity, more than 300 plants (over 127GW) have been installed worldwide [259], accounting for 99% of the total storage capacity, according to a report [285]. The basic principles of PHS are given in Chapter 1.4.

Now PHS is generally viewed as the most promising technology to increase RE penetration level and provide significant flexibility in switching operations in the power system, particularly in small autonomous island grids [286]. Currently PHS is increasingly deployed in the countries with the most RE, Western Europe, U.S. and Japan, due to its function in energy smoothing and RE integration [80, 287]. PHS is proven to be an ideal option and is being applied to confirm the variability of renewable power sources, such as wind and solar [288].

The basic concept of PHS-based RE systems is that RE surplus, during periods of low electrical demand or high RE output, can be stored by pumping water to the upper reservoir, otherwise the surplus is discarded. The stored energy is then allowed to flow back to the lower reservoir enabling discharge of electricity through a hydro generator. Another possible benefit is that the pumped storage system can be integrated with the conventional hydroelectric plants through natural steam-flow, making good use of a renewable solar, wind and hydro combination also allowing RE to remain renewable. Therefore PHS is the ideal partner for intermittent renewable integration, especially for the stand-alone application.

#### *2.4.4.1 The use of PHS for increasing RE penetration in medium and large power systems*

As indicated in the study [289], the intermittent RE supply cannot be stored on a large scale economically viable except for the use of pumped hydropower storage. The large

scale RE system is becoming increasingly popular, but stability of an electricity network and the utilization safety of terminal users can be greatly affected, once the RE share exceeds 15% [290] or 20% [291, 292]. According to [293], when medium time (some days) storage of energy with PHS is introduced, the acceptable penetration of RE in autonomous grids can reach high levels, such as from 25% to 70% on Corvo island [294].

For power system sizes beyond a few MW, PHS is proven to be the most technically mature and cost-effective storage solution, particularly suited for facilitating large scale RES integration in medium and large power systems, due to its high power and energy capacity [295, 296].

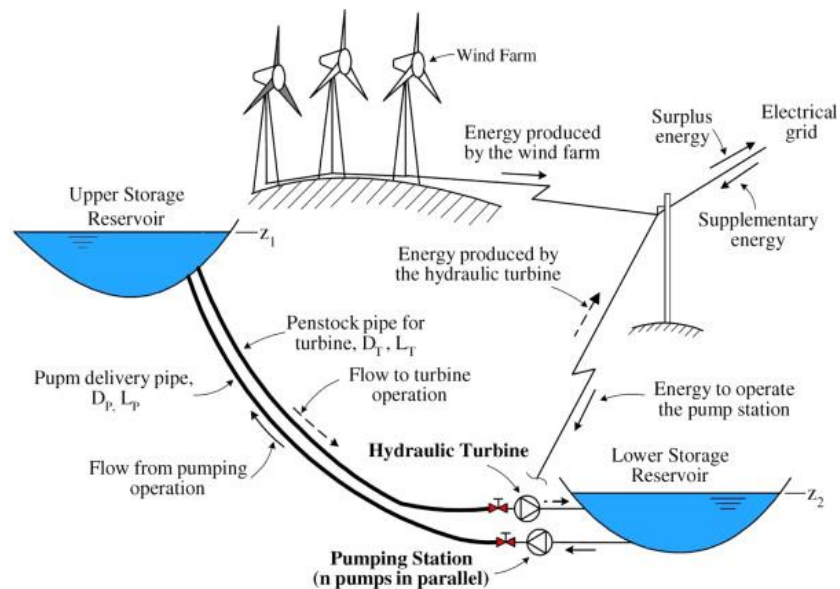


Fig. 2.8 Typical arrangement of Wind-PSP system [297]

In recent years, a considerable amount has been reported in the literature regarding the study of large-scale PHS facility integrated with the wind or solar power systems [298-308]. In particular, the combined use of wind and PHS in an island system has been the subject of substantial publications [267, 293, 295, 309-314]. These studies

demonstrate that PHS is the most suitable storage technology for allowing high wind penetration levels in medium and large autonomous power systems. A typical configuration of such hybridization is shown in Fig. 2.8. The majority of those studies are focused on several autonomous islands of different size such as Ikaria, Kasos, Crete and Rhodes in Greece [311, 313, 315-323]. In addition, other countries and regions have been studied, for example, Croatia [324], Portugal [325], Macedonia [326], and the El Hierro Island in Spain [327, 328].

These systems, in general, aim to i) explore locally available and environmentally friendly RE (especially wind) and increase their penetration; ii) minimize the imported fossil fuels consumption; iii) mitigate the power production and load demand imbalance and control sags in voltage and alleviate the effects of rapid swings on the distribution grid; iv) minimize the total cost of power production [310, 329].

The application of PHS to facilitate RE integration can constitute attractive investments, while, from a system perspective, according to the literature, the integration of a properly sized PHS may achieve significant economic benefits of the hybrid power system [329-335]. At regions where the variable tariff is applied, more significant economic benefits may be achieved by deciding on an optimal turbine and pumping schedule [336].

#### *2.4.4.2 PHS for small/micro RE-based RAPS systems*

PHS is also viewed as a promising technology for small autonomous RE systems in remote areas [292]. According to the study [337], the potential of the PHS in a decentralized electricity grid is even more important if power generation capacity of RE is below 300 kW.

The PHS was introduced in the studies [40, 338] to replace the environmentally harmful batteries for the standalone hybrid solar-wind system. It explores a novel solution for the challenging task of energy storage. PHS seems more economical than the battery for standalone applications [254], with payback periods as low as 2.5 to 5.5 years [339].

A considerable number of studies are specifically, conducted for autonomous small island systems using wind turbines for power generation and PHS for energy storage [340-349].

A patent named solar hydroelectric power plant system (Fig. 2.9) was published in 2009 by [350], aiming at supplying power for remote consumers (house, settlement, town, island). For this topic, Glasnovic and Margeta carried out a series of studies on the standalone hybrid solar PV and PHS system, for example [252, 280, 304, 351-358]. Other researchers have also examined such hybrid system [359-364].

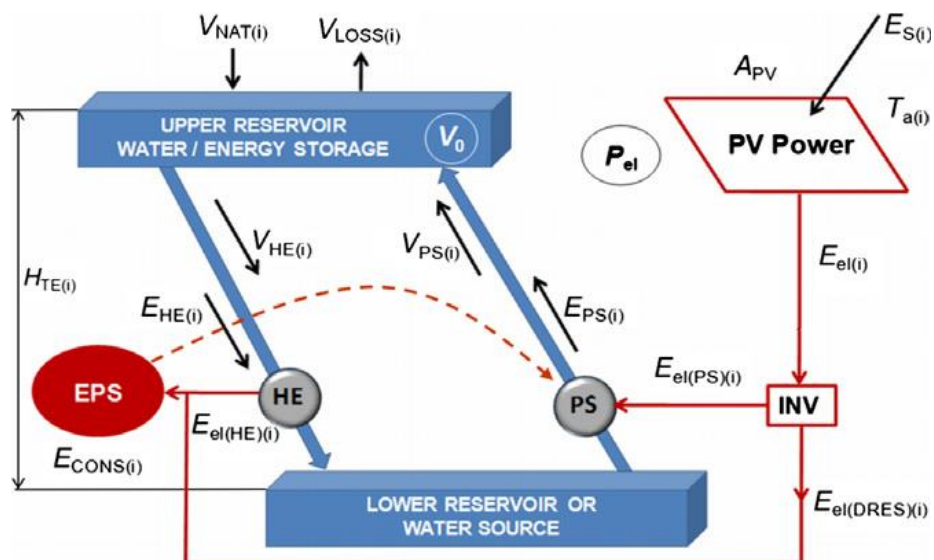


Fig. 2.9 Configuration of the proposed hybrid power plant PV-PHS [353]

In addition, the hybrid small solar and wind systems with PHS have been investigated by [40, 365-372]. A standalone desalination unit powered by such a hybrid system with a pumped storage unit was also investigated in detail by [373].

#### *2.4.4.3 Seawater pumped storage for RE system*

Seawater pumped storage has presented great potential for the PHS based RE systems on remote islands. Seawater pumped-storage power plants have several advantages such as lower civil construction cost and lower power distribution cost due to their proximity to nuclear or steam turbine power plants [374, 375]. A fundamental case study investigating seawater PHS for offshore wind parks was presented [376], and the seawater PHS for regulating the export of RE to the national grid was evaluated in [377]. These studies indicate that seawater PHS storage is technically and economically feasible allowing for high penetration of intermittent RE.

#### *2.4.4.4 System modeling, design, simulation and optimization*

Two significant variables for the design of pumped systems are the volume of the upper reservoir and the height difference between the upper and lower reservoir [259]. Other design parameters include the lower reservoir, the design of the penstock and the choice of pumps and turbines [353]. Different software has been employed for system simulation, such as H2RES [378], the combination of HOMER and Simulink [348].

The studies [366, 367] have established some simple models for the main components of a hybrid wind-solar-pumped-storage power system. PHS models specifically for micro RE systems have been developed by [379, 380], as have wind park and pumped storage station models presented by [381].

The algorithm designed to size the PHS units for increasing wind penetration in the Lesbos island has been presented in [342, 382]. In these studies [297, 314, 330, 383-386], the numerical methodology is presented for the optimum sizing of the components of a pumped-storage power plant for the recovery of wind-farms rejected energy. The optimal design of PV/wind/pumped-storage hybrid system was achieved using the GA based multi-objective optimization [370] and improved PSO method [369]. In addition, the optimal operating strategies/policies for the joint operation and schedule of PHS-based RE systems have been examined by [267, 282, 297, 311, 314, 331, 341, 373].

#### *2.4.4.5 Practical engineering projects*

Available practical applications in which PHS is used as energy storage for standalone RESs are extremely rare. The use of PV, WT and PHS for powering an island in Boston was planned in 1985 for public education and recreational use [387]. A PHS system was demonstrated in an 18kWp PV plant in Greece to partially replace batteries [360, 388, 389]. The efficiency of the water pump (6.6kW) and turbine (5.0kW) at their best operating point is 72% and 64%, respectively, leading to quite a low overall ESS efficiency, whereas significant social impacts, such as both electricity and water supply, were achieved. In Houay Se of Lao PDR, a pilot research project, composed of a micro hydropower station (80kW), a PV system (100kWp) and 8 water pumps (60kW), was developed by NEDO Japan [390]. This system has operated for several years, demonstrating its effectiveness and success in providing a sustainable power supply and improving living conditions for the local residents in an isolated countryside. In addition, wind-solar and pumped storage supply systems were built in Alishan to solve electricity problem for rural areas in the west region of China [379],

and a demonstration system with 5kW wind turbine and 720kWp solar panel was also established in Siziwangqi of Inner Mongolia, China [379]. A big water pump and a small water pump were designed for different working conditions. A demonstration of the hybrid electric/hydro energy system for standalone PV applications in remote areas has been implemented in the laboratory at Wayne State University [361]. This system functions as an educational tool to teach students the concepts of different types of energy storage and the integration of RE and ESS. An engineering example, the Eagle Mountain pumped storage project [391] with 1,300MW capacity, represents a sustainable RE dependable solution, providing reliable and clean electricity generation.

#### *2.4.4.6 Limitations*

PHS is currently the most cost effective means of storing electrical energy. The literature demonstrates that an immense potential exists for RE integration. However, some key challenges have to be overcome, to create opportunities for further technological improvements and the promotion of renewables:

- Environmental issues: must also be considered during the operation of PHS to prevent water spillage from the reservoirs.
- Site availability: the presence of the appropriate geography for two large reservoirs and pipe arrangements are a critical decision making factors.
- Water availability: an adequate water supply should be guaranteed. As regards a seawater pumped storage, some technical problems should be assessed such as the corrosive effects and possible leakage into the ground water.
- Technical viability: the majority of current PHS literature mainly focuses on the development of the technology itself, while the joint operation of RE and PHS realized in real applications has not been widely reported. Some

unknowns and technical issues remain to be solved and thus challenges are provided for much future research in this field. In addition, limited attention has been paid to system sizing optimization and techno-economic evaluation of PHS based RE power generation systems of a scale at a few hundred kW in standalone application for remote areas.

## **CHAPTER 3    SYSTEM MODELING AND EVALUATION METHODS**

System modeling of individual components is an important step before system design, simulation and optimization. In this chapter, the mathematical models for PV generator, wind power generation, battery energy storage, pumped hydro energy storage, and diesel generator are developed and described. The information of the key components used in this thesis is also presented. Finally the evaluation criteria for the hybrid systems are discussed.

### **3.1 Mathematical modeling of photovoltaic system**

With the robust growth of solar PV applications, accurate prediction of the power production of solar PV systems becomes an essential topic of research. The designers require a reliable tool to predict PV module energy production under real conditions and also to make a sound decision on selection of different PV modules. Engineers also need an accurate tool to simulate the power output from a PV plant under real operating conditions for evaluating the system's energy performance. However, PV module specifications from the manufacturer cannot determine the power production in real conditions, since the specifications are only obtained at standard test conditions (STC): incident sunlight of  $1000 \text{ W/m}^2$ , a cell temperature of  $25 \text{ }^\circ\text{C}$  and an air mass of 1.5. An accurate and reliable solar PV power prediction model for other general conditions, therefore, is urgently needed [65, 66].

The electrical behavior of a PV device is characterized by its current-voltage (I-V) curve. In this section, a novel theoretical model, offering a good compromise between accuracy and simplicity, is developed in Matlab for determining PV module parameters and then fitting the model to experimental I-V curves of a PV module/string/array. The developed model is then solved using a combined technique which integrated an algebraic simultaneous calculation of the parameters at standard test conditions (STC) with an analytical determination of the parameters under real operating conditions.

To demonstrate the feasibility of the simulation model, the parameters from the simulation and I-V characteristic curves were compared with those from the DeSoto model and other simulation software at different conditions. A series of field measurements were also carried out for a PV system to validate the simulation results. The final objective is to apply this model to predict the operational performance of PV modules and systems in the field, such as power production.

### **3.1.1 Physical configuration of PV cell, module, string, array and plant**

As illustrated in Fig. 3.1, the basic unit of a PV system is the PV cell. Dozens of PV cells are interconnected in series to form the cell series string. A group of one or more series strings is then encapsulated to produce a PV module. The modules are connected in series to increase the system voltage and form a module string. A PV array is then made up of a number of module strings connected in parallel, to increase the current of the array. The array links to a solar inverter which transforms the DC power produced by the PV array to the AC for load consumption and connection to a power grid. Generally, a PV plant is composed of a single or a number of PV arrays.

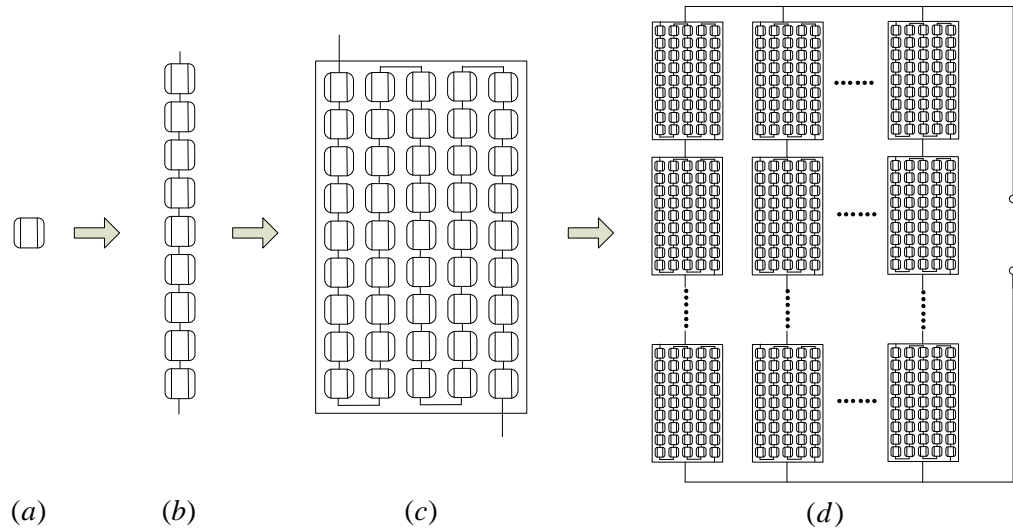


Fig. 3.1 Physical configuration of a photovoltaic cell (a), a cell series string (b), a module (c) and a PV array (d)

### 3.1.2 Simulation model and determination method developed in this study

#### 3.1.2.1 Simulation model development

A solar cell is traditionally represented by an equivalent circuit composed of a current source, a diode (D), a shunt/parallel resistance ( $R_p$ ) and a series resistance ( $R_s$ ). As shown in Fig. 3.2, available electrical power from the solar cell is modeled using this well-known five-parameter model.

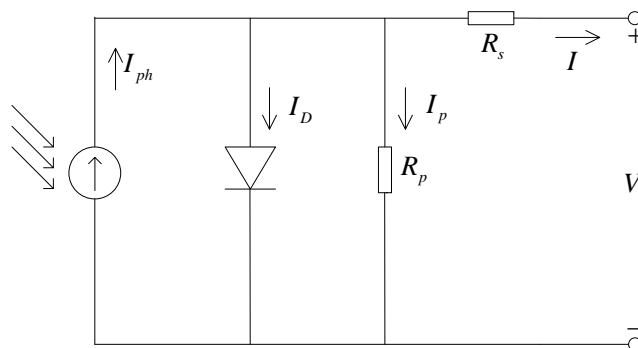


Fig. 3.2 Equivalent circuit for a solar cell (five-parameter model)

The PV generator is neither a constant voltage source nor a current source. It is modeled and described by the relationship between current and voltage. Based on the Shockley diode equation, the mathematical model (I-V characteristic) for an individual PV cell is as follows [97, 100, 106, 392]:

$$I = I_{ph} - I_D - I_p = I_{ph} - I_0 \left( e^{\frac{V+IR_s}{V_t}} - 1 \right) - \frac{V + IR_s}{R_p} \quad (3.1)$$

where  $I_{ph}$  is the photo current (A);  $I_0$  is the diode saturation current (A);  $R_s$  is the series resistance ( $\Omega$ );  $R_p$  is the shunt/parallel resistance ( $\Omega$ );  $V_t = \frac{nKT}{q}$  is the diode

thermal voltage;  $n$  is the diode ideality factor;  $q$  is the charge of the electron (1.602E-19 Coulomb);  $K$  is the Boltzmann's constant (1.381 E-23 J/K) and  $T$  is the temperature of the solar cell (K). Eq. (3.1) presents a solar cell as a nonlinear power source. Determination of an analytical solution of an implicit equation is a difficult and challenging work. Therefore, its numerical solution is employed in the present study.

This equivalent circuit is not only used for an individual solar cell, but also for a PV module with many cells, or for an array/string including dozens of modules. Therefore, the mathematical model for a PV module's power output could be deduced:

$$I = I_{ph} - I_0 \left( e^{\frac{1}{V_t} \left( \frac{V_M}{N_s} + I_M R_s \right)} - 1 \right) - \frac{1}{R_p} \left( \frac{V_M}{N_s} + I_M R_s \right) \quad (3.2)$$

where  $N_s$  represents the number of series connected cells in each module. Based on the PV module mathematical model, the output current  $I_A$  and output voltage  $V_A$  of a PV array with  $N_A$  cells in series and  $N_p$  strings in parallel can be found.

$$I = N_p I_{ph} - N_p I_0 \left( e^{\frac{1}{V_t} \left( \frac{V_A}{N_A} + \frac{I_A}{N_p} R_s \right)} - 1 \right) - \frac{N_p}{R_p} \left( \frac{V_A}{N_A} + \frac{I_A}{N_p} R_s \right) \quad (3.3)$$

This equation can be expanded to any number of solar cells in series ( $N_A$ ), and thus is not restricted to one module. Therefore, for the array with  $N_M$  modules connected in series and  $N_s$  cells in series for each module, the  $N_A$ , in the above equation, becomes  $N_M \times N_s$ .

From above analysis, the PV cell/module/array mathematical models are very similar. These models could be directly developed in Matlab/Simulink and other electromagnetic transient simulation programs, and enabling the I-V curve or P-V curve can be obtained.

Table 3.1 The key specifications of the Shell Solar SQ175-PC PV module

Characteristics	Value
Open - Circuit Voltage (Voc)	44.6V
Optimum Operating Voltage (Vmp)	35.4V
Short - Circuit Current (Isc)	5.43A
Optimum Operating Current (Imp)	4.95A
Maximum Power at STC (Pmax)	175Wp
number of cell connected in series	72
Temperature coefficient of Isc (alpha)	0.8mA/°C
Temperature coefficient of Voc (beta)	-145mV/°C
Temperature coefficient of Pmpp	-0.43%/°C

The PV module from Shell Solar is used as a sample in the present study. The key parameters for the three characteristic points: short circuit (0, Isc), maximum power point (MPP) (Vm, Im), and open circuit (Voc, 0) and other operating temperature

coefficients are summarized in Table 3.1. These parameters can be easily found in the specification datasheet from the manufacturer.

### 3.1.2.2 Parameters determination and calculation procedure

In Eq.(3.3), a total of five unknown parameters are determined:  $I_{ph}$ ,  $I_0$ ,  $V_t$ ,  $R_s$  and  $R_p$ . The objective of this research is to solve the five parameters through the product's datasheet provided by its manufacturer. To find the five parameters, at least five equations are needed. Equations which are generally based on the three characteristic points under STC are used for parameter determination.

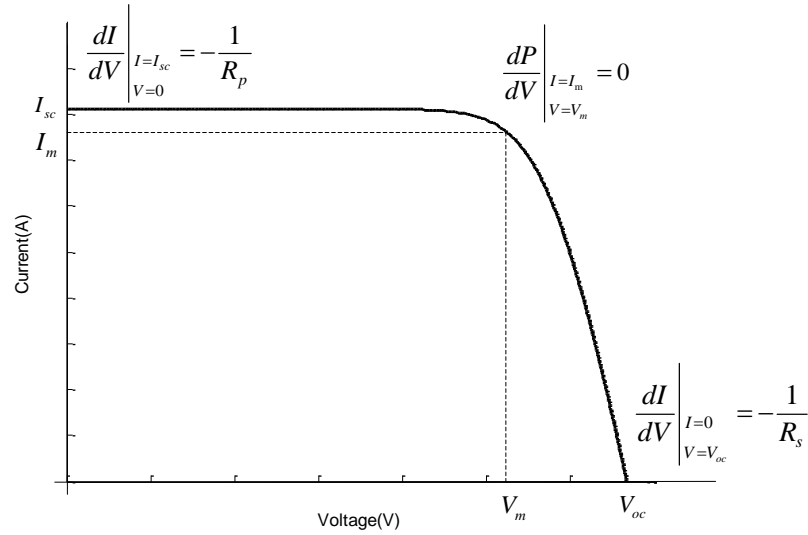


Fig. 3.3 The relationship between I-V curve,  $R_s$  and  $R_p$

(1) For an open circuit under the STC, i.e.  $I = 0$  and  $V = V_{oc}$ ,

$$0 = N_p I_{ph} - N_p I_0 \left( e^{\frac{V_{oc}}{N_s V_t}} - 1 \right) - \frac{N_p}{N_s} \frac{V_{oc}}{R_p} \quad (3.4)$$

(2) For a short-circuit under the STC, i.e.  $V = 0$  and  $I = I_{sc}$ ,

$$I_{sc} = N_p I_{ph} - N_p I_0 \left( e^{\frac{I_{sc} R_s}{N_p V_t}} - 1 \right) - \frac{I_{sc} R_s}{R_p} \quad (3.5)$$

(3) The maximum power point under STC, i.e.  $I = I_m$  and  $V = V_m$ ,

$$I_m = N_p I_{ph} - N_p I_0 \left( e^{\frac{V_m + I_m R_s}{N_p V_t}} - 1 \right) - N_p \frac{\frac{V_m}{N_s} + \frac{I_m}{N_p} R_s}{R_p} \quad (3.6)$$

(4) The derivative of the power with respect to voltage is equal to zero at the maximum power point shown in Fig. 3.3, that is,

$$\left. \frac{dP}{dV} \right|_{P=P_m} = \left. \frac{dP}{dV} \right|_{V=V_m, I=I_m} = \left. \frac{d(IV)}{dV} \right|_{V=V_m, I=I_m} = I + V \frac{dI}{dV} = 0 \quad (3.7)$$

i.e.

$$\frac{I_m}{V_m} = - \left. \frac{dI}{dV} \right|_{V=V_m, I=I_m} \quad (3.8)$$

Eq. (3.3) is a transcendent equation, which needs numerical methods to express the current and voltage. Therefore, it is rewritten as:

$$I = f(I, V) \quad (3.9)$$

By differentiating Eq. (3.9), the following equation can be obtained:

$$dI = df(I, V) = dI \frac{\partial f(I, V)}{\partial I} + dV \frac{\partial f(I, V)}{\partial V} \quad (3.10)$$

Therefore:

$$\frac{dI}{dV} = \frac{\frac{\partial f(I,V)}{\partial V}}{1 - \frac{\partial f(I,V)}{\partial I}} \quad (3.11)$$

Substituting Eq. (3.11) into Eq.(3.8), we can deduce the fourth determination equation:

$$\frac{I_m}{V_m} = - \frac{dI}{dV} \Big|_{\substack{V=V_m \\ I=I_m}} = - \frac{\frac{\partial f(I,V)}{\partial V}}{1 - \frac{\partial f(I,V)}{\partial I}} \Big|_{\substack{V=V_m \\ I=I_m}} = \frac{\frac{N_p}{N_s V_t} I_0 e^{\frac{V_m + I_m \frac{N_s R_s}{N_p}}{N_s V_t}} + \frac{1}{\frac{N_s}{N_p} R_p}}{1 + \frac{R_s}{V_t} I_0 e^{\frac{V_m + I_m \frac{N_s R_s}{N_p}}{N_s V_t}} + \frac{R_s}{R_p}} \quad (3.12)$$

(5) At this moment four equations are available. In the five-parameter model of a solar cell, the resistances  $R_p$  and  $R_s$  affect the slope of the I–V characteristic, before and after the curve “knee”, respectively. Therefore, the fifth equation could be established from the derivative of the current with voltage at the short circuit point as shown in Fig. 3.3. This can be mainly determined by the parallel resistance  $R_p$  [66, 97, 100, 117], expressed as below:

$$\frac{dI}{dV} \Big|_{\substack{I=I_{sc} \\ V=0}} = - \frac{1}{R_p} \quad (3.13)$$

Eq. (3.11) and Eq. (3.13) lead to:

$$\frac{dI}{dV} \Big|_{\substack{I=I_{sc} \\ V=0}} = \frac{\frac{\partial f(I,V)}{\partial V}}{1 - \frac{\partial f(I,V)}{\partial I}} \Big|_{\substack{V=0 \\ I=I_{sc}}} = \frac{- \frac{N_p}{N_s V_t} I_0 e^{\frac{I_{sc} \frac{N_s R_s}{N_p}}{N_s V_t}} - \frac{1}{\frac{N_s}{N_p} R_p}}{1 + \frac{R_s}{V_t} I_0 e^{\frac{I_{sc} \frac{N_s R_s}{N_p}}{N_s V_t}} + \frac{R_s}{R_p}} = - \frac{1}{R_p} \quad (3.14)$$

(6) Similarly, the reciprocal of the slopes of the I–V characteristic at the open circuit point is equal to the serial resistance at the STC [66, 97] (Fig. 3.3). This relationship can also be employed as the fifth equation:

$$\left. \frac{dI}{dV} \right|_{\substack{I=0 \\ V=V_{oc}}} = \frac{-\frac{N_p}{N_s V_t} I_0 e^{\frac{V_{oc}}{N_s V_t}} - \frac{1}{\frac{N_s}{N_p} R_p}}{1 + \frac{R_s}{V_t} I_0 e^{\frac{V_{oc}}{N_s V_t}} + \frac{R_s}{R_p}} = -\frac{1}{R_s} \quad (3.15)$$

(7) Tian et al.[102] proposed yet another solution to develop the fifth equation based on the temperature coefficient of the open circuit voltage provided by the manufacturer. The  $V_{oc}$  at other operating temperatures can be expressed as  $V_{oc} [1 + \beta_{V_{oc}} (T - T_0)]$ . Therefore,

$$0 = N_p I_{ph}(G, T) - N_p I_0(G, T) \left( e^{\frac{V_{oc} [1 + \beta_{V_{oc}} (T - T_0)]}{N_s V_t (G, T)}} - 1 \right) - \frac{N_p}{N_s} \frac{V_{oc} [1 + \beta_{V_{oc}} (T - T_0)]}{R_p(G, T)} \quad (3.16)$$

where  $\beta_{V_{oc}}$  is the temperature coefficient for  $V_{oc}$  and  $T_0$  is the solar cell temperature under STC. By using Eq.(3.16), the temperature coefficient for  $V_{oc}$  can be guaranteed.

The first four equations (Eq.(3.4), (3.5), (3.6) and (3.12)) are commonly used in the literature. To determine the most suitable fifth equation, the results from several methods with different equations (Eq.(3.14), (3.15), (3.16) and their combinations) are compared. It was found that the method combining Eq. (3.14) and Eq. (3.16) is the best, as the result can simultaneously fit the module's I-V characteristic at the short circuit point and voltage thermal performance. In addition, the above determination equations are transcendent and nonlinear, making it almost impossible to separate all

unknowns and solve them analytically. A numerical method is therefore employed. The simultaneous equations were constructed in Matlab using the nonlinear equation solver ‘fsolve’, embedded with ‘Levenberg-Marquardt (LM) algorithm [393]’ and ‘Gauss-Newton’ algorithm. This solver can solve the six simultaneous equations with five unknown parameters, with a rapid convergence. The values of the five parameters for a cell/module/array and its ideality factor are shown as in Table 3.2.

Table 3.2 Calculated parameters of PV cell/module

	I <sub>ph</sub>	I <sub>o</sub>	R <sub>s</sub>	R <sub>p</sub>	V <sub>t</sub>	n (deduced from V <sub>t</sub> )
Cell	5.449	1.20E-09	0.010	2.725	0.028	1.086
Module	5.449	1.20E-09	0.7	196.2	0.028	1.086

### 3.1.2.3 Parameter analysis under general condition

Once the parameters under STC are determined by the simultaneous equations, the I-V characteristics of the PV cell/module/string/array at the STC can be easily obtained. It is then necessary to generalize the model to other operating conditions with different solar irradiance and operating temperature. This section describes the temperature and irradiance dependence of the parameters.

The photo current  $I_{ph}$  can be described by:

$$I_{ph}(G, T) = I_{ph} [1 + \alpha_{I_{sc}} (T - T_0)] \frac{G}{G_0} \quad (3.17)$$

where  $G$  and  $G_0$  are the solar radiation intensities under real conditions/outdoor and STC, respectively;  $\alpha_{I_{sc}}$  is the relative temperature coefficient of the short-circuit

current (%/K), which represents the rate of change of the short-circuit current with respect to temperature (%).

It is well known that the diode saturation current is primarily proportional to temperature raised to the third power [393], and the relationship is expressed as [62, 90, 102, 394, 395] :

$$I_0(T) = I_0 T^3 \exp\left(\frac{-E_g}{nkT}\right) \quad (3.18)$$

where  $E_g$  is the band gap energy in eV, defined by Kim, Jeon [396] as:

$$E_g = 1.16 - 7.02 \times 10^{-4} \times \frac{T^2}{T - 1108} \quad (3.19)$$

The effect of the changing ideality factor does not have significant on the curve shape, and usually a higher ideality factor can slightly soften the knee of the curve. The present study considers the ideality factor as a constant value, following the method proposed in [102]. It means that the ideality factor would not change with respect to the operating condition. Therefore, the temperature dependence equation of the thermal voltage  $V_t$  is obtained from

$$V_t(T) = V_t \frac{T}{T_o} \quad (3.20)$$

The parallel/shunt resistance  $R_p$  represents the leakage current, which is lost mainly in the p–n interface of the diode and along the edges [90]. The study [96] and PVsyst software [397] reported that the sensibility of the model to the value of the shunt resistance is minor, in view of which a fixed  $R_p$  does not greatly affect the I-V characteristic. In this study,  $R_p$  is taken as inversely proportional to the solar irradiance,

which has been widely used in Ref. [62, 65, 66], while this assumption is opposite to that proposed in [102].

$$R_p(G) = \frac{R_p}{G/G_0} \quad (3.21)$$

Ref. [62, 90, 96, 137] concluded that it was convenient to assume that the  $R_s$  is independent of incident irradiation and temperature, which could simplify the calculation process and guarantee a sufficient degree of precision. Therefore, a constant was assumed for  $R_s$  in this study.

PV module performance depends greatly on the solar cell operating temperature, and the temperature is influenced by many factors, such as solar irradiance, wind speed, ambient temperature [151]. The relationship between the module back-surface temperature and cell temperature is simplified as [151, 398]:

$$T_c = T_m + \frac{G}{G_0} \Delta T \quad (3.22)$$

where  $T_c$  is the inside cell operating temperature in  $^{\circ}\text{C}$ ,  $T_m$  is the collected back-surface operating temperature of module in  $^{\circ}\text{C}$ , and  $\Delta T$  is a constant temperature difference between the cell and the module back surface ( $3^{\circ}\text{C}$ ).

The effects of temperature and solar irradiance under general operating conditions have been discussed above. With the PV cell temperature in Eq. (3.22) and parameters obtained at STC in Table 3.2, these parameters in Eq.(3.17), (3.18), (3.20) and (3.21) can be substituted into Eq.(3.1), (3.2)and (3.3) to obtain the I-V characteristic curves of the PV cell/module/array under any general operating conditions.

3.1.2.4 *Simulation results from the proposed model and comparison with PVsyst, INSEL and DeSoto model*

The performance of the proposed PV model under general operating conditions has been simulated, and compared with the results from the DeSoto model, PVsyst software and insel software. DeSoto model presented by DeSoto et al. is a 5-parameter PV model [62], which was developed by the Wisconsin Solar Energy Laboratory (SEL). This model is widely used to accurately predict the performance of cSi modules. PVsyst [397] is an analysis software for the PV system developed by the University of Geneva in Switzerland. It also employs the one-diode equivalent circuit model to calculate the performance of cSi modules. The basic parameters of the studied PV module can be found in the software database. The insel software [399] from Doppelintegral GmbH in Germany is a PV system analysis program, and the characteristics of the studied module can be output directly from the software using the two-diode model.

Table 3.3 Summary of parameter results

Methods	$I_{ph}$	$I_o$	$R_s$	$R_p$	$V_t$	$n$	$\alpha_{Isc}$ (mA)	$\beta_{Voc}$ (mV)	$\gamma_{Pmpp}$ (%)
Proposed model (present study)	5.449	1.20E-09	0.70	196.20	0.028	1.086	0.797	-145.3	-0.431
DeSoto model	5.457	4.67E-11	0.81	163.3	0.024	0.948	0.796	-145.2	-0.430
PVsyst software	5.43	2.00E-09	0.65	180	0.029	1.110	0.800	-144.7	-0.430
insel software	5.43	-	0.71	171.06	-	-	1.412	-144.95	-

The results from the four tools are summarized in Table 3.3. The insel software uses the two-diode model for the studied PV module (SQ175-PC), and thus it has two values for ‘ $I_o$ ’ and ‘ $n$ ’, but they could not be extracted directly from the software.

As can be seen from Fig. 3.3, the value of  $R_s$  mainly affects the slope of the I-V curve at  $V_{oc}$ . Table 3.3 indicates that the calculated  $R_s$  values from the simulation model in Matlab, Desoto model, PVsyst and insel software are similar. The small difference would not significantly influence the curves. The graphics for the I-V and P-V curves in the following section will vividly show the discrepancy. Table 3.3 also reveals that all the methods can have similar  $R_p$  values. With the exception of the temperature coefficient of the  $I_{sc}$  from the insel software, all the methods can meet the thermal performance ( $\alpha_{I_{sc}}, \beta_{V_{oc}}, \gamma_{P_{mpp}}$ ) well. These properties will determine the  $I_{sc}$  and  $V_{oc}$  values under different operating temperatures. However, the ideality factor from the DeSoto model is less than 1. With a reasonable range (usually from 1 to 2), the ideality factor value determines the knee of the I-V curve near the maximum power point.

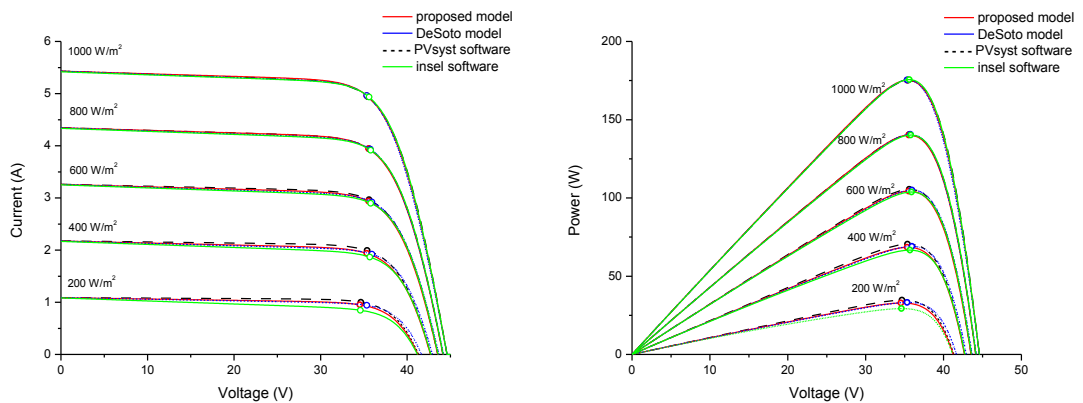


Fig. 3.4 I-V curves and P-V curves under different solar radiation levels (cell temperature=25 °C)

It is well acknowledged that two factors strongly affect the PV module performance: the cell temperature and the solar irradiance. Therefore, after obtaining the parameters in Table 3.3, the I-V characteristic curve under various irradiances and temperatures has been studied. Fig. 3.4 presents the I-V curves and P-V curves for solar radiation ranging from 200W/m<sup>2</sup> to 1000W/m<sup>2</sup> with the cell temperature at 25 °C. It can be seen

that the proposed model in the present study can agree well with Desoto model for the whole solar radiation range. However, discrepancy can be found from PVsyst model and INSEL model at the low solar radiation level, but it is not significant.

The I-V curves and P-V curves under different PV cell temperatures with irradiance  $1000\text{W}/\text{m}^2$  are illustrated in Fig. 3.5. This figure presents good agreement between the results from this proposed model and that from the DeSoto model and PVsyst software, especially at the three characteristic points. A relatively small deviation exists for the INSEL model due to the larger temperature coefficient of  $I_{sc}$ . The graphic results show that the simulation curves from the proposed model exactly match that from the DeSoto model and PVsyst software, particularly around the maximum power point. It demonstrates that the simulation model is reliable and feasible, and therefore it could be used to characterize the operating performance for general purpose in the future.

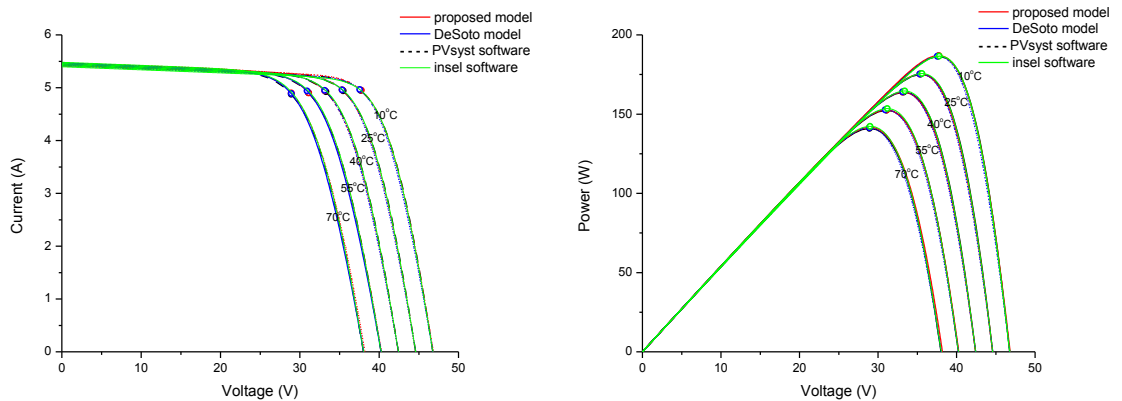


Fig. 3.5 I-V curves and P-V curves under different PV cell temperature levels (irradiance= $1000\text{W}/\text{m}^2$ )

### 3.1.3 Model validation through field measurements

#### 3.1.3.1 Experimental system

In this study, a series of outdoor measurements on a grid-connected PV system was carried out to validate the simulation results from the proposed model under different solar irradiance and temperature conditions.



Fig. 3.6 Field measurement instruments and test rig of the 22kWp PV system

A portable I-V checker MP170 from EKO was employed to measure the I-V curves of the PV module/string/array. To prevent the MP170 main unit from heat generating internally, the test interval is set at 1 minute. An overview of the test system is shown in Fig. 3.6. The output of the PV module/string/array was directly measured from the junction box attached on the back side of the module or from the subarray combiner box. To guarantee a high degree of accuracy, an external high-precision pyranometer from EKO (model: MS802; resolution:  $5 \mu\text{V}$ ), instead of the integrated small one, was used to measure solar radiation intensity. This method is also suggested by the



under real conditions. A similar conclusion can also be found in the literature [102, 400]. This phenomenon may result from many factors, collectively referred to as an as derating factor [401]. Dust is the most significant contributory factor because this PV system was sited in a heavy traffic area, and one which is also related to seasonal change. An additional consideration is the weathering of the PV modules because this system has been in operation for more than 8 years. Additionally other derating factors should be taken into account, such as the degradation of manufacturer's nameplate rating when exposed to sunlight in a real operation, the losses in DC wiring, voltage drop due to block diodes and shading by nearby structures. The I-V characteristics also vary slightly, from module-to-module.

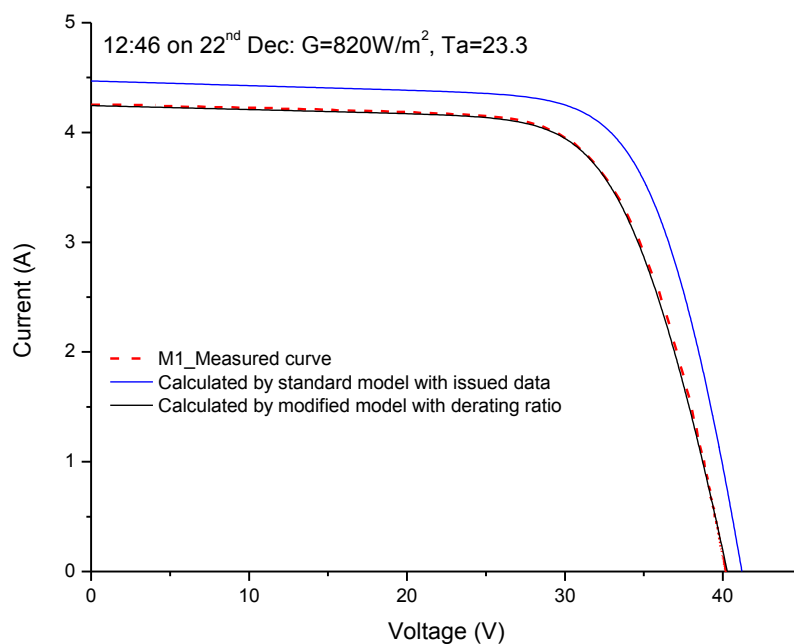


Fig. 3.8 The measured and calculated I-V curves of PV module M1

To find a specific derating factor for this PV system, a detailed analysis was performed based on the 59 reference I-V curves of the module M1 with irradiance ranging from 200 to 900 W/m<sup>2</sup> and temperature from 22 ° to 50 °C. Since the experimental measurements have been achieved at different temperatures and solar irradiances, it is

necessary to translate both curves to STC conditions [402]. By complying with the IEC 60891 Standard, each current-voltage pair on the measured I-V curve was converted to a corresponding pair under STC. Therefore, the updated module's electrical specifications were obtained from a subsequent translation. The distribution of the converted specifications is presented in Fig. 3.9. It can be seen that the average  $I_{sc}$  at STC is 5.16A, smaller than the manufacturer's nameplate data of 5.43A, and thus, derating ratio of 5% was taken into account for  $I_{sc}$ . The determination procedure for  $V_{oc}$ ,  $I_m$  and  $V_m$  derating factors is similar to that for  $I_{sc}$ . The derating factors and corrected values for the characteristic points are summarized in Table 3.4.

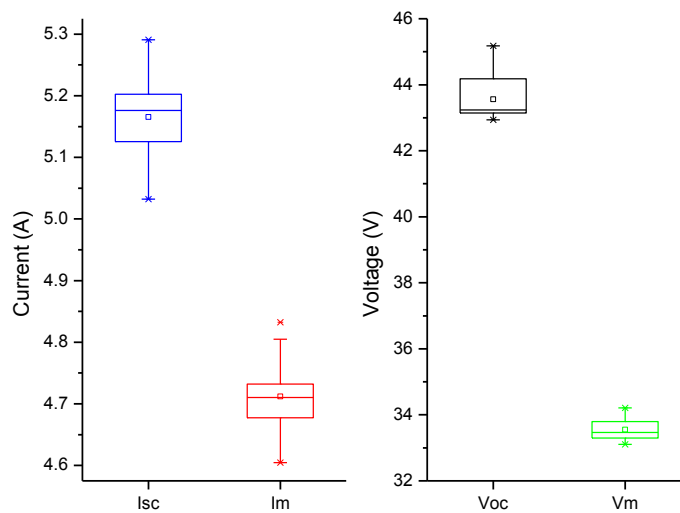


Fig. 3.9 Distribution of the converted  $I_{sc}$ ,  $I_m$ ,  $V_{oc}$  and  $V_m$  values to STC on 21<sup>st</sup>Dec 2012

Based on the corrected specifications in Table 3.4, the parameters for the new simulation model in this study were recalculated (Table 3.5) and taken as a representative for all the modules in the system. A sample with derating factor and modified specification is presented in Fig. 3.8, which reveals that the predicted curve

from the model, with modified values, is much more accurate than that with the manufacturer issued data.

Table 3.4 Comparisons between specifications under STC and corrected values with derating factor

	Manufacturer value at STC	Derating	Corrected value at STC
Isc	5.43	5%	5.16
Voc	44.6	2%	43.7
Im	4.95	5%	4.7
Vm	35.4	5%	33.6
Pmpp	175	10%	158

Table 3.5 Calculated parameter values with corrected values for PV cell/module model

	I <sub>ph</sub>	I <sub>o</sub>	R <sub>s</sub>	R <sub>p</sub>	V <sub>t</sub>	n (deduced from V <sub>t</sub> )
Cell	5.182	1.43E -09	0.0136	3.14	0.0276	1.075
Module	5.182	1.43E -09	0.98	226.3	0.0276	1.075

### 3.1.3.3 PV model validation

To validate the new simulation model, comparisons between the field measurements and the calculated results were carried out for three cases: (1) one single PV module; (2) PV string with 9 modules connected in series; (3) PV array configured with 9 modules in series and 2 strings in parallel. All these measured items are shown in Fig. 3.7.

### 3.1.3.3.1 Case I: one single module

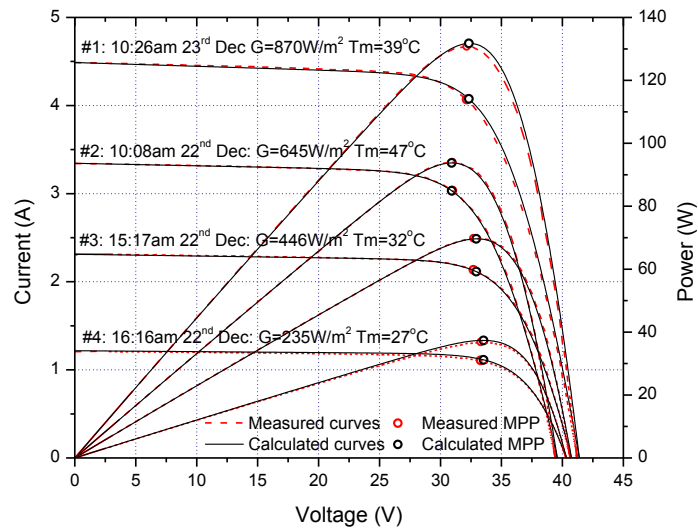


Fig. 3.10 Comparison between measured and calculated I-V curves, P-V curves and MPPs of PV module #M1

The PV module M1, taken as an example, was employed to validate the modeling results for a single PV module. Fig. 3.10 presents the I-V curves and P-V curves for four different operating conditions with solar radiation from  $235\text{W}/\text{m}^2$  to  $870\text{W}/\text{m}^2$ . It can be seen that the measured curve (red dashed line) and predicted curve from the modified model (black solid line) are consistent. Slight difference was observed only in #1 curve.

The environmental conditions, the three collected and simulated characteristic points, deviations, as well as the time and date of each experiment, are summarized in Table 3.6. Fig. 3.10 and Table 3.6 highlight that the characteristic points from the simulation model are very close to the collected data.

Table 3.6 The characteristic points (Isc, Voc and Pmmp) comparisons between PV module #M1's measured data and calculated data

Test No.	Time & date	Solar radiation (W/m <sup>2</sup> )	Module temp. (°C)	Amb. temp (°C)	Isc (A)			Voc (V)			Pmpp (W)		
					Meas.	Cal.	Devi.	Meas.	Cal.	Devi.	Meas.	Cal.	Devi.
#1	10:26, 23 Dec 2012	870	39	20	4.49	4.49	0.0%	41.22	41.39	0.4%	130.72	131.75	0.8%
#2	10:08, 22 Dec 2012	645	47	24	3.34	3.34	0.1%	39.42	39.58	0.4%	93.83	93.76	-0.1%
#3	15:17, 22 Dec 2012	446	32	23	2.31	2.31	-0.2%	40.66	40.75	0.2%	69.78	69.64	-0.2%
#4	16:16, 22 Dec 2012	235	27	20	1.21	1.22	0.9%	40.34	40.33	0.0%	36.85	37.36	1.4%

As stated above, the modified model is only based on the preliminary measurements of the model M1. To validate the model for other modules, the I-V curves of other modules M1, M2, M3 and M4 were measured and compared with the calculated curve at the solar radiation of 840W/m<sup>2</sup> (Fig. 3.11). It was found that the predicted curve and all the measured curves have a high degree of consistency at the short circuit point. Slight difference can be detected in the curve of M2, especially at the open circuit and maximum power points. This phenomenon may result from a different Voc derating factor and specific Voc temperature coefficient for M2, since these parameters can vary slightly from module to module.

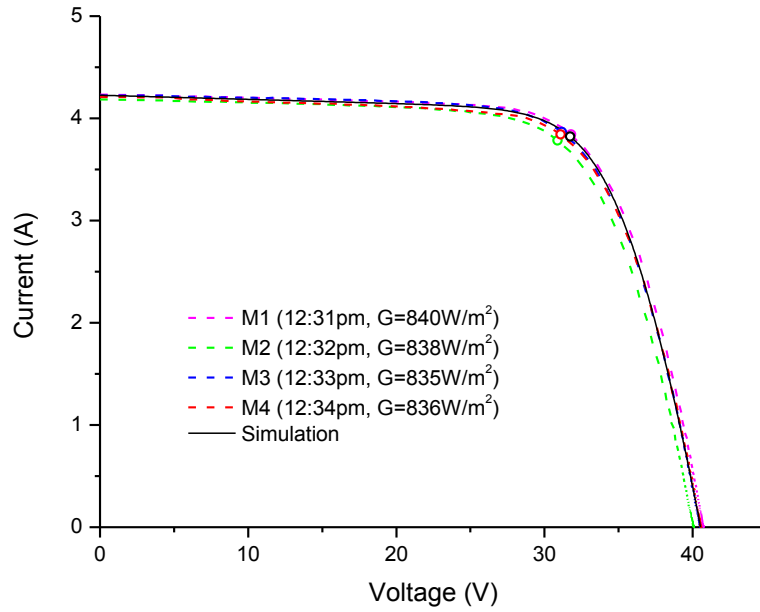


Fig. 3.11 I-V curves and MPP comparison of the four PV modules

### 3.1.3.3.2 Case II: PV string (S1)

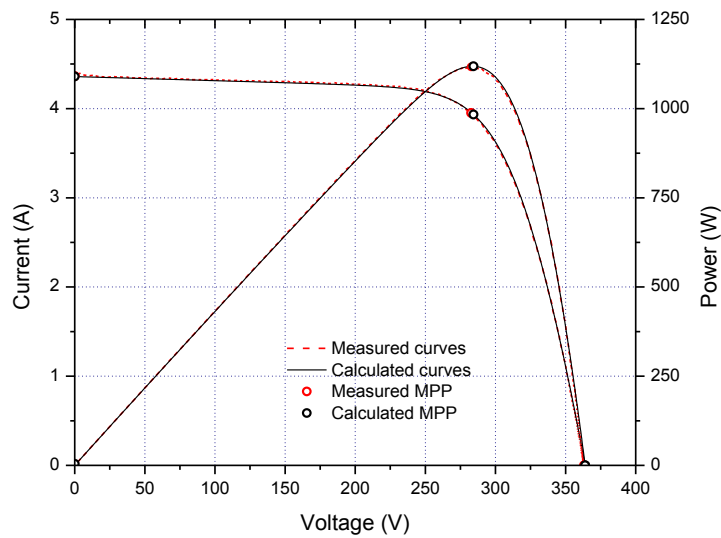


Fig. 3.12 Comparison between measured and calculated I-V curves, P-V curves and MPPs of PV string #S1

The above second case focuses on the PV string model validation. As revealed in Fig. 3.12, the proposed model, as expected, demonstrates a good agreement with the measured data both in current and power curves. The difference between the simulated

Pmpp (1118.6W) and collected Pmpp (1116.8W) is smaller than 0.5%. The practically null errors for the characteristic points demonstrate that the proposed model is indeed superior.

### 3.1.3.3.3 Case III: PV array (A1, A2, A3)

Finally, three PV subarrays A1, A2 and A3 were studied for array model validation. Once again, the A1 and A2 simulation results presented in Fig. 3.13 match well with the measured data. The difference existing in A3 possibly results from slight shading from PV string S1 at that time or other defects (such as hotspots) in A3. It is of note that the discrepancy between the maximum power point of three arrays and simulation data is particularly small.

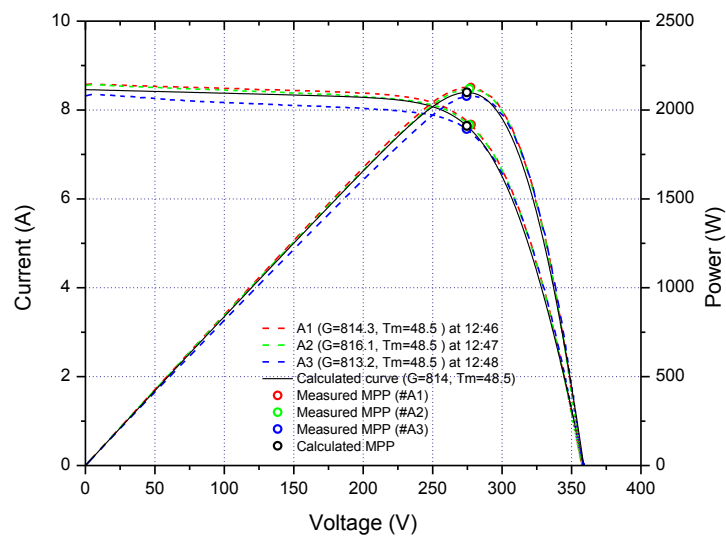


Fig. 3.13 Comparison between measured and calculated I-V curves, P-V curves and MPPs of PV array #A1, #A2, #A3

From the figures above (Fig. 3.10–Fig. 3.13), all the measured curves and the predicted curves from the module/string/array model with derating factor are fundamentally similar under different operating conditions. In addition, some defects or mismatch in

the existing systems can be detected by using the developed model. The perfect agreement between the calculated and measured results, both in the I-V curves and characteristic points, well demonstrates the reliability and accuracy of the model.

### 3.1.4 Solar PV system modeling and performance evaluation

The proposed model and determination method was further implemented in a case study on a standalone PV system (19.8kW) located on a remote island (22.3 °N, 114.2 °E) in Hong Kong [16, 254, 403]. There are two subarrays. PV array #1 consists of three parallel strings (#A, #B and #C) with 17 PV modules connected in series, and all modules are connected to one PV inverter. The subarray #2 is similarly configured as 16×3 and connected to the other inverter. This PV plant, therefore, in total, contains 99 polycrystalline modules. The key specification of the module (model: STP200-18/Ub-1) provided by the manufacturer is presented in Table 3.7.

Table 3.7 The key specifications of the Suntech STP200-18/Ub-1 PV panel

Characteristics	Value
Open - Circuit Voltage (Voc)	33.4V
Voltage at maximum power point (Vmp)	26.2V
Short - Circuit Current (Isc)	8.12A
Current at maximum power point (Imp)	7.63A
Maximum Power at STC (Pmax)	200Wp
Number of cells connected in series	54
Temperature coefficient of Voc	-(0.34±0.01)%/°C
Temperature coefficient of Isc	-(0.055±0.01)%/°C

In this PV system, the long-term environmental data and the operating performance data such as instantaneous power output have been continuously recorded by a data collection system at intervals of five minutes since the commissioning of the system.

### 3.1.4.1 Simulation results and validation with field collected data

The simulation results from the Matlab model were compared with those from the DeSoto model, PVsyst software and insel software under a wide range of cell temperatures and solar radiation levels. Fig. 3.14 presents the I-V and P-V curves for solar radiation ranging from  $200\text{W/m}^2$  to  $1000\text{W/m}^2$  when the cell temperature is  $25\text{ }^\circ\text{C}$ . Only a slight difference between the DeSoto model results and those of the other models can be found in the knee of the curves. This may be the result of the ideality factor being less than one. Other curves have good agreement. Fig. 3.15 illustrates the studied module's I-V curves and P-V curves under different cell temperatures (irradiance= $1000\text{W/m}^2$ ). Similarly, the curves from this proposed simulation model agree well with those from the PVsyst software and the insel software, and only a small difference was observed between it and the DeSoto mode results.

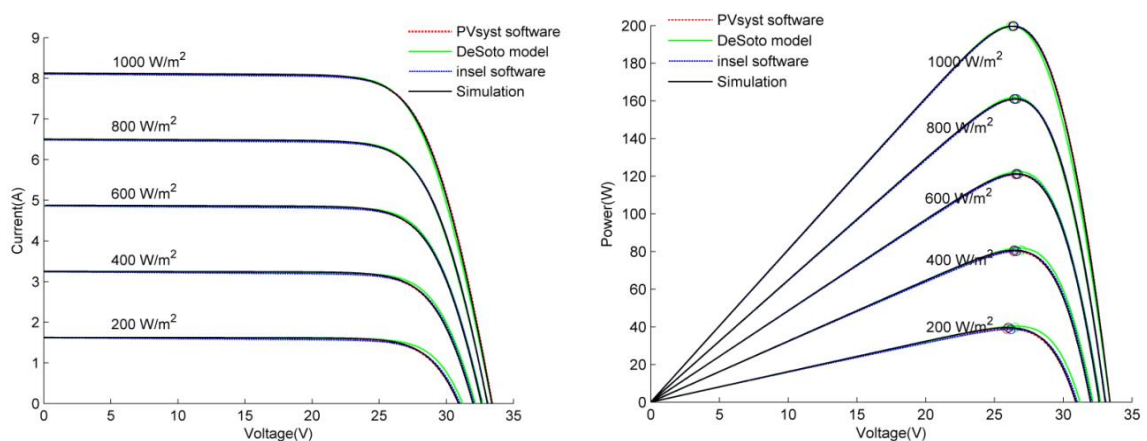


Fig. 3.14 PV module's I-V curves and P-V curves under different solar radiation intensity ( $T_c=25\text{ }^\circ\text{C}$ )

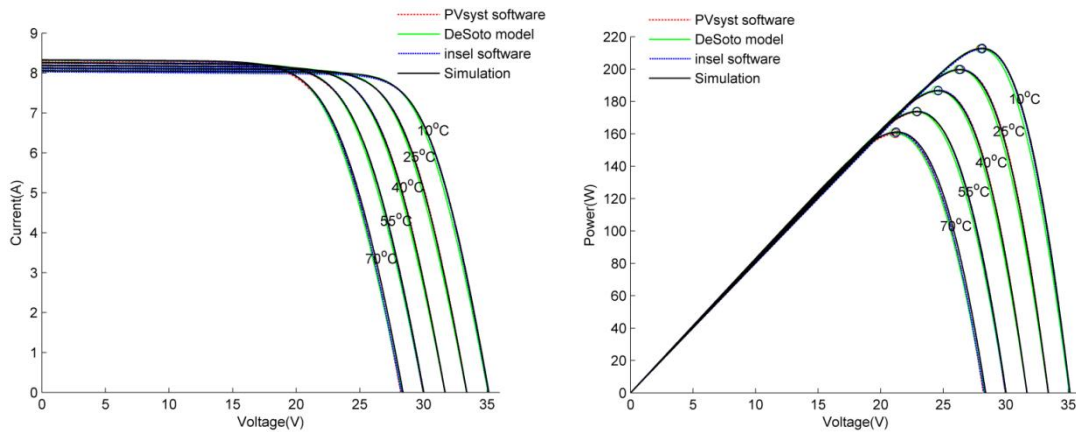


Fig. 3.15 PV module's I-V curves and P-V curves under different PV cell temperature (irradiance=1000W/m<sup>2</sup>)

The graphic results illustrate that the simulation model results of this study agree well with those from other software models, thus validating the simulation model enabling it to be used further for PV performance prediction in Section 3.1.4.4.

The accuracy of this model and determination method was further verified by comparing calculated I-V curves from the simulation model with field collected I-V curves for the six PV strings, measured on 29<sup>th</sup> December 2010. The data was collected by the portable I-V checker MP170 from EKO, which can measure specifically the onsite I-V curves of a PV module/string/array.

Using the PV string A (PV array #1) results as an example, Fig. 3.16 shows that the simulated curves coincide well with the experimental results. The relative errors of the P<sub>mpp</sub> are smaller than ±1%. Fig. 3.17 illustrates the simulation and onsite measurement results for the PV string F (PV array #2). The field collected curve shows that this PV string did not function well because an obvious inflection point can be seen around the maximum power point (MPP). Similar features were observed in other measurements relating to the PV string F. The inflection points on the PV string F measured curves indicate that the string may have defects or else is shaded.

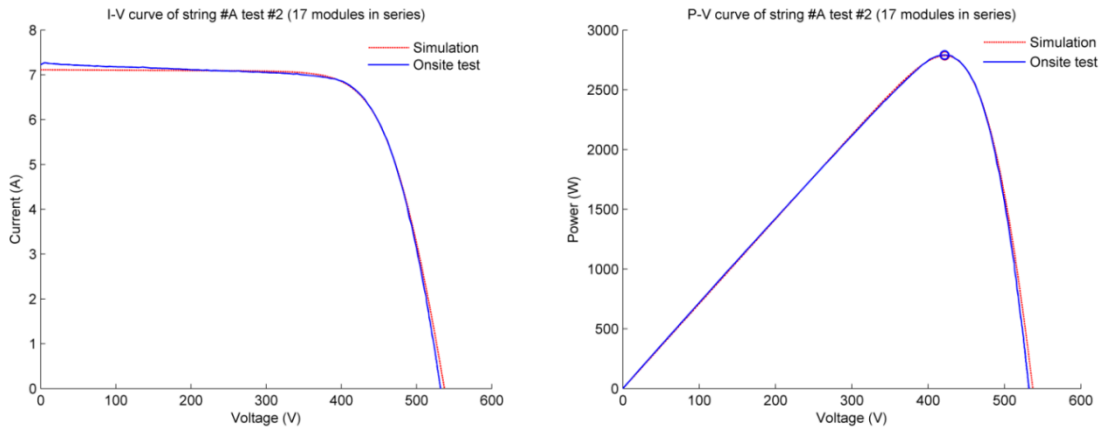


Fig. 3.16 Measurement and simulation results of PV module string A

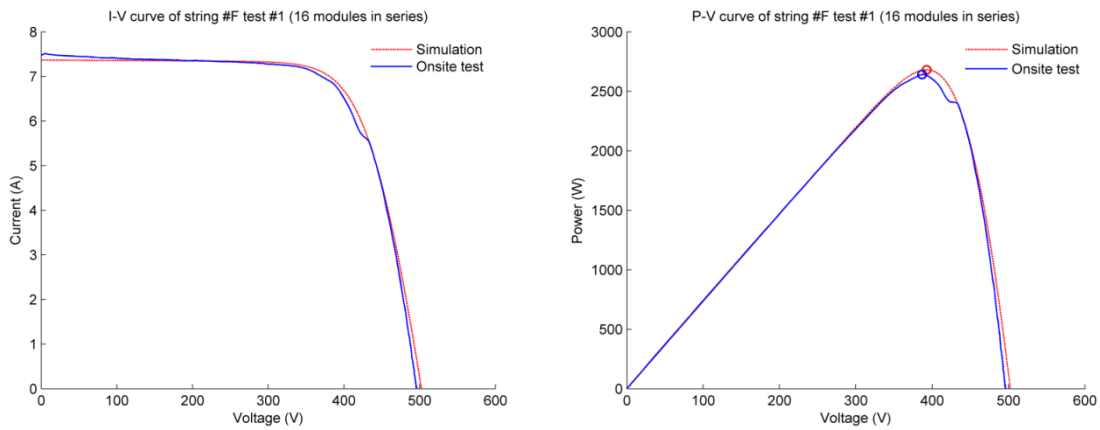


Fig. 3.17 Measurement and simulation results of PV module string F

### 3.1.4.2 PV array power output prediction

The I-V and P-V curves for any general set of weather conditions can be predicted accurately, and the maximum power output estimated using the developed model. Real-time power generated by the two PV arrays was recorded by the existing PV system. To compare the predicted power with the measured power of the PV arrays, three typical cases, i.e. sunny days, semi-cloudy days and cloudy days, were investigated. The cases had different amounts of average daily solar irradiation from 6:00 to 18:00. For each case, the simulation model was verified by selecting one

sample day with at least 120 datasets. Detailed information for the three examples is given in Table 3.8.

Table 3.8 The weather conditions of the three cases

Data type	Date	Irradiance (W/m <sup>2</sup> )		Ambient temperature (°C)		Module temperature (°C)	
		Max.	Ave.	Max.	Ave.	Max.	Ave.
		Case 1: sunny day	12 <sup>th</sup> Oct 2010	963	599	31.9	29.6
Case 2: semi-cloudy day	12 <sup>th</sup> Feb 2012	930	224	21.2	14.3	37.4	27.0
Case 3: cloudy day	16 <sup>th</sup> May 2011	509	148	27.7	24.6	40.6	33.7

#### 3.1.4.2.1 Sunny day

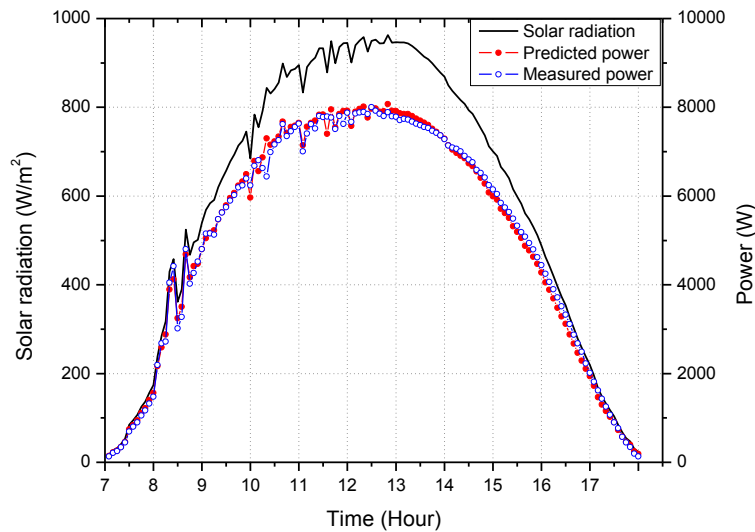


Fig. 3.18 Predicted and measured power-output profile of PV array #1 on 12<sup>th</sup> Oct 2010 (sunny day)

In the case of the sunny day, 12<sup>th</sup> October, 2010, the daily average solar irradiation was about 599 W/m<sup>2</sup>, peaking at 963 W/m<sup>2</sup> at 12:00 (Table 3.8). The predicted and measured power outputs of the PV array #1 on that day are illustrated in Fig. 3.18. The

predicted power-output curve followed the measured values trend reasonably well. Relationships with solar radiation are also presented. In the morning, the simulated and measured power output increases gradually coinciding with the irradiance intensity. However, an obvious gap between the irradiance and power profiles can be seen around the solar noon. Such a difference is mainly caused by the high PV cell temperature. In the afternoon, the cell temperature decreases with solar radiation, and thereafter the effect of temperature on power reduction is not so obvious, thus the predicted power and measured power outputs are both close to the irradiance profile.

#### 3.1.4.2.2 Semi-cloudy day

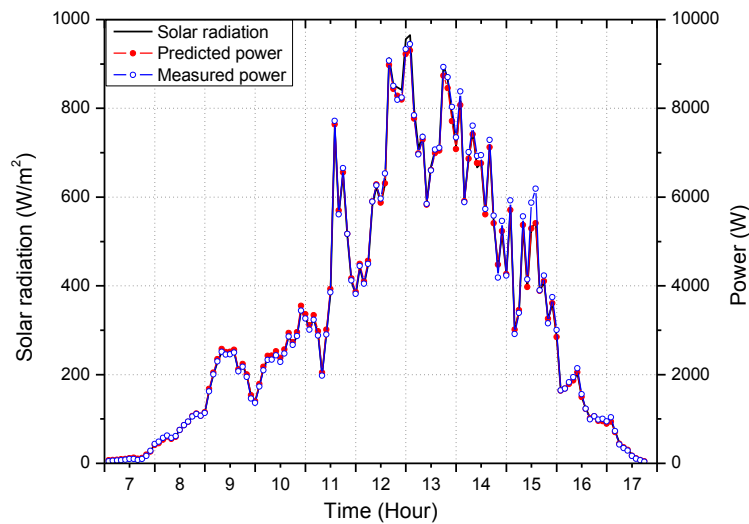


Fig. 3.19 Predicted and measured power-output profiles of PV array #1 on 12<sup>th</sup> Feb 2012 (semi-cloudy day)

The second case concerned a semi-cloudy day. On that sample day, the solar radiation fluctuated greatly from 0 to 930 W/m<sup>2</sup>, averaging at 224 W/m<sup>2</sup> (Fig. 3.19). Similarly, the modeled power-output curve is seen to match well with the measured data. Some differences are found at some peak points, which may be caused by the solar radiation sensor measurement error because of the rapid variation. The effect of the cell

temperature on PV array performance is not significant since the average module temperature was only 27 °C, very close to the standard test condition.

#### 3.1.4.2.3 Cloudy day

The measured data on 16<sup>th</sup> May, 2011, was selected to validate the simulation result for an extremely cloudy day (Fig. 3.20). It is also found that the predicted and measured data show consistent agreement throughout the day, demonstrating high accuracy for this simulation model, even under low irradiance levels. On that day, the simulation model slightly overestimated the actual current values, which may represent PV panel deterioration because of aging, soiling and other factors.

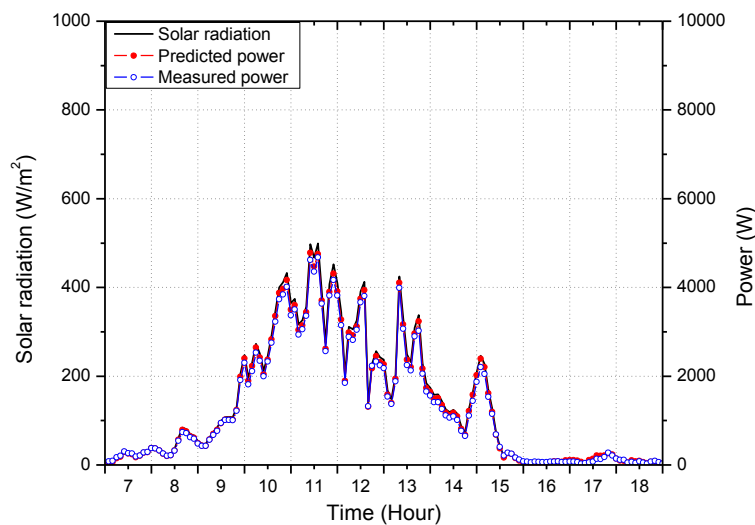


Fig. 3.20 Predicted and measured power-output profiles of PV array #1 on 16<sup>th</sup> May 2011 (cloudy day)

#### 3.1.4.2.4 Performance indicators of the simulation model

To quantify the performance/accuracy of the proposed model, the coefficient of determination  $R^2$  was employed in this study to measure how well a simulation model follows variations in onsite collected data. This indicator has been used in publications

[90, 151, 404] as a statistical tool to evaluate the simulation performance of power or current predictions. The coefficient of determination is expressed as:

$$R^2 = 1 - \frac{\sum_{i=1}^n (y_i - f_i)^2}{\sum_{i=1}^n (y_i - \bar{y})^2} \quad (3.23)$$

where  $y_i$  is the field measured/observed data,  $f_i$  is the associated modeled/predicted data, and  $\bar{y}$  is the arithmetic mean of the field data, i.e.  $\bar{y} = \frac{1}{n} \sum_{i=1}^n y_i$ .

As presented in Table 3.9, the  $R^2$  values of the arrays #1 and #2 for three weather conditions are quite high, ranging from 0.992 to 0.998. These calculated  $R^2$  values are much higher than those seen in the literature [404]. A strong correlation, therefore, exists between the predicted and measured data, demonstrating the superior performance of the simulation model for general weather conditions.

Table 3.9 performance statistic of the proposed model

Data type	$R^2$		RMSD (%)		MBE (%)	
	Array #1	Array #2	Array #1	Array #2	Array #1	Array #2
Case 1: sunny day	0.992	0.997	0.07	0.04	-0.02	-0.002
Case 2: semi-cloudy day	0.998	0.998	0.10	0.10	0.03	0.04
Case 3: cloudy day	0.997	0.993	0.26	0.29	0.03	0.06

The simulation performance was also evaluated by calculating the root mean square error (RMSE) which measures nonsystematic error, and the mean bias error (MBE) which measures systematic error. These two indicators are widely employed in the

literature [125, 151, 405]. They are nondimensional (error/power) and expressed as a percentage (%) value. The parameters are defined as:

$$RMSE = \sqrt{\frac{1}{n} \sum_{i=1}^n \left( \frac{f_i - y_i}{y_i} \right)^2} \quad (3.24)$$

$$MBE = \frac{1}{n} \sum_{i=1}^n \frac{f_i - y_i}{y_i} \quad (3.25)$$

where the field measured data  $y_i$  is considered to be the ‘real value’, and the model predicted data  $f_i$  to be the ‘calculated values’.

Table 3.9 shows that both the RMSE and the MBE values for PV arrays #1 and #2 are very low, indicating very good agreement between predicted and measured power outputs. These performance indicators demonstrate that the proposed model is not only suitable for I-V characteristics modeling but also for any general purpose power prediction.

#### 3.1.4.3 Energy production prediction

Table 3.10 Measured and predicted energy production on the three example days

Data type	PV array #1			PV array #2		
	Measured energy (kWh/day)	Predicted energy (kWh/day)	Error (%)	Measured energy (kWh/day)	Predicted energy (kWh/day)	Error (%)
Case 1: Sunny day	61.22	59.91	-2.14	56.45	56.38	-0.11
Case 2: semi-cloudy day	36.46	36.19	-0.76	33.58	34.06	1.43
Case 3: cloudy day	15.36	15.87	3.32	14.26	14.94	4.76

The measured and predicted energy production from PV arrays #1 and #2 is illustrated in Table 3.10. The differences between them are within 5% for three weather conditions, indicating the proposed model can estimate PV system energy production accurately.

#### 3.1.4.4 Performance evaluation of the PV system using this model

The operating performance of a PV system was simple to evaluate, with the aid of the validated simulation model. The potential power output was predicted using the model and compared with that from the measured data, and some possible reasons for the obvious differences were then examined.

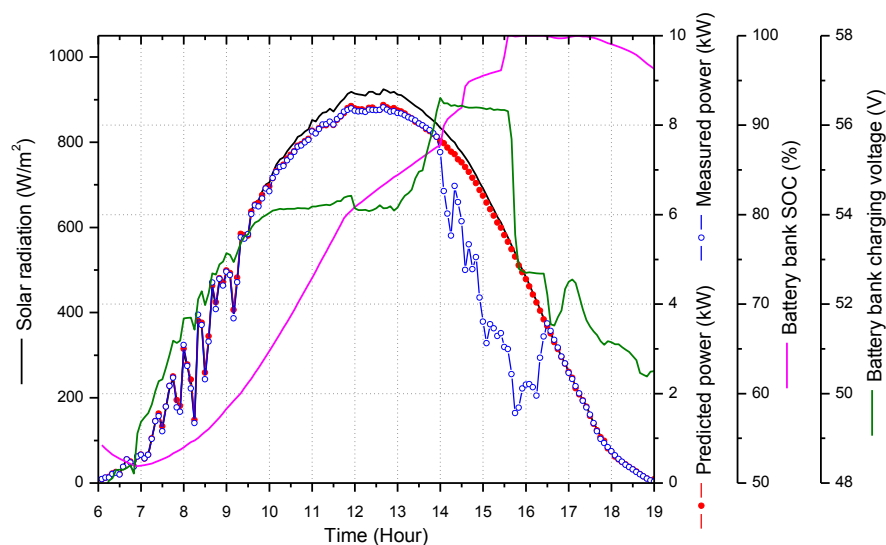


Fig. 3.21 Predicted and measured power-output of PV array #1 on 30<sup>th</sup> May 2011 with SOC and charging voltage profile

For this standalone PV plant located on a remote island, the excess power from the PV arrays after servicing the load should be delivered to the batteries. However, the battery charging rate is usually limited by two major factors, the state-of-charge (SOC) and the floating charging voltage (or the terminal voltage) [406]. When either the

charging voltage or the SOC are greater than their upper limits, the battery bank and the control centre take self-protection actions, and the PV arrays will be partially or totally shut off or disconnected from the load and the battery bank, to protect the PV arrays, battery bank and the electrical appliances on the load side.

The measured and predicted power-output profiles of the PV array #1 on 30<sup>th</sup> May 2011, used as an example to explore the reasons for PV array power reduction, are presented in Fig. 3.21. At the beginning of that day, the measured and calculated power outputs have a close relationship with the solar radiation fluctuation, while the measured power dropped suddenly at almost 14:00 in the afternoon. Thereafter an obvious difference between the measured and calculated power outputs can be observed until about 16:30. The irradiance profile and predicted power curve, however, indicate that the PV array has the potential to generate more power. This figure reveals that the PV arrays were partially shut off and disconnected from the load and battery bank. The possible reasons for this can be gauged by using the curves of the battery bank SOC and the charging voltage. The reduction in PV array power generation between 14:00 and 15:30 was possibly due to the high battery bank charging voltage being greater than the upper limit of 56.4V (2.35V for each battery cell). The continuous decrease in PV power from 15:30 to 16:30 results from the fully charged battery bank, with the SOC reaching 100%.

This is just one example to show how power reduction of the PV generator can be due to a fully charged battery storage system. In fact, many days, mostly during the afternoons of sunny days, have the potential to generate much more power, but the PV array output is partially or even totally cut off from the inverter. Theoretically, sufficient storage capacity can help to achieve higher PV power output ratios in the standalone system [403]. In addition, the training of local residents in the better

utilization of the energy supplied by the PV array and battery bank, based on the weather and the energy stored in the battery bank (i.e. SOC), could contribute to improving the mismatch between power production and consumption.

## 3.2 Mathematical modeling of wind energy system

### 3.2.1 Power output characteristics of a wind turbine

Due to differences in the power curve characteristics, different types of wind turbines (WTs) may output different power, even though they have the same rated power and are installed on the same site. Therefore, the model used to describe the performance of WTs should be different. After a comprehensive Literature Review, it was found that the following equation was commonly used to describe the power output of a WT, if its power curve was not available (Eq.(3.26)):

$$P_w(v) = \begin{cases} P_R \frac{v^k - v_c^k}{v_R^k - v_c^k} & (v_c \leq v \leq v_R) \\ P_R & (v_R \leq v \leq v_F) \\ 0 & (v < v_c \text{ and } v > v_R) \end{cases} \quad (3.26)$$

where  $P_R$  is the rated electrical power;  $v_c$  is the cut-in wind speed (the wind speed at which the turbine starts to generate usable power);  $v_R$  is the rated wind speed;  $v_F$  is the cut-off wind speed (the speed at which the turbine hits the limit of its alternator and can no longer generate more power if further increases in wind speed);  $k$  is the Weibull shape parameter.

However, for the wind turbine Proven 11(also known as KW6) used in this study, the power output is calculated based on its specific power output curve, or so called

performance characteristic curve, provided by the WT manufactory (Fig. 3.22). Based on the power curve, the power output from the wind turbine can be modeled as:

$$P(v) = 5.5 \times e^{\left(\frac{v-13.8}{4.6}\right)^2} + 2.2 \times e^{\left(\frac{v-9.15}{3.5}\right)^2} \quad (3.27)$$

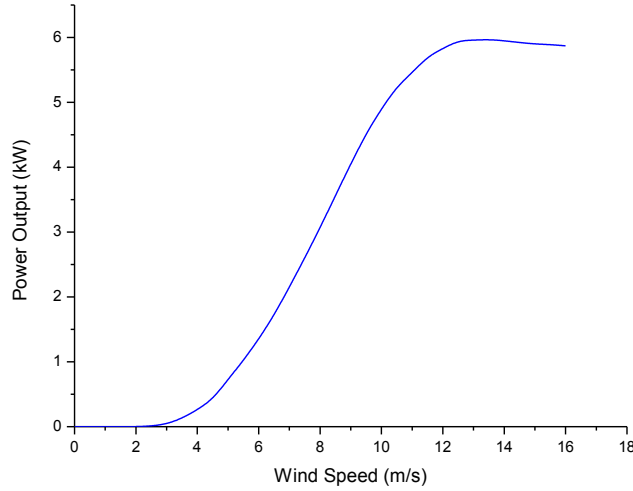


Fig. 3.22 Wind turbine power output characteristic curve of Proven 11

The details for the selected wind turbine are presented in Table 3.11.

In addition to the above, several loss factors were also considered when calculating the specified turbine output. The losses mainly include the downtime losses (6%), array losses (2%), soiling losses factor (4%) and other losses (4%). Therefore, the overall loss factor can be calculated by the combination of these loss factors using the following equation:

$$f_{WT} = 1 - (1 - f_{downtime})(1 - f_{array})(1 - f_{soiling})(1 - f_{other}) \quad (3.28)$$

### 3.2.2 The probability for WT operation

For wind turbine of Proven 11, the cut-in wind speed is 3.5 m/s and it has no cut-off speed (cut-off speed is infinite), so the probability  $p_{WT}(v \geq 3.5)$  can be calculated by Eq.(3.29):

$$p_{WT}(v \geq 3.5) = 1 - F(3.5) = \exp\left(-\left(\frac{3.5}{c}\right)^k\right) \quad (3.29)$$

Table 3.11 Details of wind turbine

<b>Wind Turbine</b>	
Manufactory	Proven / Kingspan Renewables Ltd.
Model	Proven 11 (KW6)
Rated power	5.2 kW (1 min average at 11m/s)
Peak power	6.1 kW
Reference Annual Energy	8,949 kWh (5m/s, 10m hub)
Output voltage available	<u>48V DC</u> /300V DC
Cut in speed	3.5 m/s
Cut out speed	N/A (Continuous operation)
Survival wind speed	Designed to Class 1 (70m/s)
Hub/Tower heights	9m / 11.6m / <u>15m</u> / 20m
Capital cost per unit	\$ 20,000
Replacement cost per unit	\$ 20,000
O&M cost per unit	\$ 500/year
Lifetime	20 years

### 3.3 Mathematical modeling of battery energy storage

The conventional battery energy storage technology, particularly the deep cycle lead-acid battery is widely used in off-grid RE systems. The battery from Hoppecke is employed in this thesis for the study of battery based RE systems (Chapter 5). The details are shown in Table 3.12.

Table 3.12 Details of the selected battery

Manufactory	Hoppecke
Nominal capacity	3000 Ah
Nominal voltage	2 V
Roundtrip efficiency	86%
Maximum depth of discharge	70%
Lifetime throughput	10,196 kWh
Capital cost per unit	\$ 1,644
O&M cost per unit	\$ 10/year

The sizing approach to initially determine the required number of batteries is shown below:

$$C_{Ah} = \frac{E_c}{\eta_B \cdot DOD \cdot V_B} = \frac{n_{day} \cdot E_{load}}{\eta_B \cdot DOD \cdot V_B} \quad (3.30)$$

$$n_{battery} = \frac{C_{Ah}}{C_{single}} \quad (3.31)$$

$$n_{string} = \frac{n_{battery}}{48 / V_B} \quad (3.32)$$

where  $n_{day}$  is the number of autonomous days powered solely by the battery storage bank;  $E_{load}$  is the daily energy consumption;  $E_c = n_{day} \cdot E_{load}$  is the summary of energy demand for the continuous number of autonomous days;  $\eta_B$  is the overall battery and inverter efficiency;  $V_B$  is the battery rated voltage; DOD is the allowable depth of

discharge;  $C_{single}$  is the storage capacity of a single battery;  $n_{battery}$  is the total number of batteries; and  $n_{string}$  is the string number.

The kinetic battery model [407, 408] was used to find the maximum allowable charging and discharging rates. This model treats the battery as a “two tank” system. One tank, part of the battery’s energy storage capacity, provides immediately available energy while the second is chemically bound which can only be charged or discharged at a limited rate. In addition, an optional control parameter called the set-point state of charge (SOC) was applied in this study. When a set-point SOC is applied, the RE will continue charging the battery bank until it reaches the specified SOC. Otherwise, the battery bank will start discharging as soon as it can supply the load. The set-point SOC helps avoiding situations where the battery experiences shallow charge-discharge cycles close to its minimum SOC. In real systems, such situations are harmful to battery life. Based on the cycles-to-failure curve in Fig. 3.23, the lifetime throughput, the amount of energy that can cycle through the battery before failure, can be calculated using the following equation:

$$Q = f \cdot d \cdot \frac{q_{max} V_B}{1000} \quad (3.33)$$

where  $Q$  is the lifetime throughput of a single battery (kWh),  $f$  is the number of cycles to failure,  $d$  the depth of discharge (%),  $q_{max}$  is the maximum capacity of the battery (Ah) and  $V_B$  is the nominal voltage of the battery (V).

To evaluate the life of battery banks, two independent limitations, the battery cycle life  $Y_{cycle}$  and the battery float life  $Y_{float}$ , were investigated and the minimum value chosen as the real battery bank lifetime[54].

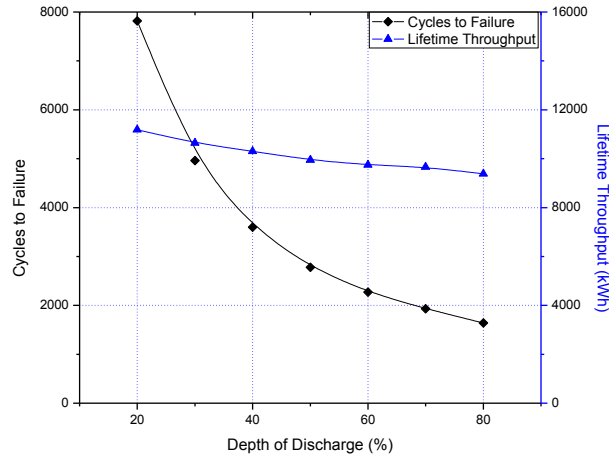


Fig. 3.23 Lifetime cycles-to-failure and throughput of the battery

Battery cycle life  $Y_{cycle}$  is the length of time that the battery will last under normal cycles before it requires replacement. It primarily depends on the depth of discharge of individual cycles. During the battery lifetime, a great number of individual cycles may occur, including charging and discharging processes, and every discharging process will result in some wear down effect to the battery. In addition, the depth of discharge also affects the performance and lifetime of battery. Therefore the lifetime throughput, which considers both cycles-to-failure and depth-of-discharge, was employed in the present research to study the battery lifetime, expressed as:

$$Y_{cycle} = \frac{n_{battery} \cdot Q}{Q_{bank,annual}} \quad (3.34)$$

where  $n_{battery}$  is the number of batteries in the battery bank,  $Q$  the lifetime throughput of a single battery, and  $Q_{bank,annual}$  the annual throughput (the total amount of energy that cycles through the battery bank in one year).

The battery float life  $Y_{float}$  is the maximum length of time that the battery will last before it needs replacement, regardless of throughput and how much or how little it is used. This limitation is typically associated with the damage caused by corrosion in

the battery, which is strongly affected by temperature. Higher ambient temperatures are more conducive to corrosion, so a battery installed in warm surroundings has a shorter float life than one installed in air-conditioned surroundings. The float life of the battery in this study is 20 years.

Considering these two lifetime limitations, the battery will die either from use or from old age. Battery bank lifetime is calculated according to the following equation:

$$Y_{battery} = \min(Y_{cycle}, Y_{float}) \quad (3.35)$$

### **3.4 Mathematical modeling of pumped storage system**

Remote islands are surrounded by sea and usually without sufficient fresh water. Therefore the seawater PHS technology can be applied in the islands, and the sea is considered as the low reservoir, resulting in a reduced construction cost of PHS system.

In this thesis, the available static head for the Town Island can be conservatively assumed as 80m and the sea is taken as the lower reservoir. Therefore, only the volume of the upper reservoir and the size of pumps and turbines should be determined. The pumped storage subsystem consists of a separated pump/motor unit and a turbine/generator unit, and they are modeled based on the law of mechanical energy (kinetic energy and potential energy). The water pumping coefficient ( $\text{m}^3/\text{kWh}$ ) and turbine generating coefficient ( $\text{kWh}/\text{m}^3$ ) are two key parameters of the pumped storage system. The modeling of the PHS system is presented as follows:

#### **3.4.1 Pump/motor unit**

In this study, the pumping station consists of a number of variable speed pumps in parallel operation. The pumps operate only when the available solar power exceeds

15% of the rated power [373]. The power source is directly supplied by the hybrid renewable energy generator. The flow rate of water sucked from the low reservoir can be expressed as Eq.(3.36). The water pumping flow rate can be considered as similar to the charging rate of the battery bank.

$$q_p(t) = \frac{\eta_p \cdot P_{RE \rightarrow p}(t)}{\rho g(h + h_f)} \quad (3.36)$$

where  $P_{RE \rightarrow p}(t)$  is the charging power from the hybrid generator to the pump (W);  $h$  is the elevating head (m);  $h_f = k \cdot q_p(t)$  is the head loss in the pipes (m);  $g$  is the acceleration due to gravity ( $9.8 \text{ m/s}^2$ );  $\rho$  is the density of water ( $1000 \text{ kg/m}^3$ );  $\eta_p$  is the overall pumping efficiency (i.e. the product of pump and electric motor efficiency); and  $C_p = \frac{\eta_p}{\rho g(h + h_f)}$  is the water pumping coefficient of the pump/motor unit ( $\text{m}^3/\text{kWh}$ );

If it is a solar pump, the overall water pumping coefficient  $C_p$  can be determined as:

$$C_p = \frac{Q}{P_{array}} \quad (3.37)$$

where  $Q$  is the rated volumetric flow rate of solar pump;  $P_{array}$  is the required PV module capacity for each pump.

If the pumping efficiency is 70%, for example, the corresponding water pumping coefficient is roughly calculated as  $4.286 \text{ m}^3/\text{kWh}$  for the elevating head of 80m (excluding the head loss in the pipe).

The head loss can be determined by the Darcy-Weisbach expression:

$$h_f = f \frac{L}{D} \frac{v^2}{2g} \quad (3.38)$$

where  $f$  is friction factor, which can be taken as 0.02 for a rough estimate;  $L$  is the length of the pipe;  $D$  is the penstock diameter, and  $v = \frac{4q_p(t)}{\pi D^2}$  is the water flow velocity in the pipe.

Therefore heat losses can be written in the terms of water flow rate:

$$h_f = \frac{fL}{2g(\pi/4)^2 D^5} q_p^2(t) \quad (3.39)$$

### 3.4.2 Turbine/generator unit

In the case of energy deficits, water is drawn from the upper reservoir in order to operate the hydro turbines. The output power from the turbine/generator unit is:

$$P_t(t) = \eta_t \rho g (h + h_f) \cdot q_t(t) \quad (3.40)$$

where  $\eta_t$  is the overall efficiency of the turbine/generator unit (i.e. the product of turbine and electric generator efficiency);  $h_f$  is the head loss in the pipes in the generating model, which has the similar expression with Eq. (3.39);  $q_t(t)$  is the water volumetric flow rate input into the turbine ( $\text{m}^3/\text{s}$ );  $C_t = \eta_t \rho g (h + h_f)$  is the overall generating coefficient ( $\text{kWh}/\text{m}^3$ ).

For instance, the efficiency of the micro turbine/generator unit is assumed as 75%, and the corresponding turbine generating coefficient is  $0.123 \text{kWh}/\text{m}^3$ . Therefore the overall efficiency of the energy storage system is 52.5% (excluding the head loss in the pipe). The pump and turbine are of variable speed, which allows the exploitation

of small amounts of excess energy produced by the PV arrays and wind turbines, and also allows covering small net load by a small quantity of water, to improve the overall energy system efficiency.

### 3.4.3 Upper reservoir (UR)

The water quantity stored in the UR should be adequate to meet the island's power demand in case of no renewable power supply for several consecutive days. The gravitational potential energy stored in the UR can be derived from the following equations:

$$E_c = n_{day} \cdot E_{load} = \eta_t \cdot \rho \cdot V_{UR} \cdot g \cdot h \quad (3.41)$$

where  $E_c$  is the energy storage capacity of a water reservoir (Joules);  $n_{day}$  is the number of days of autonomy;  $E_{load}$  is the daily load consumption (kWh/day);  $V$  is the volume or storage capacity of the water reservoir ( $m^3$ ).

During the operation of the PHS system, the potential energy associated with the head is transformed into kinetic energy. One part of this energy is associated with the velocity of a mass  $m_k$ . The other part is the pressure, with the enthalpy given by the pressure  $P$  over the density of water multiplied by the remaining mass  $m - m_k$ .

$$E_{potential} = mgh = m_k \cdot \frac{1}{2} u^2 + (m - m_k) \frac{P}{\rho} = E_{kinetic} + enthalpy \quad (3.42)$$

Therefore the required volume of UR can be calculated as:

$$V_{UR} = \frac{E_c}{\eta_t \cdot \rho \cdot g \cdot h} = \frac{E_c}{c_t} \quad (3.43)$$

Based on Eq. (3.41) and Eq.(3.43), the theoretical volume of UR is worked out to be 109,204m<sup>3</sup> for expected 5 days of autonomy (250kWh/day).

The total quantity of water stored in the UR at any time  $t$  is determined by:

$$Q_{UR}(t) = Q_{UR}(t-1)(1-\alpha) + \int_{t-1}^t q_P(t)dt - \int_{t-1}^t q_T(t)dt \quad (3.44)$$

where  $\alpha$  is the evaporation and leakage loss, similar to the self-discharge of a battery bank. For simplification, these losses in the above equations were neglected in this study.

The water level in the UR can be considered as the state of charge (SOC) of the storage tank. Therefore, the SOC of the storage system is expressed as:

$$SOC(t) = \frac{Q_{UR}(t)}{Q_{UR_{max}}} \quad (3.45)$$

In addition, the water quantity of upper reservoir is also subject to the following constraints:

$$Q_{UR_{min}} \leq Q_{UR} \leq Q_{UR_{max}} = V_{UR} \quad (3.46)$$

where  $Q_{UR_{min}}$  and  $Q_{UR_{max}}$  are the bottom and top limits of the UR(m<sup>3</sup>), and  $V_{UR}$  is the volume of the UR. The minimum storage of the UR  $Q_{UR_{min}}$  is usually set at zero.

### 3.5 Energy balance model for generation and consumption

The energy balance model of the hybrid renewable energy power generation system at time  $t$  is expressed as:

$$[P_{PV}(t) \cdot f_{PV} + P_{WT}(t) \cdot p_{WT}] \cdot \eta_{inv} = P_{RE \rightarrow l}(t) + P_{RE \rightarrow p}(t) + P_{RE \rightarrow d}(t) \quad (3.47)$$

where  $\eta_{inv}$  is the inverter efficiency, which is the ratio of the inverter's AC output power and DC input power;  $f_{pv}$  is the PV derating factor, accounting for the factors as aging, soiling, wiring losses, shading, and so on;  $f_{WT}$  is the derating factor of a WT, as shown in Eq. (3.28);  $P_{RE \rightarrow l}(t)$  is the renewable energy output directly delivered to the load;  $P_{RE \rightarrow p}(t)$  is the power transferred to the pumps for charging UR; and  $P_{RE \rightarrow d}(t)$  is the excess/wasted energy delivered to a dump load, which exists in the system with wind turbines, usually in the form of resistive loads such as air heaters.

The load demand is mainly covered by two sources, so the energy balance mode of load consumption is:

$$P_l(t) = P_{RE \rightarrow l}(t) + P_t(t) \quad (3.48)$$

where  $P_t(t)$  is the power produced by turbine/generator unit. When the net load, the difference between the actual load and the renewable energy output, is negative or zero, no supplementary energy is required and thus  $P_t(t)$  is zero; when the net load is positive, the energy storage system will be launched and  $P_t(t)$  will be positive.

## 3.6 Other components

### 3.6.1 Diesel generator (DG)

The DG is only considered as a backup in the battery based RE systems. The diesel is to meet the load when RE supply is not available or is insufficient. This can reduce the size of the battery bank and the PV and WT installations. The details of the DG selected for this study is shown in Table 3.13.

Table 3.13 Specification of diesel generator set

<b>Diesel generator</b>	
Manufactory	Huali Electromechanical Co., Ltd.
Model	HL30C
Rated Output	30kW / 37.5kVA
Standby Output	33kW / 41kVA
Engine Model	DCEC 4BT3.9-G2
Alternator Model	STAMFORD PI144J (30KW) 220V
Type	OPEN
Fuel curve intercept coefficient	0.04667 L/hour/kW rated
Fuel curve slope	0.26267 L/hour/kW output
Capital cost per unit (with ATS )	USD 7,911
Replacement cost per unit (with ATS )	USD 7,911
O&M cost per unit	USD 0.033 /hour/kW
Fuel price (pump price)	USD 1.80
Minimum load ratio	30%
Lifetime	15,000 hours

The DG usually runs under part-load conditions to cover the power difference between RE output and load demand. Thus diesel consumption and efficiency under partial load are important to system performance [34]. The fuel curve is shown in Fig. 3.24, based on the DG's specification provided by manufacturer. The intercept coefficient of the fuel curve is calculated as 0.04667 l/h/kW rated capacity (=1.4 l/h). The slope of the fuel curve is 0.26267 l/h/kW output. The partial load efficiency of the DG can be worked out, based on its fuel curve (Fig. 3.24). DG has low efficiency at low loads, dropping rapidly when operating at less than 10 kW. Hence, fuel economy considerations indicate that the generator should be stopped under lower loads. Therefore, a minimum load ratio is required for the generator under LF dispatch

strategy. In this hybrid RE-diesel system, the minimum operating threshold was set at 30% of rated capacity [20].

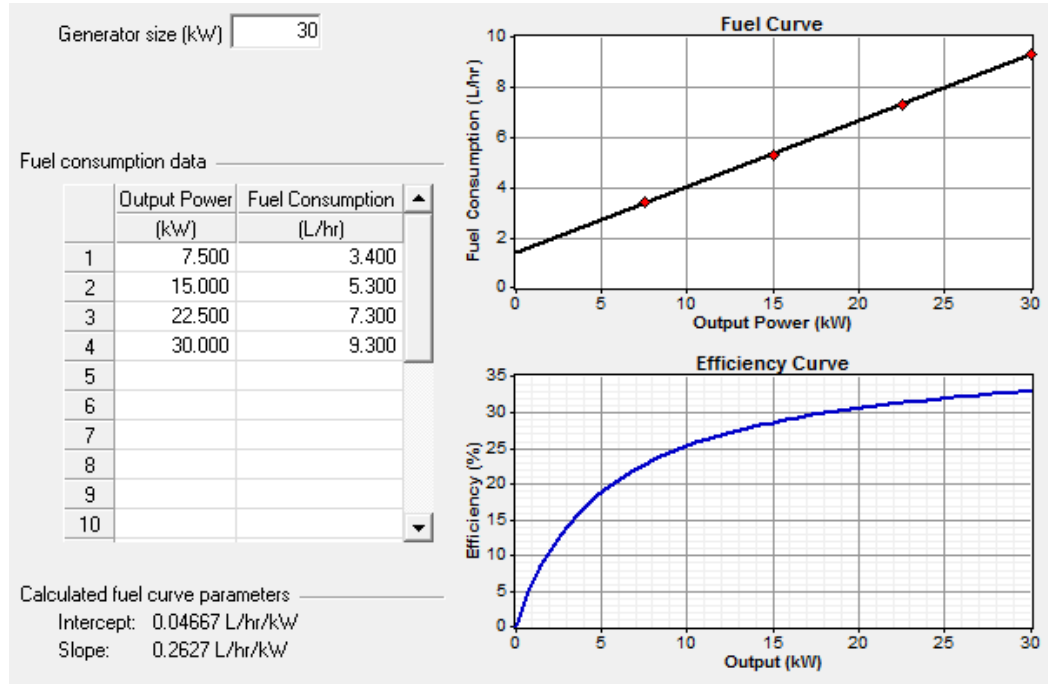


Fig. 3.24 Generator fuel curve and efficiency curve

The DG's fixed and marginal energy cost can be calculated, based on its fuel curve. There are key parameters in cost-based logic to determine which dispatch strategy should be used. The fixed cost of energy is the cost per hour of simply running the generator, without producing any electricity. It is calculated:

$$C_{fixed} = C_{O\&M} + \frac{C_{replace}}{R} + F_0 \cdot Y \cdot P_{fuel} \quad (3.49)$$

where  $C_{O\&M}$  is the O&M cost,  $C_{replace}$  the replacement cost,  $R$  is the generator lifetime in hours,  $F_0$  is the fuel curve intercept coefficient,  $Y$  is the capacity of the generator, and  $P_{fuel}$  is the price of fuel.

The marginal cost of energy is the additional cost per kWh of producing electricity from the generator. It depends on the following equation:

$$C_{marginal} = F_1 \cdot P_{fuel} \quad (3.50)$$

where  $F_1$  is the fuel curve slope.

### 3.6.2 Converters

The converter/inverter is a device that converts electric power from DC to AC (inversion) and/or from AC to DC (rectification). Rectification processes only occur in hybrid renewables with diesel since the diesel generator output is AC, the excess power may be used to charge the battery bank.

The SMA Sunny Island 5048 is employed in this study. It can perform the above directional processes. The SI5048 details are given in Table 3.14. The initial cost of the inverter was assumed to be \$4,480, which is the same as the replacement cost. There were no estimated operating and maintenance costs.

Table 3.14 Details of converter SI5048

<b>Converter</b>	
Manufactory	SMA
Model	Sunny Island 5048
Rated power	5 kW
Efficiency (for both inverter and rectifier)	90% (Max.=95%)
Nominal AC voltage (adjustable)	230 V (202 V – 253 V)
Capital cost per unit	USD 4,480
Replacement cost per unit	USD 4,480
O&M cost per unit	USD 0
Lifetime	15 years

### 3.7 System performance evaluation methods

Well recognized indicators are usually employed to evaluate the performance of RE systems in technical, economic and environmental terms [157]. The assessment criteria adopted in this study are briefly described as follows.

#### 3.7.1 Technical reliability evaluation

One objective of system evaluation and optimization is power supply reliability. In this study, the system reliability is evaluated based on the loss of power supply probability (LPSP) index, which is defined as the total power supply failure hours divided by the number of sample hours over the reporting period. The LPSP is given by the equation below, followed by the load models in Eq.(3.48).

$$LPSP = \frac{\sum_{t=1}^{8760} \text{hours}[(P_{RE \rightarrow l}(t) + P_l(t)) < P_l(t)]}{8760} \quad (3.51)$$

This index is widely used in the literature [55, 231] to evaluate whether a system is able to cater for the load demand and give the time percentage when power is insufficient. The LPSP index not only can help to size the renewable energy generator (PV and wind turbine) and UR capacity, but also it can be used to assess the reliability of a specific system.

Expected energy not supplied (EENS), also known as the loss quality of load power supply [155], is the expected energy not supplied to the load under the condition related to when load exceeds generation. On the basis of Eq.(3.51), the EENS in kWh is calculated as[409]:

$$EENS = \sum_{t=1}^{8760} L \cdot D \quad (3.52)$$

where  $L$  is the average annual demand (kW),  $D$  is the duration (h) in which load is not meet out.

The energy index of reliability (EIR) [155] on an hourly basis is then given by:

$$EIR = 1 - \frac{EENS}{\sum_{t=1}^{8760} P_t(t)} \quad (3.53)$$

Another indicator, the level of autonomy (LA) [410, 411] is given as one minus the ratio of the number of hours during which power supply failure occurs to the total number of sample hours.

$$LA = 1 - LPSP \quad (3.54)$$

In addition, the ratios of RE supplied directly to the load, to the dump load and to the pumped storage system are discussed in relations to the utilization performance of PV power generated (e.g. energy utilization rate). The final water level of UR is worked out as an indicator of the stored energy, and the differences between the maximum and minimum level of upper reservoir over the whole year studied. Finally, the system overall efficiency is examined.

### 3.7.2 Economic cost evaluation

Economic evaluation plays an essential role both in the simulation process and operating the system so as to minimize total cost, and in its optimization process, wherein it searches for the system configuration with the lowest cost.

Life cycle cost (LCC) is the total cost of ownership of machinery and equipment. LCC analysis is the most straightforward measure of economic analysis. In the optimization process, a great variety of system configurations involving different amounts of renewable or nonrenewable energy sources could fulfill the same performance

requirements but differ with respect to LCC, therefore they are compared and the most cost-effective one chosen based on the LCC analysis results. In this study, the total net present cost (NPC) was employed to represent the LCC of a system. The total NPC condenses all the costs (positive) and revenues (negative) that occur within the project lifetime into one lump sum in current dollar value. The future cash flows are discounted back to the present value using the discount rate. Please note that all monetary unit appearing in this thesis is the US dollar (\$) except indicated otherwise.

The NPC includes the costs of initial investment (equipment procurement, transportation, and installation) occurring in year zero, the replacement cost occurring each time the component needs replacing at the end of its lifetime, the O&M cost occurring each year of a project lifetime, and miscellaneous costs such as revenues. The revenues include salvage value (also called residual values or disposal costs) of a system and/or a component that occurs at the end of the study period. It can be calculated by linearly depreciating its initial or replacement costs, as shown below:

$$S = C_{rep} \frac{N_{rem}}{N_{comp}} \quad (3.55)$$

where  $S$  is the salvage value,  $C_{rep}$  the initial or replacement cost of the component (\$),  $N_{rem}$  is the remaining life of the component (years), and  $N_{comp}$  the lifetime of the component (years).

The annual real interest rate, which is also called the real interest rate, or simply interest rate, is the discount rate used to convert one-time costs and annualized costs. It is related to the nominal interest rate by the Eq.(3.56) given below[57].

$$i = \frac{i' - f}{1 + f} \quad (3.56)$$

where  $i$  is the interest rate,  $i'$  nominal interest rate, and  $f$  is the annual inflation rate.

A nominal interest rate is 6.56% and the inflation rate is 4.5% based on the statistics in China, giving an annual real interest rate of 1.97% was employed in this thesis. It can be noted that all price information is assumed as escalating at the same rate over the study period. Inflation, therefore can be factored out in the economic analysis by using the real (inflation-adjusted) interest rate. In this way, all costs become real costs, meaning that they are defined in terms of constant dollars.

The NPC can be calculated according to the Eq.(3.56) and (3.57):

$$NPC = \frac{TAC}{CRF(i,n)} \quad (3.57)$$

where  $TAC$  is the total annualized cost (\$/year), which is sum of annualized cost of individual system components,  $CRF(i,n)$  is the capital recovery factor, given by the equation,  $i$  is the annual real interest rate (the discount rate), and  $n$  is the project lifetime (years).

$$CRF(i,n) = \frac{i(1+i)^n}{(1+i)^n - 1} \quad (3.58)$$

In addition to NPC, the levelized cost of energy (COE) is also considered as a principal economic figure of merit for a RE system. It is the average cost per kilowatt-hour of useful electrical energy produced by the system, which is expressed by Eq.(3.59):

$$COE = \frac{TAC}{E_{Load}} \quad (3.59)$$

where  $TAC$  is the total annualized cost (\$/year),  $E_{Load}$  is the total amount of electrical load that the system serves per year (kWh).

In Section 6.4.1, the single-objective optimization results are ranked and based on COE index, as it is a convenient metric to evaluate the cost effectiveness of different system configurations.

### 3.7.3 Payback time

The payback time (PBT) is the number of years it takes for the cumulative annualized RES savings, when compared to the diesel system, to become positive [412]. That means during that year when payback time is achieved, the sum of the RE system costs is equal to those of a diesel-only configuration [413]. Annual savings are expressed by subtracting the annualized costs of the RESs from the diesel-only system, and thus the overall saving can be simply expressed as:

$$\sum_{j=0}^{PBT} (NCF_{RE} - NCF_{Diesel}) \geq 0 \quad (3.60)$$

where  $j$  is the year number,  $PBT$  is the calculated payback time (years);  $NCF$  represents the nominal cash flow, where outflows is recorded as negative (such as the initial cost, fuel expenditure, equipment replacements, or O&M) and inflows are positive such as equipment salvage values.

It is evident that the shorter the PBT, the better the investment. This is a criterion which values availability more than profitability.

### 3.7.4 Environmental effect evaluation

Also examined are the pollutant emissions and the subsequent environmental effect. This study assumed no cost penalty associated with pollutants (as these data cannot be collected as virtually no penalties are imposed in Hong Kong). The pollutant emission

factors in diesel power generation are summarized in Table 3.15 [408]. Therefore, the environmental benefit of the RESs is considered as avoiding such pollutants emissions.

Table 3.15 Emission factor from diesel power generation

Pollutant	Emissions factor (g/L diesel)
Carbon dioxide (CO <sub>2</sub> )	2,633
Carbon monoxide (CO)	6.5
Unburned hydrocarbons (CH <sub>x</sub> )	0.72
Particulate matter (PM)	0.49
Sulfur dioxide (SO <sub>2</sub> )	5.28
Nitrogen oxides (NO <sub>x</sub> )	58

### 3.8 Summary

In this chapter, the individual components are modeled, as a foundation to simulate the dynamic behaviour of the RE-based RAPS systems and evaluate the performance of their combined operation in the subsequent chapters. In particular, a novel PV simulation model was developed to fit the I-V curves and predict power output. The model was solved using an integrated analytical and numerical method, then validated through field measurements in a real grid-connected and a standalone PV system. It was envisaged that such proposed work would be relevant to the needs of PV power system designers and engineers who require simple, fast and accurate models for PV systems. In addition, the system evaluation methods in terms of technical, economic and environmental issues are proposed. These criteria will be employed for comparing the performance of different system types and configurations.

## **CHAPTER 4 ASSESSMENT OF RENEWABLE ENERGY POTENTIAL AND LOAD DEMAND**

An assessment of renewable energy potential and load demand of Town Island is given in this chapter. It is well acknowledged that RE output varies greatly both with time of the day and specific locations. Wind output depends on patterns of atmospheric circulation and geographic influences, while solar energy depends mainly on latitude and climate. In addition, these intermittent RE resources may experience enormous daily and seasonal variability. The availability of RE is greatly influenced by the specific configurations and economics involved in its activation. The evaluation of RE potential for a specific location is thus of great importance. In this study, a detailed analysis of the characteristics of solar irradiance and wind conditions has been conducted, and the complementary characteristics between solar and wind power analyzed. The biomass is not considered as a limited resource on this island. An additional consideration is that the measured load information is not available, a full-years' worth load data, therefore, has been synthesized in this study by selecting historical typical daily load profiles and adding some degree of randomness to them.

### **4.1 Background of Town Island**

There are three inhabited islands, namely Po Toi Island, Tung Ping Chau and Town Island, off Hong Kong and beyond the reach of the utility grid. Currently they are powered by diesel generators with fuel supplied by barge. To reduce dependence on diesel and improve power supply quality, the government is planning to explore locally available renewable energy for power generation on these islands.

Town Island, the example island involved in this study, is located in the southeastern part of the Sai Kung District of Hong Kong. The latitude and longitude of this island is 22°36'N and 114°40'E, respectively. The island is as much as 22km off the coast of Hong Kong. An organization, Operation Dawn, has run the Drug Addiction Treatment & Rehabilitation Centre on this Island since 1976. At present, the island has around 50-70 residents of different nationalities on the island and Operation Dawn is contemplating extending accommodation provision to include about 100 residents. As is the case of many similar remote islands, access to the utility grid is not available for Town Island. Three diesel power generators, therefore, are in use for which diesel fuel is transported by sea. However, before the RE scheme, the diesel power supply was available for only a limited number of hours every day owing to extremely high cost of the whole exercise, including expensive transportation costs, inventory carrying cost and the high price of diesel fuel in Hong Kong.

Realizing the difficult living conditions and constraints on the island and also those for further development because of lack of an electricity supply, a local utilities company, China Light & Power, was on the verge of deciding to install submarine cables and overhead lines to provide a constant electricity supply for this island. This proposal was finally abandoned because of various disadvantages such as high cost and ecological destruction. After an initial investigation, a far sighted decision was taken to use available RE for a local remote power supply. Reasons given were RE is environmentally friendly, more cost-effective than grid extension, and mature enough to provide utilitarian quality power supply.

Town Island has therefore been taken as an example site to test the proposed RE and storage technologies potentially useful in remote areas. This RE power supply scheme is divided into two phases, i.e. Stages 1 and 2. During Stage 1, completed in 2010, a

stand-alone 19.8kWp PV system was installed on the island. This system was used mainly to test PV system's feasibility, understand its operating characteristics, and prepare for the system implementation in next stage. A hybrid solar wind power supply system has been initiated in Stage 2, and the power generation and storage capacity may increase to tenfold that of Stage 1. Some issues are anticipated such as the capacity allocation of solar and wind energy, the selection of energy storage technology, system optimization of power generation and storage.

## 4.2 Solar energy potential

The solar PV system is proposed as the major power generator. The solar radiation data from 2008 to 2011 was collected from an adjacent meteorological station at Kau Sai Chau, about a 5 km distance from the island. As shown in Fig. 4.1, measurements of diffuse solar radiation were made by a pyranometer shaded from the sun, while direct solar radiation was measured by another pyranometer mounted on a sun tracker which ensures that the pyrliometer points directly at the sun all the times.

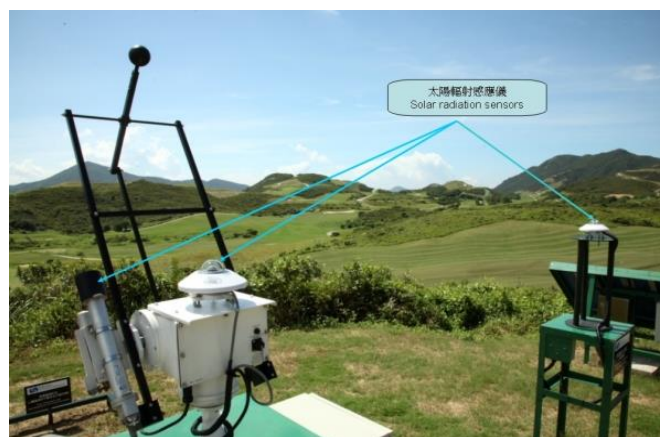


Fig. 4.1 Kau Sai Chau solar radiation station

Fig. 4.2 shows that the annual occurrence frequency of the daily total global solar radiation in comparison with a specified level. In the winter months, more than 60% of days receive less than 4.0kWh/m<sup>2</sup>/day, while less than 10% exceed 6.0kWh/m<sup>2</sup>/day.

However, in summer, from May to September, about 40% of the days are above 5.0kWh/m<sup>2</sup>/day, and a small number of days exceed 8.0kWh/m<sup>2</sup>/day. The yearly frequency distribution is quite symmetrical with respect to July, in which the occurrence frequencies of high solar radiation are significant, with 5% higher than 8.0kWh/m<sup>2</sup>/day.

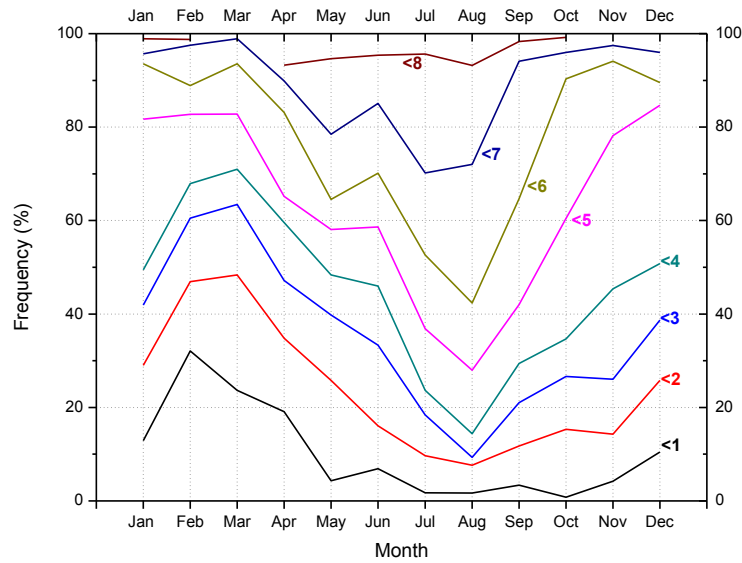


Fig. 4.2 Frequency distribution of daily average irradiation less than specified amounts (kWh/m<sup>2</sup>/day)

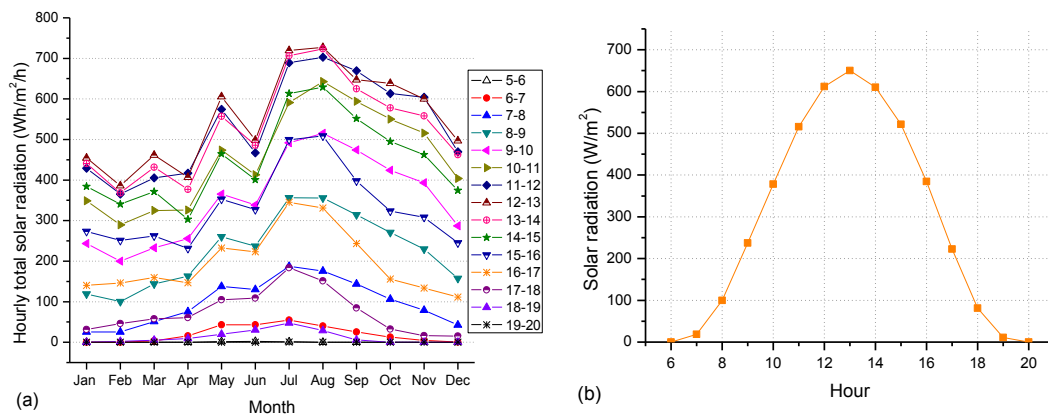


Fig. 4.3 Hourly distribution of solar radiation (a) monthly average (b) yearly average

The distributions of monthly averaged and yearly averaged solar radiation at given hourly intervals are demonstrated in Fig. 4.3. It seems that the hourly value peaks at 1:00pm and has a symmetrical distribution from 6:00am to 8:00pm. The solar resource profile indicates that for a solar energy system the PV output could cover the load during most of the daytime and that there may be considerable surplus at noon.

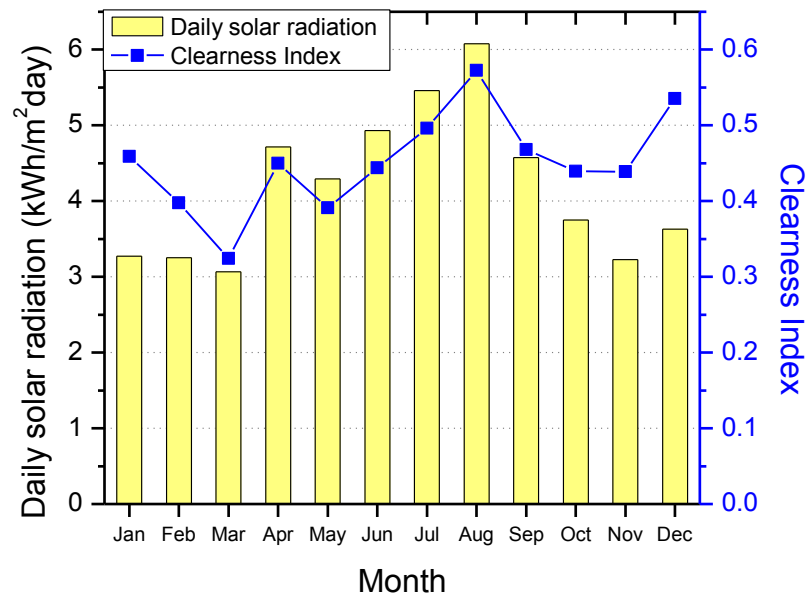


Fig. 4.4 The monthly solar radiation and the clearness index in 2009

To provide a reference for PV system modeling and design at its optimum angle, the solar radiation incident at the tilted angle of  $22.5^\circ$  was studied for year 2009. The results are presented in Fig. 4.4. The monthly average data is in the range of 3.17 to 5.84kWh/m<sup>2</sup>/day, and yearly mean is 4.34kWh/m<sup>2</sup>/day. Fig. 4.4 also illustrates that higher irradiation can be expected between April and September, with less between November and March. Such season distribution is consistent with the typical subtropical climate in Southern Asia. The low value and exceptionally large fluctuations in the months of March and November are mainly due to unstable climate conditions during transition from cold to warm weather and vice versa [338]. The

clearness index, the ratio of the solar radiation striking Earth's surface to that striking the top of the atmosphere, is similar to the trend of solar radiation, as presented in Fig. 4.4.

### **4.3 Wind energy potential**

Wind power is one of the most potential renewable energy resources for Hong Kong, as the small territory is characterized by a long coastline and numerous islands. The surrounding strong winds on the islands provide good opportunities for wind power applications.

In Stage 1 of the RE scheme, a small meteorological tower equipped with an anemometer was installed on this island. However, the collected data could not reflect the actual wind conditions on the island due to some problems with the measurement system. Therefore, the 10-year wind data from the Waglan Island weather station was selected to represent the wind condition on the involved island. Finally the wind data was synchronized with the solar radiation data in 2009 over hourly time steps.

#### **4.3.1 Assessment procedure**

##### *4.3.1.1 Weibull distribution function*

The Weibull distribution function, based on the occurrence frequency distribution, is employed in this thesis for wind power evaluation. Published research [414, 415] has proven that the Weibull distribution. In particular, it can give a good fit to a wide collection of recorded wind data and provide a useful model to estimate the potential of wind energy.

Wind speed distribution is fitted using the two-parameter Weibull Distribution, and its probability distribution function (PDF) can be described as [416]:

$$f(v) = \frac{k}{c} \cdot \left(\frac{v}{c}\right)^{k-1} \exp\left[-\left(\frac{v}{c}\right)^k\right] \quad (k > 0, v > 0, c > 0) \quad (4.1)$$

The cumulative distribution function is given by:

$$F(v) = \int_0^v f(v)dv \quad (4.2)$$

where  $v$  is wind speed (m/s);  $c$  (m/s) and  $k$  are the respective scale parameter and shape factor of the Weibull distribution. The scale parameter is related to the average wind speed, indicating the degree of strength of the wind. The dimensionless shape factor reflects the breadth of the distribution, with lower value corresponding to broader distributions.

Once the mean value and variance of the wind speed are known, the following acceptable approximation [417] can be used to calculate the Weibull parameters.

$$k = \left(\frac{\sigma}{\bar{v}}\right)^{-1.086} \quad (1 \leq k \leq 10) \quad (4.3)$$

$$c = \frac{\bar{v}}{\Gamma(1 + 1/k)} \quad (4.4)$$

where the average wind speed is:

$$\bar{v} = \frac{1}{n} \sum_{i=1}^n v_i \quad (4.5)$$

The variance  $\sigma^2$  of wind speed recordings is:

$$\sigma^2 = \frac{1}{n-1} \sum_{i=1}^n (v_i - \bar{v})^2 \quad (4.6)$$

The gamma function of  $x$  can be calculated as:

$$\Gamma(x) = \int_0^{\infty} e^{-u} u^{x-1} du \quad (4.7)$$

#### 4.3.1.2 Wind-speed variation with height

Wind speed changes with height, which requires an equation predicting wind speed at one height based on the measured speed at another height. For a wind turbine, it is also necessary to know the wind speed at its hub center. The most common method is the power law:

$$v = v_0 \left( \frac{z}{z_0} \right)^\alpha \quad (4.8)$$

where  $v$  is the wind speed estimated at a desired height (wind turbine hub height);  $v_0$  is wind speed measured at the reference height  $z_0$ ;  $\alpha$  is the ground surface friction coefficient. A power law exponent of 0.143 (one-seventh) is applied in this thesis.

#### 4.3.1.3 The average power in the wind

The theoretical mean value of wind speed is given by:

$$\bar{v} = \int_0^{\infty} v f(v) dv \quad (4.9)$$

The average power in the wind passing through an area  $A$  perpendicular can be expressed as:

$$\overline{P}_w(v) = \frac{1}{2} \rho A v^3 = \frac{1}{2} \rho A \int_0^{\infty} v^3 f(v) dv \quad (4.10)$$

If the wind PDF  $f(v)$  can meet the Weibull distribution in Eq. (4.1), the average power becomes:

$$\overline{P_w}(v) = \frac{\rho A v^3 \Gamma(1+3/k)}{2\Gamma(1+3/k)^3} \quad (4.11)$$

So the wind power density used to compare different regions is given by:

$$\frac{\overline{P_w}(v)}{A} = \frac{1}{2} \rho \int_0^\infty v^3 f(v) dv = \frac{\rho v^3 \Gamma(1+3/k)}{2\Gamma(1+3/k)^3} \quad (4.12)$$

Based on Eqs. (4.10), (4.11) and (4.12), the available wind energy can be calculated for any defined period of time. The energy output is commonly calculated in watts per square metre (W/m<sup>2</sup>).

### 4.3.2 Analysis of the collected data

The wind speed profile in 2010 is presented in Fig. 4.5 as an example to display wind condition on this island. The wind data was collected at anemometer height of 82m.

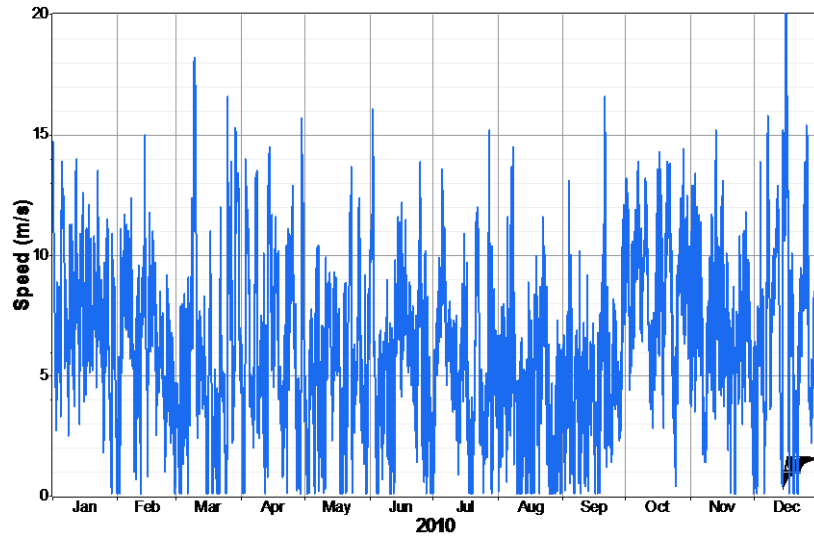


Fig. 4.5 Wind speed collected in 2010

The diurnal wind speed profiles in 12 months are presented in Fig. 4.6. From October to March, the wind speed is strengthened at nighttime, reaching a peak in the early morning and declining to the lowest after the sunset, while the tendency is contrary during the summer months from April to August. The wind speed magnitude in

summer, 5.6m/s, is much lower than in winter (6.7m/s). The diurnal wind speed profile can reflect the condition of wind resources at different hours in a day and can provide a guide for customers to best use wind energy depending on the diurnal wind power distribution.

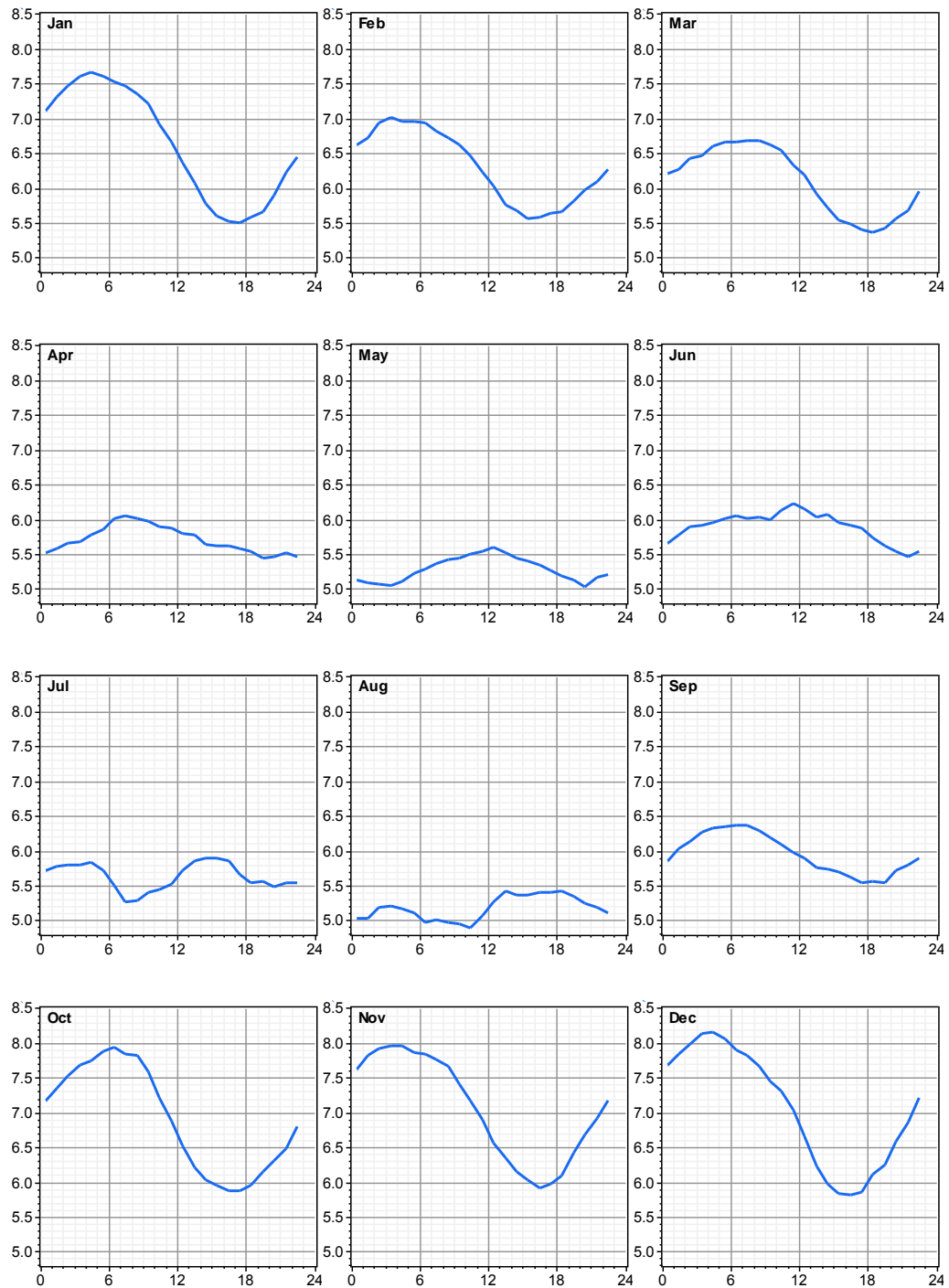


Fig. 4.6 Diurnal wind speed profile in different months (10 years mean)

The prevailing wind directions can provide important information to determine the WT orientation to maximize the power output. The statistical result of wind direction by frequency rose during the 10-year period is presented in Fig. 4.7. Overall, the wind rose pattern indicates that the prevailing wind direction on the island is mainly in the eastern and north-eastern directions.

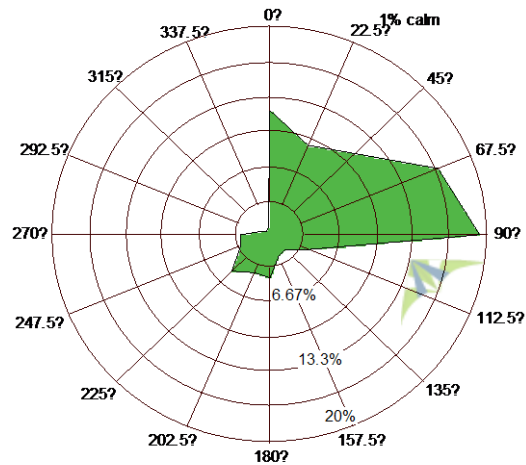


Fig. 4.7 Wind direction frequency rose during 10 years

### 4.3.3 Analysis of wind power potential

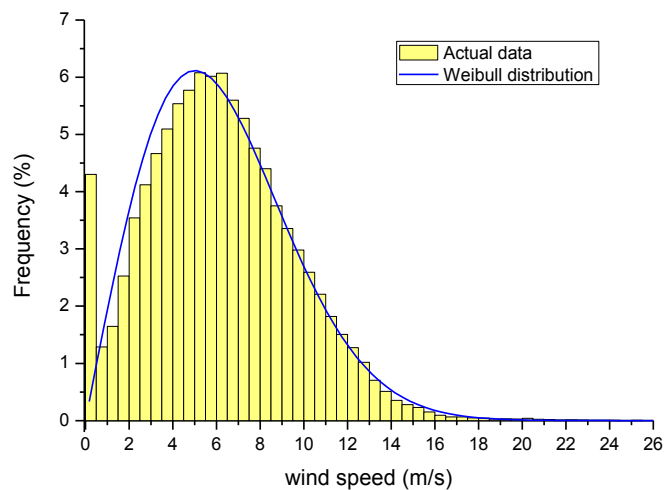


Fig. 4.8 Wind speed Weibull distribution (10 years data)

The frequency distribution of 10-year wind speed data is presented in Fig. 4.8. This distribution fits by Weibull distribution. The overall scale parameter and shape factor

is 7.05m/s and 2.02, indicating that the island possesses satisfactory wind resources and has a relatively broad wind distribution.

Two typical monthly wind speed frequency distributions are given in Fig. 4.9. The fitted curves show that the scale parameter in August is much lower than that in December, indicating that low and moderate winds are common in August. A low shape parameter in August indicates that the wind distribution in that month tends to be fairly narrow and concentrated on a central point. In contrast, the wind distribution in December is broad and peaks at a strong wind speed value.

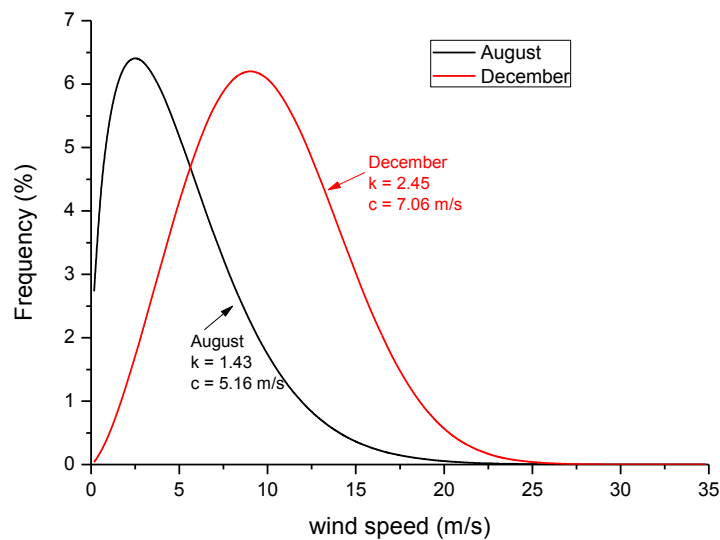


Fig. 4.9 Wind speed Weibull distribution in August and December

The 10 years averages of monthly mean wind speeds and theoretical wind power densities ( $W/m^2$ ) are given in Fig. 4.10. The results demonstrate that the potential wind power in the summer months from May to September is much lower than those in other months. The variation of monthly wind power density and average wind speed has a similar trend. However, sometimes they can show an opposite tendency as the wind power is determined not only by the mean speed but also by the Weibull shape parameter (see Eq.(4.12)). For example, the mean wind speed in August is only 5.16m/s, lower than that in July (5.64m/s), while the estimated power density in

August is higher than that in July. This phenomenon results mainly from the wide distribution and great fluctuation of wind speeds in July.

Over the 10 years, the yearly average power density is calculated at 283 W/m<sup>2</sup> under the anemometer height of 27m. Therefore, the potential annual wind power can be theoretically estimated as 2,480kWh/m<sup>2</sup>.

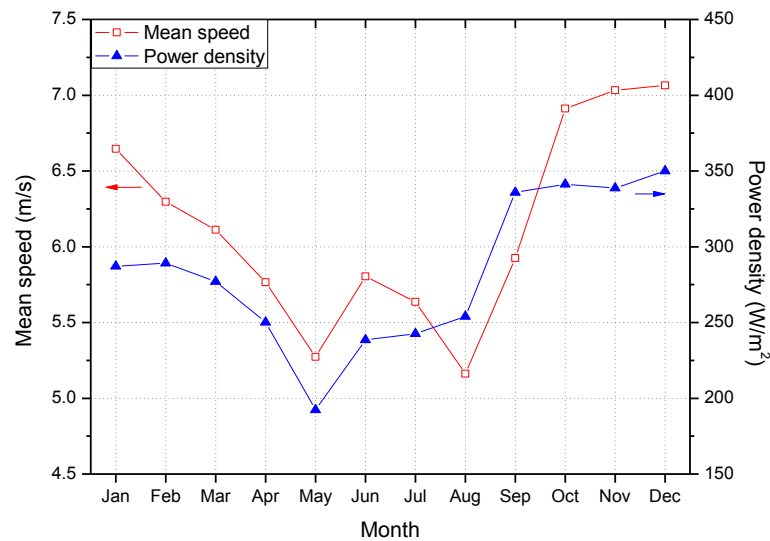


Fig. 4.10 Monthly (and yearly) average wind power density and average wind speed

#### 4.3.4 Analysis of wind power at different hub heights

To investigate the wind power generated from a specific wind turbine, the wind turbine Proven 11 with four hub heights, i.e. 9m, 11.6m, 15m and 20m is studied. The wind speeds at the four heights were calculated based on the wind data at the anemometer height (27m).

The mean wind speed, Weibull parameters, and power density at the four hub heights are shown in Table 4.1. It is observed that wind distributions at the four heights have the same pattern (shape parameter), while the magnitude and power density increases with the hub height.

The turbine operating performance was also simulated (Table 4.2) based on the wind turbine power curve. When the hub heights increase, the zero output time decreases and the operating hours increase proportionally, resulting in an increase in wind power output and capacity factors. The availability of wind turbine output at 20m is very high at 88.5%.

When the hub height changes from 9m to 20m, the mean daily energy output increases by 27.3%, due to the fact that wind energy is proportional to the cube of wind velocity and the operating time at high hub height has also increased.

Table 4.1 Wind distribution results for different hub heights

Hub height (m)	Mean speed (m/s)	Shape parameter k	Scale parameter c (m/s)	Power density (W/m <sup>2</sup> )
9	5.24	2.02	6.03	176.6
11.6	5.44	2.02	6.25	196.9
15	5.64	2.02	6.48	219.9
20	5.88	2.02	6.75	248.8

Table 4.2 Turbine operating performance results at different hub heights

Hub height (m)	Time at zero output (%)	Time at rated output (%)	Net capacity factor (%)	Mean daily energy output (kWh/day)
9	12.77	4.07	21.7	27.1
11.6	12.06	5.09	23.6	29.4
15	12.12	6.25	25.5	31.8
20	11.53	7.98	27.7	34.5

#### 4.3.5 Predicted performance of the turbine at the hub height of 15m

The hub height at 15m was selected, as an example, to study the operating performance. The predicted results are presented in Table 4.3. The daily average energy output varies from 21kWh/day in August to 41.3kWh/day in November, resulting in a yearly mean of 31.8kWh/day. The predicted annual capacity factor is 25.5%, with monthly values ranging from 16.9% to 33.1%. These values are consistent with typical wind turbine capacity factors of 20-40% throughout the world.

Table 4.3 Monthly wind turbine operating performance (for hub height at 15m)

Month	Hub Height	Time At	Time At	Mean Net	Capacity
	Wind Speed (m/s)	Zero Output (%)	Rated Output (%)	Energy Output (kWh)	Factor (%)
Jan	6.11	6.35	5.77	1,141	29.5
Feb	5.79	11.02	7.8	960	27.5
Mar	5.62	12.74	7.36	1,010	26.1
Apr	5.3	15.43	6.24	876	23.4
May	4.85	16.7	2.8	720	18.6
Jun	5.34	13.75	4.33	861	23
Jul	5.18	13.57	3.72	774	20
Aug	4.75	20.41	4.83	652	16.9
Sep	5.45	16.57	6.47	850	22.7
Oct	6.35	7.35	8.8	1,251	32.3
Nov	6.47	6.18	8.49	1,238	33.1
Dec	6.49	5.44	8.51	1,269	32.8
Overall	5.64	12.12	6.25	11,605	25.5

#### 4.4 Solar and wind energy complementary characteristic

The hourly meteorological data on this island was synchronized throughout 2009. Fig. 4.11a presents the average solar and wind energy resources monthly. The inherent complementary nature is displayed. The summer provides a relative good solar energy resource but poor wind conditions, while a crosscurrent is present in the winter. Usually, the wind speed is higher during seasons of low insolation and low for high insolation. Fig. 4.11b demonstrates an example of hourly and daily complementary characteristics illustrating that the wind often blows when the sun does not shine and vice versa. The figures show that solar and wind energy, together, give greater value than they do individually, therefore, a better utilization factor for the available RE can be achieved and less energy storage capacity is needed.

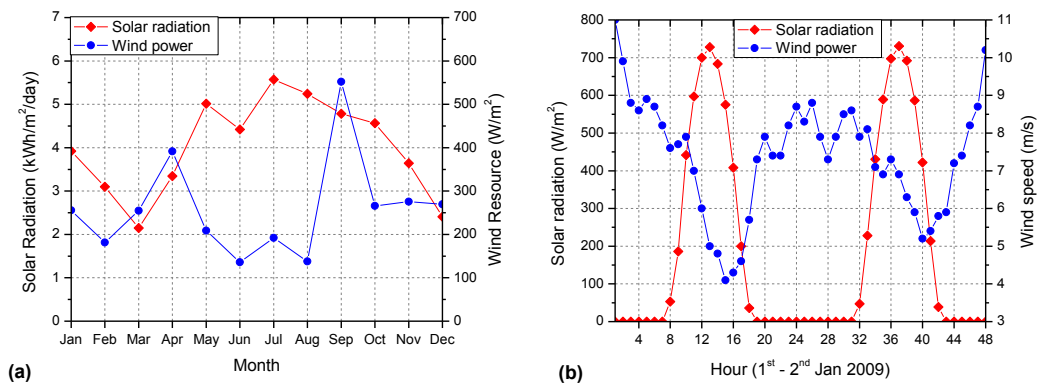


Fig. 4.11 The solar and wind energy resource on the island (a) monthly energy density in 2009 (b) Daily solar radiation and wind speed distribution on 1<sup>st</sup>-2<sup>nd</sup> January 2009

To express the complementary characteristics numerically, a correlation coefficient between solar and wind energy was calculated using Matlab. This coefficient is used to see if employing the hybrid system is beneficial. If the correlation coefficient is close to 1, a positive relationship between the data columns is suggested and if the

correlation coefficient is close to -1, the implication is that one column of data has a negative relationship to another, also called as anticorrelation. In this case, the correlation coefficient of monthly distribution and daily distribution was calculated at -0.12 and -0.60, respectively, indicating that the two sources of energy approach opposite paths, i.e. when one is approaching its maximum quantity, the other is approaching its minimum. This will improve the reliability of the hybrid solar and wind system. For example, when there is insufficient wind energy supply, a considerable amount of solar energy available.

#### **4.5 Island load demand profile**

A key element of any power generation system is the load itself, which has a pronounced effect on system configuration [34]. The power generated by the PV plant in Stage 1 was recorded by the data collection system. However, the load data cannot reflect the real electricity consumption on this island since part of the power was supplied by the backup diesel generator. In addition, the power demand will increase due to the growing number of residents.

As measured hourly load information is not available, a full-years' data load, therefore, were synthesized by specifying typical daily load profiles and then adding some degree of randomness for different days. The typical daily power demand was artificially estimated with reference to [418, 419]. The average daily power demands for major electric appliances are given in Table 4.4. All these loads are assumed as AC load.

The hourly load profile over a day was created based on the assumed electrical appliances and the subsequent estimated power demand. A sample of the 24-hour load

profile is displayed in Fig. 4.12. The sample demonstrates that peak loads occur in the afternoon and early evening.

Table 4.4 Average daily power demands of major components in Town Island

Load components	Power (kW)	Operating hours (h/day)	Power demand (kWh/day)
Light bulbs	8	5	40
A/C Load	25	5	125
Cooker	5	5	25
Radio	0.2	5	1
TV set	5	4	20
Refrigerator	1	24	24
Other appliances	5	3	15
<b>Total</b>			<b>250</b>

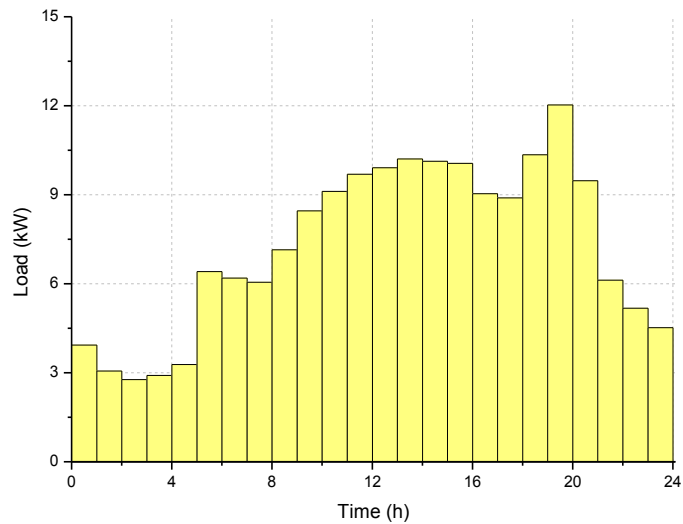


Fig. 4.12 A sample daily load profile for this island

As would be expected, the daily load profile for this island depends on the season. To specify the monthly load data throughout the year, load coefficients were applied for

each month, based on the Hong Kong typical climate and load profile reported by other studies [420]. The load coefficients for the autumn months from October to November were set at 1, meaning that the energy consumption in this season is equal to the average load. The spring months between March and April require slightly less electricity than those of autumn with a coefficient of 0.9, followed by the winter months from December to February (175kWh/day), with 0.7 of the average energy consumption. The highest power consumption occurs in summer due to the cooling load, when the coefficients range from 1.1 to 1.4, peaking at August. It can be noted that energy demand for the summer is about twice that in the winter. The monthly load coefficient and the daily and monthly electricity demand are summarized in Table 4.5.

Table 4.5 Monthly load coefficient and total electricity demand

Season	Month	Number of days	Monthly load coefficient	Average daily load (kWh/day)	Monthly load (kWh)
Winter	Jan	31	0.7	175	5,425
	Feb	28	0.7	175	4,900
Spring	Mar	31	0.9	225	6,975
	Apr	30	0.9	225	6,750
Summer	May	31	1.1	275	8,525
	Jun	30	1.2	300	9,000
	Jul	31	1.3	325	10,075
	Aug	31	1.4	350	10,850
	Sep	30	1.1	275	8,250
Autumn	Oct	31	1	250	7,750
	Nov	30	1	250	7,500
Winter	Dec	31	0.7	175	5,425

The shape and magnitude of the load profiles, in fact, vary day by day and hour by hour. To avoid daily precise repeats of load profiles for each month, a daily and hourly perturbation factor was added. The daily factor prompts the load profile magnitude to vary randomly from day to day, while the hourly factor affects the shape of the load data distribution without affecting its size.

The correction of the basic 24 hour data is based on the multiplication factor  $\alpha$  :

$$\alpha = 1 + \delta_d + \delta_h \quad (4.13)$$

where  $\delta_d$  is the daily perturbation factor and  $\delta_h$  is the hourly perturbation factor.

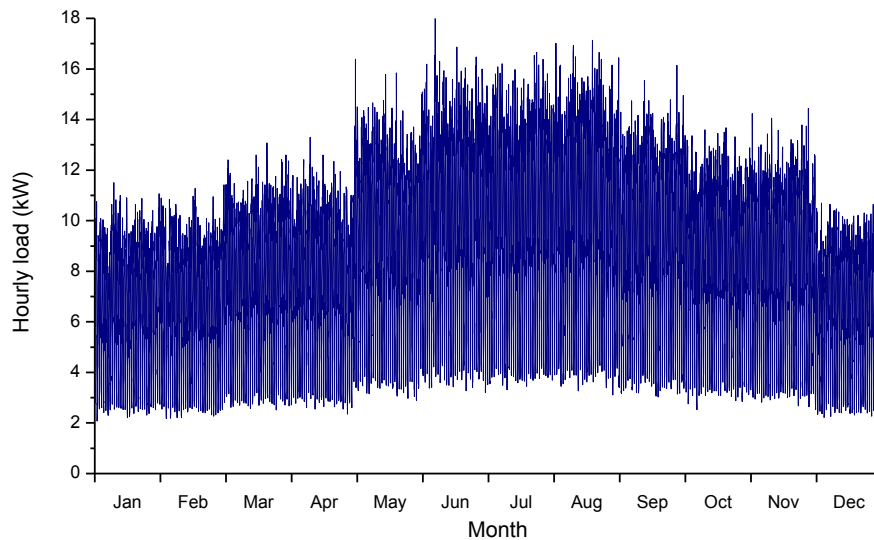


Fig. 4.13 Yearly load profile on this island

User-defined perturbation factors in the range 2% to 20% have been reported in the literature [12, 13, 57]. In this study, a daily and hourly perturbation factor of 5% was employed, given that the residents on this island have regular lifestyles and a relatively stable energy demand. A plot of the hourly average power demand during a year is

shown in Fig. 4.13. A realistic-looking load profile is generated with the coupling of daily and hourly perturbation in Eq.(4.13).

In summary, the scaled total energy demand of the island is 91,250kWh/year, and the daily demand averages 250kWh/day with a maximum power demand of 27.3kW.

## **CHAPTER 5 DEVELOPMENT OF BATTERY-BASED RENEWABLE ENERGY SYSTEMS**

The intermittent characteristic of a solar, wind or their hybrid prevents the standalone RE system from being fully reliable without suitable energy storage capability. In this chapter, a study of the traditional energy storage technology, battery, to support the microgrid RE power generation system at a few hundred kW scale, is carried out. Hourly simulations of possible combinations of the four technologies (solar, wind, diesel and battery) with a wide variety of configurations have been performed to achieve an optimal system configuration based on techno-economic analysis results. The performances of the potential eight options have been evaluated. A sensitivity analysis on the effects of load variation on system configuration and cost has also been conducted. Finally two typical options, the 100% RE system and RE system with backup diesel, were selected for elaborate analysis. Emphasis was also placed on examining the effects of the PV, wind turbine, diesel generator, and battery bank capacity on the system's reliability and economic performance.

### **5.1 System configuration of battery-based power generation systems**

In this section, two typical system types, the 100% RE system and RE system with backup diesel, are discussed with respect to the system configuration, control and dispatch strategy.

### 5.1.1 100% renewable energy system

The system architecture for the hybrid solar–wind system with battery storage is shown in Fig. 5.1. The system mainly consists of a PV array, WT, battery bank, inverter, controller, dump load and other accessory devices such as cables. The DC power output from the PV array and WT is converted into AC by the inverter to supply the load, while available excess energy is fed into the battery bank. When no more energy is needed and the battery bank fully charged, the surplus energy is dumped. The battery bank releases power to the load when the RE output is unavailable or is insufficient to supply the load. The main power distribution component is the inverter, to which the AC and DC buses are connected.

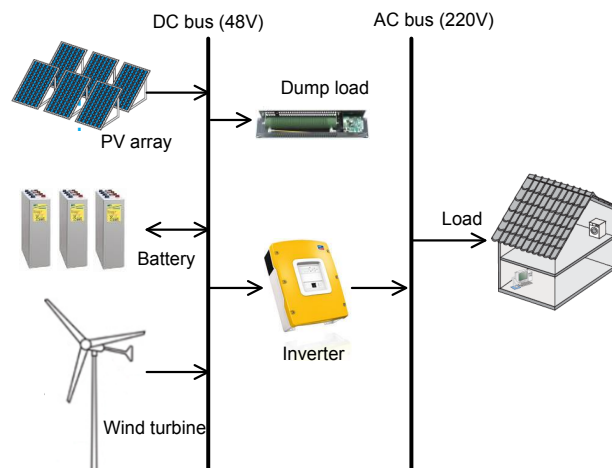


Fig. 5.1 Energy flow diagram of the hybrid solar–wind system with battery storage

The system can be easily controlled because there is only one dispatchable power source, i.e. the battery bank. Whenever the net load, the difference between the actual load and the renewable power output, is negative, meaning that the RE output is sufficient to serve the load, the excess energy is used to charge the battery bank and any further surplus is dumped. Whenever the net load is positive, the only supplementary power source battery bank releases energy to satisfy the load. The operation strategy of this kind system is shown in Fig. 5.2.

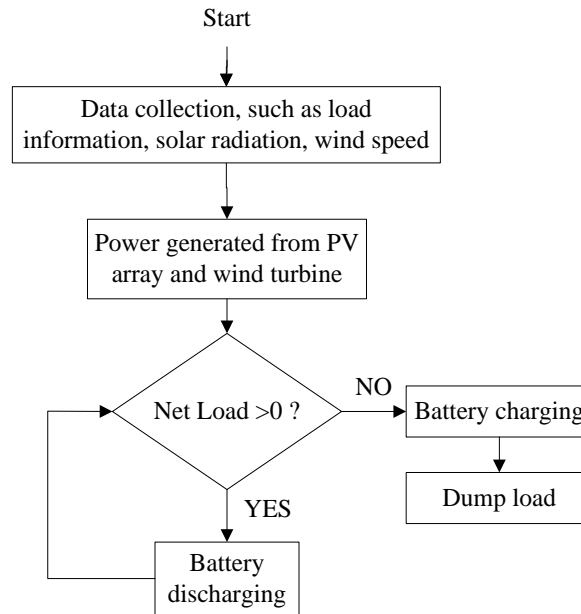


Fig. 5.2 Operating strategy of this hybrid solar -wind system employing a battery bank

### 5.1.2 Renewable energy system with backup diesel

Recently the International Energy Agency has released a report on RE development in remote areas [36], suggesting that it is possible to provide renewable electricity at the 100% level. However, that is most readily achieved when intermittent RE generators are combined with dispatchable generation such as diesel. A system combining only RE and a storage device can be achieved. Technical barriers, however, will arise when the system capacity is excessively large due to the fluctuating nature of RE. Therefore, a diesel generator is introduced in the hybrid renewable energy system. To guarantee high renewable energy penetration, a minimum renewable energy supply fraction in this study was set at 90%.

#### 5.1.2.1 System configuration and description

The schematic diagram of a hybrid solar-wind-diesel-battery system is similar to that in Fig. 5.1, except that one diesel generator has been added. Solar and wind energy

typically provide bulk energy, whereas the diesel generator, in the form of a backup, provides the reliability that end-users demand. When all RE output cannot meet the load demand, the dispatchable components (battery and diesel generator) are launched, and the rules are subject to cost-based dispatch logic (discussed in Section 5.1.2.3). This inverter is bidirectional. It not only converts the DC output from RE or batteries to AC load but may also convert the diesel surplus energy to charge the battery. Whether to use the surplus capacity from the diesel generator to charge batteries is subject to the selected dispatch strategies, explained in Section 5.1.2.4.

#### *5.1.2.2 The role of the diesel generator for standalone RE systems*

One advantage of including a DG is the significant decrease in both storage and RE generator capacities, hence reducing system cost, whilst an optimal combination of PV, WT and batteries can limit fuel consumption of the generator. Studies [20, 56] have demonstrated that it is more cost-effective to employ a diesel generator than to increase the size of the battery bank or RE generator. The diesel generator covers the peak load and supplies load demand when continuously poor weather limits RE availability. The diesel generator provision can ramp up down, to accommodate the intermittent RE output. In addition, reliability can be supported through specialized diesel controls [36], such as an automatic starter and minimum load ratio, both of which can maximize the benefit from RE and improve the diesel performance in such hybrid systems. In the study presented in this thesis, the role of the backup generator in the hybrid system regarding its purpose to reduce system cost and enhance the power supply reliability is investigated, and the threshold load size at which it is the most cost-effective examined.

### 5.1.2.3 System control of dispatchable components

The control strategy is of vital importance for hybrid systems with more than one dispatchable component. Fig. 5.3 demonstrates the operating strategy for a system with two dispatchable power sources, i.e. diesel generator and battery bank. Whenever the net load is negative, the excess power will charge the battery bank and any further surplus dumped. Whenever the net load is positive, the system will have three options: 1. launch the DG, 2. discharge the battery, 3. combine 1 and 2, to serve the load deficit. If the three alternatives are capable of supplying the net load, the alternative selected is based on a cost-based fundamental principle that the solution fulfills the load demand and operating reserve with cheapest cost being chosen.

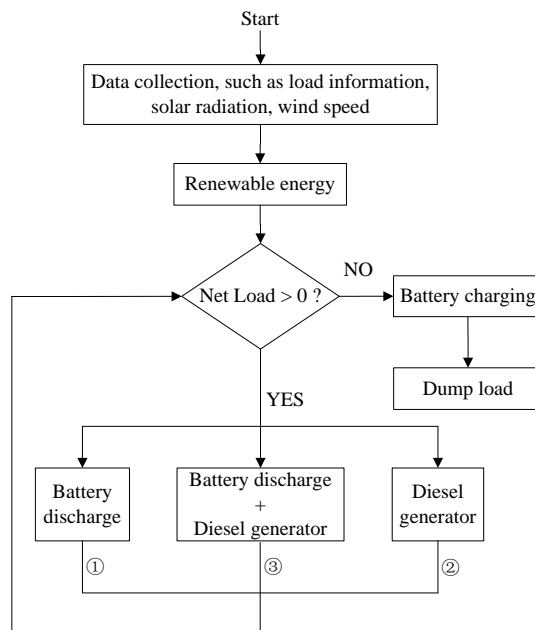


Fig. 5.3 Control strategy of dispatchable system components

### 5.1.2.4 Dispatch Strategy

Dispatch strategy contains rules relating to how to choose system charges a battery bank [170]. This rule is irrelevant in the case of a 100% RE system as the only medium to charge the battery bank is the surplus RE. However, for systems comprising a

battery bank and diesel generator, an additional aspect of system operation has to be considered and that is, whether and how the generator should charge the battery bank. The solution relates to the reliability of RE resources in subsequent hours.

Two simple dispatch strategies were studied to govern the operation of the generator and the battery bank: load-following (LF) and cycle-charging (CC). Under the LF strategy, a generator produces only enough power to meet the load demand, and never to charge the battery bank. Under the CC strategy, whenever a generator is needed, it operates at its maximum rated capacity, or as close as possible to reach the maximum efficiency, and charges the battery bank with the surplus power [421]. However, when the diesel is under LF, a minimum load ratio, such as 30%, should be set to ensure acceptable diesel generator efficiency, thus the excess power, after serving the net load, is charged into the battery bank to avoid energy waste. In this study, both strategies have been simulated and compared for the solar-wind-battery-diesel system, to find the more cost-effective one.

## **5.2 System modeling and constraints**

### **5.2.1 System modeling and components information**

The design and analysis of standalone microgrid RE systems can be challenging, due to the many design options and the uncertainty regarding key parameters. Based on a literature review, of the energy-modeling software available, HOMER's capabilities appear to provide the best option for modeling and investigating such scenarios [20]. Therefore, HOMER software is employed in this chapter for system simulation and optimization.

The main components of the system under study include the power generator, energy storage device, and inverter. The technical data and cost information of WT, diesel generator, battery, and inverter have been presented in Chapter 4. The PV module specification is presented in Section 4.1. The cost of PV modules fluctuates greatly depending on the market but has declined gradually in recent years. The initial capital cost was assumed as \$2.0/W<sub>p</sub>, including installation costs. The replacement cost is considered to be the same as the initial cost although, in this specific study, replacement cost is not relevant since the PV lifespan is assumed to be equal to the study period of 25 years. The operating and maintenance cost was assumed to be zero since it is negligibly small [13].

## 5.2.2 Constraints

The constraints include some technical parameters that control system operation and performance. A feasible system configuration must satisfy the specified constraints examined as follows:

### 5.2.2.1 Operating reserve

Operating reserve (also called spinning reserve) is the surplus power generation capacity required above the load. This safety margin, provided by the battery or diesel generator, can compensate for a sudden increase in the load or a sudden decrease in RE supply, so as to avoid outages. Operating reserve is defined as percentages of hourly load and renewable resources. In this study, 10% was specified for load reserve, 25% for PV power reserve and 50% for wind power reserve, as suggested by previous research [12, 13, 57, 408, 412, 422, 423]. The hourly operating reserve required for the system can be calculated as below:

$$\text{Operating reserve} = \%_L \times P_L + \%_{PV} \times P_{PV} + \%_{WT} \times P_{WT} \quad (5.1)$$

where  $\%_L$ ,  $\%_{PV}$ ,  $\%_{WT}$  is the percent of hourly load reserve, PV power output and wind power output reserve, respectively.  $P_L$ ,  $P_{PV}$ ,  $P_{WT}$  is the power required by the load and the power generated by PV and WT, respectively.

#### 5.2.2.2 Renewable fraction (RF)

The RF is only applied in the case of a hybrid RE system with backup diesel. The RE refers to the proportion of the system's total energy production generated by renewable power sources, such as WT and PV arrays, divided by the total energy production. The equation for renewable fraction is given below:

$$RF = \frac{E_{RE}}{E_{total}} \quad (5.2)$$

where  $E_{RE}$  is the RE electricity production and  $E_{total}$  is the total electricity production (kWh/yr).

The RF greatly influences the system configuration, economic performance and environmental benefits. The literature review given in Chapter 2 indicates that the effects of the RF are not widely reported. In this study, the minimum RF for the hybrid RE-diesel system is set at 90%. A sensitivity study was then conducted to examine the effects of RF values at 60%, 70% and 80%.

### 5.3 Overall results of the battery-based power generation options

#### 5.3.1 Overall results of the eight options

The categorized optimization results, based on the least net present cost (NPC) for eight different power generation options, are summarized and shown in Table 5.1. The results contain only those with a RF higher than 90% (does not apply to the diesel-

only and diesel-battery system), meaning that systems with renewable outputs lower than 90% of load were discarded, even though lower NPC values could be achieved. It is seen in Table 5.1 that each row represents an optimal system configuration, with the lowest NPC in that specified option. The first and second columns give the option serial numbers and system types. The next four columns show the required capacities of the PV array, WT, diesel and battery, followed by the dispatch optimal strategy for each system type. Some economic results, namely, the initial cost (IC), yearly operating cost, the total NPC and the levelized cost of energy (COE), are highlighted in the following five columns. The RF, annual diesel consumption and operating hours of the diesel generator are provided in the last three columns for the hybrid RE with a diesel generator.

Overall, the hybrid solar-wind-diesel-battery system (Option 1) with 95% RF was the most cost-effective, ranking the first in the table. This system consists of an 80 kWp PV array, 2 WTs and 48 batteries. The total NPC and COE was \$456,002 and \$0.391/kWh, respectively, much less than those for a 100% RE system (Option 3 and Option 4). The total diesel operating time was 637 hours and the fuel consumption was 2,414L during the simulated year. It is believed that implementation of this hybrid system with 95% RF on the island would be a good choice as the RE contribution is quite significant whilst GHG emission is not high.

The hybrid solar-diesel-battery system with 100 kW PV and 72 batteries was considered as the second choice for the island (Option 2). The NPC was \$538,887, about 18% higher than that of Option 1. The diesel consumption was also higher than that of Option 1, resulting in a RF at 91%. The results show that in such an option, a decrease in RF could lead to a reduced NPC. As there was no wind contribution, the capacities of the PV and battery bank were relatively higher than those of Option 1,

indicating that the complementary nature of solar and wind resource is beneficial for standalone RE systems.

To achieve a target of 100% RE, two approaches are feasible: solar-wind-battery system (Option 3) and solar-battery system (Option 4). The COEs of these two systems were \$0.595 and \$0.734, respectively. Compared with Option 1, these two system types both had a remarkably high PV array and battery bank capacity, hence a total NPC increase. They could be perfect choices of a total RE power generation system on the island since the RE is sustainable and environmentally-benign.

The wind-battery system could not ensure zero capacity shortage and 90% RF, although this target could be achieved by adding a diesel generator to form a wind-diesel-battery system (Option 5). This system was composed of 12 WTs, one diesel generator, 96 batteries and 5 converters. The dispatch strategy was also subjected to the LF. An IC of Option 5 (\$270,691) was the least among the first five options, but the operating cost was much higher than that of the other four options. Compared with Option 1, 5% decrease in RF could lead to almost double the diesel consumption.

Further down on the list are the diesel-battery (Option 6) and diesel-only (Option 7) systems without any RE contribution. The COE of the diesel-battery system was \$0.832, which had zero wasted energy because of the inclusion of batteries. For the diesel-only system, the IC was low, while the O&M cost was unreasonably high, occupying more than 80% of the total NPC due to high fuel consumption. The comparison between Option 6 and option 7 demonstrate that the deployment of a battery bank is more cost effective than increasing diesel consumption.

Table 5.1 Categorized options with lowest net present cost

Option No.	System type	PV (kW)	Wind turbine (unit)	Diesel generator (kW)	Battery (unit)	Converter (kW)	Dispatch strategy	Initial cost (\$)	Operating cost (\$)	Total NPC (\$)	COE (\$/kWh)	Renewable fraction (%)	Diesel (L)	Diesel operation (hour)
1	Solar-wind-diesel-battery	80	2	30	48	25	LF	324,539	10,284	456,002	0.391	95%	2,500	637
2	Solar-diesel-battery	100	-	30	72	25	LF	348,679	14,879	538,887	0.462	91%	5,065	1,288
3	Solar-wind-battery	145	2	-	168	30	-	608,932	6,585	693,114	0.595	100%	-	-
4	Solar-battery	240	-	-	168	30	-	783,072	5,655	855,365	0.734	100%	-	-
5	Wind-diesel-battery	-	12	30	96	25	LF	520,031	28,379	882,807	0.757	90%	7,344	1,591
6	Diesel-battery	-	-	30	24	15	-	60,807	71,133	970,131	0.832	-	33,443	4,648
7	Diesel-only	-	-	30	-	-	-	7,911	83,762	1,078,672	0.925	-	39,234	8,760
8	Solar-wind-diesel	140	10	30	-	25	-	586,891	39,707	1,094,478	0.938	90%	14,307	3,574

The last option was the solar-wind-diesel system without storage. Although this would achieve the same high RF of 90% as the Option 5 system, the diesel consumption was double. Because there is no storage device, up to 72.4% of the total energy production was dumped. In this sense, an energy storage subsystem is extremely important for RESs, particularly for those with high RE penetration.

All possible combination of the four technologies (solar, wind, diesel and battery) with a wide variety of system configurations were simulated but only the 8 options were compared and studied in detail. Solar-diesel, wind-diesel or wind-battery were not considered because they proved not feasible during simulation or they could not satisfy the necessary technical constraints such as operating reserve and renewable fraction.

### 5.3.2 Sensitivity analysis of the load demand

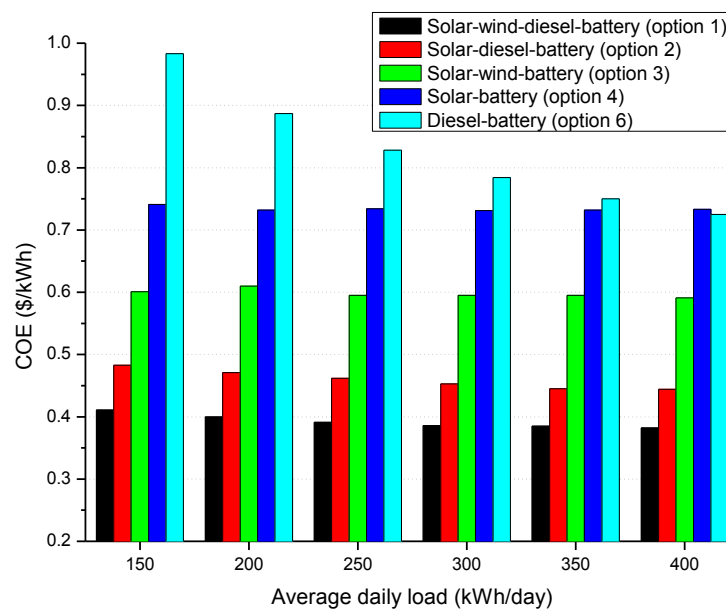


Fig. 5.4 Cost of energy of five power supply options versus load consumption

As stated in Chapter 3, the daily load consumption was assumed as 250kWh. To ensure an acceptable power supply margin for the island, a sensitivity analysis was performed to investigate the effects of load variation on system performance. Fig. 5.4 illustrates

the COEs of the five system options with load demands varying from 150 to 400 kWh. Overall, as load increases, the PV capacity, WT number, battery number, and converter size all gradually increase, while a downward COE trend is evident. Option 1 always had the lowest COE of the whole load range, indicating this option to be the most cost-effective. The solar-diesel-battery system, with 18% average increase in COE came second to Option 1. The 100% RE system (Option 3) ranked as third, with a COE of about 1.5 times that of Option 1. The solar-battery system type (Option 4) seems to be technically feasible, but the high capital cost made it not economically viable. Compared with Option 4, the hybrid solar-wind-battery system of Option 3 required less storage capacity and had lower COE values. Such benefits of the hybrid system became more significant as load demand increase. The diesel-battery system (Option 6) had high COEs under low load levels, but a decrease proportional with that load, to the extent that it was lower than that of Option 4 in which the load was 400kWh/day, indicating that a diesel power generation system may be comparable with a PV system when the load exceeds some threshold.

### 5.3.3 Sensitivity analysis of renewable energy resources

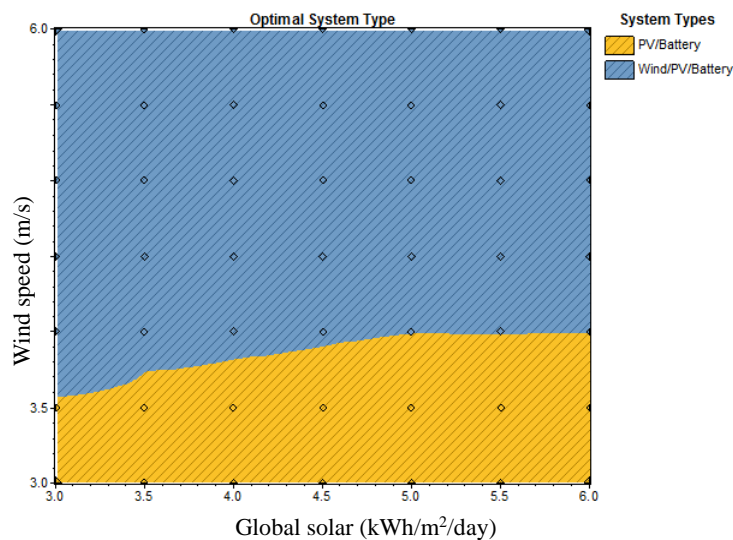


Fig. 5.5 Optimal system type against with solar radiation and wind speed

The impact of the available RE potential of the selection of a 100% RE system was also examined. The optimal system type graph under various solar radiation intensities and wind speeds is presented in Fig. 5.5. If the average wind speed is lower than 3.5m/s, the solar-battery systems provide the lowest COE, because the WT cannot start or else outputs little energy at such low wind speeds. For an average wind speed of between 3.5 and 4m/s, solar-wind-battery systems are cost effective for low solar radiation values and solar-battery systems for high solar radiation values. When the average wind speed is larger than 4m/s, it is more cost-effective to adopt a hybrid solar-wind-battery system.

### 5.3.4 Payback time

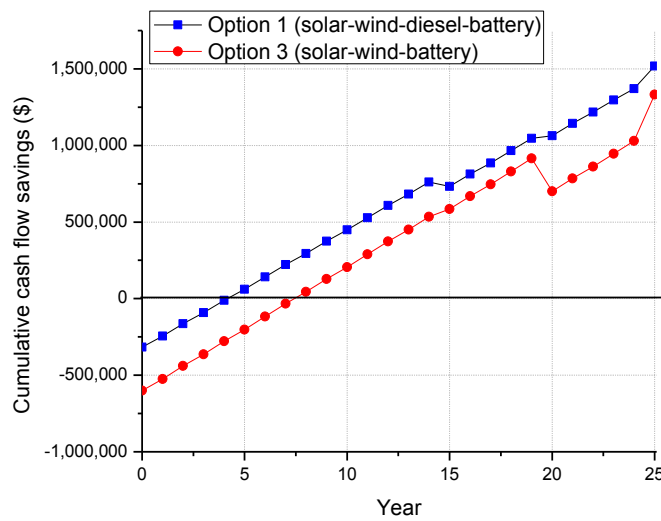


Fig. 5.6 Cumulative cash flow savings for the Option1 and Option 3 compared to diesel-only system

The payback time of Option 1 and Option 3 were studied. The summary of annual nominal cash flow savings of the two systems are given in Fig. 5.6. The cash flow of year 0 was negative as the initial costs of the two options greatly exceeded that of the diesel-only system (Option 7). From the year 1 onwards, the annualized savings were positive figures because the operating cost was less than that of a diesel-only system.

Between years 4 and 5, the cumulative cash savings of option 1 intersect the zero line and become positive. This implies the payback time of this option is 4.2 years, a similar result can be found in the studies [422, 424]. The payback time of Option 3 is a little longer at 7.3 years as it is a 100% RE system. When the replacement of the system component was due, an obvious increase in nominal cash flow would occur and thus the net saving might be negative in such a year. A significant decrease in cumulative cash flow of Option 3, for example, can be seen in the year 20, due to the replacement of the battery bank. Similarly, the obvious increase in cumulative cash flow at the end of the project (year 25) results from the positive salvage value of system components.

## **5.4 Simulation performance of a 100% RE system**

Simulation results show that the optimal configuration of the 100% RE system, i.e. solar-wind-battery system, comprises PV array (145 kW), WT (2 units, 10.4 kW), battery bank (144 units, 6 stings, totally 706 kWh) and converter (6 units, 30 kW). The performance of this optimal system is discussed in the following sections with detailed analysis. A sensitivity analysis on the key parameters is then conducted to identify their impact on the results.

### **5.4.1 Simulation performance of system components**

A summary of operating performance and some economic results of PV, WT and battery bank is presented in Table 5.2. It can be seen that the PV array and WT capacity factors are relatively low due to large amounts of wasted energy. The levelized costs for the PV and WT were \$0.128 and \$0.2 per kWh, respectively. The energy cost for the battery bank was zero because the only charging source is the surplus power from PV and WT. However, battery wear cost of \$0.174/kWh was significantly high,

accounting for approximately 30% of the COE. The battery cost was even higher than that of the PV module. This could explain why, in some cases, the end-users might cut down or discard the energy storage devices and introduce more RE generators. Such an approach, however, is likely to result in a substantial waste of energy.

Table 5.2 Components operating performances of solar-wind-battery during the simulated year

Parameters	Data	Units	Parameters	Data	Units
<b>1. PV</b>			<b>3. Battery</b>		
Rated capacity	145	kW	Batteries number	144	
Mean output	20	kW	Strings in parallel	6	
Capacity factor	14	%	Usable nominal capacity	605	kWh
Total production	177,882	kWh/yr	Autonomy	58.1	hr
Hours of operation	4,392	hr/yr	Lifetime throughput	1,468,224	kWh
Levelized cost	0.128	\$/kWh	Energy in	37,829	kWh/yr
<b>2. Wind</b>			Energy out	32,561	kWh/yr
Total rated capacity	10.4	kW	Battery wear cost	0.174	\$/kWh
Mean output	3.4	kW	Expected life	20	year
Capacity factor	32.5	%			
Hours of operation	7,688	hr/yr			
Total production	29,584	kWh/yr			
Levelized cost	0.2	\$/kWh			

The monthly mean electricity production from PV array and WTs is presented in Fig. 5.7. It is noted that solar production predominated, providing almost 84% of the total production during the simulation year. The PV output was extremely high in the summer months from July to October. This is a favorable characteristic since electricity demand is strong in the summer due to the high cooling load demand. In

contrast, wind energy contribution was found to be significant in January, April and September but less in other months.

The simulation results for the battery bank SOC are presented in Fig. 5.8. SOC values between 90% and 100% existed for approximately 74% of the time, and more than 90% of the time witnessed the SOC values higher than 80%, indicating that the battery bank was only used in “shallow” fashion for most of the time. In only two months high depth of discharge occurred: the lowest SOC values appeared in March and August at 35% and 30%. This can be explained by relatively poor RE availability in March and a high cooling load in August. Thus there must be sufficient battery bank capacity to supplement the energy supply during those two months, to ensure a continuous power supply.

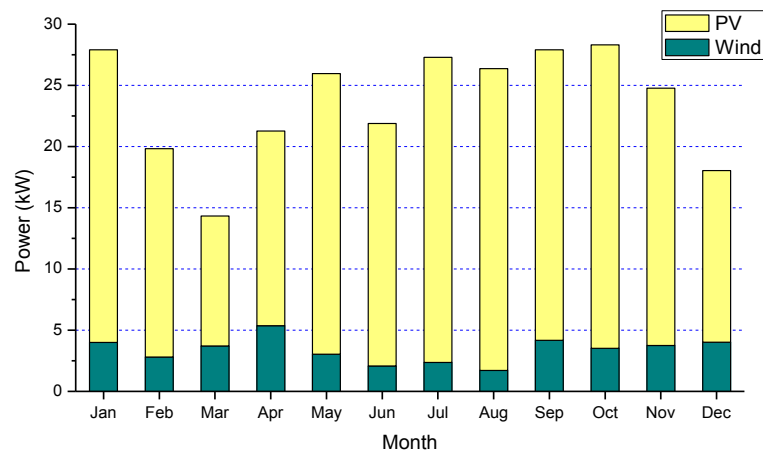


Fig. 5.7 Daily mean powered generated by PV and wind in different months

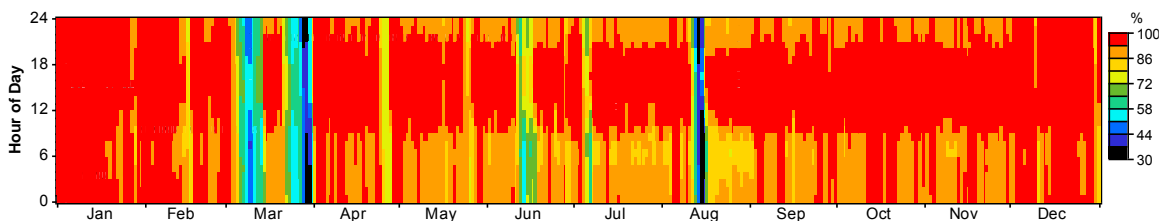


Fig. 5.8 rainbow profile of battery bank SOC during the simulated year

### 5.4.2 Total cost break-down

The cash flow break-down by components and cost type is shown in Fig. 5.9. The IC and NPC of the above system were \$608,932 and \$693,114, respectively. The corresponding COE was \$0.595/kWh, approximately three times of the current electrical tariff in Hong Kong [314, 425]. However, it is still considered as a cost-effective solution in comparison with the diesel generator or grid extension by submarine cables and overhead lines.

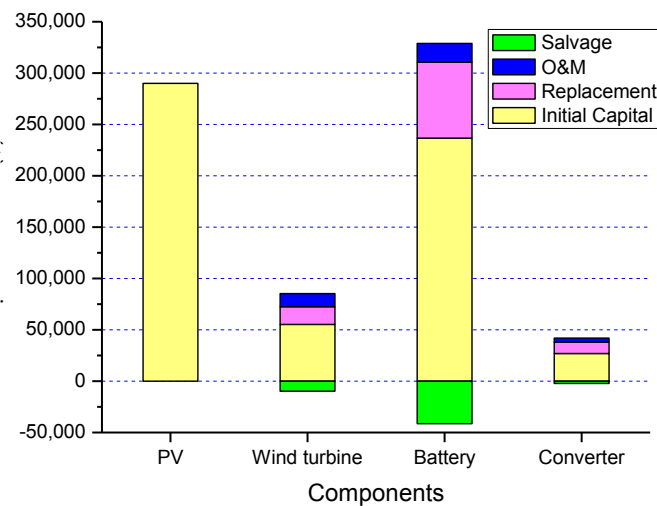


Fig. 5.9 Cash flow break-down by components and cost type

The breakdown of the total NPC shows that about half is shared by the battery bank, indicating that the cost of energy storage in a stand-alone hybrid RE system is dominant. The cost of the PV array, IC only, accounted for 36% of the total NPC, followed by the WT, which takes up approximately 10%. The least cost item is the converter, at 5% of the total NPC.

### 5.4.3 Hourly simulation results

An example of the hourly simulation results during four consecutive days is illustrated in Fig. 5.10. The red line of the hollow circles and the blue line of the hollow diamonds

display the respective PV and WT outputs. Usually the wind energy resource was excessive late at night and during the early morning hours. Surplus solar energy was typically available during the middle of the day. The black line illustrates the load profile for this island. After serving the load, the excess electricity was used to charge the battery bank. The top violet line illustrates the battery SOC and indicates the amount of energy stored in the battery bank. If the excess electricity was more than enough to fully charge the battery bank, the surplus was then fed into the dump load, represented by the green line of hollow triangles.

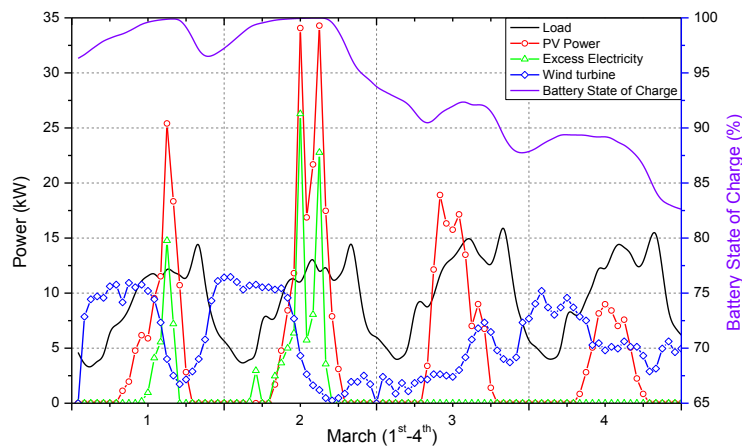


Fig. 5.10 Hourly sample simulation results for four consecutive days (1<sup>st</sup> to 4<sup>th</sup> March)

During 1<sup>st</sup> and 2<sup>nd</sup> March, the solar and wind resources were good and able to cater for the demand. Thus excessive power was produced in the afternoon. It was noticed that for some hours the surplus energy was not fully transferred to the battery bank even though its SOC had not reached a 100% level. This is because it is limited by the maximum allowable charging rate and current of the selected battery. The SOC is also dependent on the recent charging and discharging history of the batteries, which is the basic principle of the kinetic battery model [407]. The battery bank was periodically charged or discharged during the first two days, while the SOC values dropped during

the third and fourth day due to poor solar radiation. It was found that the lowest value of 82% occurred on the fourth day, but was still much higher than the allowable minimum SOC.

#### 5.4.4 The effects of PV, wind turbine, battery capacity on simulation results

The effect of variation in PV capacity and battery number on the total NPC is shown in Fig. 5.11. The WT and converter were fixed at 2 units and 30kW, respectively. The results indicate that an increase in PV capacity can reduce the battery bank size, while only the optimal system configuration chosen in the study has the lowest NPC.

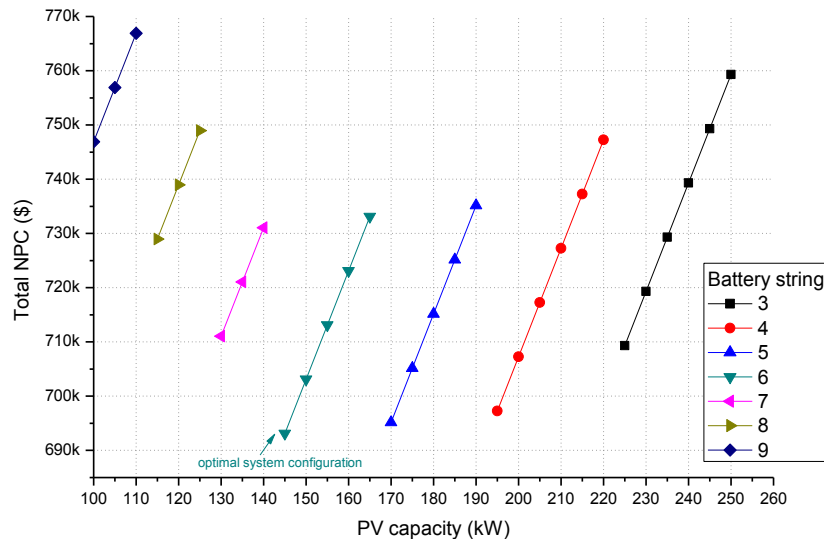


Fig. 5.11 The effect of PV capacity and battery string number on total NPC

Fig. 5.12 demonstrates how PV capacity, number of battery strings, total NPC, and excess electricity produced vary with the number of WTs. It can be seen that if no WTs are installed, the PV-only system (Option 4) has an extremely high PV capacity (240kW) with 6 strings of batteries. The system would be very expensive, with a COE at \$0.734. In addition the dumped energy is also high. The system with two WTs is considered to be the optimal system type (Option 3) because it has the lowest cost and lowest dumped electricity. The PV size was reduced to a reasonable value for this

option. As the WT number increases, the battery bank can be reduced but the system cost and dumped electricity each grow gradually.

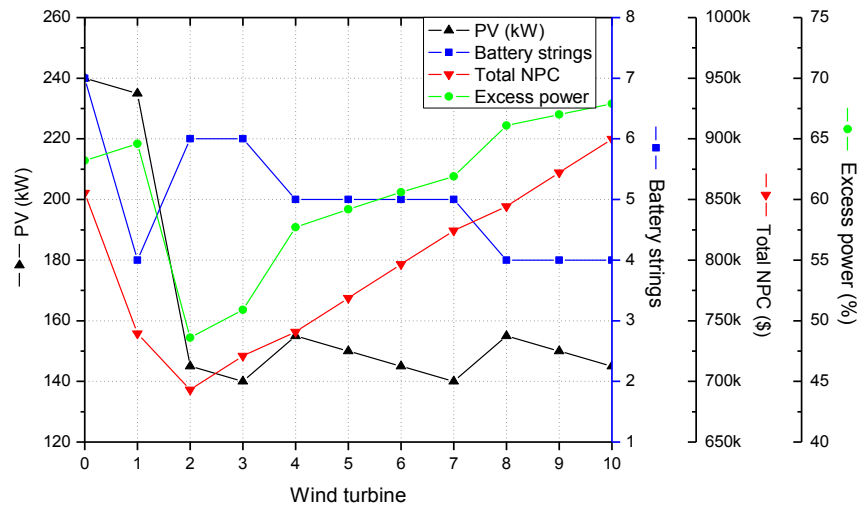


Fig. 5.12 PV, battery, NPV and excess power versus WT number

### 5.5 Simulation performance of a RE system with backup DG

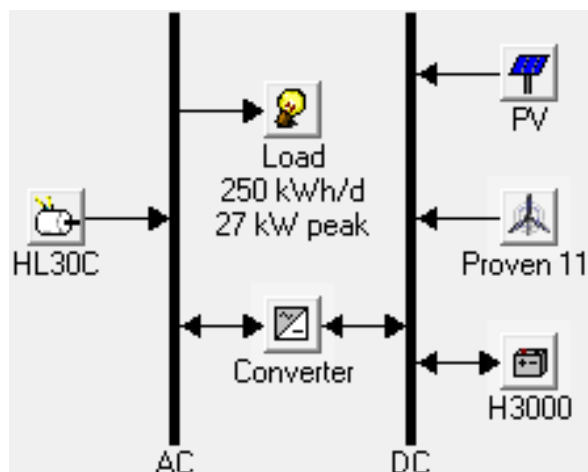


Fig. 5.13 System diagram of the hybrid solar-wind-diesel-battery system developed in HOMER

Renewable and non-renewable energy sources have remarkably different economic characteristics. The high initial capital cost possibly is still the biggest barrier to RE, while the diesel generator tends to have high operating cost. Therefore, a trade-off

between RE and diesel should be carefully considered with respect to the technical feasibility, economical cost, and environmental impact. In this section, the hybrid solar-wind-diesel-battery system (Option 1) was selected to study the hybrid RE with diesel system in detail.

The system diagram of the hybrid solar-wind-diesel system with the battery developed in HOMER is shown in Fig. 5.13. The system comprised 80 kW PV panels, 2 WTs, 1 diesel (30kW), 2 battery strings (288 kWh) and 5 converters (25kW). The total NPC and COE for this system are \$456,002 and \$0.391/kWh, respectively.

### **5.5.1 Simulation performance of system components**

The simulation results for the main components are presented in Table 5.3, including the rated capacity, power production, hours of operation, capacity factor, levelized cost and other parameters.

The monthly mean electricity production from the PV array, WTs and the diesel generator are presented in Fig. 5.14. Compared with Option 3 in Section 5.4, the PV output was still the dominating component, accounting for about 73% of total production during the simulation year, followed by the wind output (22%). The electricity provided by the diesel was only 5%, thereby resulting in a RF at 95%.

For Option 1, only 48 batteries with 19.4 hours of autonomy were required because the diesel could be used to cover the peak load in the period of continuously poor weather. The storage capacity is only one third of the 100% RE system in Option 3. Therefore, the cost of energy storage is significantly reduced. However, the lifetime of the batteries in this option, 14.6 years, was shorter than that of option 3 (20 years), as they were cycled more frequently in the hybrid system.

Table 5.3 Components of operating performance for the solar-wind-diesel-battery system (option 1)

Parameters	Data	Units	Parameters	Data	Units
<b>1. PV</b>			Fuel consumption	2,500	L/yr
Rated capacity	80	kW	Specific fuel consumption	0.408	L/kWh
Mean output	11.2	kW	Mean electrical efficiency	24.9	%
Capacity factor	14	%	Electrical production	6,120	kWh/yr
Total production	98,142	kWh/yr	Operational life	23.5	yr
Hours of operation	4,392	hr/yr	Fixed generation cost	4	\$/hr
Levelized cost	0.128	\$/kWh	Marginal generation cost	0.473	\$/kWh
<b>2. Wind</b>			<b>4. Battery</b>		
Total rated capacity	10.4	kW	Batteries number	48	
Mean output	3.4	kW	Strings in parallel	2	
Capacity factor	32.5	%	Usable nominal capacity	288	kWh
Hours of operation	7,688	hr/yr	Autonomy	19.4	hr
Total production	29,584	kWh/yr	Lifetime throughput	489,408	kWh
Levelized cost	0.2	\$/kWh	Energy in	35,897	kWh/yr
<b>3. Diesel generator</b>			Energy out	30,988	kWh/yr
Total rated capacity	30	kW	Battery wear cost	0.174	\$/kWh
Hours of operation	637	hr/yr	Expected life	14.6	year

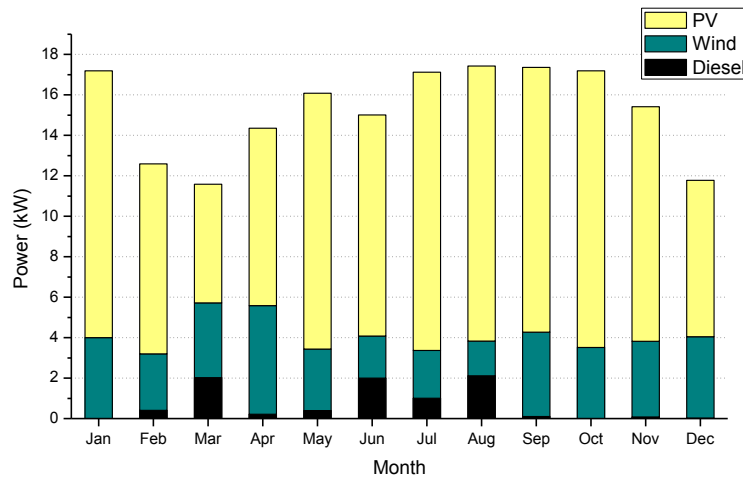


Fig. 5.14 Hourly mean power generated by PV, wind and diesel by month

The battery bank's SOC distribution is presented in Fig. 5.15. The SOC distributions in Option 1 and Option 3 were distinctly different. In Option 1, the SOC values at the two extremes were very high. SOC values from 95% to 100% were achieved for 16% of the time period, followed by the SOC values from 30% to 35%. The battery bank hourly SOC profile illustrates that some hours in March, June and August reached the maximum depth of discharge. The main reason for this phenomenon seems to be the relatively poor availability of RE resources in March and June, and high cooling loads from June to August. It can also be inferred that the diesel generator operates frequently during those three months in order to meet the energy shortage, proved in Fig. 5.14.

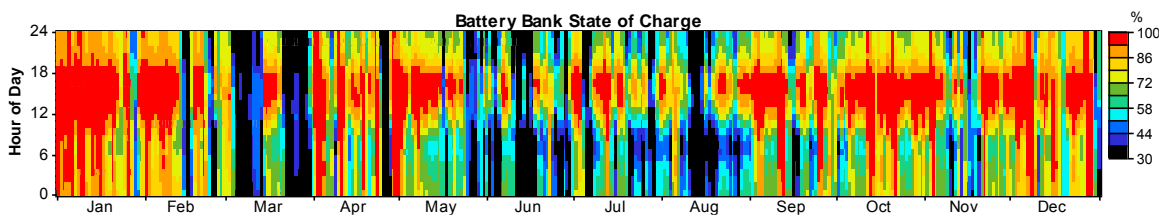


Fig. 5.15 Coarse rainbow profile of battery bank state of charge during the simulated year

### 5.5.2 Total cost break-down

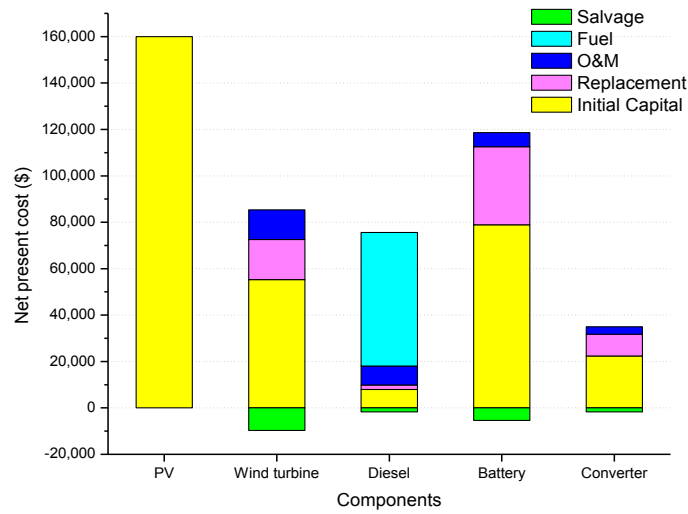


Fig. 5.16 Cash flow break-down by components and cost type

The total NPC of the optimal system configuration in Option 1 was \$456,002, much less than that of the 100% RE system in Option 3 (\$693,114). The corresponding levelized COE was only \$0.391. As shown in Fig. 5.16, the PV system costs account for the major share at 35% of the total NPC, followed by the battery and WT cost. The diesel generation cost takes up 16.2% of the total NPC due to high fuel cost, while diesel only contributed 5% of the energy supply.

### 5.5.3 Energy flow or energy balance analysis

Fig. 5.17 summarizes the energy flow for Option 1. 5% of the total energy production was contributed by the diesel generator, and the rest was by the PV array (73%) and the WTs (22%). However, 21% of total production was surplus to demand and had to be dumped. If more batteries were to be employed, the surplus energy would drop but the total NPC would increase. Battery and converter losses took up 14% of the total energy used.

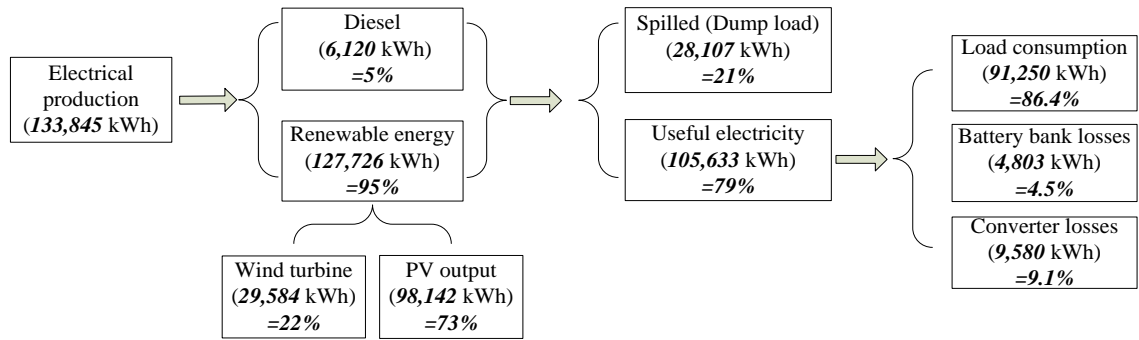


Fig. 5.17 Summary of the energy flow during the simulated year

### 5.5.4 Hourly simulation results

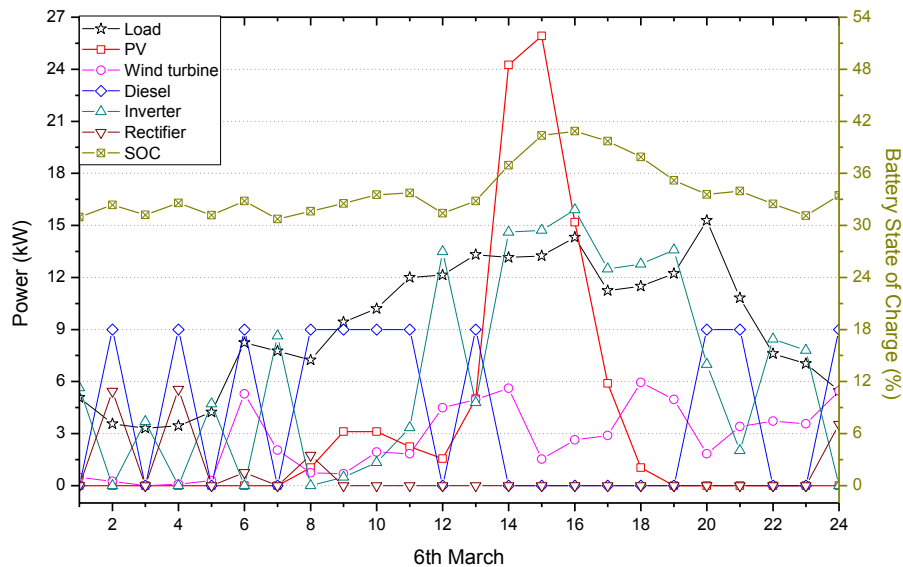


Fig. 5.18 Hourly sample simulation results on 6<sup>th</sup> March

The hourly simulation result on 6<sup>th</sup> March of the year is illustrated in Fig. 5.18. At 4:00am, for example, the PV output was zero and wind output only 0.086 kW. To cater for the load of 3.488kW, the diesel generator operated at its minimum load ratio of 30% (9kW). The AC output from the diesel generator was sufficient to meet the load, thus the surplus power (5.552 kW) was delivered into the battery bank through the rectifier. The DC wind output was also in excess and directly charged into the battery bank. Therefore, the total input power to the battery bank (5.083kW) was the sum of the

rectifier output (4.997kW) and entire WT output (0.086kW). During the next hour, beginning at 5:00am, the energy stored in the battery bank and wind output was able to meet the load of 4.24 kW. To do this, the power input into the inverter should be equal to 4.711kW DC, contributed by the wind turbine (0.286 kW) and battery discharge (4.425kW). In summary, with the aid of the diesel generator, no energy shortfall and wastage occurred on that day.

### **5.5.5 Renewable fraction**

Based on the overall results, in the following case, the cost of a 100% RE system is less than that of a diesel power generation system as a result of the high diesel price. Therefore, the greater the RE contribution, the less expensive the energy supply. However, the inclusion of diesel to serve periods of peak load and poor RE resources availability, can avoid the need to provide excessively large RE generation and storage capacity, thus a hybrid RE with diesel system is a more economically viable option, even with high fuel costs. In this study, sensitivity to minimum RF was explored by testing of the inclusion of RF values of between 50% and 100%. The simulations show that the RF at 95% is the most cost-effective. Intermittent running of the diesel generator not only greatly cuts down the capacity of the PV and WT installations but also significantly reduces overall system costs and wasted energy.

### **5.5.6 Dispatch strategy**

The cost-based dispatch logic, based on the fixed and marginal cost of energy, explains how to choose the cheapest dispatch source between the battery bank and diesel. Fig. 5.19 presents the cost of the battery bank and diesel generator with two fuel prices. The fuel price of \$1.8/L is the price in Hong Kong. The price at \$0.1/L [34] in Saudi Arabia was adopted for comparison.

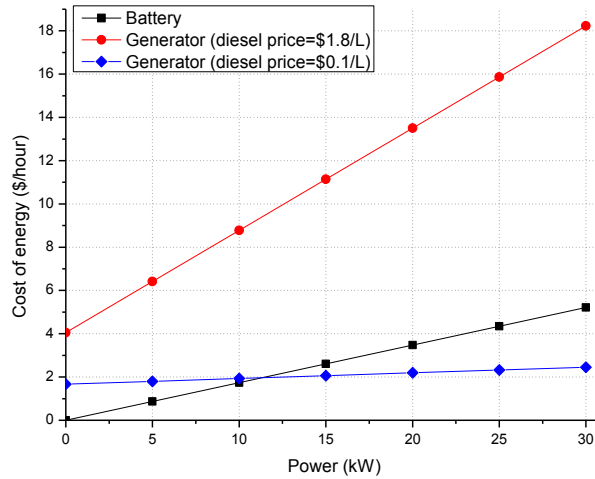


Fig. 5.19 Cost comparisons of battery and diesel generator for different fuel prices

As presented in Fig. 5.19, the diesel's marginal cost of energy (line slope) (\$0.473/kWh) is much higher than the battery cost (\$0.174/kWh) in Hong Kong, and thus the difference between them grows with power increase, indicating that the LF strategy should be employed as the cost of diesel for charging the battery is much higher than the cost of enlarging the battery bank. Although the LF strategy was adopted in for the hybrid system, the excess electricity from diesel was charged into the battery bank only when the diesel was under the minimum load ratio of 30% to avoid wasting energy. No excess electricity was generated by the diesel under high load ratios as the total energy produced was used to serve the load. For the system in Option 1: over the simulation period, 573kWh of electricity, about 9.4% of the total 6,120 kWh of diesel generated power, was in excess and stored in the battery bank.

For a fuel price of \$0.1/L, the diesel's fixed cost was \$1.67/h (the intercept of cost line). The marginal cost was \$0.026/kWh, much lower than that of the battery. Therefore, the cost lines of the battery bank and diesel crossed at the power of 11.3 kW, which means that if the net load was less than 11.3kW, the batteries would be cheaper for supplying the load; otherwise, the diesel would be chosen to supply the

net load, even if the battery bank was capable of serving the load. However, the dispatch strategy not only depends on the cost of energy but also on the minimum RF. If the minimum RF was set at 90%, the LF strategy would be the only suitable method. If there was no RF limitation, the CC strategy would be better when net load is greater than 11.3kW.

### 5.5.7 The effect of diesel price

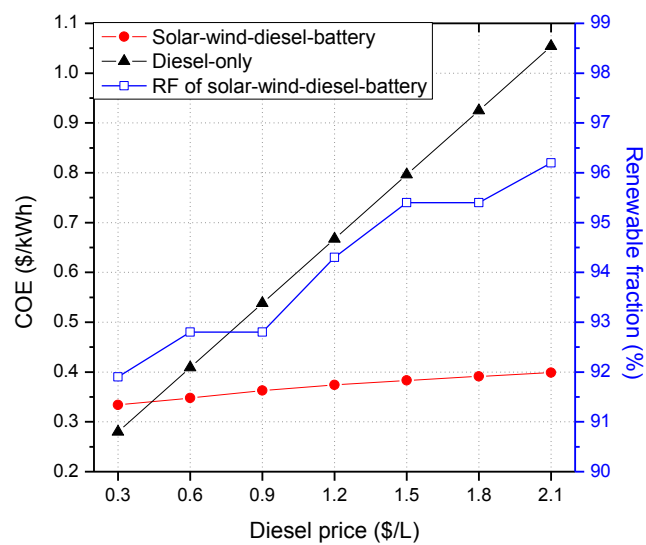


Fig. 5.20 COE of two systems types against with diesel price

The COE comparison between Option 1 and Option 7 (diesel-only) was made for different diesel prices from \$0.3/L to \$2.1/L (Fig. 5.20). The COE for Option 1 intersects that for Option 7 at the lower diesel prices of between \$0.3/L to \$0.6/L, indicating that Option 7 might be economically feasible for those areas with a low diesel price, providing the environmental impacts are not taken into account. The COEs for the two options increase in proportion to the increase of diesel price, but the growth trend for Option 7 is much greater than that for Option 3. When the diesel price reaches \$2.1/L, the COE of Option 7 can be 2.6 times that of Option 3. It is obvious that further increase in diesel price can enhance the cost effectiveness of the hybrid

RE with diesel when compared with that of a diesel only system. In addition, the RE of Option 1 grows, i.e. tending to use more RE, as diesel price increases.

### 5.5.8 The effect of PV, number of WT and battery capacities on the result of Option 3

As a final remark, an attempt was made to study the effects of changing the key variables on the simulation results of Option 1. Fig. 5.21a illustrates that, for the majority of systems, the optimal battery string number is two. Excluding two infeasible configurations, the COE values are in the range of \$0.39-\$0.50/kWh (Fig. 5.21b) and diesel consumption from 768 to 4,872 L/year (Fig. 5.21c). The majority of diesel consumption is less than 2000L.

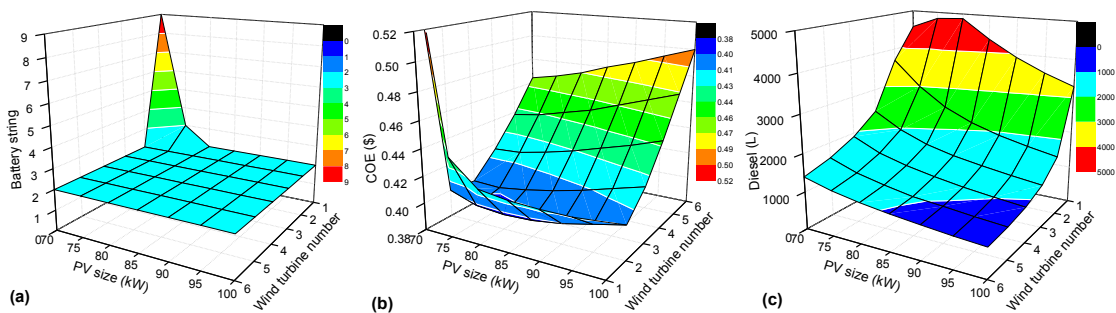


Fig. 5.21 The optimal system configuration versus PV size and WT number in Option 1: (a) optimal string of batteries; (b) COE values and (c) diesel consumption. Similarly, the optimal number of WTs against variation of PV and battery bank sizes is presented in Fig. 5.22a. In most cases, the optimal WT number is 2, a number which is also proved by Fig. 5.22b. With the optimal WT number, the effects of battery bank and PV capacity on COE are displayed in Fig. 5.22b, indicating that the results are more sensitive to battery bank size than PV size. Diesel consumption with this optimal WT number fluctuates greatly with variations in PV array size and battery capacity (Fig. 5.22c).

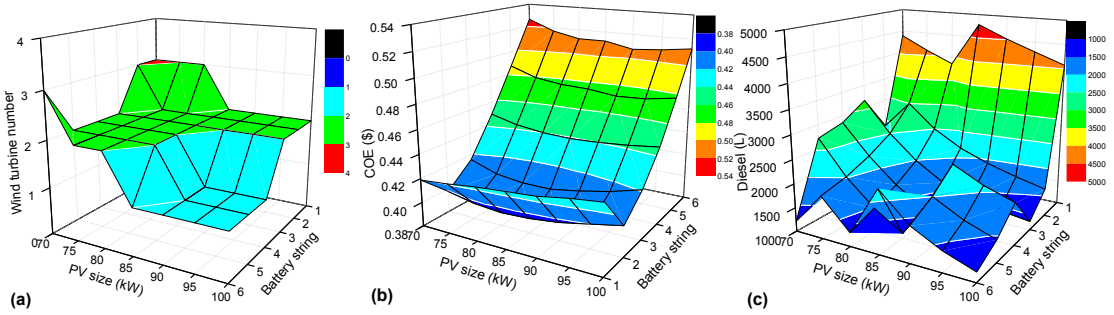


Fig. 5.22 The optimal system configuration versus PV size and battery strings in Option 1: (a) optimal WT number; (b) COE values; (c) diesel consumption

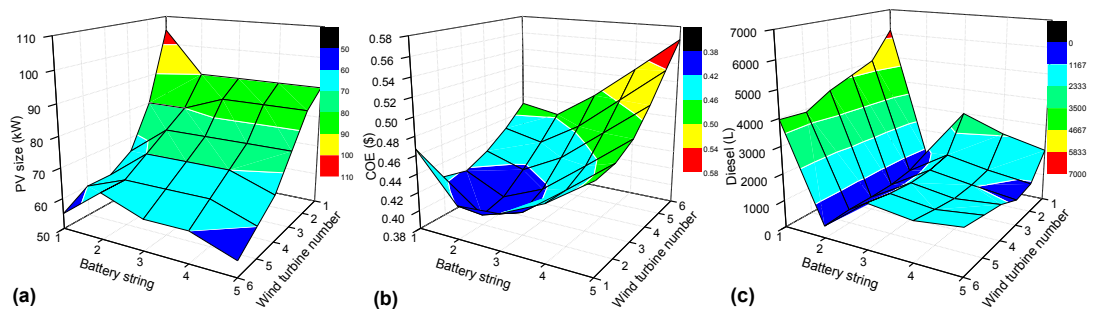


Fig. 5.23 The optimal system configuration versus WT number and battery strings in Option 1: (a) optimal PV size; (b) COE values; (c) diesel consumption

Finally, the optimal PV array capacity in relation to variations in the number of WTs and battery bank size was studied, and the results are presented in Fig. 5.23. For the system with one WT and one battery string, the optimal PV size is 105kW, and the corresponding diesel consumption is extremely high, 6148L/year (91% RF), and the COE is \$0.467/kWh. With increase in WT, the PV sizes decrease gradually, whereas the COE and diesel consumption remain largely unchanged.

In summary, sensitivity analysis of PV capacity, the number of WT and battery systems show that the system configuration under study (i.e. 80 kW PV, 2 WTs and 2 battery strings) is the optimal one.

## 5.6 Summary of this chapter

In this study, eight battery storage based power generation options were investigated for the Town Island from the techno-economic point of view. Two options are fully examined and analysed. Based on the simulation results, the following conclusions are drawn:

- The simulation results of Option 3 (solar-wind-battery) show that the island could be powered by a 100% RE system. The combination of solar energy, wind energy and battery storage can supply a continuous power to this island. The optimal configuration is capable of saving a large amount of diesel and greatly reducing GHG. This fully renewable power generation with battery storage could be an ideal solution from the point of view of environmental conservation and the energy provision. However, the cost of energy may be much higher than the electricity tariff. With expected continuing rapid development in the renewable energy industry and upgrades in storage technology, the system's cost should be reduced and hence off-grid RESs sited in remote places could be more promisingly evident.
- The introduction of a diesel generator into the RE system can make the hybrid system (Option 1: solar-wind-diesel-battery) more economically viable, particularly for those areas experiencing low diesel cost. The solution, a compromise between RE and diesel generation, has great potential to replace the existing diesel generators on the island, as this solution provides a reasonable COE value and high RE fraction (95%). The COE and payback time for this option would be much lower than those of a fully renewable energy system described in Option 3. The generator is scheduled only to assist the RE generator to cater for peak loads, thus little diesel is consumed, and a higher RE penetration level is still

able to be guaranteed. However, such systems will emit GHG due to the 5% energy diesel contributed, making this system type not so favourable.

- The diesel-only and diesel-battery systems not only provide the highest COE but emit massive GHG amounts every year. This could cause environmental problems from a long-term perspective. Therefore, the option of diesel should be abandoned. The addition of a battery bank is recommended if the diesel system has to be applied.

In summary, the study demonstrates that the existing diesel generation system on this island could be fully replaced by a 100% renewable energy power generation system, and the addition of a back-up diesel generator makes the hybrid energy system a more economically viable option. It can be expected that in the near future the transition from diesel to high renewable energy penetration will be increasingly popular in remote areas for power generation.

It is believed that the outcome of this study could serve as a starting point for the design of a renewable energy system on the island. The methodology of this study can also be viewed as a benchmark for planning and sizing hybrid renewable systems suitable for other similar remote areas.

# **CHAPTER 6 DEVELOPMENT OF PUMPED STORAGE BASED-RENEWABLE ENERGY SYSTEMS**

The battery-based renewable energy system is widely used for remote areas. However, some barriers concerning batteries, for example high costs and negative environmental impacts, limit wider usage and future applications. The pumped hydro storage is introduced in this chapter, as an alternative to support standalone microgrid RE systems. This technology provides a new energy storage solution to serve intermittent solar and wind energy systems in remote areas where there is no access to the utility grid.

A novel operating principle for the pumped storage-based RE system has been developed, and the initial design process is presented below. The performance of the system was simulated hour-by-hour throughout a complete year. The genetic algorithm, along with the Pareto optimality concept, was used for system techno-economic optimization, to maximize power supply reliability and minimize system cost. A case study based on Town Island research project was made, using the method developed and the proposed system. The optimized system configuration under zero loss of power supply probability (LPSP) was examined. In addition, the system performances of hybrid solar-wind, solar-only and wind-only systems with pumped storage for LPSP values from 0 to 5% were investigated and compared. Sensitivity analysis in relation to several key parameters, such as load demand and renewable energy cost, was also performed to examine their effects on system performance.

## 6.1 System configuration and operation principle

### 6.1.1 Pumped storage-based renewable energy systems

As illustrated in Fig. 6.1, the hybrid solar and wind system with pumped storage is equipped with a PV array, wind turbine (WT), pumped hydro storage, an end-user and a control station.

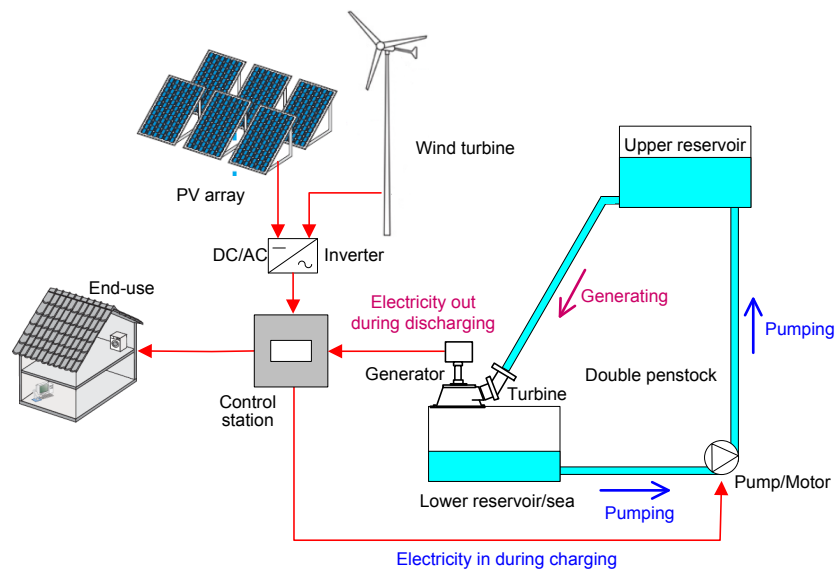


Fig. 6.1 System schematic of a hybrid solar-wind system with pumped storage system

The locally available solar energy matches well with the load demand, so it is reasonable to use solar panels to convert sunlight to generate power in the daytime. The WTs usually produce more power at night and on rainy days. Therefore, this complementary characteristic of solar and wind energy can reduce not only the installed capacity of the renewable generator but also the amount of energy storage needed. An inverter transforms the output DC to 220V AC supply load via the power distribution network. Any surplus power is used to pump water to a high elevation reservoir. A pump-turbine set, converting renewable electrical energy into mechanical energy and vice versa. In this system, there are two separate penstocks, one only used

for pumping water and the other only for generating electricity. The two processes, therefore, charging and discharging, can occur simultaneously [257]. This double-penstock system is popularly used because it makes easier the stabilization of power voltage and frequency.

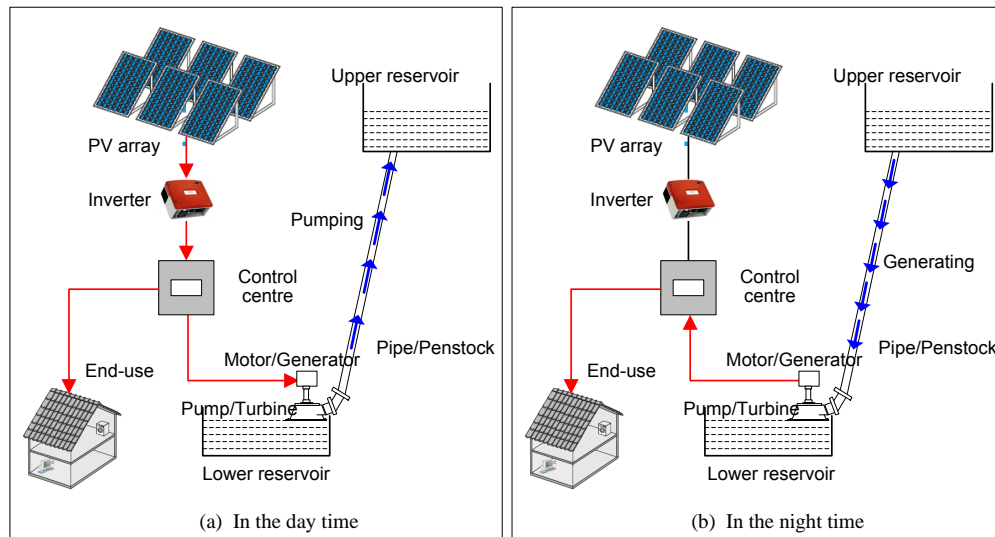


Fig. 6.2 System schematic of a pumped storage-based PV power generation system

Similarly, a stand-alone solar PV system with pumped storage is presented in Fig. 6.2 as appropriate for areas lacking sufficient wind energy. The pumped storage as shown is a simpler and single-penstock system, but it is unable to charge and discharge power at the same time.

The systems of Fig. 6.1 and Fig. 6.2 are isolated from the utility grid, and hence called standalone systems, designed for remote areas where utility extension is either overly expensive or impossible. The whole microgrid system in a standalone mode is managed by a control centre, an essential element for load management and energy distribution.

The pumped storage-based RE system can be fully integrated with natural conditions because it can make use of local streams and collect rain water in the UR. In this way,

some of the evaporation and leakage in the UR can be offset. Therefore, the discharging of water through a turbine mode relies on a combination of the water previously pumped to UR and collected rain water/natural inflow, while the charging mode relies only on the sea water [292].

### **6.1.2 Operation principle**

The pumped storage subsystem plays an important role in shifting energy surpluses, mitigating the intermittency of RE sources, and also in balancing fluctuations in supply and demand. The operating principle of the system is given briefly as follows. During the charging/pumping mode, the pumped storage system is based on two vertically-separated water reservoirs. The pump elevates water from the lower reservoir (sea or river or an artificial pool) to the UR using excess RE output after meeting the load. During the discharging/generating mode, the stored water flows down to the lower reservoir, enabling the production of electricity as a result of passing through a turbine/generator unit. This occurs during periods of high electrical demand whenever there is insufficient renewable energy production.

In such a manner, a sustainable and continuous power supply can be guaranteed throughout the 24 hours of a day, and the potential environmental problems due to the use of batteries can be avoided, although the cyclic processes will suffer from some conversion losses. Pumped storage, therefore, is ideal for integrating intermittent RE supplies, and is an environmentally favourable alternative to batteries, especially for stand-alone applications.



where  $P_{PV}$  and  $P_{WT}$  are the power generated by a single PV panel and a specified wind turbine, respectively;  $N_{PV}$  and  $N_{WT}$  represent the number of PV panels and wind turbines employed.

Therefore, the total generated and required energy over a period  $T$  can be written in terms of the generated solar/wind power  $E_{gen}$  and the load demand  $E_{dem}$  as follows:

$$E_{gen} = \sum_{t=1}^T (N_{PV} P_{PV} + N_{WT} P_{WT}) \cdot t \quad (6.2)$$

$$E_{dem} = \sum_{t=1}^T P_{dem} \cdot t \quad (6.3)$$

where  $T$  is the total time period, and  $t$  is the time interval between the successive samples taken, which in this case is one hour.

#### 6.2.2.1 The initial value of PV panels and wind turbine number

In the proposed system, solar panels and the wind turbines are seen as an integrated power generator supplying the load. The average power obtained from the power generator should be larger than the average load power required, i.e.

$$\overline{P_{gen}} \geq \overline{P_{dem}} \quad (6.4)$$

Therefore the combination of the required number of solar panels and wind turbines can be calculated. As wind turbine numbers change from 0 to 10, the corresponding PV panel numbers are determined.

### 6.2.2.2 The initial upper reservoir volume

It was observed in the literature [259] that the most significant variables in the design of pumped hydro systems are the volume of the upper reservoir and the height difference between the upper and lower reservoirs. In the current study, the height difference was fixed at 60 m based on the geography of the island concerned. The sea provided the lower reservoir. Only the volume of the upper reservoir, therefore, had to be initially determined.

In order for a generated electricity load to balance over a given period of time, the curve of  $\Delta E$  over that time must average at least zero. Note that positive values of  $\Delta E$  indicate the availability of surplus power, and negative  $\Delta E$  indicates a shortage of generated power. An equation relating energy to  $\Delta E$  can be obtained by integrating  $\Delta P$  :

$$\Delta E = \int \Delta P dt = E_{gen} - E_{dem} \quad (6.5)$$

The energy curve of Eq. (6.5) can be used to find the initial volume of the UR  $V_{UR}$ . On an average day, the pump and turbine are required to cycle between the positive and negative peaks of the energy curve. Therefore, the UR in the pumped storage system should have a capacity at least equal to the difference between the positive and negative peaks of the energy curve.

$$E_{PHS} \geq \text{Max}(\int \Delta p dt) - \text{Min}(\int \Delta p dt) \quad (6.6)$$

Hence, the required volume of the upper reservoir can initially be calculated:

$$V_{UR} = \frac{E_{PHS}}{\eta_t \rho g h} \quad (6.7)$$

where  $\eta_t$  is the efficiency of turbine (%),  $\rho$  is the density of water ( $\text{kg/m}^3$ );  $V_{UR}$  is the volume of the upper water reservoir ( $\text{m}^3$ );  $g$  is the gravitational acceleration ( $9.81 \text{ m/s}^2$ );  $h$  is the total head (m).

### **6.2.3 Simulation and optimization**

The simulation study was performed using a one hour time-step and for one whole year's duration. The hourly interval is sufficiently small to model the intermittency of the RE resources and fluctuating electrical load with fair accuracy, yet not too small to require an excessive increase in the computation complexity. Thus, the design simulation process will be practical.

#### *6.2.3.1 Rationale for system optimization*

Standalone autonomous RE systems are usually unreliable power sources due to the intermittent nature of weather conditions. A combination of RE generation and energy storage, however, can provide reliable and sustainable energy autonomy for remote areas. However, the combination should be optimized to ensure that the load can be met at all times, as well as to balance between generator and storage capacities [426].

If a large pumped storage system is used and the RE generation system is underdesigned, the upper water reservoir may be left in a discharged state for long periods of time resulting in unmet loads. This situation would be dangerous, especially for the primary load, which has to be met at the time of need. In contrast, if the RE generation system is oversized, the overcharging of UR may occur and waste of energy will result. Therefore, system optimization should specifically aim to size the system components as sufficient to simultaneously meet load requirement and minimize system costs.

### 6.2.3.2 Optimization methodology and algorithm

The principle objective of system optimization is to determine the optimal combination of the number of PV modules  $N_{PV}$ , the number of wind turbines  $N_{WT}$ , and the volume of the upper reservoir  $V_{UR}$ , after meeting the technical and economic constraints. That is the co-called techno-economic optimization. The optimization technique simulates all possible configurations satisfying the technical system reliability constraints and determines that with the lowest system lifecycle cost, in other words the “optimal”.

Many studies have been conducted regarding the sizing and optimization of RE systems because of the recent wide utilization [229, 427-429]. Among the optimization methods, the genetic algorithm (GA) approach has been extensively studied. The basic GA principle is based on the Darwinian Theory of natural selection (survival of the fittest) [430, 431], i.e. the strongest is likely to be the victor in a competing environment [432]. This approach performs a stochastic global search (optimization) simulating the metaphor of real biological evolution [433]. Basically, the GA operates on a population of individuals represented by chromosomes, which are evaluated, selected, merged, mated, and mutated along the generations to find the best solution according to the predefined fitness function [171]. The flow chart of GA optimization is illustrated at the bottom of Fig. 6.4.

For the single-objective optimization, the LPSP was predefined as 0%, and therefore the only fitness function is the COE of the system. If two objectives are employed for technical-economic analysis, i.e. both COE and LPSP, the general approach is the determination of a Pareto optimal solution set or a representative subset [434]. A Pareto optimal solution set is often preferred to a single solution because of its

practicality for real-life problems, as the final solution of the decision-maker is always a trade-off. The ultimate goal of a double-objective optimization algorithm is the identification of solutions in the Pareto optimal set.

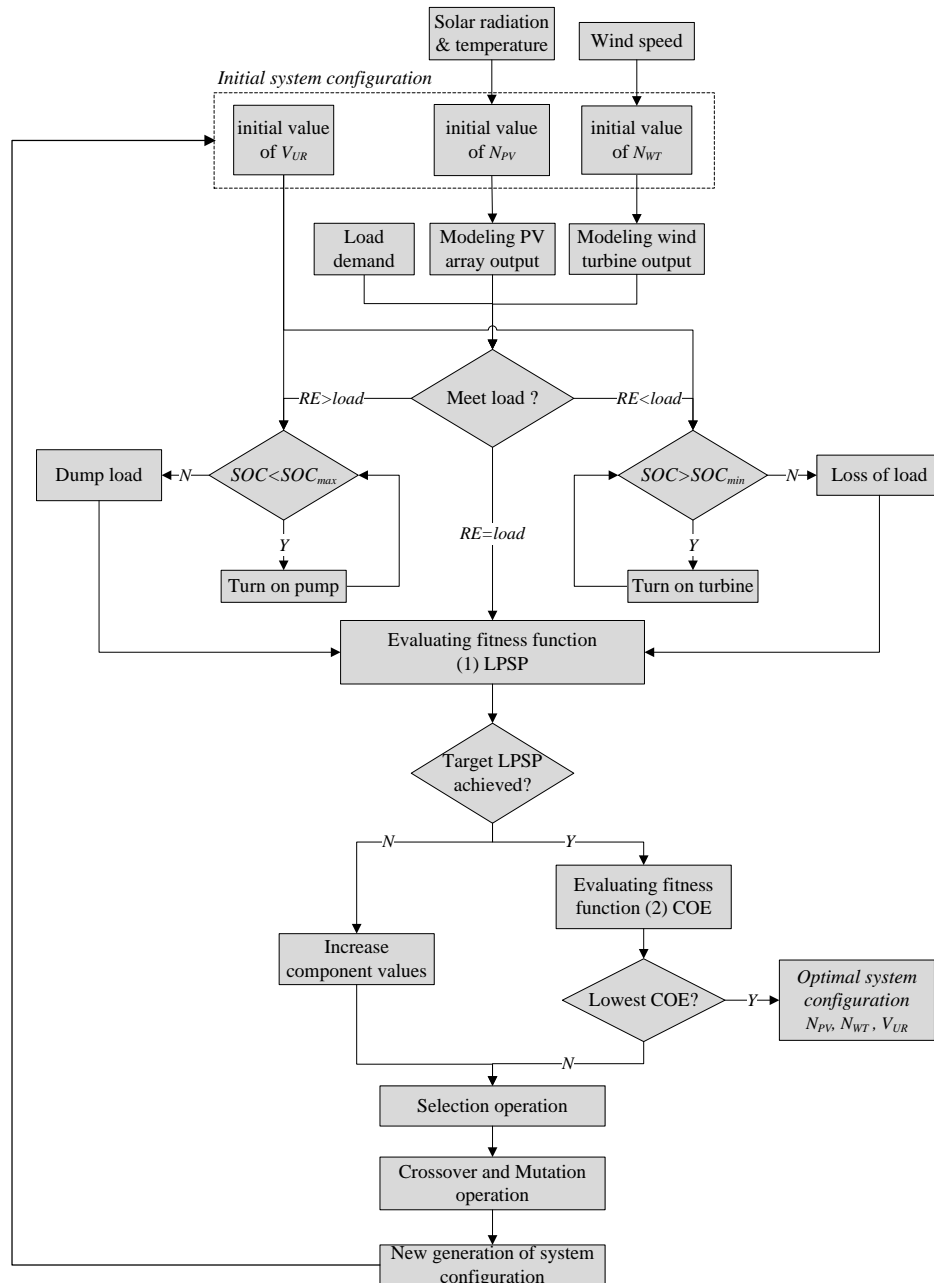


Fig. 6.4 Flowchart of the system optimization process using GA

The system simulation and optimization flowchart is illustrated in Fig. 6.4. The inputs data to this algorithm are: the hourly weather data throughout the year including solar radiation, wind speed and ambient temperature, the desired LPSP value for one year

and specifications and cost information for different systems components. The mathematical models make clear that the relationship between decision variables is not linear and only techno-economic analysis with GA optimization, therefore, can identify the optimal system combination of  $N_{PV}$ ,  $N_{WT}$  and  $V_{UR}$ . Firstly, two fitness functions, LPSP and COE, are evaluated. If the LPSP requirement is met and the lowest COE applies, the optimal system configuration is then obtained. If the system configuration is not able to meet the targeted LPSP or has a higher COE, the combination is discarded, and then goes to the GA optimization process, i.e. selection, crossover and mutation operation. A new system combination is then generated and the cycle, simulation, evaluation and optimization is repeated until the desired LPSP values are met simultaneously with the lowest COE values.

### **6.3 Technical feasibility study**

Technical feasibility of the pumped storage-based RE system is examined in this section. Together with the wind capacity ranging from 0 to 20.8 kW in steps of 5.2 kW (the rated power of one WT) and PV size from 100 to 170 kWp in steps of 10 kWp, 40 cases in total were simulated. During simulation, a zero energy deficit was set for all cases, and the initial quantity of water in the UR was assumed to be at maximum capacity. Using the simulation program developed by the author, the required minimum UR capacity can be derived for each PV and wind turbine combination. For example, in theory, if the number of wind turbines is two and PV size is 120kWp, the required minimum UR size was calculated at 6100 m<sup>3</sup>.

The overall results are presented in Fig. 6.5. For the first scenario, there were no wind turbines i.e. a PV-alone system with pumped storage. The lowest UR capacity (6,100 m<sup>3</sup>) can be achieved when the PV size is 170 kW. The UR capacity increases gradually

as the PV size decreases. For a PV of 120kW, for example, the UR soars up to 12,700 m<sup>3</sup>. If PV size is further decreased, the UR becomes unreasonable at over 31,300 m<sup>3</sup>.

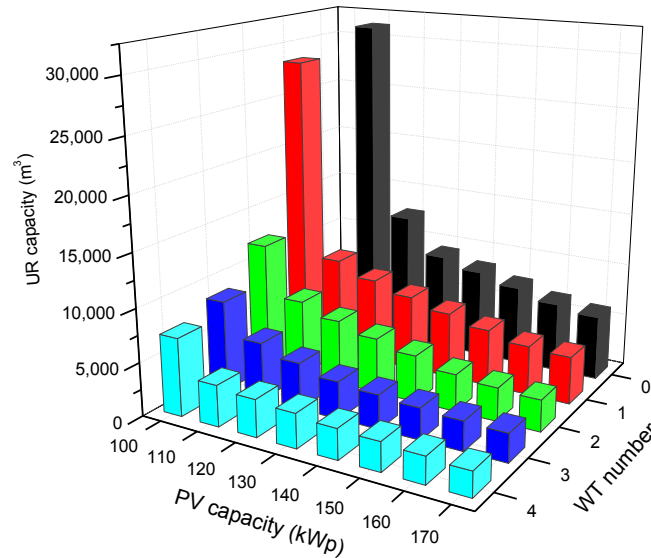


Fig. 6.5 Overall simulation results

For the second scenario, a single wind turbine was assumed. Due to the complementary characteristics in the timing of solar and wind energy outputs, the required UR size can obviously be reduced. For the same PV size, the UR size can be reduced by about 30% compared to the PV-alone system. Similar trends can be found for the wind turbine numbers 2 to 4. More wind turbines reduces both PV and UR capacities.

### 6.3.1 Sizing curve

The minimum UR capacity required to achieve 0% LPSP were connected to generate the sizing curve. As shown in Fig. 6.6, similar characteristics can be found between the sizing curves of different system configurations. Fig. 6.6 demonstrates that for a fixed number of turbines, UR decreases as PV is increased and that this decrease trend becomes much less evident at the larger PV values. Indeed the curves indicate a

minimum level of storage is needed however big the PV array and the number of WTs, if energy autonomy is to be provided whereby power supply can be sustained for several days in circumstances of no wind and no sun.

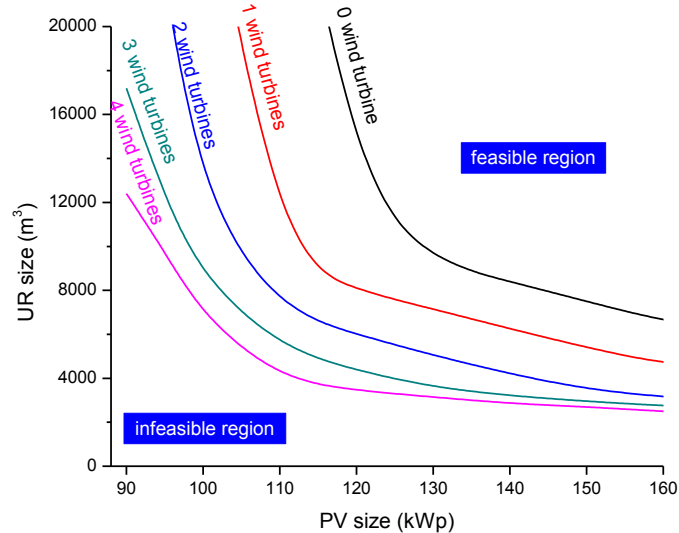


Fig. 6.6 sizing curve for pumped storage-based renewable energy system

Similarly, for the same PV size, increase in the number of WTs also reduces the UR size. The phenomenon is particularly obvious at the smaller PV sizes. Compared with the PV-alone system, significant reductions in UR size can be observed for the hybrid systems.

The curves in Fig. 6.6 also demonstrate that the space over the each sizing curve is the feasible design space for each scenario, while the space below is the infeasible region. Within the design space, any combination of WT numbers, PV and UR capacities is technically feasible. The actual decision is to a large extent dependent on the economic effectiveness of the combination. Therefore, optimized sizing, which must take economic and reliability into account, should be developed. Such a study is described in the following Section 6.5.

### 6.3.2 Wind turbine alone system

The wind turbine alone system with UR at 2,5000 m<sup>3</sup> was also studied. As illustrated in Fig. 6.7, when the wind turbine number increases from 10 to 70, the LPSP value decreases from 18.7% to 0%. A significant improvement in the reliability of power supply can be observed when the number of turbines changes from 10 to 20. Further increase in WT numbers continues to increase power supply reliability but less effectively. It seems that without PV panels a large number of WTs are required to achieve a zero LPSP power supply system.

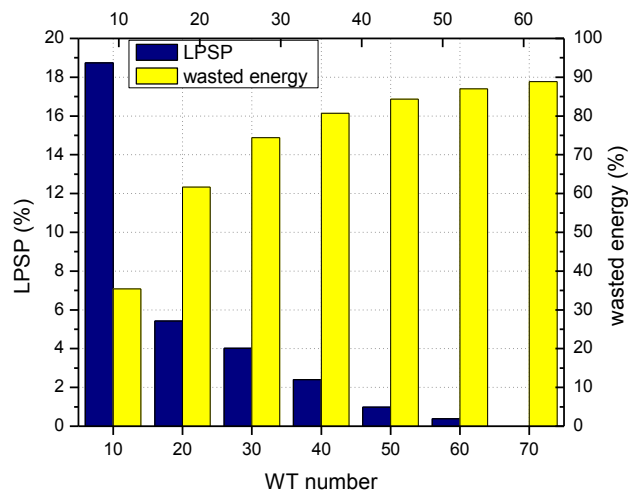


Fig. 6.7 LPSP and excess energy percentage of the wind-alone system

Since the WT output pattern cannot conform to the daily and seasonal load consumption profile, the excess power grows with the increase WT number. Up to 87.5% (2,423kWh per day in average) of the electricity production was wasted in the case of 70 wind turbines due to the limited energy storage capacity. The amount of energy spilled is much greater than the energy required. Indeed, the energy storage system is even more important for wind turbine alone systems, as the production of WT fluctuates rather more than PV production.

Based on the results of the PV-alone and wind-alone systems, it is clear that PV arrays and wind turbines working together can provide greater value than either technology forms acting alone. Better utilization of the available energy and thus less energy storage capacity is needed.

## 6.4 Techno-economic optimization of PV-PHS

### 6.4.1 Single-objective and two-objective optimization

In this section, a hybrid solar PV and pumped storage system is studied as an example to enable a comparison of the performance of the one-objective and two-objective optimization approaches.

#### 6.4.1.1 Single-objective optimization

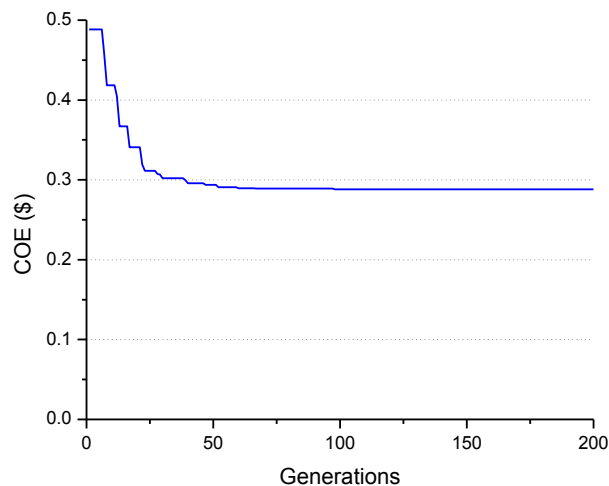


Fig. 6.8 Progress chart (variations of COE during GA optimization process)

During the single-objective optimization, LPSP was set to zero, meaning that no energy shortfall was allowed. The single objective to be optimized was the COE. The COE variation during the GA optimization process (200 generations) is shown in Fig. 6.8, demonstrating that a near optimal solution can be obtained very quickly during

the generation evolutions of GA optimization. The lowest COE was \$0.289/kWh, and was considered to be the optimal case.

The system configuration under single-objective optimization is presented in Fig. 6.9. During the simulation, the number of PV modules changed from 400 to 900 in steps of 1, and UR volume changed from 0 to 160,000 m<sup>3</sup> in steps of 1 m<sup>3</sup>. The lowest COEs for the different system combinations are presented in the curve of black dots. Each point on the curve represents a system configuration which can satisfy the technical target. For the single-objective optimization, the only benchmark for evaluating system performance is the economic index COE, thus the point with the lowest COE is the optimal configuration. Based on Fig. 6.9, the main components in the optimal system configuration consist of PV arrays (595 modules, 119 kWp), pumped storage subsystem (UR: 13,205 m<sup>3</sup>, pump: 90kW, turbine: 28kW) and inverter (30kW), and the corresponding NPC and COE figures are \$413,850 and \$0.289/kWh, respectively.

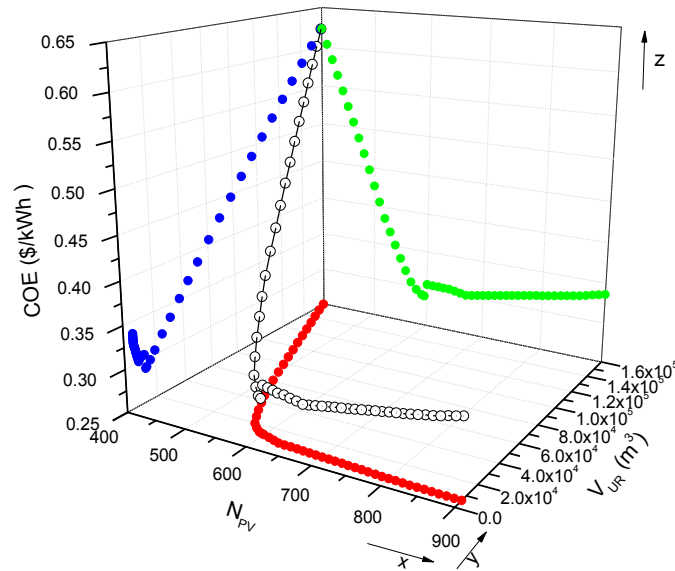


Fig. 6.9 COE vs. system configuration when LPSP is fixed at 0% under single-objective optimization

The relationship between the COE and system configuration parameters  $N_{PV}$  and  $V_{UR}$  was also investigated. As indicated in Fig. 6.9, the red points in the XY surface, i.e. the projection of the black curve, are used to generate the sizing curve for the proposed system if economics are not taken into account. In addition, the green points in the XZ surface depict the relationship between COE and the number of PV panels. It can be seen that as the number of PV modules grows, the COE decreases rapidly until the PV number is 595, after which the COE begins to increase gradually. A similar trend is found in the relationship between COE and the UR volume (the blue points in YZ surface). In summary, the lowest COE is indeed achieved at the optimal system configuration.

#### 6.4.1.2 Double-objective optimization

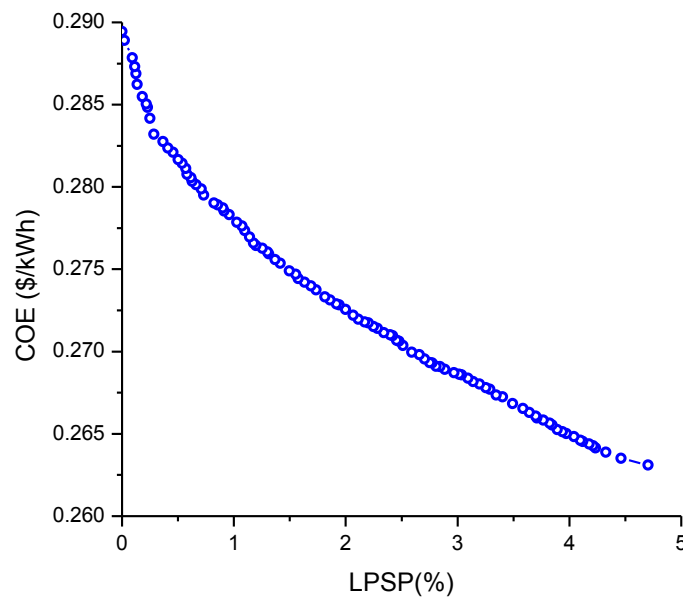


Fig. 6.10 Pareto front in the double-objective optimization

The double-objective optimization approach was based on the LPSP and COE criteria, and the Pareto optimality concept was used for the system techno-economic optimization using the GA technique. Fig. 6.10 illustrates the Pareto optimal solution

set obtained, meaning that there is no single optimal solution, but a set of infinite solutions. All of the optimum design points in the Pareto front are non-dominated and could be chosen with equal validity as optimum system configurations. Obviously, choosing a better value for any one objective function in the Pareto front would result in a poorer value for the other objective. The final solution of the decision-maker, therefore, is subject to a trade-off between technical and economic targets. Greater power supply reliability will result in a higher cost, and vice versa.

In this technical-economic optimization, the optimal system configuration under zero LPSP is the same as that for single-objective optimization. COE declines dramatically as LPSP increases. COE was reduced by 3.8% and 5.5% respectively for LPSPs at 1% and 2%. The cost could be further decreased by about 9.3% (COE: \$0.262/kWh) if an LPSP of 5% were to be allowed.

Table 6.1 Optimal system configurations under different LPSP values

Targeted LPSP	N <sub>PV</sub>	V <sub>UR</sub> (m <sup>3</sup> )	NPC (\$)	COE (\$)	Excess power (kWh)	Resulting LPSP
0%	595	13,205	413,850	0.289	18,263 (12.2%)	0.00%
1%	594	9,960	397,734	0.278	19,183 (12.9%)	0.99%
2%	592	8,535	389,843	0.273	19,913 (13.4%)	1.99%
3%	575	8,430	384,195	0.269	16,670 (11.5%)	2.99%
4%	564	8,040	378,847	0.265	14,980 (10.6%)	4.00%
5%	564	7,200	374,352	0.262	16,127 (11.4%)	5.00%

Optimal system configurations under different LPSP values were also investigated. The results were derived from double-objective optimization and are summarized in

Table 6.1, which demonstrates that the number of PV modules decrease slightly with an increase in targeted LPSP, and the volume of UR reduces greatly. A LPSP of 1% could bring a dramatic decrease in the volume of UR, which could be further reduced to 7,200 m<sup>3</sup> if a LPSP of 5% was allowed. The effect of LPSP values on excess power is not obvious because the number of PV modules and the UR volume decreased in unison. With the aid of double-objective optimization, it can be concluded that if not meeting some small proportion of the load can be accepted, significant reductions in capital cost, PV module numbers and UR size can be achieved.

#### **6.4.2 The optimal configuration assuming zero LPSP**

The performance of the optimal system case is examined as follows.

##### *6.4.2.1 Economic cost analysis*

The total NPC for the optimal system configuration was \$413,850, and the corresponding COE was \$0.289/kWh, i.e. HK\$2.243/kWh. Currently, the general service tariff in Hong Kong is HK\$0.973-1.206/kWh depending on the amount of electricity consumed and the power supply company fuel costs [435]. However, the tariff, including basic tariff and fuel clause charge, increases at for about 5% annually due to wider use of cleaner but more expensive fuel, and as existing electricity generation facilities are to be retired [436]. Therefore, the cost of this RE system will be probably lower than the retail electricity price 15 years later. In addition, if the electricity were to be supplied by a diesel generator with fuel transported by sea, the cost would be much higher than the RE solution. Compared to extending the grid by submarine cables and overhead lines, the economic and environmental benefit of the proposed system would be significant.

The breakdown of the system's NPC by components and cost type is illustrated in Fig. 6.11. Of interest is that the cost of a pumped storage system, including pumps, turbines, and UR, accounts for about 47% of the total system NPC, followed by the cost of PV modules which assume initial capital costs only. The least costly item is the inverter, at nearly 10% of the total NPC. Compared with battery-based RE power generation systems in Chapter 5 [16], the cost share of the energy storage subsystem is similar, indicating the importance of energy storage in standalone RE systems. However, the pumped storage cost is much less than battery storage costs, demonstrating the benefit of pumped storage solutions.

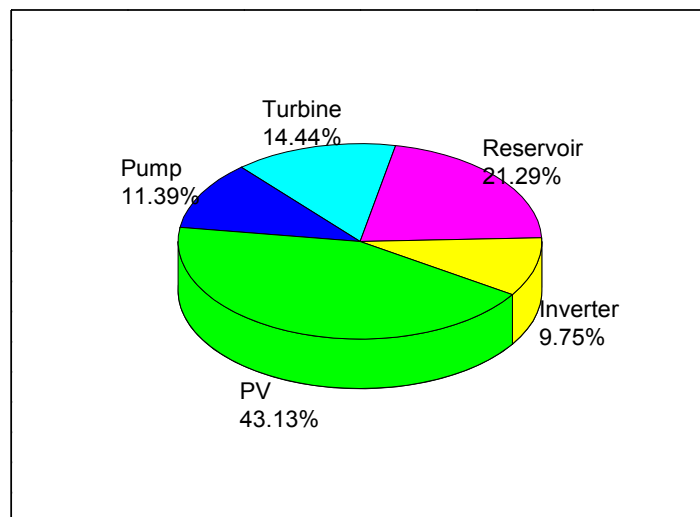


Fig. 6.11 Break-down of NPC by components

#### 6.4.2.2 Energy balance analysis

The optimal case simulation results reveal that the year-round energy output from the PV plant was 157,404kWh with the peak output at 105kW. The daily average PV generator output was 410 kWh after the deduction of the inverter conversion losses, and can be further divided into three components (Fig. 6.12): About 31.4% was used to supply the end-users directly, and 56.4% was taken up by the pump/motor unit,

meaning that on average 990 m<sup>3</sup> of water was pumped every day from the lower reservoir to the upper one for storage. About 12.2% (50kWh/d) of the total PV production, however, was lost in the “dump load”, usually in the afternoons when the available sunlight produced more power than needed while the UR was already full.

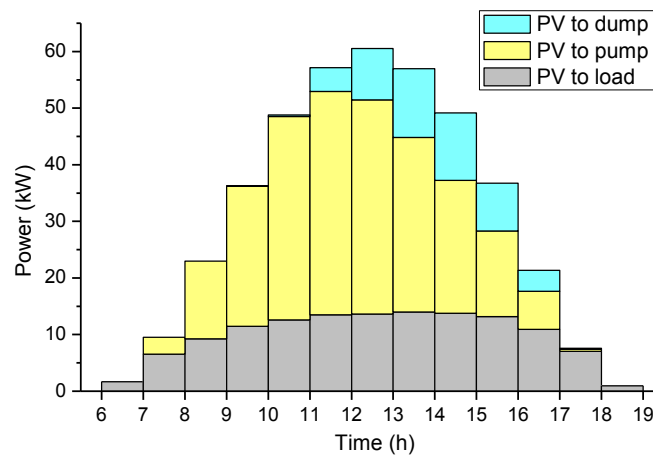


Fig. 6.12 Breakdown of PV output after the PV inverter

The average hourly load shared by the PV output and turbine/generator unit is shown in Fig. 6.13. As expected, the PV could satisfy the majority of the load in the daytime between 7:00am and 6:00pm. From 7:00pm until the next morning 5:00am, the load was met, totally, by the turbine output due to non-availability of solar radiation. As a result, the PV supplied directly to the load ratio was 51.4% and the corresponding turbine to load ratio was 48.6%.

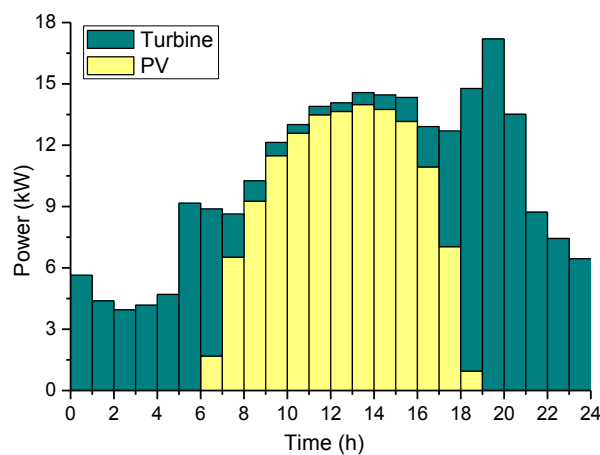


Fig. 6.13 Hourly load shared by PV direct output and turbine

6.4.2.3 Energy storage system performance

Fig. 6.14 illustrates the UR's SOC distribution frequency from 0% to 100%. About 81% of the SOC values are above 50%. Additionally, a fully charged status was available for 430 hours and dissipation of excess energy was likely to occur at that time. As a whole, the total amount of dumped energy in this case was 50kWh/d due to insufficient UR capacity.

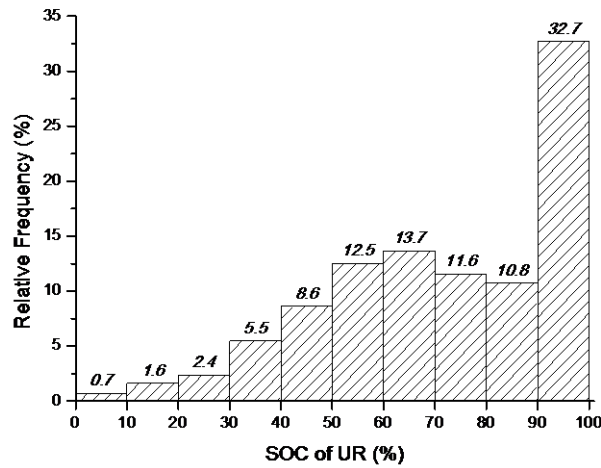


Fig. 6.14 Frequency distribution of UR's SOC

Based on Eq.(3.41), the UR stored water could supply energy for this island for about 6.5 days without RE backup. Such a design allows power to be supplied for several consecutive days of poor or even no PV output. During the year, the electricity input to the pumping system was 84,367kWh and output from the turbine generator was 44,347 kWh, giving an overall efficiency of the storage subsystem of 52.6%.

6.4.2.4 Sample hourly simulation result analysis

A plot of the hourly simulation results for 1<sup>st</sup> July is given as an example in Fig. 6.15. It can be seen that no energy was dumped on that day as the water level in the UR did

not reach its maximum, and also, there was no energy deficit, since the UR never became empty. As illustrated, the PV array began to generate electricity and served the load from 7:00. The excess power after meeting the load was used to pump water, and thus water level in the UR increased gradually. At 19:00, PV output could only serve part of the load and so the turbine cut in to restore the balance. The turbine then operated continuously to supply the total load demand until 7:00am the next morning and then went to another cycle. During the discharging period during the night, the volume of water stored in the UR reduced steadily. The result demonstrates that the pumped storage system effectively compensates for the unpredictable nature of solar energy by absorbing excess energy when the production exceeds load levels and then releasing it when the opposite is the case, hence ensuring a reliable and continuous power supply.

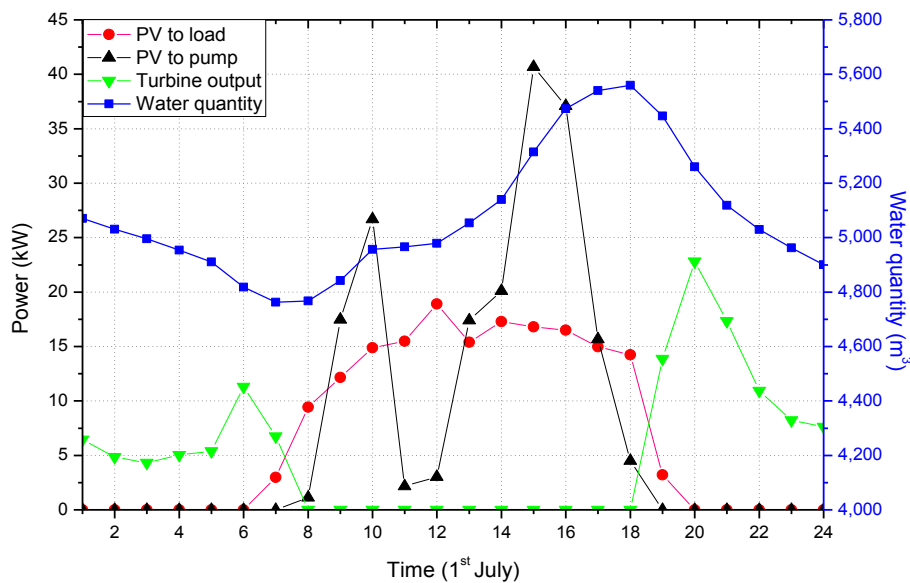


Fig. 6.15 Hourly simulation results on a sample day

## 6.5 Techno-economic optimization of PV-wind-PHS systems

The optimization of a standalone hybrid solar-wind-pumped storage system is described. The techno-economic optimization results of the hybrid system are discussed, and compared with the solar-pumped storage and the wind-pumped storage systems.

### 6.5.1 Performance analysis of the optimized, oversized and undersized systems

The techno-economic optimization demonstrated that the optimal system configuration consists of 553 PV panels (110.6kWp), 9220 m<sup>3</sup> upper reservoir and 1 wind turbine (5.2 kW), with a resultant COE of US\$0.286 (HK\$2.219). The use of only one wind turbine is due to the relatively high cost of the selected turbine, which should survive typhoons.

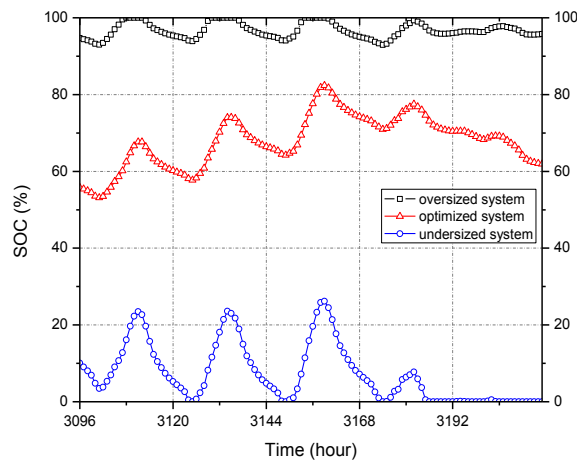


Fig. 6.16 SOC of the energy storage system under different system configurations

To examine the effectiveness of optimization, two other system configurations, i.e. oversized and undersized, were studied and compared with the optimized system. Fig. 6.16 shows the SOC distribution of the energy storage system for the three systems.

System configurations and the resultant performance indices, including COE, LPSP and excess energy percentage, are summarized in Table 6.2. It can be seen that the oversized system has a high reliability but the COE is significantly higher than the optimized system. UR, for most of the time was fully charged and therefore about 43% of excess energy had to be dumped. The undersized system cost was much lower but reliability was badly affected. The LPSP was 17%, meaning no power supply for about 4 hours per day. In addition 8% of the electricity produced was dumped as the energy storage capacity was limited. It is obvious, therefore, that only the optimized system under study balances both technical and economic targets to produce the optimal/best solution.

Table 6.2 System configuration and resultant performance index

	PV (kW)	UR (m3)	WT (kW)	COE (\$)	LPSP (%)	Excess energy (%)
Oversized system	140	14000	10.4	0.369	0	42.9%
Optimized system	110.6	9220	5.2	0.286	0	19.7%
Undersized system	80	4000	5.2	0.233	16.9%	8.0%

## 6.5.2 The optimal configuration assuming zero LPSP

### 6.5.2.1 Monthly average energy production from PV arrays and WTs

The daily average WT and PV power generation for each month of the year are presented in Fig. 6.17. It can be noted that solar power production dominates the power supply, contributing almost 91% of the total production during the simulated year. In addition, the PV output was extremely high in the summer months. This is a favourable

characteristic since electricity demand was also high in summer because of a high cooling load. Therefore, in this hybrid system, the PV contribution to the load was significantly higher than that of the wind turbines. Similar findings were seen in previous studies [42, 437]. The wind energy contribution was found to be significant from Jan to March and from Sep to Dec.

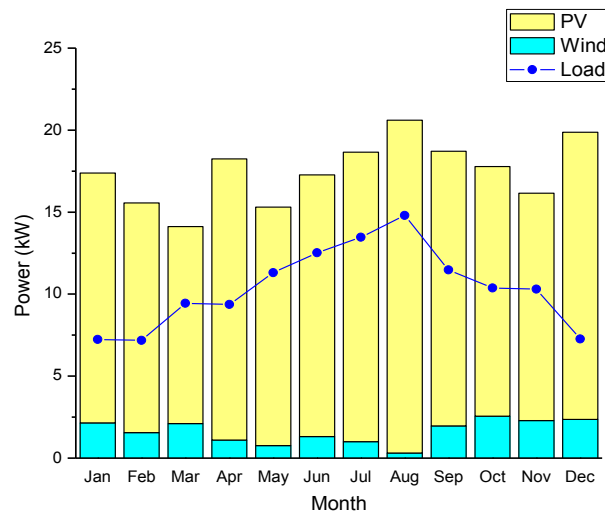


Fig. 6.17 Daily mean renewable energy power production and load demand

### 6.5.2.2 Energy flow and water flow

Fig. 6.18 summarizes the daily average electricity flow and water flow for the optimal case. The red lines and blue lines represent the electrical energy flow and water flow, respectively. PV contributed 91% of the RE output and WTs contributed 9%. Among the total useful electricity (419.7kWh/day), about 36.6% was directly consumed by the end-users, and 43.7% was transferred to the pump/motor unit for lifting water to UR for storage. Almost 19.7% (82.8kWh/day) of the total output, however, was in excess of requirements and had to be dumped.

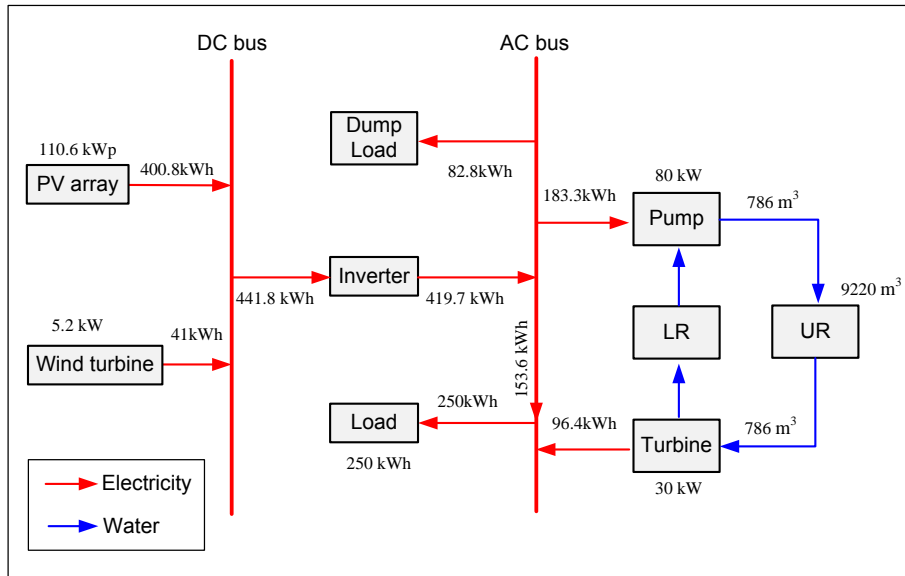


Fig. 6.18 Summary of daily average electricity flow and water flow

### 6.5.2.3 State of charge of the UR

The results shown in Fig. 6.19 illustrate the hourly SOC of the UR during the simulated year. It can be seen that SOC figures are relatively high. For the yearly distribution, values between 90% and 100% apply for 48% of the time, indicating the UR was fully or nearly fully charged for quite a considerable time. Therefore a large part of the generated energy was wasted because of limited storage capacity. The daily pattern is that the storage system was usually charged in the afternoons and discharged late at nights and in the early mornings.

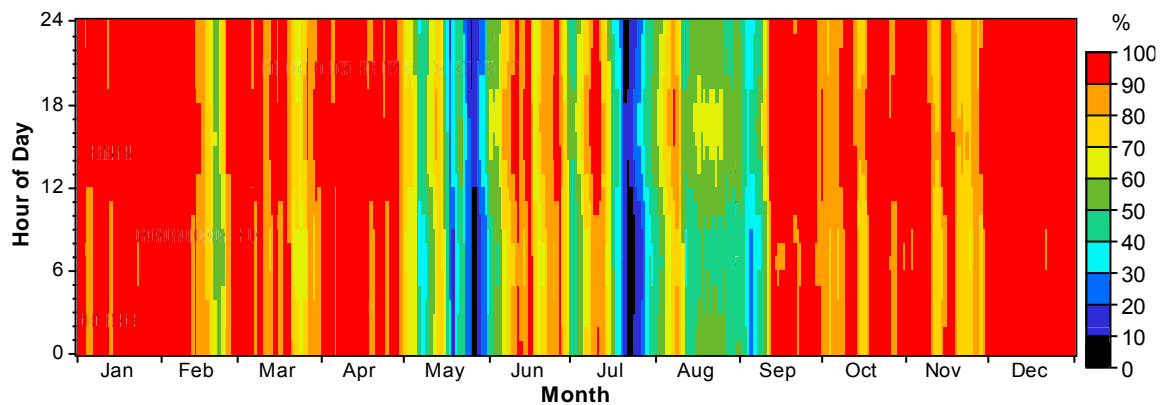


Fig. 6.19 Rainbow profile of UR's state of charge during the simulated year

High depth of discharge occurs in May and July, because of the high cooling load during these months. The minimum amount of water stored in the UR ( $0.921\text{m}^3$ ) was at 7:00am on 26<sup>th</sup> May. Therefore, to ensure sustainable and continuous power, sufficient RE and UR capacities should be available during those two months.

#### 6.5.2.4 Energy surplus and deficit of the optimized system

The performance of the optimal system configuration under zero LPSP was examined. Fig. 6.20 presents the power surplus and deficit duration over the simulated year. As seen in Fig. 6.20, the sum of areas B and C under the power surplus curve gives the total energy absorbed by the pumped storage charging system. Similarly, the sum of areas A and B under the power deficit curve gives the total energy provided by the pumped storage discharging system. By integrating the areas over time, the charged and discharged energy in the year was 66,902 and 35,174 kWh, respectively. Therefore, the overall efficiency was 52.6%. This value is in harmony with the mathematical model presented in Section 3.3 and the result in Section 6.4.2.3.

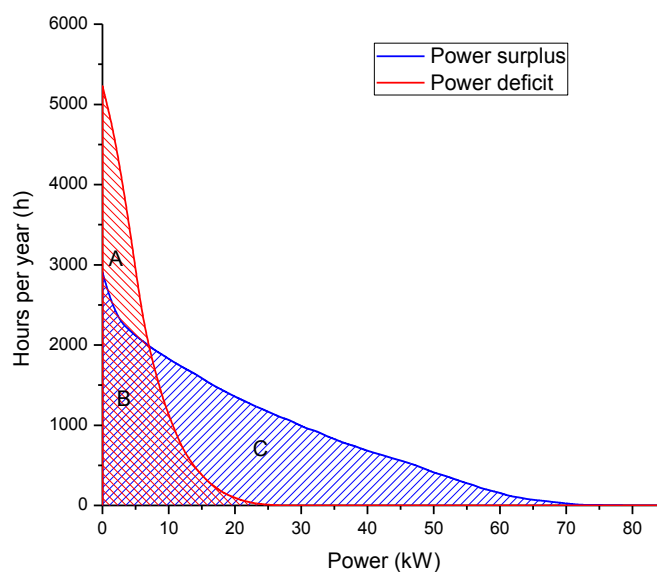


Fig. 6.20 Annual duration curves of power surplus and deficit

In addition, the required sizes of the pump and turbine can be determined based on the maximum surplus power (79.2kW) and the maximum power deficit (27.1 kW). For example, a single variable speed pump or a combination of several pumps rated above 79.2kW value should be used for the system. Usually a combination of several pumps or turbines can improve the efficiency and utilization ratios of each.

#### 6.5.2.5 Energy distribution analysis for the optimized system

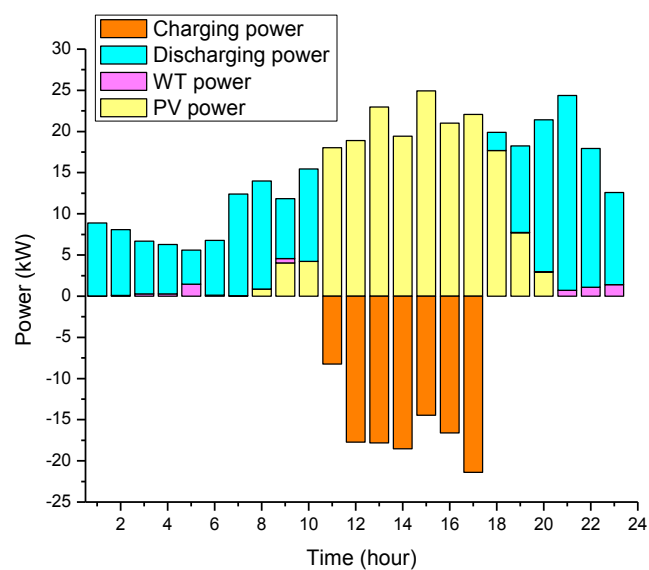


Fig. 6.21 Energy distributions for a typical day

The energy flow for a typical day for the optimal system configuration is presented in Fig. 6.21. It is obvious that during daytime, PV panels produced power, while wind speed was very low, meaning that there was little or even no wind power production. In Fig. 6.21, above the zero line represents the load demand, which was totally covered by the PV panels during the sunshine hours, and ensured by the wind power and energy storage system at other times. In summary, 52% of the energy demand was covered by PV panels, 2% by wind turbine and 46% by the energy storage system. In such a way, the combined system contributes a continuous power supply. In addition, below

the zero line in Fig. 6.21 represents the charging power, totally provided by the PV surplus power (38% of PV production). No power was stored in the evening because of low wind speed and the absence of solar radiation.

#### 6.5.2.6 Sensitivity analysis

Finally, a sensitivity analysis was performed in relation to several key input parameters: PV panel cost, wind turbine cost, UR construction cost, load consumption, solar energy resource and wind energy resource. The effects of a  $\pm 25\%$  deviation in the parameter values on the COE results were examined and the results are displayed in Fig. 6.22.

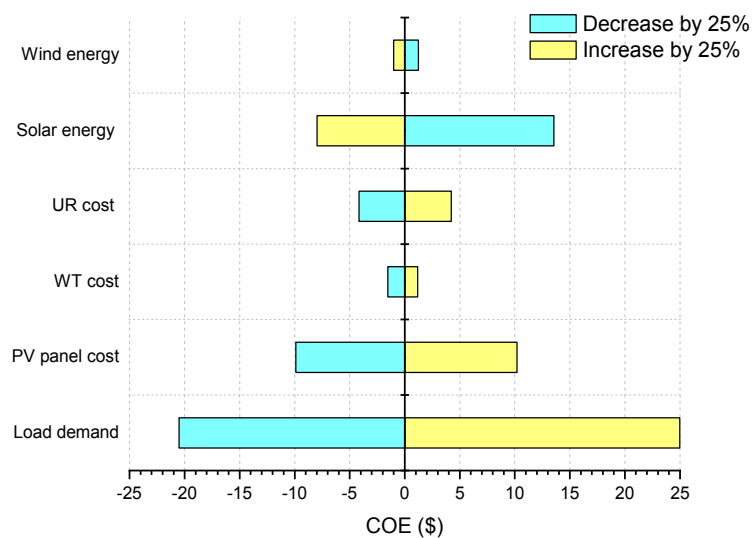


Fig. 6.22 Sensitivity analysis results on several key parameters

The load demand was a key parameter in determining system capacity and cost. It can be seen that a 25% increase in load had a higher impact (+25%) on COE than the impact (-20%) of a 25% decrease. For the costs of the key components, COE was quite sensitive to PV cost. In particular a 25% increase in PV panel cost produces a 10% higher COE value. The changes in COE for the 25% deviation of wind turbine cost,

however, were small because the single wind turbine was always needed in the optimal system configurations, and, it is worthy of note that the cost of the wind turbine was only 6.8% of that of the whole system. The 25% variation in UR construction cost resulted in a 4% increase or decrease in COE. In addition, a deviation of 25% in wind speed affected the COE by 1% inversely, and the effect of solar energy variation was more significant as regards system cost. A 13% increase in COE resulted from a 25% decrease in solar radiation. Overall, the results in Fig. 6.22 demonstrate that the significant contributors to the system economic cost include load demand, RE resource availabilities, and the cost of key components.

### 6.5.3 Comparison with solar-pumped storage and solar-wind-PHS

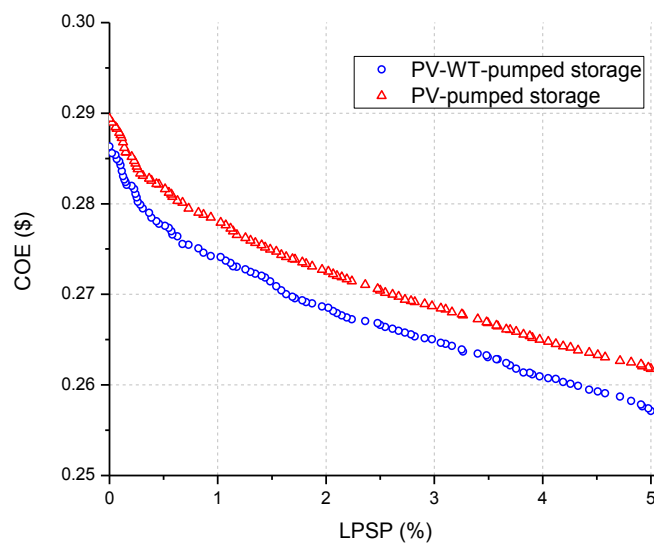


Fig. 6.23 System COE under various LPSP

After the techno-economic optimization, the lowest COE values for the hybrid solar-wind-pumped storage system and the solar-pumped storage system for different power supply reliabilities were obtained. Fig. 6.23 depicts the COE values as a function of LPSP from 0% to 5%. For a critical load, the LPSP should be set at 0, while for a

noncritical load, the LPSP maybe set in the range of 0%-5%, to balance costs against reliability. It is obvious that the hybrid solar and wind system can achieve lower costs than the solar alone system. The COE difference becomes significant as the LPSP increases.

The cost of the wind turbine is quite high because they have to have sufficient stability to survive typhoons. Only one wind turbine was used in the hybrid system and hence the wind power contribution to total energy production was not very high. However, the benefit of adding just that one wind turbine was significant, in that it made such a hybrid system more economically and technically viable. Therefore, to design an optimal power supply system, a combination of wind and solar energy sources should be considered.

Table 6.3 Optimal system configurations of different system types

<b>LPSP=0%</b>	PV (kW)	WT (kW)	UR (m3)	COE (\$)	Excess energy (%)
Solar-wind-pumped storage	110.6	5.2	9,220	0.286	19.7%
Solar-pumped storage	119	0	13,205	0.289	12.2%
Wind-pumped storage	0	286	29,552	1.376	85.6%
<b>LPSP=5%</b>					
Solar-wind-pumped storage	102.2	5.2	3,840	0.256	17.6%
Solar-pumped storage	112.8	0	7,200	0.262	11.4%
Wind-pumped storage	0	20	28,800	0.621	61.4%

Wind powered pumped storage was also studied. However, as displayed in Table 6.3, a wind turbine only system would be extremely expensive. The number of wind turbines and required energy storage capacity were also high due to the different distributions during the 24 hours of wind power generation and load demand.

The study has demonstrated that the feasibility of hybrid solar-wind energy system heavily depends on solar radiation and wind energy availability at the site, and the cost of the PV panels and wind turbines. It should be acknowledged that if the wind speed is extremely low or the wind turbine cost is remarkably high, the solar-pumped system may be better than a solar-wind-pumped storage system, but usually, integrating PV and wind energy produced in a complementary manner at different periods in the day can reduce energy storage capacity and lead to high energy supply reliability.

Fig. 6.23 and Table 6.3 show that a lower COE can be achieved if a very small energy deficit is acceptable. Notably, about a 45% reduction in UR size can be achieved as LPSP changes from 0% to 5%. This indicates that allowing some peak power demand not to be met when extremely bad weather exists can achieve cost-effective solutions. In addition, if a secondary energy storage system were employed, the pumped storage capacity could be greatly reduced and power supply reliability can be simultaneously improved. The author believes that introducing a small battery bank or supercapacitor bank is of vital importance in a pumped storage-based renewable power supply system. The battery/supercapacitor would only be used to cover the peak load in May and July and greatly reduces the UR size in such a hybrid energy storage system. To better balance the energy flow between supply and demand, a small battery bank has been incorporated in the pumped storage system [305, 360, 389], and this will be considered for future study in relation to the optimization procedure developed by the author.

## 6.6 Summary of this chapter

In this chapter, investigations into pumped storage-based renewable energy systems at the scale of a few hundred kW scale for the island concerned were described. The effectiveness of the proposed models and optimization algorithm has been presented. The relationship between system configurations and their corresponding COE values shows that the unavailable periods of RE necessitate a minimum UR capacity to supply the load, no matter how big the RE generator capacity. The effects of changing targeted LPSP indicate that if it can be accepted that a small proportion of load demand will not be met, significant reductions in capital cost,  $N_{PV}$  and  $V_{UR}$  can be achieved. In addition, it has been demonstrated that the complementary characteristic between solar and wind energy output can provide greater value than either a PV alone or a wind alone system. Therefore, in designing an optimal power supply system, a combination of wind and solar energy sources should be considered.

System simulation and optimization results indicate that pumped storage technology can effectively compensate for the intermittent nature of RE, although the overall energy efficiency of such a micro system is not high. However, a reliable, sustainable and environmentally friendly power supply solution can be provided by the hybrid system, demonstrating that pumped storage is an ideal partner for a standalone 100% RE power supply system in remote areas.

The pico PHS system can achieve an overall efficiency of 52.6%, which is considered low if compared to massive PHS system. However, its suitability in respect of technical, economic and environmental terms, make this kind of storage a feasible alternative to battery.

The COEs of the optimal solar-wind-pumped storage system and solar-pumped storage system under zero LPSP are \$0.286 and \$0.289/kWh, respectively. From the perspective of long-term sustainability and environmental factors, it can be expected that the RE-based power supply system for remote areas will become more competitive and cost-effective than diesel-based power generation systems. Therefore, implementation of this novel technology in remote regions has promising prospects.

## **CHAPTER 7 DEVELOPMENT OF HYBRID ENERGY STORAGE TECHNOLOGIES**

An investigation of battery-based and pumped hydro storage-based RE systems has been presented in Chapters 5 and 6, and it is shown that a combination of more than one storage technology is able to better complement the fluctuating RE output and dynamic power demand. Hence, a hybrid energy storage system (HESS), which combines battery for long-term energy management and supercapacitor (SC) for fast dynamic power regulation, is proposed and examined in this chapter. The operation of a passive connected HESS was studied via both theoretical analysis and numerical simulation using Matlab/Simulink. An electric inductor was further introduced to improve the performance of the HESS. An experimental test bench was developed to validate the simulation results. It was demonstrated that the HESS can stabilize energy provision, not only for the intermittent renewable energy, but also for fluctuating load applications. Another type of HESS, combining pumped hydro storage and battery energy storage, was analyzed and to find any advantages of this type, a physical representation of the system was experimentally studied.

### **7.1 Introduction**

Energy generated by renewable sources has many advantages over conventional supplies, but a negative aspect is that the supply that it is stochastic in nature and consequently difficult to control. To regularize an intermittent RE output, an appropriate energy storage component with high specific power and at the same high specific energy over periods minutes or hours is required [438, 439]. The PHS system

proposed in Chapter 6 offers a good solution, but subject to site limitation in respect of available water elevations. In addition, compressed air energy storage is normally used for long-term energy storage, and a flywheel is usually incorporated to cope with the short-term peak power demand.

The battery energy storage studied in Chapter 5 could be a good solution for remote RE projects because of its technical maturity and wide availability. However, on one hand, batteries are only efficient at supplying low and steady loads, and on other hand, RE outputs are not ideal for battery charging as the output fluctuates greatly depending on weather conditions [440, 441]. It is difficult for batteries to recover from rapid power fluctuations without a dramatic reduction in their lifetime. In addition, the charge/discharge rate of battery is limited because of its low power density [442]. This imposes severe stress on the batteries under conditions of quick supply/load fluctuations, resulting in extended periods of low state of charge and also in more charge/discharge cycles. The lifespan of the battery is, thereby, significantly reduced [443, 444]. Furthermore, high startup currents are required by some typical appliances. Water pumps, for example, its starting current can be 6-10 times greater than the rated current [426]. Even though these large current spikes only exist for a short duration, the battery must be sized large enough to supply the current spike, leading to the necessity for an excessively high battery storage capacity.

A promising energy buffer device, the supercapacitor (also known as an ultracapacitor or electronic double layer capacitor) has become increasingly interesting in the above regard because of its higher power density, longer cycle life and higher charging-discharging efficiency compared with that of the traditional battery. Its only disadvantage is a low energy density [445]. Since the supercapacitor and the battery are complementary in technical characteristics, it is reasonable to combine them to

create a hybrid energy storage system (HESS) where the battery absorbs/supplies long term continuous energy and the supercapacitor responds speedily to the dynamic and instantaneous power demands.

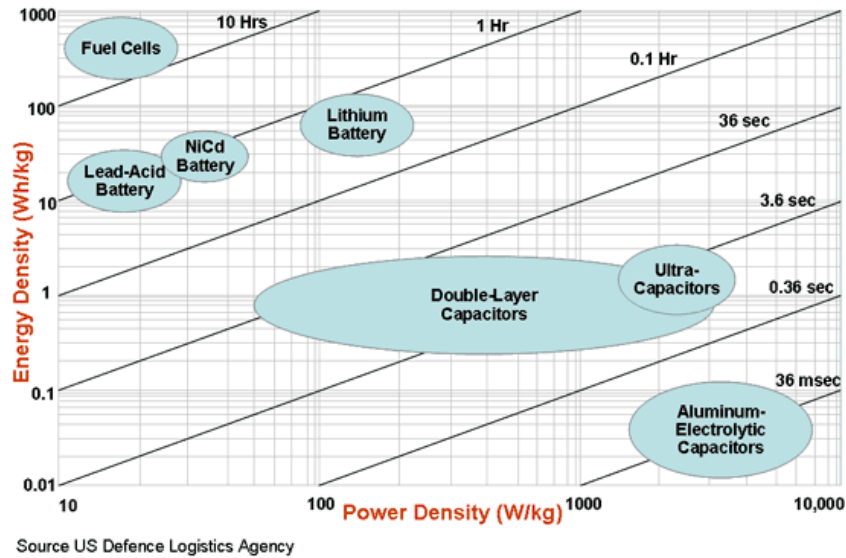


Fig. 7.1 Ragone Plot of energy storage technologies

The Ragone plot, i.e. specific power versus specific energy ranges of various energy storage technologies, is displayed in Fig. 7.1. The plot shows the lead-acid batteries have high energy density of the order of 10–100 Wh/kg, while the power density is low at around 100W/kg, resulting in long charging/discharging times of 0.3–3 hours in microgrid RE systems. Thus batteries cannot respond immediately under severe load fluctuations. In contrast, supercapacitors possess high power densities in the range of 1000 to 5000 W/kg and long life of around 500000 cycles at 100% depth-of-discharge. The charge/discharge efficiency is very high (95%), at a fast rate over a time in the range of 0.3 to 30s. Hence, supercapacitors are usually used for the quick power fluctuations [443, 446, 447]. The proposed HESS, therefore, is a good combination of the high energy density of the battery with the high power density of the supercapacitor.

The combination in fact, can yield benefits greater than if the two components were to act separately [448].

In the literature, hybrid battery-supercapacitor energy storage was first explored as an alternative to the traditional battery system when subjected to pulsed loads in digital communication applications [449], and is now popularly applied in electric vehicles since they have frequent motor startups and braking events. The addition of the supercapacitor has the potential to reduce the size and improve battery life [450-452]. The HESS is also being considered for standalone renewable energy applications [448, 450, 453-455], as such battery–supercapacitor combinations result in better reliability and a longer battery life.

This study aims at exploring the advantages of both batteries and supercapacitors, to make the hybridization of two technologies able to cope with long duration power charging/discharging and short duration peak power surges, and further extending the lifetime of the energy storage devices.

## 7.2 System description of the passive hybrid

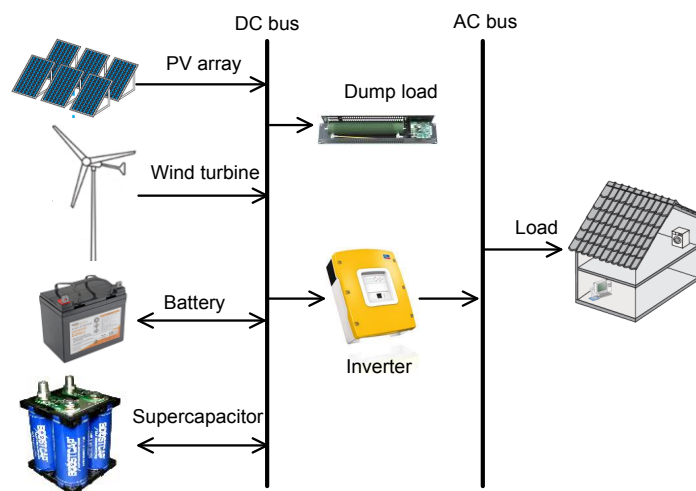


Fig. 7.2 Standalone RE system with passive hybrid energy storage system

There are three basic configurations of a hybrid battery-supercapacitor, i.e. passive, semi-active and fully active connection [456]. Among these, the passive hybrid is the simplest and cheapest arrangement. It achieves a better system performance than a single energy storage technology, although the power flow in and out of the HESS is not controlled.

A schematic diagram of a micro-grid RE system with HESS is presented in Fig. 7.2. The major components are the RE generator, HESS, inverter, controller, and load. The supercapacitor is directly connected in parallel with the battery bank, which is the so-called passive connection. In the standalone RE system with HESS configuration, the batteries provide the primary energy buffer for long duration, and super-capacitors only serve for “peak power smoothing” and “emergency reserve”. It is expected that this system can not only meet stable RE output and load requirements, but can also meet sudden peak power output and peak load demands.

### 7.3 Mathematical models

#### 7.3.1 Numerical analysis of the HESS

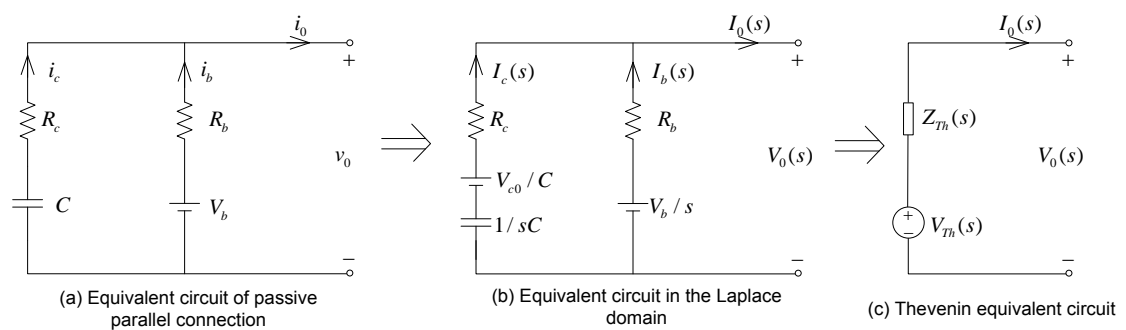


Fig. 7.3 Equivalent circuit of a supercapacitor in parallel connection with a battery

In this study, the mathematical models of the battery and supercapacitor are simplified to make the analysis tractable. The battery is represented by an ideal voltage source  $V_b$  and an internal resistance  $R_b$ , and the supercapacitor is represented as a single lumped constant capacitance  $C$  together with an internal lumped resistance  $R_c$ , [457]. The equivalent circuit of the direct connection is displayed in Fig. 7.3(a), and its equivalent circuit in the Laplace domain and its Thevenin equivalent are presented in Fig. 7.3(b) and Fig. 7.3(c), respectively.

Based on the analysis presented in [457, 458], the equivalent circuit is transformed into the frequency domain using the Laplace transform.

$$V_{Th}(s) = V_b \frac{R_c}{R_b + R_c} \frac{s + \alpha}{s(s + \beta)} + V_{c0} \frac{R_b}{R_b + R_c} \frac{1}{s + \beta} \quad (7.1)$$

$$Z_{Th}(s) = (R_b + \frac{1}{sC}) \parallel R_b = \frac{R_b R_c}{R_b + R_c} \frac{s + \alpha}{s + \beta} \quad (7.2)$$

where  $s$  is the complex frequency,  $V_{c0}$  is the initial voltage of the supercapacitor, and

$$\alpha = \frac{1}{R_c C} \quad (7.3)$$

$$\beta = \frac{1}{(R_b + R_c)C} \quad (7.4)$$

Therefore, the inverse Laplace transform of the Thevenin voltage source in Eq. (7.1) leads to:

$$v_{Th}(t) = V_b + \frac{R_b}{R_b + R_c} (V_{c0} - V_b) e^{-\beta t} \quad (7.5)$$

When the mathematical model of the Thevenin equivalent circuit is obtained, it is possible to connect a power charging source or load to this HESS. As displayed in Fig. 7.3(a), a positive value (downward flow) of  $i_0$  is defined as load consumption and a negative value is defined as a power charging source.

To investigate the behaviour of HESS when there is a charging source/load, suddenly fluctuating from one level to another, a pulsed source is assumed in this chapter. The analytical approach is presented as follows.

The pulsed charging/load current with pulse duty ratio  $D$  and period  $T$  and for  $N$  pulses can be expressed as:

$$i_o(t) = I_0 \sum_{k=0}^{N-1} [\Phi(t - kT) - \Phi(t - (k + D)T)] \quad (7.6)$$

where  $\Phi(t)$  is the unit step function and  $I_0$  is the amplitude of the charging/load current. By operating the Laplace transform on Eq.(7.6), the current in the frequency domain is:

$$I_0(s) = \sum_{k=0}^{N-1} \left[ \frac{e^{-kT \cdot s}}{s} - \frac{e^{-(k+D)T \cdot s}}{s} \right] \quad (7.7)$$

For the given form of charging current, the internal voltage drop  $V_i(s)$  in Fig. 7.3(c) is:

$$V_i(s) = Z_{Th} I_0(s) \quad (7.8)$$

Through an inverse Laplace transform, the corresponding expression in the time domain is:

$$v_i(t) = R_b I_0 \sum_{k=0}^{N-1} \left\{ \left(1 - \frac{R_b}{R_b + R_c} e^{-\beta(t-kT)}\right) \Phi(t-kT) \right. \\ \left. - \left(1 - \frac{R_b}{R_b + R_c} e^{-\beta[t-(k+D)T]}\right) \times \Phi[t-(k+D)T] \right\} \quad (7.9)$$

From the circuit in Fig. 7.3c, the output/power source voltage can be expressed as:

$$V_0(s) = V_{Th}(s) - V_i(s) \quad (7.10)$$

By combining Eq. (7.5) and (7.9), the above Eq. (7.10) in the time domain can be expressed as:

$$v_0(t) = v_{Th}(t) - v_i(t) \\ = V_b + \frac{R_b}{R_b + R_c} (V_{c0} - V_b) e^{-\beta t} - R_b I_0 \sum_{k=0}^{N-1} \left\{ \left(1 - \frac{R_b}{R_b + R_c} e^{-\beta(t-kT)}\right) \Phi(t-kT) \right. \\ \left. - \left(1 - \frac{R_b}{R_b + R_c} e^{-\beta[t-(k+D)T]}\right) \times \Phi[t-(k+D)T] \right\} \quad (7.11)$$

Finally, the currents in the battery and supercapacitor can be derived based on the resolved output/power source voltage in Eq. (7.11):

$$i_b(t) = \frac{1}{R_b} [V_b - v_0(t)] \quad (7.12)$$

$$i_c(t) = i_0(t) - i_b(t) \quad (7.13)$$

### 7.3.2 Currents under steady state conditions

If the battery voltage reaches to supercapacitor voltage, a steady state exists, i.e.

$V_{0c} = V_b$ . The battery voltage can then be found using Eqs. (7.11) and (7.12):

$$i_{bss}(t) = I_0 \sum_{k=0}^{N-1} \left\{ \left(1 - \frac{R_b}{R_b + R_c} e^{-\beta(t-kT)}\right) \Phi(t-kT) - \left(1 - \frac{R_b}{R_b + R_c} e^{-\beta[t-(k+D)T]}\right) \times \Phi[t-(k+D)T] \right\} \quad (7.14)$$

Similarly, the supercapacitor current under steady state conditions is:

$$i_{css}(t) = \frac{R_b I_0}{R_b + R_c} \sum_{k=0}^{N-1} \left\{ e^{-\beta(t-kT)} \Phi(t-kT) - e^{-\beta[t-(k+D)T]} \Phi[t-(k+D)T] \right\} \quad (7.15)$$

### 7.3.3 Performance of HESS in peak power enhancement

Based on Eq. (7.14), the peak current of battery appears at the end of the pulsed charging current, i.e  $t = (k+D)T$ . With time increasing,  $n$  tends towards infinity, and the expression for peak battery current is:

$$I_{bpeak} = I_0 \left[ 1 - \frac{R_b e^{-\beta DT}}{R_b + R_c} \frac{1 - e^{-\beta(1-D)T}}{1 - e^{-\beta DT}} \right] = I_0 (1 - \zeta_c) = \frac{I_0}{\gamma} \quad (7.16)$$

where  $\zeta_c$  is the current sharing factor of the supercapacitor at the peak charging current:

$$\zeta_c = \frac{R_b}{R_b + R_c} \frac{e^{-\beta DT} (1 - e^{-\beta(1-D)T})}{1 - e^{-\beta DT}} \quad (7.17)$$

$\gamma$  is the power enhancement factor:

$$\gamma = \frac{1}{1 - \zeta_c} \quad (7.18)$$

It can be seen that if there is no supercapacitor,  $\zeta_c = 0$ ,  $\gamma = 1$ , and then  $I_{bpeak} = I_0$ , meaning that there is no enhancement, the battery would absorb all charging current by itself alone.

If the rated current for the battery is  $I_{rated}$ , the charging source current will be:

$$I_0 = \gamma \cdot I_{rated} \quad (7.19)$$

The instantaneous peak power at the rated current is then:

$$P_{peak} = I_0 V_b = \gamma \cdot I_{rated} V_b = \gamma P_{rated} \quad (7.20)$$

where  $P_{rated}$  is the rated battery power .

Eq. (7.20) indicates that the peak power absorbed by the HESS is enhanced. A factor  $\gamma$  is introduced to measure the extent of power enhancement.  $\gamma$  is larger than 1 when a supercapacitor is introduced, and therefore the factor represents the extra power provided by the HESS when compared to a battery system alone.

## 7.4 Numerical simulation

### 7.4.1 Numerical simulation using Matlab/Simulink

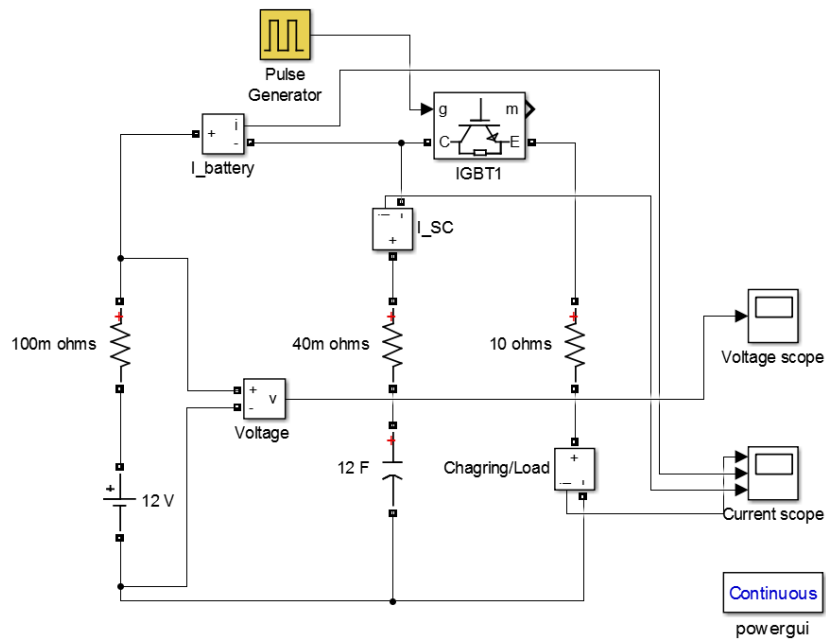


Fig. 7.4 Simulation model formatted in Matlab/Simulink

For pumped storage-based and battery-based RE systems, simulations are usually carried out using a one hour time-step, which is sufficiently small to model the intermittency of the RE supply and the fluctuating electrical load with fair accuracy. However, for the HESS proposed in this chapter, although the charge/discharge duration of the batteries is rated in hours, supercapacitor has very small time constant and thus it can only cope with very short-time high power charge/discharge pulses, usually over only seconds, due to their very low internal resistances. Therefore, a microsecond interval simulation instead of hour is conducted for the HESS using the Matlab/Simulink software.

A particular case of the passive hybrid energy storage system with  $R_b = 0.1\Omega$ ,  $R_c = 0.04\Omega$  and  $C = 12F$  was studied to verify the above analytical results. The simulation model implemented in Matlab/Simulink is illustrated in Fig. 7.4. The period and duty ratio of the pulsed charging source or load are 10s and 50%, respectively. Other parameters are also shown in this figure.

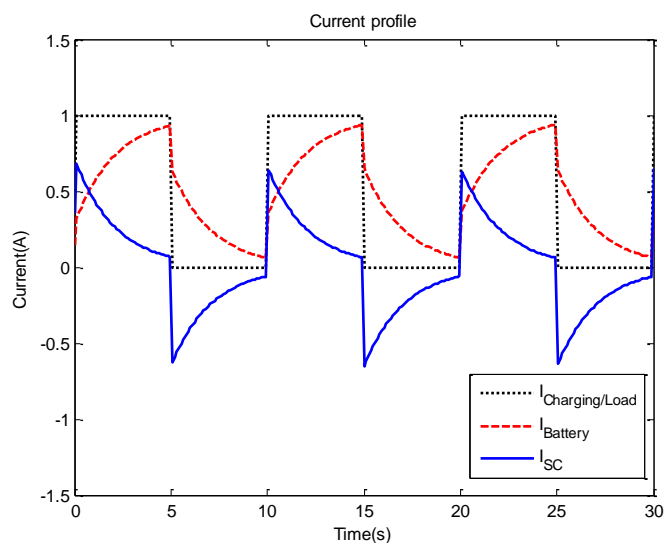


Fig. 7.5 Currents of battery and SC in reaction to a pulsed charging source or load

The battery curves and supercapacitor currents in reaction to a pulsed charging source are plotted in Fig. 7.5. It is observed that when the charging power is turned on suddenly, the supercapacitor, with high power density, jumps rapidly to a high value and charging takes place with a current descending exponentially. When there is no charging power, the supercapacitor current flow changes quickly to the opposite polarity, releasing the stored energy to the battery during the off-state period.

The reaction of the battery is different. During the charging power on-state period, the battery's current starts at a low value and then gradually increases. During the off-state period, it falls off to a value equal to the supercapacitor current, but in the opposite direction, keeping on absorbing energy from the supercapacitor. As a result, the battery is under charge for the whole cycle, while the influence on the battery from the variable charging source is greatly reduced.

Based on the above simulation results, it is obvious that the battery current, which otherwise should be equal to the charging current, has been reduced significantly due to the existence of the supercapacitor. The supercapacitor can absorb some of the charging current, thereby relieving stress on the battery and improving the performance of the hybrid system in absorbing fluctuating/peak charging power. Similar trends are also found for the HESS under pulsed loads.

Based on the analysis in Section 7.3.3, the power enhancement factor  $\gamma$  of the hybrid system is calculated as 2.5, meaning that 2.5 times as much power can be absorbed and supplied by the hybrid system compared to a battery-alone system.

#### 7.4.2 Performance enhancement through an inductor

The passive connection of the hybrid system can be improved with an upgraded connection, which is realized by connecting an inductor in series with the battery branch (Fig. 7.6). Due to the filtering effect of the inductor, the battery output current can be stabilized.

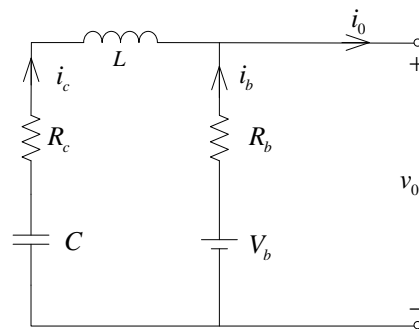


Fig. 7.6 Semi-active connection of the hybrid system

A simulation model of the improved connected hybrid energy storage system was also developed in Matlab/Simulink under the pulsed charging source, and the simulation results are plotted in Fig. 7.7. The parameters are the same as the case in Fig. 7.5 except for the added inductor. The results demonstrate that the power enhancement effect of the semi-active hybrid system is the same as that of the passive connected system. However, the battery performance is obviously improved. The battery current ranges from 0.3A-0.8A, are much smaller than those in the passive hybrid system in Fig. 7.5. The battery current waveform is also smoother. Most of the fluctuating current is shared by the supercapacitor, thereby relieving the battery stress. In such a way, the lifetime of the battery in the hybrid system can be prolonged.

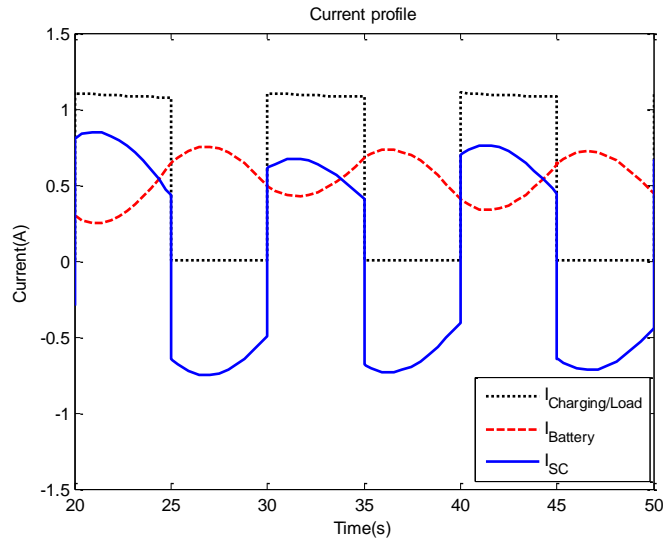


Fig. 7.7 Currents profile of semi-active connected hybrid energy storage system

### 7.4.3 Comparison between hybrid energy storage and battery alone system

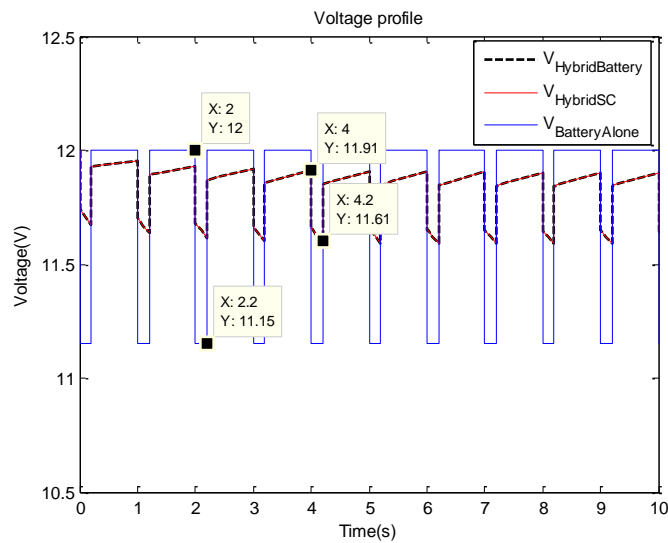


Fig. 7.8 Voltage profiles of the HESS and battery-alone system

The voltage profiles of the HESS and battery-alone system as a function of time are presented in Fig. 7.8. The simulations are based on a pulsed load at a period of 1s and duty ratio of 0.1. For the hybrid system, the variation of supercapacitor voltage follows the uniform battery voltage trend during the whole simulation period, because they are connected in parallel in the circuit. However, for the battery alone system, the voltage

variation is much more significant. Based on the data points sketched in Fig. 7.8, the average gap between the voltage peaks and valleys in the battery alone system is 0.85V, which the hybrid system reduces to 0.3V, indicating a marked reduction of 65% in voltage variation can be achieved. The results demonstrate a significant benefit of the hybridization in reducing the fast and large battery terminal voltage transients.

## 7.5 Experimental validation

### 7.5.1 Experiment tests of the passive connected system

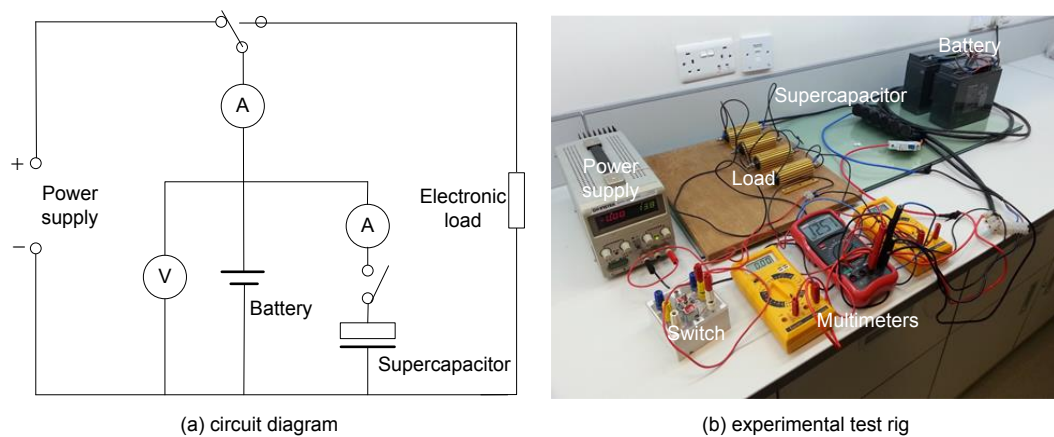


Fig. 7.9 Experimental layout of the hybrid battery-supercapacitor storage system

An experimental test bench was designed, and the experimental results were analyzed, to validate the simulation results using software Matlab/Simulink. Fig. 7.9 shows the circuit diagram and experimental test rig. In this test system an adjustable power supply (0~3A 0~30V) was used as the charging source to simulate the power generated from a renewable energy system. An 83F supercapacitor module and a 12V/17Ah lead acid battery were used in this test system as a HESS. A voltage meter (0~20V) is connected in parallel at both ends of the lead-acid battery to measure the system voltage. Two current meters (0~10A) were used to measure the total current and the supercapacitor branch current. This enabled the lead-acid battery branch current to be

extrapolated through the two measured currents. Four  $22\Omega$  resistors, connected in parallel, were adopted as the load. A switch controlled the test system operation and test.

To investigate the performance of the HESS in response to the fluctuating renewable energy generator, a pulsed charging source was applied. The charging current was set as within 1A-2A, lasting for about 30s on-state, and the power supply then cut off for 30s observation before repeating the cycle. Usually a test lasted for about 3-5 minutes. The currents and voltages of the battery and supercapacitor were recorded every second by the data logger.

### 7.5.2 Experimental results and data analysis

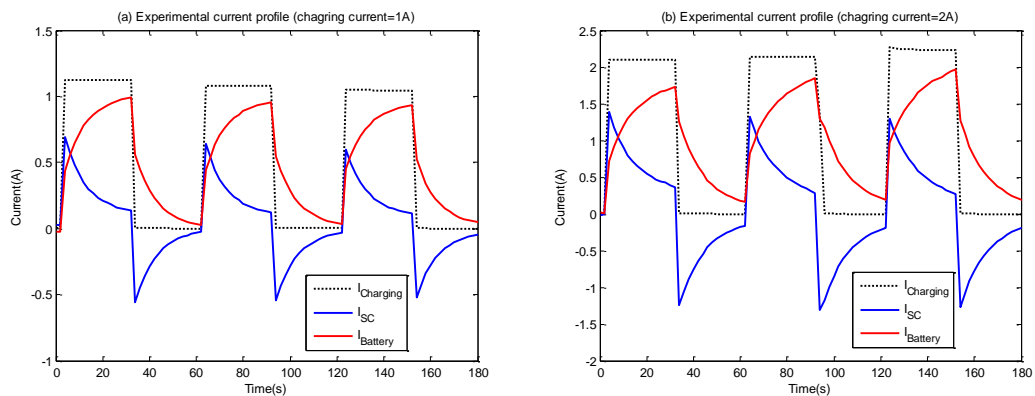


Fig. 7.10 System experimental currents for the hybrid energy storage system

The measured currents of the hybrid energy storage system under different power sources are presented in Fig. 7.10. Compared with the numerical simulation results in Matlab/Simulink (Fig. 7.5), it is observed that the simulated current profile coincides well with the experimental results. The SC absorbed peak power during the power supply on-state and released the stored energy to the battery during the off-state, while the battery was being charged during the whole cycle due to its high energy density.

Therefore, the experimental data can be used to validate the analytical and simulated results.

### 7.5.3 Experiment tests of the improved passive HESS

The passive HESS with the added inductor was also experimentally tested, to examine the benefits of the existence of an inductor. The circuit diagram of the experimental system is presented in Fig. 7.11. The inductance of the newly added inductor was 1mL.

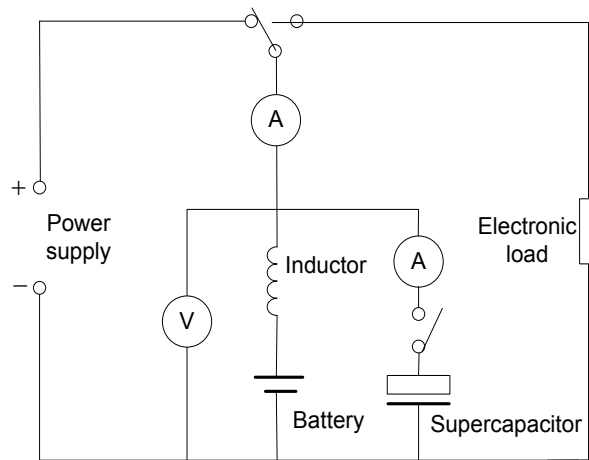


Fig. 7.11 Circuit diagram of the experimental semi-active connected system

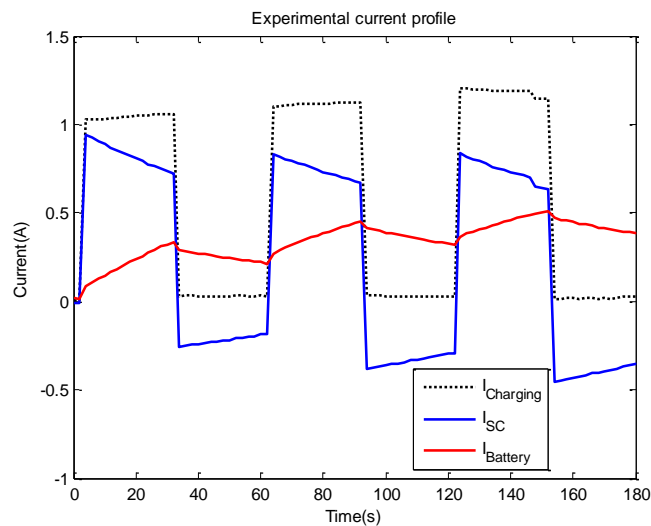


Fig. 7.12 Experimental currents for the passive HESS with inductor

The measured current profile is given in Fig. 7.12. Compared to the passive connected system in Fig. 7.10a, the current share taken by the supercapacitor is markedly higher than in the HESS case. The majority of the charging current, particularly the peak current, was absorbed by the supercapacitor, and a quite stable battery current can be therefore guaranteed, which benefitting battery performance and lifetime. The measured results agree well with the simulation in Section 7.4.2 as well.

## **7.6 Experimental study on the hybrid PHS-battery energy storage system**

The study findings in Chapter 6 suggest that if a secondary energy storage system were employed, the capacities of PHS facilities could be greatly reduced and power supply reliability could be simultaneously improved. In this section, the benefits of a small battery bank added to a PHS-based RE system are analyzed, and such a HESS is examined experimentally.

### **7.6.1 The benefit of a battery bank for the pumped energy storage system**

Introducing a small battery bank is important in a PHS-based RE system, for the following reasons:

#### 1) Balancing demand and supply in discharging mode of the pumped storage system

Consumption load is unsteady since residents turn their electrical appliances on and off as they see fit. In the traditional hydro turbine powered village, the surplus energy when demand is lower than production is transferred into a dump load. This is a simple but wasteful approach. Therefore, a small battery bank, which is employed to match demand at all times, can maintain output voltage and frequency at levels that do not damage appliances. A bidirectional inverter can be utilized to deliver any excess power

to a battery bank and to convert the DC output from batteries to serve the AC load. The detailed operating conditions of a small battery bank in a pumped storage based RE system can be divided into several cases:

- When the load demand falls to levels suitable for the battery bank is able to supply that load, the controller should turn off the turbine completely and switch to battery bank supply as a bridge until the maximum depth of discharge is reached or the load rises. At that point the turbine comes back on again and the process cycle is repeated. This approach avoids frequent stops and starts of the turbine/generator unit.
  - When the load demand is low while it is still larger than the existing energy stored in the battery bank, and the turbine/generator should start up. To ensure reasonable “partial load” efficiency, usually the turbine should keep operating at its minimum load ratio of 50%. If the required power is 30%, for instance, the turbine still operates at its 50% capacity, with the 20% surplus power used to charge the battery bank. In this way, the inefficient and life-shortening “partial load” operation for the turbine can be avoided.
  - When the electric load suddenly increases and an extreme peak load occurs, the controller combines outputs from both turbine and batteries to meet the load. This action can cater for a brief period of peak demand thereby avoiding the need to provide a turbine and upper reservoir big enough to meet that peak demand on its own.
- 2) Balancing RE output and water pumping in charging the model of the pumped storage system

The presence of a small battery bank can also be used to interpose between the stochastic RE output and motors/pumps, to provide a stable voltage and current for driving these machines. This approach is popular with traditional PV water pumping systems. The roles of the batteries in the HESS are as follows:

- When system surplus RE output is slightly insufficient to start up the pumps, the batteries release some power to fill the gap and assist in starting up the pumps;
- When system surplus RE output is far below the launching power needed by the pumps, the available energy is directly fed into battery bank through the inverter, avoiding frequent starting and stopping of the motors/pumps unit and ensuring the pumps efficiencies;
- When system surplus RE output is greater than the rated power of pumps, the excess can be stored in the batteries, which can cut the peak RE output and absorb the energy to avoid excessive pump/motor sizing;
- When the UR reaches its maximum capacity, the battery bank might also absorb the RE production if not already fully charged, and the wasted energy can thus be reduced and a high energy utilization rate ensured.
- The batteries act to better distribute the times spent water pumping and battery charging /discharging. The pumps are therefore operated more steadily and lifting efficiency is further improved.

These multiple effects of the small battery bank play a vital role in the scheduling of energy dispatch, managing the remote microgrid PHS-based RE systems, reducing dumped energy and ensuring high efficiency for the pump and turbine. An effective

controller is also necessary to manage the energy distribution between RE output, the pump/motor unit, the turbine/generator unit, the batteries and the load. Settings and operating principles need to be developed such as turbine minimum load ratio, pump and turbine rated capacity and battery bank capacity. The drawback is that the overall efficiency of a pumped storage scheme when combined with a battery bank will slightly decrease, as batteries and inverters need extra energy conversion processes and losses will be introduced. Investment is thus increased and the environmental benefits of the purely pumped storage scheme are somewhat diminished.

### 7.6.2 Experimental test system

Mathematical modeling and simulation of the hybrid pumped hydro and battery energy storage system will be conducted in future work. However, the operating performance of such hybrid energy storage system has been examined experimentally.

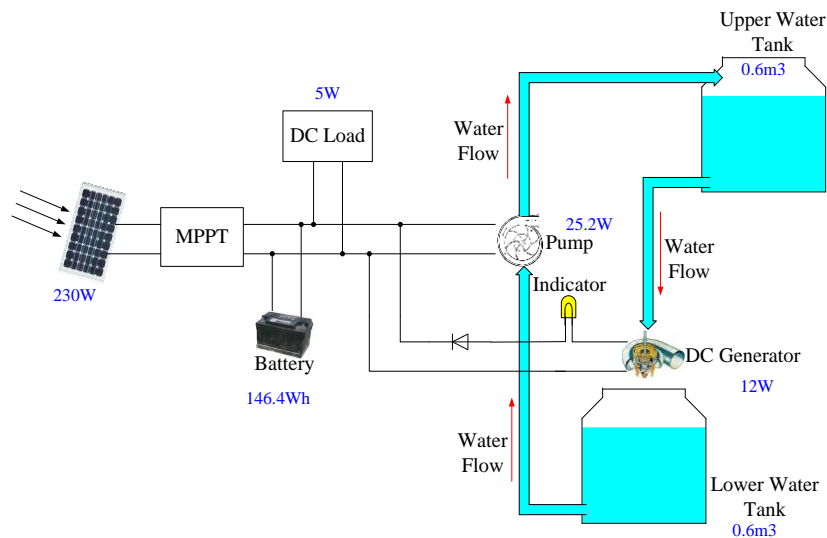


Fig. 7.13 Schematic of a micro PV system with hybrid PHS and battery energy storage

A demonstration of a micro PV system with the hybrid energy storage was developed in the laboratory, at the Center for Electric Vehicle and Smart Grid in Wayne State

University. The experimental tests were conducted by for three days by Dr. Junhui Zhao in that university.

The system diagram of a micro PV system with hybrid pumped hydro and battery energy storage is shown in Fig. 7.13 [361]. This is a demo system for experimental tests and educational purposes. This demo contains a 230W solar panel, a 146.4Wh battery, a 25.2W pump, a 12W DC generator, two 0.6m<sup>3</sup> tanks, a 5W light bulb as load and a central controller. They are all connected through a 12V DC bus. The laboratory implementation of the real hybrid energy storage system is presented in Fig. 7.14. In this system, the solar panel is the sole energy generation source to meet load demands and charge the hybrid energy storage system. A battery bank is the primary energy storage system, so the excess power will charge the battery bank first and the extra, if any, will be used for pumping the water to the upper tank, taken as the secondary storage system.

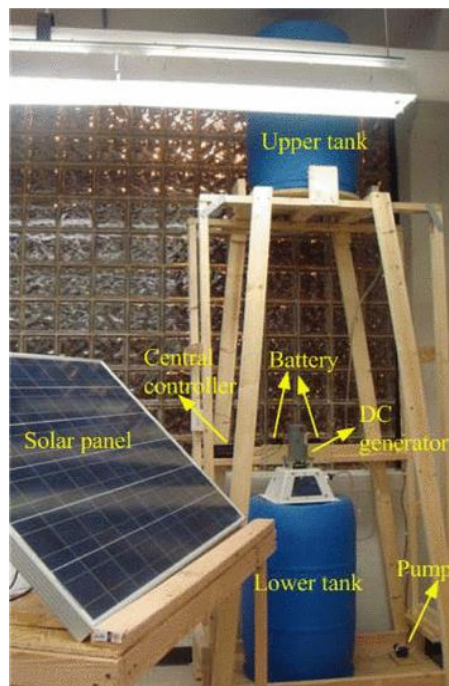


Fig. 7.14 Laboratory implementation of the hybrid energy storage system for PV [361]

### 7.6.3 Experimental results and analysis

The two tables below (Table 7.1 and Table 7.2) present the original data collected on 2 July 2014. The solar radiation, PV output, water level in lower tank, battery voltage and generator/pump current data were recorded. The electrical load was cut off during the tests to focus on investigating the operational performance of the hybrid energy storage system only.

Based on the collected original data, it is obvious that the system operation can be divided into three cases. The first case is when the battery is charged by the PV output plus power from the turbine. The second case is when the PV and battery outputs together drive the pump in storing energy in the upper tank. The third case is when the PV charges both energy storage systems simultaneously.

Table 7.1 Experimental data collected under charging status

Time (min)	Solar radiation (W/m <sup>2</sup> )	PV power (W)	Water level in lower tank (cm)	Battery voltage (V)	Generator current (mA)
0	750	7.875	8.5	14.4	75.2
1	690	7.56	11.2	14.1	70
2	680	6.93	21	14.1	61.2
3	740	7.36	28.8	14.1	55
4	810	6.4	36.5	14.1	47.9
5	750	5.985	43.5	14.2	41.3
6	759	6.93	52	14.2	38

Table 7.2 Experimental data collected under discharging status

Time (min)	Solar radiation (W/m <sup>2</sup> )	PV power (W)	Water level in lower tank (cm)	Battery voltage (V)	Pump current (A)
0	850	11.7	52	13.3	1.33
5	747	9.35	45.5	12.4	1.27
10	782	10.92	40.5	12.5	1.26
15	956	15.13	36.5	12.6	1.28
20	921	15.67	32.5	12.6	1.28
25	951	17.67	26	12.7	1.3
30	950	20.16	21.5	12.8	1.33
35	946	21.09	15	12.9	1.33
40	935	22.96	12	13.2	1.35
45	863	22.12	8.5	13.4	1.1

The collected original data was processed and is presented in Table 7.3. The energy balance for the three cases was examined. In case 1, the efficiency of the turbine/generator unit, i.e. PHS discharging model was calculated at 9.4%, based on the reduced gravitational potential energy in the upper tank and the energy produced by the generator. In cases 2 and 3, the PHS system is being charged so the efficiency of the pump/motor unit was calculated at 6.8%, based on the stored energy in the upper tank and the input energy to the water pump. Therefore the overall efficiency of the pumped storage system could be extremely low, owing to the conversion losses of the micro pump-turbine set and the losses induced in the pipe line. The system performance could be potentially enhanced through optimizing system operation and introducing superior system components. It is noted that this experimental system

functions as an educational tool to demonstrate different technology concepts of energy storage and integration of RE and energy storage systems, therefore, operation demonstration is the focus of this system rather than its efficiency.

Table 7.3 Energy balance of the hybrid energy storage system under three cases

	<i>PV power (W)</i>	<i>Generator power (W)</i>	<i>Battery power (W)</i>
Case 1: PV + pumped storage = battery	7.88	1.08	8.96
	7.56	0.99	8.55
	6.93	0.86	7.79
	7.36	0.78	8.14
	6.40	0.68	7.08
	5.99	0.59	6.57
	6.93	0.54	7.47
	<i>PV power (W)</i>	<i>Pump power (W)</i>	<i>Battery power (W)</i>
Case 2: PV + battery = pumped storage	11.70	17.69	-5.99
	9.35	15.75	-6.40
	10.92	15.75	-4.83
	15.13	16.13	-1.00
	15.67	16.13	-0.46
Case 3: PV= battery + pumped storage	17.67	16.51	1.16
	20.16	17.02	3.14
	21.09	17.16	3.93
	22.96	17.82	5.14
	22.12	14.74	7.38

For other practical engineering projects studying micro pumped storage for RE systems [389], where the efficiency of the water pump (6.6kW) and the turbine (5.0kW) was 72% and 64%, respectively, at the best operating points. In the literature [361], the rated efficiencies of the micro water pump (10kW) and turbine (7.5kW) were 68% and 39%. In a real engineering project in Laos [459], the pump efficiency was 50%, and the efficiency of the turbine 65%. Usually, a roundtrip efficiency of a micro pumped storage system in practice is about 50%.

## **7.7 Summary of this chapter**

The main purpose of this study is to assess the possibility and benefit to combine supercapacitors and traditional batteries for achieving a complementary performance between two devices. The numerical analysis, simulation and experimental results demonstrate that the passive hybrid leads to improved energy storage performance. The battery in the HESS performs as the primary energy source for longer periods and the supercapacitor as the auxiliary power source for “peak power smoothing” and “emergency reserve”. The combination makes energy storage possessing both high power and energy density, and extending battery life as well.

In addition, the benefits of the hybrid pumped storage and battery energy storage system was analyzed and a demo of the system experimentally studied, as an illustration of the various types of operational state of such hybrid energy storage technology.

## **CHAPTER 8 PERFORMANCE EVALUATION OF A REMOTE RENEWABLE ENERGY SYSTEM**

As introduced in Chapter 1, a 19.8 kWp PV system was installed on Town Island to supply power to the local residents during Stage 1 of the RES scheme which began in 2008. The PV system in Stage 1 is mainly used to test its feasibility, understand its operating characteristics, and prepare for the system implementation in next stage. As a part of the collaborative project, this section gives a detailed investigation on the Stage 1 system operation after more than one year's joint effort. Currently, this part of the work has already been published [15].

To find the actual power generation of the first-stage PV system and better understand its operating characteristics, and to facilitate the system design of the Stage 2 hybrid solar-wind power project, a data acquisition system was installed on the existing PV system and several site visits were made to understand both the local environment and geography of the island. During these trips, the data acquisition devices were examined and calibrated to ensure accurate data measurement.

After several months of testing and commissioning, the system environmental and operating data over a complete year in 2011 were collected at 5-minute intervals. A check for any anomalies in the recorded data was carried out before processing and detailed analysis. The data was evaluated in respect of the performance of the PV array, inverters, battery bank and the entire PV system performance which was analyzed in terms of daily energy balance, normalized parameters and system overall energy performance (efficiency/ratio).

## 8.1 System description

Fig. 8.1 shows the installed PV system located on this island. The 19.8 kWp PV array consists of 99 solar panels from Suntech (Model: STP200-18/Ud). As shown in Fig. 8.2, this system has two subarrays, one with three parallel strings of 17 modules connected in series and linked to one PV inverter and another one with configuration of  $16 \times 3$  linked to the other inverter. All the PV panels are positioned in a fixed direction facing south at an inclined angle of  $22.5^\circ$ .



Fig. 8.1 The installed PV system on a remote island in Hong Kong (19.8kWp)

Unlike typical standalone systems, this system uses an AC busbar to couple all system components. This architecture has greater flexibility in accommodating additional generating capacities and/or load in the future. In such condition, this stand-alone PV system employs two different types of inverter: five bidirectional inverters SI5048 and two PV inverters SMC10000TL. The five bi-directional inverters connected to the load side, PV inverters and battery bank have two functional modes, i.e. charging mode and discharging mode (inverter mode). During the charging mode (net load is positive), the inverter converts AC to DC and then charges the battery bank using the surplus energy provided on the AC side. During the discharging mode, the inverter

provides 220 VAC output using the energy stored in the batteries, allowing stable operation of the connected loads when solar energy is not available and yet electricity demand still exists. The five parallel-operation battery inverters are operated in a master-slave-standby configuration [460, 461]. The two Sunny Mini Center (SMC) PV inverters directly transform the DC PV output to supply 220VAC to the load while any surplus energy is used to charge the battery bank via the SI5048 inverters. The battery tank comprises 96 deep cycle cells made by Sonnenschein Exide. 24 cells are connected in series to provide a 48 volts nominal storage voltage.

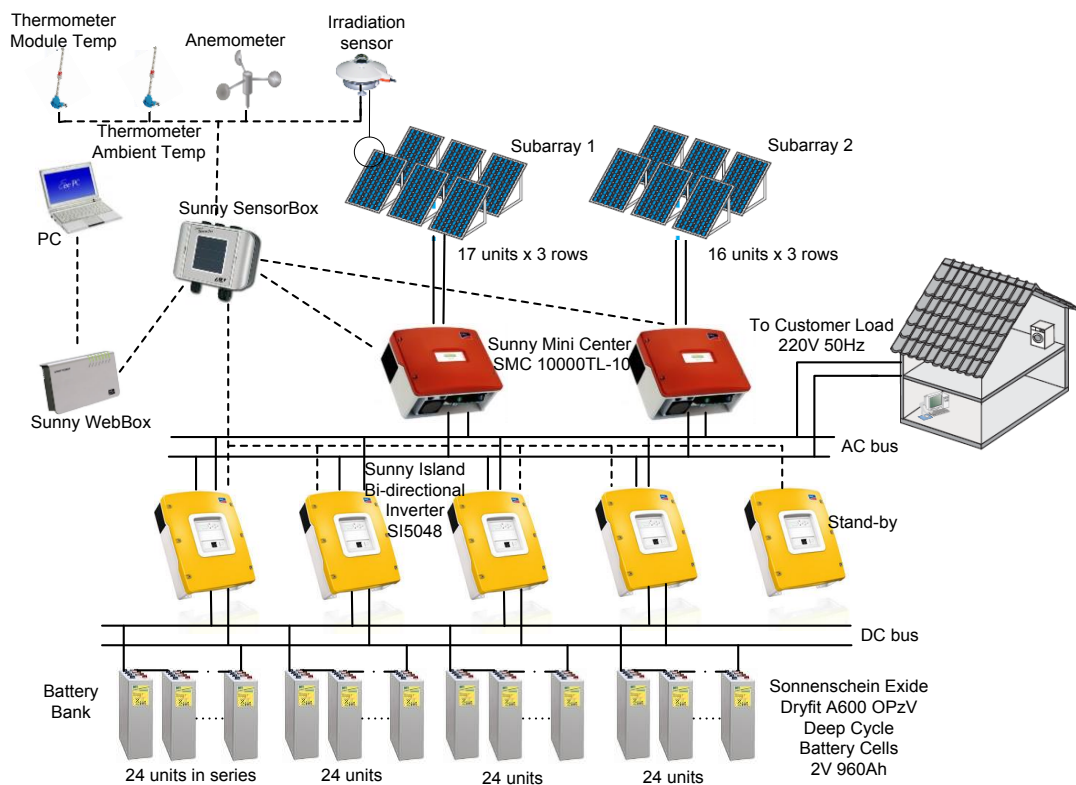


Fig. 8.2 Schematic diagram of the standalone PV system

The long-term environmental data such as solar irradiation and wind speed and the operation performance data such as power output, battery bank SOC and electricity consumption were continuously recorded by the Sunny SensorBox at intervals of 5 minutes, as shown by the dashed lines in Fig. 8.2.

## 8.2 System performance evaluation methods

The system performance was evaluated based on the PV array, SMC/SI inverters, battery bank and the entire PV plant. The overall system performance was analyzed in terms of normalized parameters and energy performance indices (efficiencies/ratio). The normalized performance parameters are usually employed as indicators to compare different PV system performances. These indicators in units of kWh/kWp/day (simplified as 'h/d') are obtained by relating the energies actually used to the nominal power of the PV array. Those parameters were evaluated following the guidelines of IEC Standard 61724 [462].

The array yield  $Y_A$  represents the number of hours per day that the array would need to operate at its nominal power  $P_0$  to contribute the same quantity of energy to the system as that actually measured in practice.

The final yield  $Y_F$  is the usable portion (i.e. used by the load) of the energy derived from the entire PV system. The yield is delivered to the load per kilowatt peak of installed PV array.

The reference yield  $Y_R$  is the theoretically possible energy output of the PV plant, which is defined as the anticipated output from the same system with nominal efficiency determined under Standard Tests Conditions (STC) of PV modules.

Energy losses indicate the amount of time during which the array would be required to operate at its nominal power  $P_0$  to produce power compensating for the losses. The losses mainly include system losses  $L_S$  and array capture losses  $L_C$ .

The following formulae were used to calculate the above normalized parameters [341, 463]:

Array yield:

$$Y_A = \frac{E_A}{P_0} \quad (kWh / d / kW_p) \quad (8.1)$$

Load consumption:

$$E_{PV} = \frac{E_{Load}}{1 + \frac{E_{BU}}{E_A}} = E_{Load} \quad (kWh) \quad (8.2)$$

Final yield:

$$Y_F = \frac{E_{PV}}{P_0} = \frac{E_{Load}}{P_0} \quad (kWh / d / kW_p) \quad (8.3)$$

Reference yield:

$$Y_R = \frac{\int G_i dt}{G_{STC}} = \frac{A \cdot \eta_{STC} \cdot \int G_i dt}{P_0} \quad (kWh / d / kW_p) \quad (8.4)$$

Capture losses:

$$L_C = Y_R - Y_A \quad (kWh / d / kW_p) \quad (8.5)$$

System losses:

$$L_S = Y_A - Y_F \quad (kWh / d / kW_p) \quad (8.6)$$

where  $E_A$  is the daily array energy output (kWh/d);  $P_0$  is the PV array peak power (kW<sub>p</sub>);  $E_{use}$  is daily energy delivered to the load (kWh/d);  $G_i$  is the irradiance

incident on the tilted PV array ( $\text{W}/\text{m}^2$ );  $E_{PV}$  is the actual energy amount contributed to the load by the PV plant;  $E_{Load}$  is the energy consumed by the load;  $E_{BU}$  is the energy consumption provided by the back-up system. In this system, the back-up generator output was not an input to this data acquisition system, so that  $E_{BU} = 0$  and  $E_{Load} = E_{PV}$ ;  $A$  is the total PV array area and  $\eta_{STC}$  is the PV module nominal efficiency at STC according to the manufacturer's specifications.

According to the above definitions, the relationships between these normalized parameters are briefly shown in Fig. 8.3. One completed year is usually used for analyzing the energy performance of a PV system [327]. In this study, the data collected in 2011 is employed.

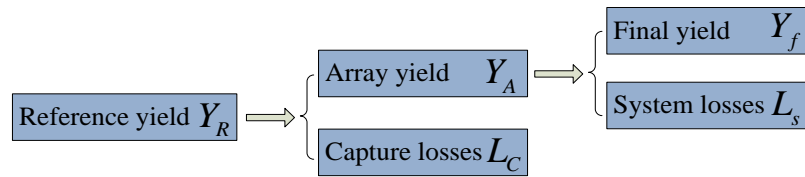


Fig. 8.3 Relationship between these normalized parameters

### 8.3 Performance evaluation results and analysis

#### 8.3.1 PV array performance analysis

The PV array DC power output from 1<sup>st</sup> to 10<sup>th</sup> May 2011, as an example, is presented in Fig. 8.4, which clearly illustrates that the PV DC output power, represented by the scatter points, is linearly dependent on the solar radiation level. To show their inherently close relationship, the tendency of instantaneous PV DC power per kW peak versus solar radiation on 10<sup>th</sup> May is shown in Fig. 8.5.

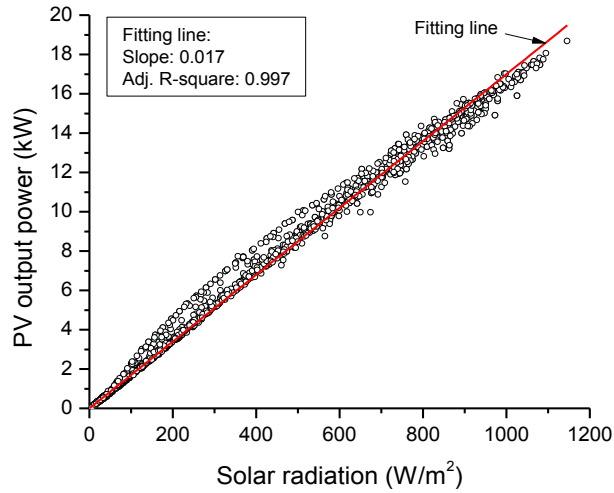


Fig. 8.4 The PV array DC output power versus solar irradiance (1<sup>st</sup> to 10<sup>th</sup> May 2011)

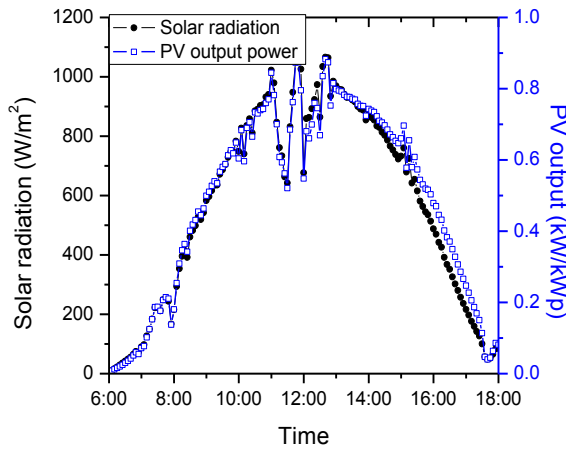


Fig. 8.5 The output power per peak watt versus solar irradiance on 10<sup>th</sup> May 2011

The daily energy production from this PV plant over the whole period is presented in Fig. 8.6. The gross electricity generation in the year was 22,322 kWh with a daily average value of 61.2 kWh. It is clear that the daily electricity production varies greatly from 5.5 to 115.5 kWh with the highest daily mean output in Aug (98.4kWh/day) and the lowest in Jan (24kWh/day). The production in the summer months was considerable higher owing to good solar irradiation resources and load side utilization ratio. However, production in winter and spring months (Nov-Apr) was very limited, particularly in Jan and Feb.

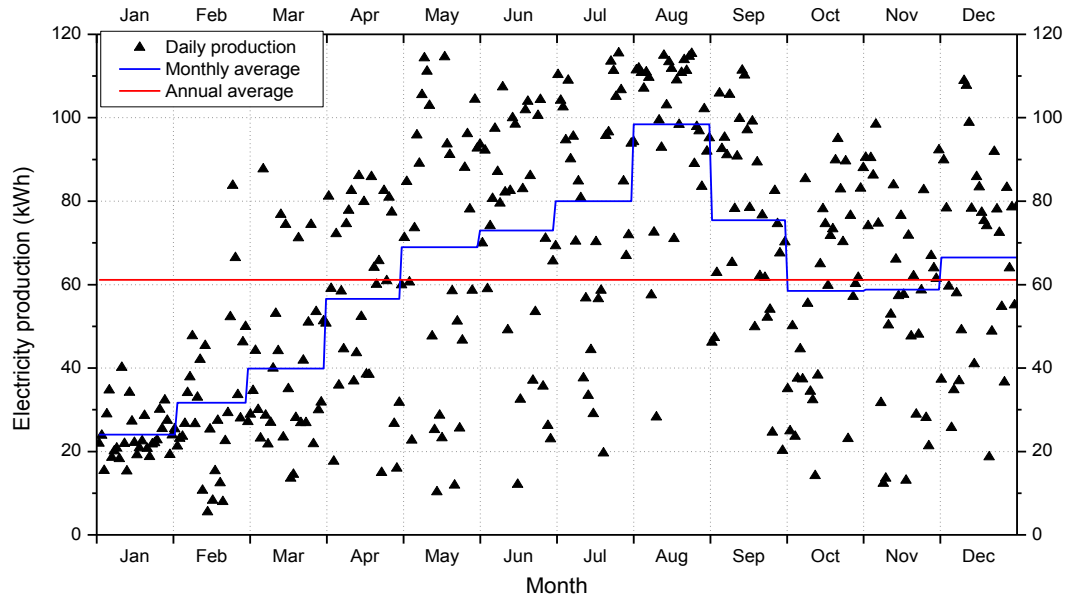


Fig. 8.6 Electricity generation profile in 2011

Fig. 8.7 gives the statistical daily average AC power output ratio of the PV modules during the studied period. This ratio mainly includes the PV module conversion efficiency, energy losses in SMC inverter for transforming DC to AC power and the energy losses during the PV modules switched off. For the on-site situation, the AC power output ratio, rather than the PV module efficiency, was usually employed as an indicator to evaluate PV array energy conservation performance under the non-standard condition. It was also found that the monthly mean PV module AC power output ratio ranged from 6.0% to 12.3%. The deviation between on-site AC power output ratio and PV module efficiency under STC may result from the non-standard test condition. Generally, the PV module would have lower conversion efficiency than the nominal value when the solar radiation drops to fairly low levels, say, 100 - 300 W/m<sup>2</sup>. The onsite recorded data show that for a great deal of time solar radiation was less than the level for rated efficiency. Another phenomenon observed is that for most of the time the working temperature was higher than 25 °C, and PV module voltage decreases significantly with the increase in cell temperature. In addition, sometimes

the PV array was switched off and disconnected during the best sunshine hours when the output was much higher than the load demand and the battery bank was already fully charged. In such conditions, the PV array has the potential to generate more electricity. Under the circumstances, we cannot take for granted that the PV array performed poorly. Other factors such as energy losses in SMC inverters for converting DC power to AC, the accumulation of dirt on the PV modules surface and shading may also affect the PV generator's power output and efficiency.

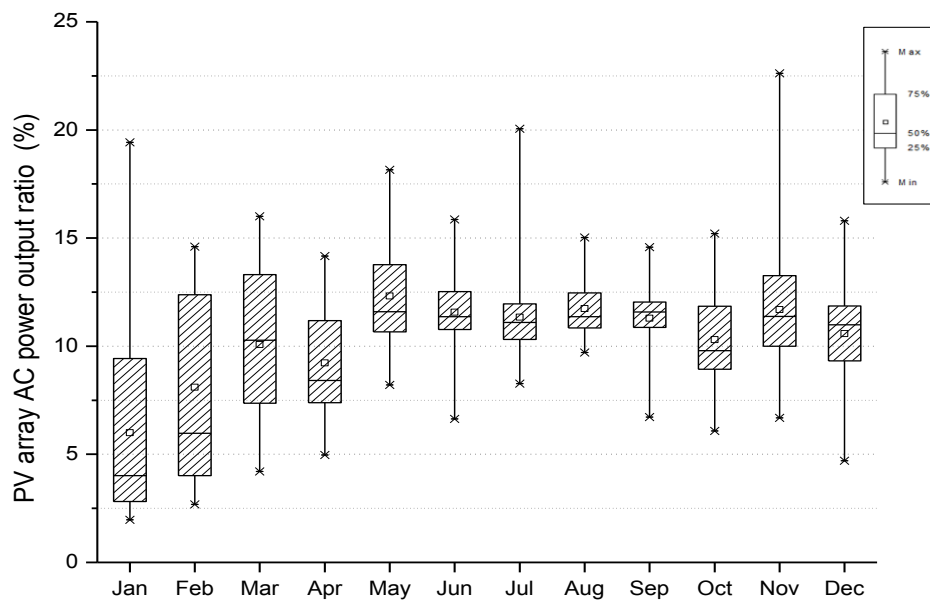


Fig. 8.7 Daily average AC power output ratio of PV module during 2011

Fig. 8.8 shows the onsite daily mean temperatures over the reporting period. The variations in module, battery and ambient temperature show a similar trend. The average ambient temperatures in the summer months from May to September were between 25 °C and 30 °C, and the PV module temperatures were greater than 35 °C. The yearly average temperature of batteries and modules were about 4.7 °C and 9.4 °C higher than ambient. The peak difference between battery and ambient temperatures can reach 12 °C, while the peak difference between module and ambient temperature can be greater than 30 °C.

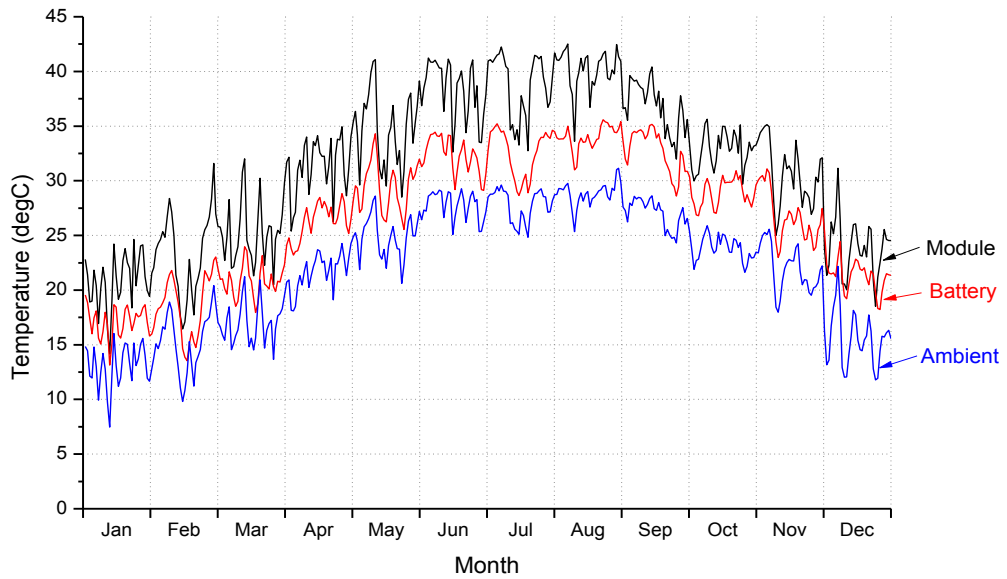


Fig. 8.8 Daily average temperatures of ambient, battery and PV module

### 8.3.2 SMC inverter performance analysis

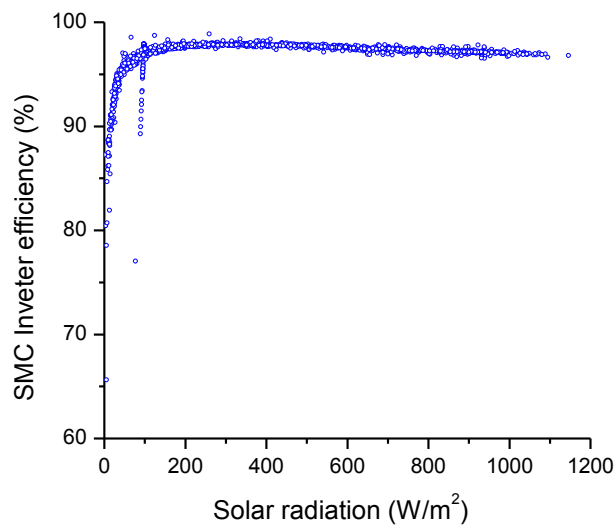


Fig. 8.9 SMC inverter efficiency from 1<sup>st</sup> to 10<sup>th</sup> May 2011

In this study, one of the two inverters with similar characteristics was chosen as an example. Only 10 consecutive days were chosen to analyze the inverter's performance. Fig. 8.9 shows that the SMC operates well with high efficiency from 95% to 100% if the solar radiation is greater than 100 W/m<sup>2</sup>. The mean efficiency over the whole solar

radiation range is 97.1%, very close to the value of 97.5 % provided by the manufacturer. Furthermore, the scatter points in this figure indicate that when the efficiencies reach the peak value at a solar radiation of about  $200\text{W}/\text{m}^2$ , they are followed by a slight descending tendency, which coincides with the experimental test results provided by the SMA Company.

### 8.3.3 SI inverter performance analysis

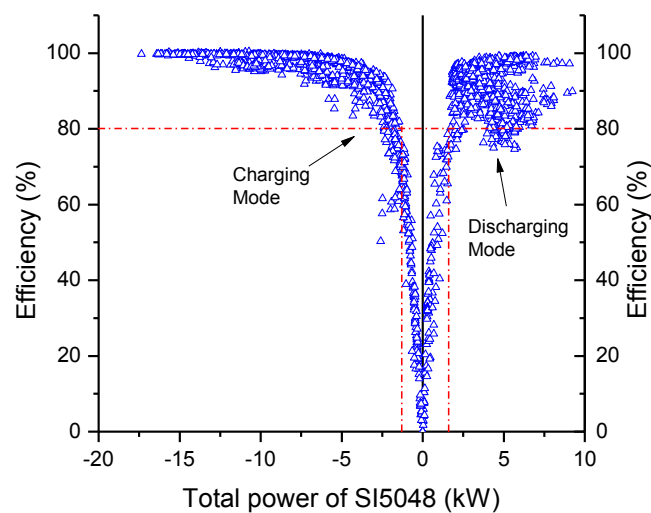


Fig. 8.10 Sunny Island bi-directional inverter efficiency from 1st to 10th May 2011

The master SI bidirectional inverter operating data for 10 days is presented in Fig. 8.10 which demonstrates that the two functional modes behave differently. In the charging mode, the average efficiency was 87.2%. In the discharging mode, the average efficiency was 89.4%. The difference shows that discharging is more effective than charging, which might result from the different input powers of each mode. The input power to the inverter during charging model is the output from the SMC, which comes from the PV generator and largely dependent on the fluctuating solar irradiation. However, the input power for discharging is the battery output where the voltage is quite constant and stable. For the SI to operate with an acceptable efficiency above

80%, the input powers of the SI during charging and discharging modes are about 1.3kW and 1.5kW respectively, as shown by the dashed line in Fig. 8.10.

### 8.3.4 Battery bank performance analysis

The ten-day data (1<sup>st</sup>-10<sup>th</sup> May 2011) in Fig. 8.11 illustrate battery status in detail including the battery SOC and battery charging and discharging power. During this period, the SOC ranged from 40% to 100%. The lowest SOC occurred during the early morning of each day after several continuous hours of discharging, and the peak SOC appeared in the afternoon lagging a couple of hours behind the peak solar radiation. The increase in SOC indicates that the battery bank stores surplus energy from the PV array after supplying power to the load. It also demonstrates that the depth of discharge (DOD) of the battery bank was not too high, which helps to prolong battery life and guarantee high energy efficiency.

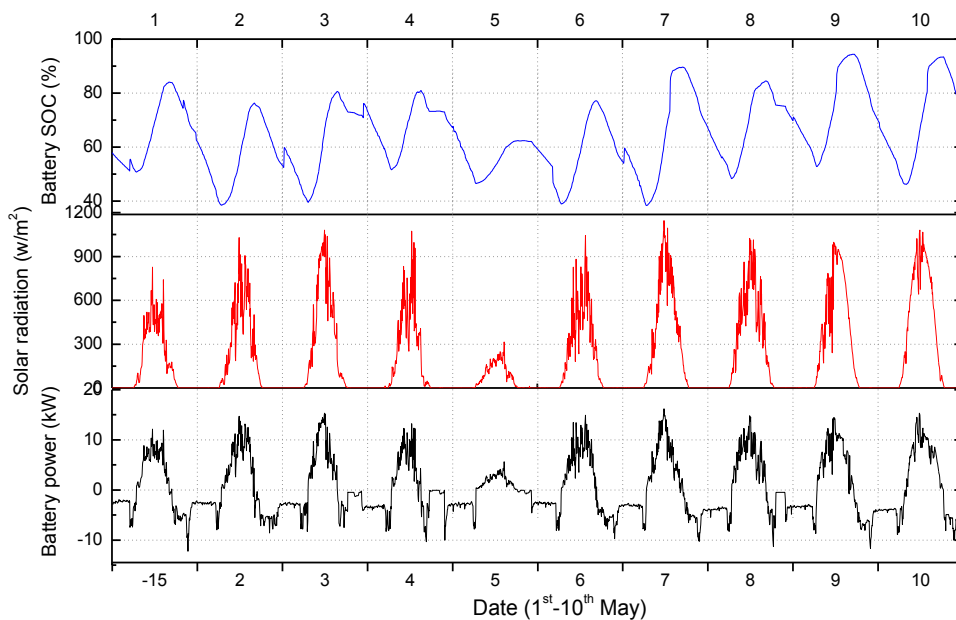


Fig. 8.11 The status of battery bank from 1<sup>st</sup> to 10<sup>th</sup> May 2011

The maximum battery bank charging and discharging power were found to be 16.2kW and 13.4kW, respectively. The charging rate was lower than 10kW for most of time

except for the peak value at noontime under bright sunlight. Also for most of time, the discharging power was less than 10kW, and the stable value was around 4 kW, which closely relates to the load demand. Another finding is of an obviously common sharp increase in discharging power at around 6:00am and 6:00pm. One possible reason for this phenomenon is that the load includes some appliances requiring a lot of power during these periods such as lighting. Taking solar radiation into consideration, it is obvious that the SOC and battery charging and discharging power bear a very close relationship to it.

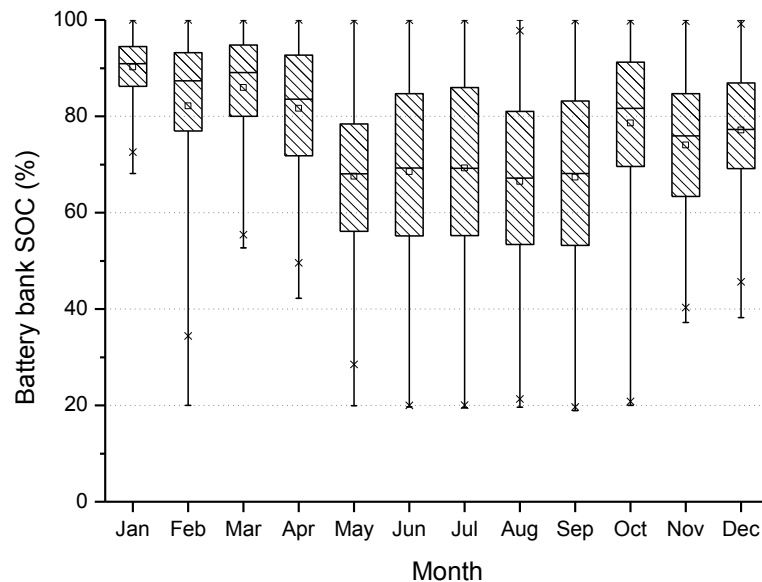


Fig. 8.12 Monthly battery SOC profile during 2011

The monthly SOC distribution is statistically presented in Fig. 8.12 which demonstrates that the SOC seasonal changes were very marked. The smallest SOC values occurred in the summer from May to Sep when the monthly averages were lower than 70%. Probably the main underlying reason is that refrigeration and air-conditioning cooling loads during summer are high even though solar resources are good during this period. The monthly average values from Jan to April and from Oct

to Dec were relatively high. The allowable minimum SOC value is 20% and the maximum allowable DOD is 80%. If this upper DOD limit is exceeded, the batteries will suffer from over-discharge, and prolonged over-discharge may result in permanent damage to the battery.

The hourly average battery bank SOC over the whole year is depicted in Fig. 8.13, demonstrating that the daily smallest and highest SOC values occurred at about 7:00am (60.6%) and 5:00pm (88%), respectively. At 7:00am, solar radiation is increasing and the battery bank is being recharged, and thus a significant increase in SOC can be observed. The SOC growth rate is greater, before the peak solar radiation at about 1:00pm. This growth trend ends at about 5:00pm when load consumption is balanced by energy supply. Thereafter, the SOC declines continuously until 7:00am next morning.

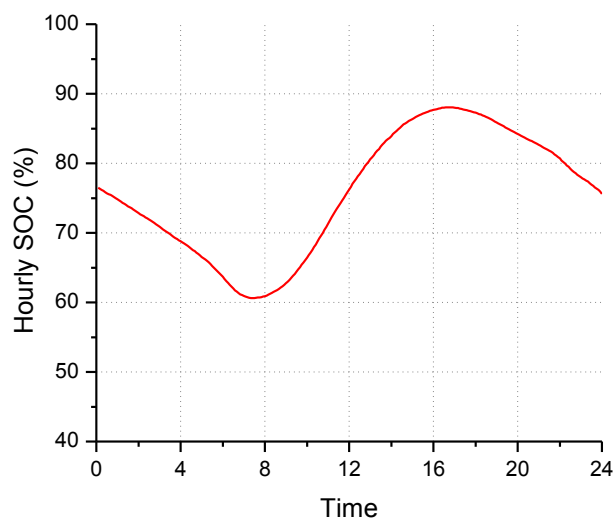


Fig. 8.13 Battery SOC hourly variation (time interval: 5 minutes)

Fig. 8.14 presents the SOC distribution probability (or occurrence frequency) ranging from 10% to 100%. The results indicate that the battery bank in this project is well

controlled. About 88 percent of its SOC values were above 50% and 45 percent above 80%.

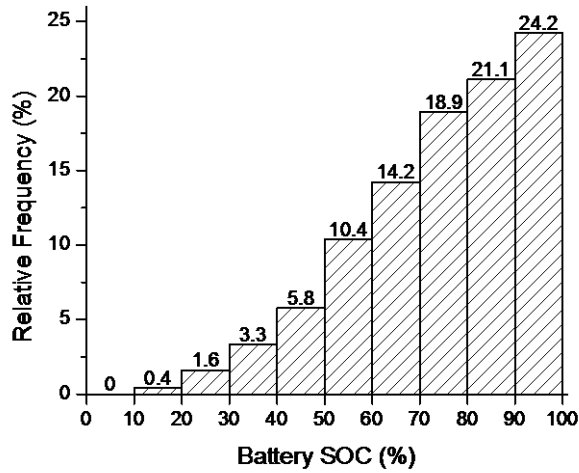


Fig. 8.14 Frequency distribution of battery bank's state of charge (SOC) during 2011

In general, the variations of solar output do not match well the fluctuations of demand. Therefore, a certain degree of oversizing of the storage system is required to guarantee power supply reliability. The total storage capacity of the current battery bank, 184.32kWh, is much higher than the mean daily load demand (49.5kWh) in order to allow power supply for the several consecutive days of poor solar radiation. That is the reason why the battery bank is always fully charged, and consequently the PV array sometimes needs to be disconnected and thus cannot work at its maximum efficiency. In a word, all these statistics demonstrate the need for rational system design and operation. As a consequence, a long cycle life for the batteries can be ensured.

The battery bank's SOC was 89.1% at the beginning of year and 77.6% by the end. Thus the net energy stored in the battery bank was 21.1kWh. Throughout the year, in total 16,308 kWh solar energy was input to the battery bank but only 12,090 kWh of energy was discharged. Therefore, about 4,239kWh energy was dissipated during the

charging, discharging and storing periods. As a result, the battery bank roundtrip efficiency is approximately 74.3% on an annual basis.

### 8.3.5 Entire system performance analysis

The variation of daily energy production, consumption, and battery bank input or output energy in May, as an example, is displayed in Fig. 8.15 to show the daily energy balance. Daily energy production is in the range of 10 to 115kWh and the daily energy consumption is between 16 and 88 kWh. The differences between them are offset by charging or discharging the battery bank. The total energy input to the battery bank (1,613kWh) is much greater than the output (1,182kWh), where the differences may result from battery self-discharging and the cyclic processes of charging and discharging. Obviously, this quantity of energy loss is dependent on the battery's energy efficiency.

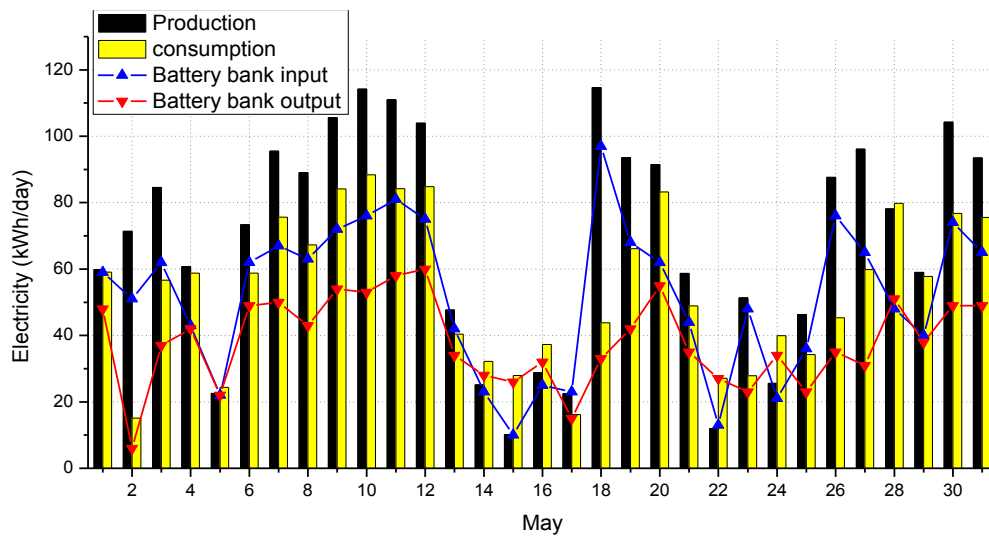


Fig. 8.15 Daily electricity generation and load consumption in May 2011

The daily average solar radiation, PV AC power production, load side energy consumption, and whole system energy performance are summarized in Table 8.1. The table illustrates that the annual total solar energy resource incident on the tilted

PV array is 1,586 kWh/m<sup>2</sup> (=4.34 kWh/m<sup>2</sup>/day). The monthly solar radiation distribution peaks in August and reaches its minimum value in March. It can also be seen that solar radiation in winter is significantly lower than in summer.

Table 8.1 Summary of the entire system energy performance

Month	Solar radiation	PV AC power production	PV AC power output ratio	Load consumption	System overall energy utilization ratio
Unit	kWh	kWh	%	kWh	%
Jan	17,731	744	4.2	519	2.9
Feb	15,157	886	5.8	684	4.5
Mar	14,318	1,236	8.6	967	6.8
Apr	20,522	1,697	8.3	1,419	6.9
May	18,261	2,138	11.7	1,678	9.2
Jun	19,746	2,189	11.1	1,810	9.2
Jul	22,701	2,480	10.9	1,994	8.8
Aug	26,363	3,051	11.6	2,601	9.9
Sep	20,423	2,263	11.1	1,762	8.6
Oct	18,702	1,813	9.7	1,482	7.9
Nov	16,391	1,764	10.8	1,457	8.9
Dec	20,510	2,061	10.1	1,697	8.3
Ave.	19,235	1,860	9.5	1,506	7.7

The average electricity production is 61.2kWh/day and the energy consumption is 49.5kWh/day. The difference between the PV AC power production and load side energy consumption results from energy stored in the battery bank, energy losses in the BOS including SI inverters, battery bank, and conduction losses in distribution

cables. The PV AC power output ratio by month ranges from 4.2% to 11.7%, averaging at 9.5%, and system overall energy utilization by month is within 2.9% and 9.9%, averaging at 7.7%. It is obvious that the load side consumption coincides with the time distribution of production. When energy consumption reaches its peak, with a high cooling load, the PV array generates the most power due to the highest solar radiation levels.

It is significant that the AC power production and load side energy consumption in Jan and Feb were extremely low, though the solar energy resource is not too bad. The key reason is that residents on the island did not know, at first, how to interpret the battery bank's SOC and therefore tended to restrict their consumption. This could also explain the low demands in Jan and Feb and the high battery bank SOC value. Therefore, the PV array was sometimes shut down by the control system due to the fully charged battery bank, to protect the battery bank and PV panels. The power output was then affected and lower energy consumption is observed. According to the discussion with project engineers responsible for the operation of this PV plant, local residents were able to tailor their demands according to the SOC level after their education, leading to a somewhat human driven intelligent system. From then on, in the following months, high energy utilization was recorded.

The difference between PV AC power production and electricity consumption is expressed as a load side energy utilization ratio. It is obvious that Jan and Feb have the lowest energy utilization during the year, while the SOC during these two months was very high (Fig. 8.12), which further suggests that the residents did not know how to use the system depending on the energy stored in the battery bank, i.e. SOC.

To improve the PV power output ratio and load side energy utilization ratio, one solution was to train local residents for better utilization of energy from the PV array and battery bank based on local weather and energy stored in the battery bank (i.e. SOC). On the other hand, if sufficient storage capacity and/or a backup generator can be guaranteed, a greater PV power output ratio and utilization ratio in the standalone system should be achievable. However, in reality a project has to be optimized between technical and economic performance. An appropriate compromise between system total cost, energy efficiency, supply reliability and future expansion would provide a cost effective RES option with satisfactory supply quality matching the nearby power grid (a normal expectation of the customers).

A summary of the normalized performance parameters is presented in Fig. 8.16, which reveals that the monthly final yield fluctuated greatly with a minimum value of 0.84 h/d in Jan and a peak of 4.24 h/d in Aug. The results indicates that the total hours of power production at less than the rated capacity during the whole year was 910 hours, meaning that only an equivalent energy of 2.49 kWh/kWp/day was consumed by the load.

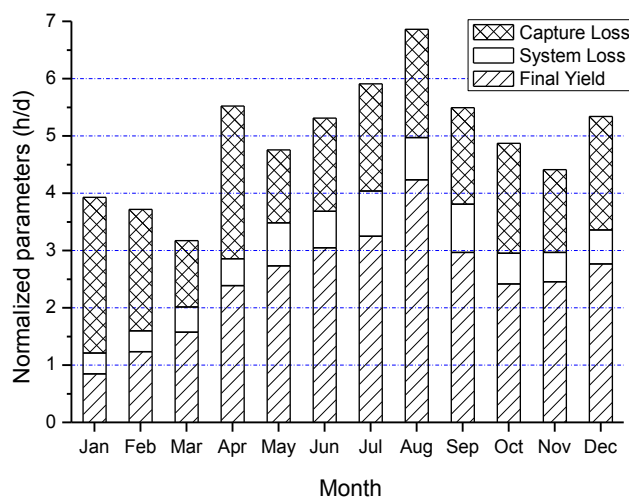


Fig. 8.16 Monthly Normalized parameters

Fig. 8.16 also shows that the system losses ranged from 0.36 to 0.84 h/d, averaging 0.59h/d. The system losses mainly result from the inverter conversion process (DC-AC or AC-DC) and battery storage cycles. Another contribution to system losses is the capacity mismatch between load and PV generator. When the energy demand during sunshine hours is lower than the PV output and the battery bank is already fully charged, the excess energy is wasted and the PV array only partially operates or is fully cut off.

The mean daily capture loss was about 1.86 h/d, indicating that about half of the array yield was lost. The capture loss in January was 2.72h/d, much higher than the final yield of 0.84h/d, representing an extremely low PR of 18.3%. The array capture loss is a big problem for this system and was split between thermal losses and other miscellaneous losses. The power output of a PV is a decreasing function of cell temperature. The power temperature-coefficient for a crystalline silicon solar cell is about -0.65%/K [464]. Therefore, when the cell temperature is higher than the STC of 25 °C, the PV performance is affected resulting in thermal capture losses. Other miscellaneous capture losses include low irradiance, string diodes, partial shading, contamination, and reduction of array power caused by inverter failures or by fully charged accumulators, spectral losses and losses caused by glass reflections.

The theoretical reference yield, the sum of the above three parameters (see Fig. 8.3), varied from 3.17 to 6.86 h/d and averaged 4.94h/d. The findings in Fig. 8.16 also display the array yield. The sum of final yield and system losses (see Fig. 8.3), was 3.08h/d. These parameters demonstrate that the anticipated output of the PV array was 4.94 kWh/kWp/day, but actually the array AC output was 3.08 kWh/kWp/day, of which only 2.49 kWh/kWp/day was ultimately used to supply the load.

## 8.4 Summary of this chapter

In this chapter, an overall evaluation of the stand-alone solar PV system operational performance for the whole of 2011 was conducted covering the following aspects: the PV array, inverters, the battery bank and overall system performance. The following conclusions can be drawn:

- The average electricity production from the PV system was 61.2kWh/day and the electrical energy consumption was 49.5kWh/day. The available solar radiation incident on the PV array was 4.34kWh/m<sup>2</sup>/day so that the average AC power output ratio of PV array and entire system energy utilization ratio were 9.5% and 7.7%. These values are satisfactory.
- The SMC and SI operated well, with high efficiencies close to the manufacturer's specifications.
- The roundtrip efficiency of the battery bank during the year was 74.3%, with SOC values above 50% for 88% of the year.
- The average yield, system losses and capture losses during the year were 2.49h/d, 0.59h/d and 1.86h/d, respectively. The resultant array yield was 3.08h/d.
- Training local residents for better utilization of the renewable energy output can help PV array to produce more power in some situations and eventually improve the utilization ratio.
- The low load side energy utilization ratio and mismatch between the power production and consumption demonstrate that an optimal design selection of PV array and battery bank capacities is quite necessary, which should consider technical issues (e.g. supply quality/reliability, energy efficiency), economic

issues (e.g. cost of energy) and social issues (future expansion). In that sense, academic and industrial considerations should be merged together for a practical renewable energy supply project. A detailed energy performance simulation model needs to be developed for this purpose.

In summary, the long term system monitoring enabled a detailed understanding of the system operating performance from the technical point of view. It also provided useful reference information for future PV system design and operation. This study is also a useful case study of real practical relevance to future applications of renewable energy supply on remote islands.

## **CHAPTER 9 SUMMARY AND SUGGESTIONS FOR FUTURE STUDY**

The research findings, main conclusions and recommendations for future work are summarized in this chapter.

### **9.1 Summary of research findings/contribution**

To achieve the goal of remote area power supply (RAPS), a comprehensive study of stand-alone renewable energy (RE) systems using different energy storage solutions has been presented in this thesis. Meaningful research outputs, potentially useful in remote areas, have been achieved. Town Island, a remote inhabited island off the coast of Hong Kong, has been chosen as the site on which to test the proposed RE and storage technologies. The major findings achieved by this research are summarized as follows.

#### **9.1.1 System modeling and evaluation**

Mathematical models of the key components have been developed and are given in Chapter 3, which is a foundation on which to simulate the dynamic behaviour of battery-based and pumped hydro storage (PHS)-based RE systems. In particular, a novel PV device simulation model has been developed and solved using an integrated analytical and numerical method. The effectiveness of the proposed model has been firstly demonstrated by comparing the predicted results with those from other models, and then validated through field measurements from two PV systems under different conditions. It is shown that the proposed model is simple and quick for calculation,

with a sufficient degree of precision and rapid enabling convergence. This model has been further employed to predict a standalone PV system energy output on a remote island. It is demonstrated that the model is of superior value, offering a good compromise between simplicity and accuracy. The predictions agree well with the PV plant field collected data, indicating that this model can be helpful in accurately determining the I-V curves and predicting power output of any PV devices.

To evaluate the system simulation and operation performance, some criteria have been proposed in terms of technical, economic and environmental issues. These criteria enable comparison of the performance of different system types and configurations

### **9.1.2 Development of the battery-based RE systems**

To determine an optimal system configuration of various combinations of four technologies, i.e. PV, WT, DG, and battery, and investigate the system dynamic performance, a total of 8 battery-based power generation options have been studied (Chapter 5), regarding simulation, techno-economic optimization and sensitivity analysis. Two options were fully examined and analyzed. Based on the simulation results, the following conclusions are drawn:

- It is found that this island could be powered by a 100% RE system, i.e. Option 3 solar-wind-battery system. This fully renewable power generation could be an ideal solution from the point of view of environmental conservation and energy provision, although, the cost of energy (COE) may be a little high (\$0.595/kWh). With the rapid development of the RE industry, however, the cost is expected to be reduced and hence this option could be increasingly viable.

- The introduction of a diesel generator (DG) could increase the economic viability of the hybrid system (Option 1: solar-wind-diesel-battery), particularly in those areas experiencing low diesel cost. It is found that this solution is a compromise between renewable and nonrenewable generation, therefore its COE (\$0.391/kWh) and payback time would be much lower than those of a fully RE system described in Option 3. The DG was scheduled only to assist the RE generator to cater for peak loads, thus a higher RE penetration level (95%) is still able to be guaranteed. However, such systems need the contribution of a small fraction of diesel energy with negative environmental impact, thus making this system type not so favourable.

### **9.1.3 Development of the PHS-based RE systems**

To find an alternative to battery power, which has some environmental problems and high initial cost, the PHS has been proposed in Chapter 6. A novel operating principle and design process for the PHS-based RE systems has been developed in this thesis. The effectiveness of the proposed models and optimization algorithm has also been examined. It is found that unavailable periods of RE necessitate a minimum UR capacity to supply the load, no matter how large the RE generator capacity. The results of changing the targeted loss of power supply probability (LPSP), suggest that significant reductions in COE,  $N_{PV}$  and  $V_{UR}$  can be achieved, if it is acceptable for a small proportion of load demand not to be met.

The COEs of the optimal solar-wind-pumped storage system under zero LPSP is \$0.286/kWh, much lower than that of the battery-based RE systems. It has also been demonstrated that the complementary characteristics of solar and wind energy output can provide greater value than either a PV or a wind system used individually.

Therefore, when designing an optimal RE power supply system, wind and solar energy sources, in combination, should be considered.

A new concept of energy storage to compensate for the intermittent nature of RE has been proposed in this study. Even though the overall efficiency of the micro-scaled PHS is not high, a sustainable and environmentally friendly power supply solution is able to be provided, indicating that the PHS is one future ideal partner for RE power supply systems, and that implementation of this novel technology in remote areas has promising prospects.

#### **9.1.4 Development of hybrid energy storage system**

A hybrid energy storage system (HESS), which combines batteries for long-term energy management with supercapacitors for fast dynamic power regulation, has been proposed in this study. The main purpose was to examine the possibility and benefit of the HESS in the achievement of a two device complementary performance. Mathematical models of the hybrid energy storage system (HESS) have also been developed and validated experimentally. It is found that the HESS enables improved performance in energy provision, not only for intermittent RE, but also for fluctuating load applications. The battery in the HESS is the primary energy source for longer periods and the supercapacitor is the auxiliary power source for “peak power smoothing” and “emergency reserve”. It also found that the performance of HESS can be further improved by the addition of an electric inductor. Such a combination contributes to the achievement of energy storage which has both high power and density, and also extends battery life.

In addition, the operation of another kind of HESS, namely a combination of PHS and battery, has been examined experimentally, as an illustration of practical operation of such hybrid energy storage technology.

#### **9.1.5 Performance evaluation of a RE system**

To evaluate the operation performance of an existing PV-battery system on the test island, a yearlong testing campaign has been conducted. Satisfactory values were achieved in that the average daily electricity production from the PV system was 61.2kWh and AC power output ratio of PV array was 9.5%. The average yield, system losses and capture losses during the year were 2.49h/d, 0.59h/d and 1.86h/d, respectively, thus the resultant array yield was 3.08h/d. The roundtrip efficiency of the battery bank during the year was 74.3%. The low load side energy utilization ratio demonstrated an optimal design of PV array and energy storage capacity was quite necessary. Considered should be technical issues (e.g. supply quality and energy efficiency), economic issues (e.g. cost of energy) and social issues (future expansion). Thus it is evident that, academic and industrial considerations should be merged for a practical RE supply project.

This research enables a detailed understanding of the operation performance the PV-battery system from a technical view point. This case study is also of practical relevance in that it can provide guidance for future renewable energy supply applications on remote areas.

In conclusion, this study enables a good utilization of RE sources for RAPS. The choices form a bank of RE resource possibilities from which interested parties can make suitable selections to enable satisfactory matching of resources with the needs and conditions of individual remote areas of interest. Hence the research presented in

this thesis contributes to the current related literature by providing good reference material, not only for the possibility of the selection of a good “match” but also a basis for further development of RE and energy storage technologies. The methodology presented can also be viewed as a starting point for planning and designing RE systems for remote communities around the world.

## **9.2 Recommendations for future research**

Although this research work does provide a comprehensive study of RE applications for RAPS using the newly proposed PHS and HESS, limitations of time and experimental facilities have led to a degree of insufficiency. It is both necessary and worthwhile to conduct further research on RE systems for remote regions, particularly as regards the PHS technology and the HESS.

RE power generation for remote areas is sustainable and environmental friendly, however several challenges need to be addressed, such as high initial cost and low overall energy utilization ratio. Although achievement has been made in the study presented in this thesis, optimum use of the RE sources to ensure reliable power supply and satisfactory economics still require further study and validation.

Storing the electricity harnessed from the RE sources at a reasonable cost is another critical issue and important challenge, to promote RE for RAPS, which is essential if such areas are to keep pace with worldwide developments. This study has demonstrated that the proposed PHS is a promising means for standalone RE systems in remote areas to meet the above. However, as is well known, such technology is still at the infancy stage and further research is necessary, such as is expressed below:

- One deficiency of this study is lack of sufficient experimental tests, although the battery-based RE system on the island has been evaluated, a whole year testing campaign for a standalone PHS-based RE system is recommended, to achieve sound knowledge of the long term performance of the proposed system. A comparison of the results with those achieved by simulation would be of value.
- This thesis has demonstrated that the passive hybrid battery-supercapacitor can achieve a better performance than the battery-alone system. However, the power flow in and out of the supercapacitor is not controllable. Therefore, it would be meaningful to add a power converter to control the HESS. Thus, the active or semi-active connected HESS needs to be studied in the future.
- While PHS for remote RE systems achieves satisfactory performance, pairing with battery storage may be a more practical option. The operating performance of a micro-scale hybrid PHS and battery energy storage has been examined experimentally for only several days due to time limitations. Therefore, a comprehensive mathematical modeling and numerical simulation of this type of HESS is recommended for future work, followed by long term experimental tests of different operation conditions. Another issue affecting the HESS is the high cost. Therefore, optimum sizing of the components in HESS based on a techno-economic analysis is also necessary in future work.
- The management and control strategies of the microgrid RE systems with PHS are also the subject of future work because such systems face real challenges of robustness when used in remote areas. System control has not been the focus in this thesis, the concern has been primarily with technical-economic feasibility study and optimization. In the above context, some state-of-the-art techniques,

such as microgrid management system, variable frequency converters, modern efficient reversible pump-turbines, as well as HESS, can be explored in future to optimize system control and simplify the system operation.

- Currently the distributed RE system is very popular, while various technical issues occur in the integration of RE sources into a grid, such as power quality and reliability. Therefore, the PHS system can be further applied for grid energy storage with high RE penetration, thus extending the study in this thesis which focuses only on the remote off-grid RE systems.
- Lack of water resources and suitable site present challenges the successful use of PHS in some remote areas. Underground reservoirs and seawater offer potential solutions, and thus deserve future research. In addition, the combination of PHS with other auxiliary systems, for example water supply, irrigation and desalination, is suggested for future study, to enable an enlargement of the contribution of this study in the form of social impacts.

## REFERENCES

1. IEA, *World Energy outlook*. 2013, International Energy Agency
2. NASA. *Earth at Night* <http://apod.nasa.gov/apod/ap001127.html>. 2000.
3. Hansen, U., *Technological options for power generation*. Energy Journal, 1998. 19(2): p. 63-87.
4. Qoaider, L. and D. Steinbrecht, *Photovoltaic systems: A cost competitive option to supply energy to off-grid agricultural communities in arid regions*. Applied Energy, 2010. 87(2): p. 427-435.
5. Bala, B.K. and S.A. Siddique, *Optimal design of a PV-diesel hybrid system for electrification of an isolated island—Sandwip in Bangladesh using genetic algorithm*. Energy for Sustainable Development, 2009. 13(3): p. 137-142.
6. Raman, P., et al., *Opportunities and challenges in setting up solar photo voltaic based micro grids for electrification in rural areas of India*. Renewable and Sustainable Energy Reviews, 2012. 16(5): p. 3320-3325.
7. Chakrabarti, S. and S. Chakrabarti, *Rural electrification programme with solar energy in remote region—a case study in an island*. Energy Policy, 2002. 30(1): p. 33-42.
8. Newnham, R.H., *Chapter 14 - Remote-area Power-supply (RAPS) Systems and the Valve-regulated Lead-Acid Battery*, in *Valve-Regulated Lead-Acid Batteries*, D.A.J.R.G.T.M.D. Parker, Editor. 2004, Elsevier: Amsterdam. p. 467-490.
9. Moseley, P.T., *Energy storage in remote area power supply (RAPS) systems*. Journal of Power Sources, 2006. 155(1): p. 83-87.

10. Tan, Y., L. Meegahapola, and K.M. Muttaqi, *A review of technical challenges in planning and operation of remote area power supply systems*. *Renewable and Sustainable Energy Reviews*, 2014. 38(0): p. 876-889.
11. Butler, D., *Requirements for batteries in remote-area power-supply systems based on technical modelling and field experience*. *Journal of Power Sources*, 1996. 59(1–2): p. 99-105.
12. Bekele, G. and G. Tadesse, *Feasibility study of small Hydro/PV/Wind hybrid system for off-grid rural electrification in Ethiopia*. *Applied Energy*, 2012(0).
13. Lau, K.Y., et al., *Performance analysis of hybrid photovoltaic/diesel energy system under Malaysian conditions*. *Energy*, 2010. 35(8): p. 3245-3255.
14. Elhadidy, M.A. and S.M. Shaahid, *Parametric study of hybrid (wind + solar + diesel) power generating systems*. *Renewable Energy*, 2000. 21(2): p. 129-139.
15. Ma, T., H. Yang, and L. Lu, *Performance evaluation of a stand-alone photovoltaic system on an isolated island in Hong Kong*. *Applied Energy*, 2013. 112(0): p. 663-672.
16. Ma, T., H. Yang, and L. Lu, *A feasibility study of a stand-alone hybrid solar–wind–battery system for a remote island*. *Applied Energy*, 2014. 121(0): p. 149-158.
17. Newnham, R.H. and W.G.A. Baldsing, *Advanced management strategies for remote-area power-supply systems*. *Journal of Power Sources*, 2004. 133(1): p. 141-146.
18. Tong, W., *Wind power generation and wind turbine design*. 2010, Southampton ; Boston: WIT Press.
19. Pearson, N.O., *Solar cheaper than diesel making India's Mittal believer: Energy*. <http://www.bloomberg.com>, February, 2012.

20. Givler, T., P. Lilienthal, and L. National Renewable Energy. *Using HOMER software, NREL's micropower optimization model, to explore the role of gensets in small solar power systems case study: SRI Lanka*. 2005; Available from: <http://purl.access.gpo.gov/GPO/LPS68114>.
21. Kanase-Patil, A.B., R.P. Saini, and M.P. Sharma, *Sizing of integrated renewable energy system based on load profiles and reliability index for the state of Uttarakhand in India*. *Renewable Energy*, 2011. 36(11): p. 2809-2821.
22. Kaldellis, J.K., *Stand-alone and hybrid wind energy systems : technology, energy storage and applications*. 2010, Cambridge : Boca Raton, Fla: Cambridge : Woodhead Pub. Boca Raton, Fla. : CRC Press, 2010.
23. Dagdougui, H., et al., *Modeling and optimization of a hybrid system for the energy supply of a "Green" building*. *Energy Conversion and Management*, 2012. 64(0): p. 351-363.
24. Zhao, J., et al., *A Review of Active Management for Distribution Networks: Current Status and Future Development Trends*. *Electric Power Components and Systems*, 2014. 42(3-4): p. 280-293.
25. Nair, N.-K.C. and N. Garimella, *Battery energy storage systems: Assessment for small-scale renewable energy integration*. *Energy and Buildings*, 2010. 42(11): p. 2124-2130.
26. Mahmoud, M.M., *On the storage batteries used in solar electric power systems and development of an algorithm for determining their ampere-hour capacity*. *Electric Power Systems Research*, 2004. 71(1): p. 85-89.
27. Mohammed, Y.S., M.W. Mustafa, and N. Bashir, *Hybrid renewable energy systems for off-grid electric power: Review of substantial issues*. *Renewable and Sustainable Energy Reviews*, 2014. 35(0): p. 527-539.

28. Krauter, S.C.W., *Development of an integrated solar home system*. Solar Energy Materials and Solar Cells, 2004. 82(1–2): p. 119-130.
29. Bernal-Agustín, J.L. and R. Dufo-López, *Simulation and optimization of stand-alone hybrid renewable energy systems*. Renewable and Sustainable Energy Reviews, 2009. 13(8): p. 2111-2118.
30. Kanase-Patil, A.B., R.P. Saini, and M.P. Sharma, *Integrated renewable energy systems for off grid rural electrification of remote area*. Renewable Energy, 2010. 35(6): p. 1342-1349.
31. Strupczewski, A., *Accident risks in nuclear-power plants*. Applied Energy, 2003. 75(1–2): p. 79-86.
32. Skoglund, A., et al., *On the physics of power, energy and economics of renewable electric energy sources - Part II*. Renewable Energy, 2010. 35(8): p. 1735-1740.
33. Akella, A.K., R.P. Saini, and M.P. Sharma, *Social, economical and environmental impacts of renewable energy systems*. Renewable Energy, 2009. 34(2): p. 390-396.
34. Shaahid, S.M. and I. El-Amin, *Techno-economic evaluation of off-grid hybrid photovoltaic–diesel–battery power systems for rural electrification in Saudi Arabia—A way forward for sustainable development*. Renewable and Sustainable Energy Reviews, 2009. 13(3): p. 625-633.
35. Himri, Y., et al., *Techno-economical study of hybrid power system for a remote village in Algeria*. Energy, 2008. 33(7): p. 1128-1136.
36. IEA, *Renewable Energies for Remote Areas and Islands*. April, 2012.

37. Upadhyay, S. and M.P. Sharma, *A review on configurations, control and sizing methodologies of hybrid energy systems*. Renewable and Sustainable Energy Reviews, 2014. 38(0): p. 47-63.
38. Voutetakis, S., *Design, optimization, and control of stand-alone power systems using renewable energy sources and hydrogen production*. 2011, New York: New York : Nova Science Publishers, c2011.
39. Farret, F.A. and M.G. Simoes, *Integration of alternative sources of energy*. 2006: John Wiley & Sons.
40. Ma, T., et al., *Technical feasibility study on a standalone hybrid solar-wind system with pumped hydro storage for a remote island in Hong Kong*. Renewable Energy, 2014. 69(0): p. 7-15.
41. Prasad, A.R. and E. Natarajan, *Optimization of integrated photovoltaic–wind power generation systems with battery storage*. Energy, 2006. 31(12): p. 1943-1954.
42. Zhou, W., et al., *Current status of research on optimum sizing of stand-alone hybrid solar–wind power generation systems*. Applied Energy, 2010. 87(2): p. 380-389.
43. Bagul, A.D., Z.M. Salameh, and B. Borowy, *Sizing of a stand-alone hybrid wind-photovoltaic system using a three-event probability density approximation*. Solar Energy, 1996. 56(4): p. 323-335.
44. Bajpai, P. and V. Dash, *Hybrid renewable energy systems for power generation in stand-alone applications: A review*. Renewable and Sustainable Energy Reviews, 2012. 16(5): p. 2926-2939.

45. Kaldellis, J.K., E. Kondili, and A. Filios, *Sizing a hybrid wind-diesel stand-alone system on the basis of minimum long-term electricity production cost*. Applied Energy, 2006. 83(12): p. 1384-1403.
46. Sopian, K., et al., *Optimal operational strategy for hybrid renewable energy system using genetic algorithms*. WSEAS Trans. Math., 2008. 7(4): p. 130-140.
47. Notton, G., M. Muselli, and A. Louche, *Autonomous hybrid photovoltaic power plant using a back-up generator: A case study in a Mediterranean island*. Renewable Energy, 1996. 7(4): p. 371-391.
48. Ghoddami, H., M.B. Delghavi, and A. Yazdani, *An integrated wind-photovoltaic-battery system with reduced power-electronic interface and fast control for grid-tied and off-grid applications*. Renewable Energy, 2012. 45(0): p. 128-137.
49. Sreeraj, E.S., K. Chatterjee, and S. Bandyopadhyay, *Design of isolated renewable hybrid power systems*. Solar Energy, 2010. 84(7): p. 1124-1136.
50. Ould Bilal, B., et al., *Optimal design of a hybrid solar-wind-battery system using the minimization of the annualized cost system and the minimization of the loss of power supply probability (LPSP)*. Renewable Energy, 2010. 35(10): p. 2388-2390.
51. Diaf, S., et al., *A methodology for optimal sizing of autonomous hybrid PV/wind system*. Energy Policy, 2007. 35(11): p. 5708-5718.
52. Dihrab, S.S. and K. Sopian, *Electricity generation of hybrid PV/wind systems in Iraq*. Renewable Energy, 2010. 35(6): p. 1303-1307.
53. Yang, H., L. Lu, and W. Zhou, *A novel optimization sizing model for hybrid solar-wind power generation system*. Solar Energy, 2007. 81(1): p. 76-84.

54. Yang, H., et al., *Optimal sizing method for stand-alone hybrid solar–wind system with LPSP technology by using genetic algorithm*. Solar Energy, 2008. 82(4): p. 354-367.
55. Yang, H.X., L. Lu, and J. Burnett, *Weather data and probability analysis of hybrid photovoltaic–wind power generation systems in Hong Kong*. Renewable Energy, 2003. 28(11): p. 1813-1824.
56. Colle, S., S. Luna Abreu, and R. R üther, *Economic evaluation and optimization of hybrid diesel/photovoltaic systems integrated to utility grids*. Solar Energy, 2004. 76(1–3): p. 295-299.
57. Ngan, M.S. and C.W. Tan, *Assessment of economic viability for PV/wind/diesel hybrid energy system in southern Peninsular Malaysia*. Renewable and Sustainable Energy Reviews, 2012. 16(1): p. 634-647.
58. Rehman, S., et al., *Feasibility study of a wind–pv–diesel hybrid power system for a village*. Renewable Energy, 2012. 38(1): p. 258-268.
59. Shaahid, S.M., et al., *Potential of autonomous/off-grid hybrid wind-diesel power system for electrification of a remote settlement in Saudi Arabia*. Wind Engineering, 2004. 28(5): p. 621-628.
60. Dufo-L ópez, R. and J.L. Bernal-Agust ín, *Design and control strategies of PV-Diesel systems using genetic algorithms*. Solar Energy, 2005. 79(1): p. 33-46.
61. Razak, J.A., et al., *Optimization of PV-Wind-Hydro-Diesel Hybrid System by Minimizing Excess Capacity* European Journal of Scientific Research, 2009. 25(4).
62. De Soto, W., S.A. Klein, and W.A. Beckman, *Improvement and validation of a model for photovoltaic array performance*. Solar Energy, 2006. 80(1): p. 78-88.

63. Dongue, S.B., et al., *Modeling Of Electrical Response of Illuminated Crystalline Photovoltaic Modules Using Four- And Five-Parameter Models*. International Journal of Emerging Technology and Advanced Engineering, 2012. 2(11): p. 612-619.
64. Carrero, C., J. Amador, and S. Arnaltes, *A single procedure for helping PV designers to select silicon PV modules and evaluate the loss resistances*. Renewable Energy, 2007. 32(15): p. 2579-2589.
65. Lo Brano, V., A. Orioli, and G. Ciulla, *On the experimental validation of an improved five-parameter model for silicon photovoltaic modules*. Solar Energy Materials and Solar Cells, 2012. 105(0): p. 27-39.
66. Lo Brano, V., et al., *An improved five-parameter model for photovoltaic modules*. Solar Energy Materials and Solar Cells, 2010. 94(8): p. 1358-1370.
67. Saloux, E., A. Teyssedou, and M. Sorin, *Explicit model of photovoltaic panels to determine voltages and currents at the maximum power point*. Solar Energy, 2011. 85(5): p. 713-722.
68. Ishaque, K., et al., *A critical evaluation of EA computational methods for Photovoltaic cell parameter extraction based on two diode model*. Solar Energy, 2011. 85(9): p. 1768-1779.
69. Ishaque, K. and Z. Salam, *An improved modeling method to determine the model parameters of photovoltaic (PV) modules using differential evolution (DE)*. Solar Energy, 2011. 85(9): p. 2349-2359.
70. Ishaque, K., Z. Salam, and H. Taheri, *Simple, fast and accurate two-diode model for photovoltaic modules*. Solar Energy Materials and Solar Cells, 2011. 95(2): p. 586-594.

71. Aparicio, M.P., et al., *Modeling of Photovoltaic Cell Using Free Software Application for Training and Design Circuit in Photovoltaic Solar Energy*. New Developments in Renewable Energy. 2013.
72. Eicker, U., *Solar technologies for buildings*. 2003, Chichester: Wiley.
73. Mazhari, B., *An improved solar cell circuit model for organic solar cells*. Solar Energy Materials and Solar Cells, 2006. 90(7–8): p. 1021-1033.
74. Luque, A. and A. Martí *Increasing the Efficiency of Ideal Solar Cells by Photon Induced Transitions at Intermediate Levels*. Physical Review Letters, 1997. 78(26): p. 5014-5017.
75. Shockley, W. and H.J. Queisser, *Detailed Balance Limit of Efficiency of p - n Junction Solar Cells*. Journal of Applied Physics, 1961. 32(3): p. 510-519.
76. Han, L., et al., *Modeling of an equivalent circuit for dye-sensitized solar cells*. Applied Physics Letters, 2004. 84(13): p. 2433-2435.
77. Villalva, M.G., J.R. Gazoli, and E.R. Filho, *Comprehensive Approach to Modeling and Simulation of Photovoltaic Arrays*. Power Electronics, IEEE Transactions on, 2009. 24(5): p. 1198-1208.
78. Massi Pavan, A., A. Mellit, and V. Lughi, *Explicit empirical model for general photovoltaic devices: Experimental validation at maximum power point*. Solar Energy, 2014. 101(0): p. 105-116.
79. Tan, Y.T., D.S. Kirschen, and N. Jenkins, *A model of PV generation suitable for stability analysis*. IEEE Transactions on Energy Conversion, 2004. 19(4): p. 748-755.
80. Mellit, A., M. Benghaneim, and S.A. Kalogirou, *Modeling and simulation of a stand-alone photovoltaic system using an adaptive artificial neural network*:

- Proposition for a new sizing procedure. Renewable Energy, 2007. 32(2): p. 285-313.*
81. Kou, Q., S.A. Klein, and W.A. Beckman, *A method for estimating the long-term performance of direct-coupled PV pumping systems. Solar Energy, 1998. 64(1-3): p. 33-40.*
  82. Gonzalez, L. and M. Francisco, *Model of photovoltaic module in Matlab, in CIBELEC. 2005.*
  83. Yusof, Y., et al. *Modeling and simulation of maximum power point tracker for photovoltaic system. in Power and Energy Conference, 2004. PECon 2004. Proceedings. National. 2004.*
  84. Weidong, X., W.G. Dunford, and A. Capel. *A novel modeling method for photovoltaic cells. in Power Electronics Specialists Conference, 2004. PESC 04. 2004 IEEE 35th Annual. 2004.*
  85. Yeong-Chan, K., L. Tsorng-Juu, and C. Jiann-Fuh, *Novel maximum-power-point-tracking controller for photovoltaic energy conversion system. Industrial Electronics, IEEE Transactions on, 2001. 48(3): p. 594-601.*
  86. Chakrasali, R.L., V.R. Sheelavant, and H.N. Nagaraja, *Network approach to modeling and simulation of solar photovoltaic cell. Renewable and Sustainable Energy Reviews, 2013. 21(0): p. 84-88.*
  87. Townsend, T.U., *A method for estimating the long-term performance of direct-coupled photovoltaic systems. 1989.*
  88. Ghoneim, A.A., *Design optimization of photovoltaic powered water pumping systems. Energy Conversion and Management, 2006. 47(11-12): p. 1449-1463.*
  89. Chenni, R., et al., *A detailed modeling method for photovoltaic cells. Energy, 2007. 32(9): p. 1724-1730.*

90. Celik, A.N. and N. Acikgoz, *Modelling and experimental verification of the operating current of mono-crystalline photovoltaic modules using four- and five-parameter models*. Applied Energy, 2007. 84(1): p. 1-15.
91. Karamirad, M., et al., *ANN based simulation and experimental verification of analytical four- and five-parameters models of PV modules*. Simulation Modelling Practice and Theory, 2013. 34(0): p. 86-98.
92. Ma, T., H. Yang, and L. Lu, *Development of a model to simulate the performance characteristics of crystalline silicon photovoltaic modules/strings/arrays*. Solar Energy, 2014. 100(0): p. 31-41.
93. Bai, J., et al., *Development of a new compound method to extract the five parameters of PV modules*. Energy Conversion and Management, 2014. 79(0): p. 294-303.
94. Chouder, A., et al., *Modeling and simulation of a grid connected PV system based on the evaluation of main PV module parameters*. Simulation Modelling Practice and Theory, 2012. 20(1): p. 46-58.
95. Jung, T.H., et al., *Output characteristics of PV module considering partially reverse biased conditions*. Solar Energy, 2013. 92(0): p. 214-220.
96. de Blas, M.A., et al., *Selecting a suitable model for characterizing photovoltaic devices*. Renewable Energy, 2002. 25(3): p. 371-380.
97. Hadj Arab, A., F. Chenlo, and M. Benghanem, *Loss-of-load probability of photovoltaic water pumping systems*. Solar Energy, 2004. 76(6): p. 713-723.
98. Ciulla, G., et al., *A comparison of different one-diode models for the representation of I–V characteristic of a PV cell*. Renewable and Sustainable Energy Reviews, 2014. 32(0): p. 684-696.

99. De Soto, W., *Improvement and Validation of a Model for Photovoltaic Array Performance*. 2004, University of Wisconsin-Madison. p. 235.
100. Sera, D., R. Teodorescu, and P. Rodriguez. *PV panel model based on datasheet values*. in *Industrial Electronics, 2007. ISIE 2007. IEEE International Symposium on*. 2007.
101. Karatepe, E., M. Boztepe, and M. Colak, *Neural network based solar cell model*. *Energy Conversion and Management*, 2006. 47(9–10): p. 1159-1178.
102. Tian, H., et al., *A cell-to-module-to-array detailed model for photovoltaic panels*. *Solar Energy*, 2012. 86(9): p. 2695-2706.
103. Kumari, J.S. and C.S. Babu, *Mathematical Modeling and Simulation of Photovoltaic Cell using Matlab-Simulink Environment*. *International Journal of Electrical and Computer Engineering*, 2012. 2(1): p. 26~34.
104. Sukamongkol, Y., S. Chungpaibulpatana, and W. Ongsakul, *A simulation model for predicting the performance of a solar photovoltaic system with alternating current loads*. *Renewable Energy*, 2002. 27(2): p. 237-258.
105. Kharb, R.K., et al., *Modeling of solar PV module and maximum power point tracking using ANFIS*. *Renewable and Sustainable Energy Reviews*, 2014. 33(0): p. 602-612.
106. Gow, J.A. and C.D. Manning, *Development of a photovoltaic array model for use in power-electronics simulation studies*. *Electric Power Applications, IEE Proceedings -*, 1999. 146(2): p. 193-200.
107. Yordanov, G.H., O.-M. Midtgård, and T.O. Saetre, *Series resistance determination and further characterization of c-Si PV modules*. *Renewable Energy*, 2012. 46(0): p. 72-80.

108. Hyvärinen, J. and J. Karila. *New analysis method for crystalline silicon cells*. 2003.
109. Gow, J.A. and C.D. Manning. *Development of a model for photovoltaic arrays suitable for use in simulation studies of solar energy conversion systems*. in *Power Electronics and Variable Speed Drives, 1996. Sixth International Conference on (Conf. Publ. No. 429)*. 1996.
110. Kurobe, K.-i. and H. Matsunami, *New Two-Diode Model for Detailed Analysis of Multicrystalline Silicon Solar Cells*. Japanese Journal of Applied Physics, 2005. 44(12): p. 8314.
111. Nishioka, K., et al., *Analysis of the Temperature Characteristics in Polycrystalline Si Solar Cells Using Modified Equivalent Circuit Model*. Japanese Journal of Applied Physics, 2003. 42(Part 1, No. 12): p. 7175.
112. Chowdhury, S., et al. *Modelling, simulation and performance analysis of a PV array in an embedded environment*. in *Universities Power Engineering Conference, 2007. UPEC 2007. 42nd International*. 2007.
113. Silvestre, S., A. Boronat, and A. Chouder, *Study of bypass diodes configuration on PV modules*. Applied Energy, 2009. 86(9): p. 1632-1640.
114. Ishaque, K., Z. Salam, and Syafaruddin, *A comprehensive MATLAB Simulink PV system simulator with partial shading capability based on two-diode model*. Solar Energy, 2011. 85(9): p. 2217-2227.
115. Chih-Tang, S., R.N. Noyce, and W. Shockley, *Carrier Generation and Recombination in P-N Junctions and P-N Junction Characteristics*. Proceedings of the IRE, 1957. 45(9): p. 1228-1243.

116. McIntosh, K.R., P.P. Altermatt, and G. Heiser, *Depletion-region recombination in silicon solar cells: when does  $mDR=2$ ?*, in *16th European photovoltaic Solar Energy Conference 2000*.
117. Chan, D.S.H. and J.C.H. Phang, *Analytical methods for the extraction of solar-cell single- and double-diode model parameters from I-V characteristics*. *Electron Devices, IEEE Transactions on*, 1987. 34(2): p. 286-293.
118. Nishioka, K., et al., *Analysis of multicrystalline silicon solar cells by modified 3-diode equivalent circuit model taking leakage current through periphery into consideration*. *Solar Energy Materials and Solar Cells*, 2007. 91(13): p. 1222-1227.
119. Duffie, J.A. and W.A. Beckman, *Solar engineering of thermal processes (3rd ed.)*. 2006: Wiley
120. Ulleberg, Ø., *Stand-alone power systems for the future: Optimal design, operation and control of solar-hydrogen energy systems*. 1998, NUST. p. 225.
121. Jung, T.-h., et al., *A mathematical model for cell-to-module conversion considering mismatching solar cells and the resistance of the interconnection ribbon*. *Solar Energy*, 2014. 103(0): p. 253-262.
122. Haouari-Merbah, M., et al., *Extraction and analysis of solar cell parameters from the illuminated current-voltage curve*. *Solar Energy Materials and Solar Cells*, 2005. 87(1-4): p. 225-233.
123. Ortiz-Conde, A., F.J. García Sánchez, and J. Muci, *New method to extract the model parameters of solar cells from the explicit analytic solutions of their illuminated I-V characteristics*. *Solar Energy Materials and Solar Cells*, 2006. 90(3): p. 352-361.

124. Chan, D.S.H. and J.C.H. Phang, *ANALYTICAL METHODS FOR THE EXTRACTION OF SOLAR-CELL SINGLE- AND DOUBLE-DIODE MODEL PARAMETERS FROM I-V CHARACTERISTICS*. IEEE Transactions on Electron Devices, 1987. ED-34(2): p. 286-293.
125. Marion, B., *A method for modeling the current–voltage curve of a PV module for outdoor conditions*. Progress in Photovoltaics: Research and Applications, 2002. 10(3): p. 205-214.
126. Marion, B., S. Rummel, and A. Anderberg, *Current–voltage curve translation by bilinear interpolation*. Progress in Photovoltaics: Research and Applications, 2004. 12(8): p. 593-607.
127. Arab, A.H., et al., *Performance of PV water pumping systems*. Renewable Energy, 1999. 18(2): p. 191-204.
128. Almonacid, F., et al., *Characterisation of Si-crystalline PV modules by artificial neural networks*. Renewable Energy, 2009. 34(4): p. 941-949.
129. Liu, S. and R.A. Dougal, *Dynamic multiphysics model for solar array*. Energy Conversion, IEEE Transactions on, 2002. 17(2): p. 285-294.
130. Chegaar, M., Z. Ouennoughi, and A. Hoffmann, *A new method for evaluating illuminated solar cell parameters*. Solid-State Electronics, 2001. 45(2): p. 293-296.
131. Matagne, E., R. Chenni, and R. El Bachtiri. *A photovoltaic cell model based on nominal data only*. in *Power Engineering, Energy and Electrical Drives, 2007. POWERENG 2007. International Conference on*. 2007.
132. Khouzam, K., et al. *Simulation and real-time modelling of space photovoltaic systems*. in *Photovoltaic Energy Conversion, 1994., Conference Record of the*

*Twenty Fourth. IEEE Photovoltaic Specialists Conference - 1994, 1994 IEEE First World Conference on. 1994.*

133. Cameron, C.P., W.E. Boyson, and D.M. Riley. *Comparison of PV system performance-model predictions with measured PV system performance.* in *Photovoltaic Specialists Conference, 2008. PVSC '08. 33rd IEEE.* 2008.
134. Al-Ibrahim, A.M., *Optimal Selection of Direct-Coupled Photovoltaic Pumping System in Solar Domestic Hot Water Systems,* in *Mechanical Engineering.* 1996, University of Wisconsin-Madison.
135. Badescu, V., *Dynamic model of a complex system including PV cells, electric battery, electrical motor and water pump.* *Energy*, 2003. 28(12): p. 1165-1181.
136. Williams, P.M., *Development and Analysis Tool for Photovoltaic-Powered Solar Water Heating Systems.* 1996, University of Wisconsin-Madison.
137. Ahmad, G.E., H.M.S. Hussein, and H.H. El-Ghetany, *Theoretical analysis and experimental verification of PV modules.* *Renewable Energy*, 2003. 28(8): p. 1159-1168.
138. Glass, M.C. *Improved solar array power point model with SPICE realization.* in *Energy Conversion Engineering Conference, 1996. IECEC 96., Proceedings of the 31st Intersociety.* 1996.
139. Salmi, T., et al., *MATLAB/simulink based modelling of solar photovoltaic cell.* *International Journal of Renewable Energy Research*, 2012. 2(2): p. 213-218.
140. Nema, S., R.K.Nema, and G. Agnihotri, *Matlab/simulink based study of photovoltaic cells/modules/array and their experimental verification.* *International Journal of Energy and Environment*, 2010. 1(3).

141. Altas, I.H. and A.M. Sharaf. *A Photovoltaic Array Simulation Model for Matlab-Simulink GUI Environment*. in *Clean Electrical Power, 2007. ICCEP '07. International Conference on*. 2007.
142. Tsai, H.-L., C.-S. Tu, and Y.-J. Su, *Development of generalized photovoltaic model using Matlab/Simulink*, in *World Congress on Engineering and Computer Science 2008: San Francisco, USA*.
143. Omid, M., *Design of an expert system for sorting pistachio nuts through decision tree and fuzzy logic classifier*. *Expert Systems with Applications*, 2011. 38(4): p. 4339-4347.
144. Ishaque, K., et al., *Modeling and simulation of photovoltaic (PV) system during partial shading based on a two-diode model*. *Simulation Modelling Practice and Theory*, 2011. 19(7): p. 1613-1626.
145. Jervase, J.A., H. Bourdoucen, and A. Al-Lawati, *Solar cell parameter extraction using genetic algorithms*. *Measurement Science and Technology*, 2001. 12(11): p. 1922.
146. Moldovan, N., R. Picos, and E. Garcia-Moreno. *Parameter Extraction of a Solar Cell Compact Model usign Genetic Algorithms*. in *Electron Devices, 2009. CDE 2009. Spanish Conference on*. 2009.
147. da Costa, W.T., et al. *Identification of photovoltaic model parameters by Differential Evolution*. in *Industrial Technology (ICIT), 2010 IEEE International Conference on*. 2010.
148. Ye, M., X. Wang, and Y. Xu, *Parameter extraction of solar cells using particle swarm optimization*. *Journal of Applied Physics*, 2009. 105(9): p. 094502-094502-8.

149. Elhagry, M.T., et al. *Fuzzy modeling of photovoltaic panel equivalent circuit*. in *Circuits and Systems, 1997. Proceedings of the 40th Midwest Symposium on*. 1997.
150. Lalouni, S. and T. Rekioua. *Modeling and Simulation of a Photovoltaic System Using Fuzzy Logic Controller*. in *Developments in eSystems Engineering (DESE), 2009 Second International Conference on*. 2009.
151. Almonacid, F., et al., *Characterisation of PV CIS module by artificial neural networks. A comparative study with other methods*. *Renewable Energy*, 2010. 35(5): p. 973-980.
152. Celik, A.N., *Artificial neural network modelling and experimental verification of the operating current of mono-crystalline photovoltaic modules*. *Solar Energy*, 2011. 85(10): p. 2507-2517.
153. Bonanno, F., et al., *A radial basis function neural network based approach for the electrical characteristics estimation of a photovoltaic module*. *Applied Energy*, 2012. 97(0): p. 956-961.
154. Tina, G. and S. Gagliano, *Probabilistic analysis of weather data for a hybrid solar/wind energy system*. *International Journal of Energy Research*, 2011. 35(3): p. 221-232.
155. Tina, G., S. Gagliano, and S. Raiti, *Hybrid solar/wind power system probabilistic modelling for long-term performance assessment*. *Solar Energy*, 2006. 80(5): p. 578-588.
156. Bucciarelli Jr, L.L., *Estimating loss-of-power probabilities of stand-alone photovoltaic solar energy systems*. *Solar Energy*, 1984. 32(2): p. 205-209.
157. Luna-Rubio, R., et al., *Optimal sizing of renewable hybrids energy systems: A review of methodologies*. *Solar Energy*, 2012. 86(4): p. 1077-1088.

158. Kaldellis, J.K., D. Zafirakis, and E. Kondili, *Optimum autonomous stand-alone photovoltaic system design on the basis of energy pay-back analysis*. Energy, 2009. 34(9): p. 1187-1198.
159. Diaf, S., et al., *Design and techno-economical optimization for hybrid PV/wind system under various meteorological conditions*. Applied Energy, 2008. 85(10): p. 968-987.
160. Dufo-López, R., J.L. Bernal-Agustín, and F. Mendoza, *Design and economical analysis of hybrid PV–wind systems connected to the grid for the intermittent production of hydrogen*. Energy Policy, 2009. 37(8): p. 3082-3095.
161. Khatod, D.K., V. Pant, and J. Sharma, *Analytical Approach for Well-Being Assessment of Small Autonomous Power Systems With Solar and Wind Energy Sources*. Energy Conversion, IEEE Transactions on, 2010. 25(2): p. 535-545.
162. Ashok, S., *Optimised model for community-based hybrid energy system*. Renewable Energy, 2007. 32(7): p. 1155-1164.
163. Kaldellis, J.K., D. Zafirakis, and K. Kavadias, *Minimum cost solution of wind–photovoltaic based stand-alone power systems for remote consumers*. Energy Policy, 2012. 42(0): p. 105-117.
164. Nikhil, P.G. and D. Subhakar, *Sizing and Parametric Analysis of a Stand-Alone Photovoltaic Power Plant*. Photovoltaics, IEEE Journal of, 2013. 3(2): p. 776-784.
165. Chauhan, A. and R.P. Saini, *A review on Integrated Renewable Energy System based power generation for stand-alone applications: Configurations, storage options, sizing methodologies and control*. Renewable and Sustainable Energy Reviews, 2014. 38(0): p. 99-120.

166. Mellit, A., et al., *Artificial intelligence techniques for sizing photovoltaic systems: A review*. Renewable and Sustainable Energy Reviews, 2009. 13(2): p. 406-419.
167. Holland, J.H., *Adaptation in natural and artificial systems*. 1975: University of Michigan Press, Ann Arbor
168. Konak, A., D.W. Coit, and A.E. Smith, *Multi-objective optimization using genetic algorithms: A tutorial*. Reliability Engineering & System Safety, 2006. 91(9): p. 992-1007.
169. Shaahid, S.M. and M.A. Elhadidy, *Optimal sizing of battery storage for stand-alone hybrid (photo-voltaic + diesel) power systems*. International Journal of Sustainable Energy, 2005. 24(3): p. 155-166.
170. Bernal-Agustín, J.L., R. Dufo-López, and D.M. Rivas-Ascaso, *Design of isolated hybrid systems minimizing costs and pollutant emissions*. Renewable Energy, 2006. 31(14): p. 2227-2244.
171. Koutroulis, E., et al., *Methodology for optimal sizing of stand-alone photovoltaic/wind-generator systems using genetic algorithms*. Solar Energy, 2006. 80(9): p. 1072-1088.
172. Yang, H., et al., *Optimal sizing method for stand-alone hybrid solar-wind system with LPSP technology by using genetic algorithm*. Solar Energy, 2008. 82(4): p. 354-367.
173. Yang, H., Z. Wei, and L. Chengzhi, *Optimal design and techno-economic analysis of a hybrid solar-wind power generation system*. Applied Energy, 2009. 86(2): p. 163-169.

174. Lagorse, J., D. Paire, and A. Miraoui, *Sizing optimization of a stand-alone street lighting system powered by a hybrid system using fuel cell, PV and battery*. *Renewable Energy*, 2009. 34(3): p. 683-691.
175. Senjyu, T., et al., *Optimal configuration of power generating systems in isolated island with renewable energy*. *Renewable Energy*, 2007. 32(11): p. 1917-1933.
176. Zagrouba, M., et al., *Identification of PV solar cells and modules parameters using the genetic algorithms: Application to maximum power extraction*. *Solar Energy*, 2010. 84(5): p. 860-866.
177. Fadaee, M. and M.A.M. Radzi, *Multi-objective optimization of a stand-alone hybrid renewable energy system by using evolutionary algorithms: A review*. *Renewable and Sustainable Energy Reviews*, 2012. 16(5): p. 3364-3369.
178. Lee, T.Y. and C.L. Chen, *Wind-photovoltaic capacity coordination for a time-of-use rate industrial user*. *Renewable Power Generation, IET*, 2009. 3(2): p. 152-167.
179. Lingfeng, W. and C. Singh. *PSO-Based Multidisciplinary Design of A Hybrid Power Generation System With Statistical Models of Wind Speed and Solar Insolation*. in *Power Electronics, Drives and Energy Systems, 2006. PEDES '06. International Conference on*. 2006.
180. Paliwal, P., N.P. Patidar, and R.K. Nema, *Determination of reliability constrained optimal resource mix for an autonomous hybrid power system using Particle Swarm Optimization*. *Renewable Energy*, 2014. 63(0): p. 194-204.
181. Kashefi Kaviani, A., G.H. Riahy, and S.M. Kouhsari, *Optimal design of a reliable hydrogen-based stand-alone wind/PV generating system, considering component outages*. *Renewable Energy*, 2009. 34(11): p. 2380-2390.

182. Sa, et al. *Optimal sizing of a hybrid renewable system*. in *Industrial Technology (ICIT), 2010 IEEE International Conference on*. 2010.
183. Mahor, A., V. Prasad, and S. Rangnekar, *Economic dispatch using particle swarm optimization: A review*. *Renewable and Sustainable Energy Reviews*, 2009. 13(8): p. 2134-2141.
184. Niknam, T., H.Z. Meymand, and M. Nayeripour, *A practical algorithm for optimal operation management of distribution network including fuel cell power plants*. *Renewable Energy*, 2010. 35(8): p. 1696-1714.
185. Mellit, A., et al., *An adaptive artificial neural network model for sizing stand-alone photovoltaic systems: application for isolated sites in Algeria*. *Renewable Energy*, 2005. 30(10): p. 1501-1524.
186. Hontoria, L., J. Aguilera, and P. Zufiria, *A new approach for sizing stand alone photovoltaic systems based in neural networks*. *Solar Energy*, 2005. 78(2): p. 313-319.
187. Kalogirou, S.A., *Optimization of solar systems using artificial neural-networks and genetic algorithms*. *Applied Energy*, 2004. 77(4): p. 383-405.
188. Kirkpatrick, S., C.D. Gelatt, and M.P. Vecchi, *Optimization by simulated annealing*. *science*, 1983. 220(4598): p. 671-680.
189. Askarzadeh, A., *A discrete chaotic harmony search-based simulated annealing algorithm for optimum design of PV/wind hybrid system*. *Solar Energy*, 2013. 97(0): p. 93-101.
190. Askarzadeh, A., *Developing a discrete harmony search algorithm for size optimization of wind–photovoltaic hybrid energy system*. *Solar Energy*, 2013. 98, Part C(0): p. 190-195.

191. Kumar, R., R.A. Gupta, and A.K. Bansal, *Economic analysis and power management of a stand-alone wind/photovoltaic hybrid energy system using biogeography based optimization algorithm*. Swarm and Evolutionary Computation, 2013. 8(0): p. 33-43.
192. Ammar, M.B., M. Chaabene, and A. Elhajjaji, *Daily energy planning of a household photovoltaic panel*. Applied Energy, 2010. 87(7): p. 2340-2351.
193. Jurado, F. and J.R. Saenz, *Neuro-fuzzy control for autonomous wind–diesel systems using biomass*. Renewable Energy, 2002. 27(1): p. 39-56.
194. Baños, R., et al., *Optimization methods applied to renewable and sustainable energy: A review*. Renewable and Sustainable Energy Reviews, 2011. 15(4): p. 1753-1766.
195. Hajela, P. and C.Y. Lin, *Genetic search strategies in multicriterion optimal design*. Structural and Multidisciplinary Optimization, 1992. 4(2): p. 99-107.
196. Goldberg, D.E., *Genetic algorithms in search, optimization, and machine learning*. 1989: Addison-Wesley Pub. Co. .
197. Abbas, D., A. Martinez, and G. Champenois, *Life cycle cost, embodied energy and loss of power supply probability for the optimal design of hybrid power systems*. Mathematics and Computers in Simulation, 2014. 98(0): p. 46-62.
198. Katsigiannis, Y.A., P.S. Georgilakis, and E.S. Karapidakis, *Multiobjective genetic algorithm solution to the optimum economic and environmental performance problem of small autonomous hybrid power systems with renewables*. Renewable Power Generation, IET, 2010. 4(5): p. 404-419.
199. Maheri, A., *Multi-objective design optimisation of standalone hybrid wind-PV-diesel systems under uncertainties*. Renewable Energy, 2014. 66(0): p. 650-661.

200. Yongping, Y., et al., *Study on multi-objective optimization of load dispatch including renewable energy and CCS technologies*. International Journal of Energy Research, 2010. 34(8): p. 702-715.
201. Bernal-Agustín, J.L. and R. Dufo-López, *Multi-objective design and control of hybrid systems minimizing costs and unmet load*. Electric Power Systems Research, 2009. 79(1): p. 170-180.
202. Dufo-López, R. and J.L. Bernal-Agustín, *Multi-objective design of PV–wind–diesel–hydrogen–battery systems*. Renewable Energy, 2008. 33(12): p. 2559-2572.
203. Pelet, X., D. Favrat, and G. Leyland, *Multiobjective optimisation of integrated energy systems for remote communities considering economics and CO2 emissions*. International Journal of Thermal Sciences, 2005. 44(12): p. 1180-1189.
204. Kulkarni, G.N., S.B. Kedare, and S. Bandyopadhyay, *Determination of design space and optimization of solar water heating systems*. Solar Energy, 2007. 81(8): p. 958-968.
205. Arun, P., R. Banerjee, and S. Bandyopadhyay, *Optimum sizing of battery-integrated diesel generator for remote electrification through design-space approach*. Energy, 2008. 33(7): p. 1155-1168.
206. Arun, P., R. Banerjee, and S. Bandyopadhyay, *Sizing curve for design of isolated power systems*. Energy for Sustainable Development, 2007. 11(4): p. 21-28.
207. Muselli, M., G. Notton, and A. Louche, *DESIGN OF HYBRID-PHOTOVOLTAIC POWER GENERATOR, WITH OPTIMIZATION OF ENERGY MANAGEMENT*. Solar Energy, 1999. 65(3): p. 143-157.

208. Arun, P., R. Banerjee, and S. Bandyopadhyay, *Optimum sizing of photovoltaic battery systems incorporating uncertainty through design space approach*. Solar Energy, 2009. 83(7): p. 1013-1025.
209. Roy, A., S.B. Kedare, and S. Bandyopadhyay, *Application of design space methodology for optimum sizing of wind–battery systems*. Applied Energy, 2009. 86(12): p. 2690-2703.
210. Roy, A., S.B. Kedare, and S. Bandyopadhyay, *Optimum sizing of wind-battery systems incorporating resource uncertainty*. Applied Energy, 2010. 87(8): p. 2712-2727.
211. Badejani, M.M., M.A.S. Masoum, and M. Kalantar, *Optimal design and modeling of stand-alone hybrid PV-wind systems*, in *Power Engineering Conference (AUPEC 2007)*. 2007: Australasian Universities. p. 1-6.
212. Hocaoglu, F.O., Ö.N. Gerek, and M. Kurban, *A novel hybrid (wind–photovoltaic) system sizing procedure*. Solar Energy, 2009. 83(11): p. 2019-2028.
213. Ai, B., et al., *Computer-aided design of PV/wind hybrid system*. Renewable Energy, 2003. 28(10): p. 1491-1512.
214. Borowy, B.S. and Z.M. Salameh, *Methodology for optimally sizing the combination of a battery bank and PV array in a wind/PV hybrid system*. Energy Conversion, IEEE Transactions on, 1996. 11(2): p. 367-375.
215. Elhadidy, M.A., *Performance evaluation of hybrid (wind/solar/diesel) power systems*. Renewable Energy, 2002. 26(3): p. 401-413.
216. Nasiraghdam, H. and S. Jadid, *Optimal hybrid PV/WT/FC sizing and distribution system reconfiguration using multi-objective artificial bee colony (MOABC) algorithm*. Solar Energy, 2012. 86(10): p. 3057-3071.

217. Katsigiannis, Y.A., P.S. Georgilakis, and E.S. Karapidakis, *Hybrid Simulated Annealing&#x2013;Tabu Search Method for Optimal Sizing of Autonomous Power Systems With Renewables*. Sustainable Energy, IEEE Transactions on, 2012. 3(3): p. 330-338.
218. Mellit, A., et al. *Neural network adaptive wavelets for sizing of stand-alone photovoltaic systems*. in *Intelligent Systems, 2004. Proceedings. 2004 2nd International IEEE Conference*. 2004.
219. Chakraborty, S., et al., *Optimal Thermal Unit Commitment Integrated with Renewable Energy Sources Using Advanced Particle Swarm Optimization*. IEEE Transactions on Electrical and Electronic Engineering, 2009. 4(5): p. 609-617.
220. Gupta, A., R.P. Saini, and M.P. Sharma, *Design of an optimal hybrid energy system model for remote rural area power generation*. Proceedings of IEEE, Pakistan, 2007: p. 1-6.
221. Chedid, R. and S. Rahman, *Unit sizing and control of hybrid wind-solar power systems*. IEEE Transactions on Energy Conversion, 1997. 12(1): p. 79-85.
222. Santarelli, M. and D. Pellegrino, *Mathematical optimization of a RES-H2 plant using a black box algorithm*. Renewable Energy, 2005. 30(4): p. 493-510.
223. Margeta, J. and Z. Glasnovic, *Feasibility of the green energy production by hybrid solar&#xa0;+&#xa0;hydro power system in Europe and similar climate areas*. Renewable and Sustainable Energy Reviews, 2010. 14(6): p. 1580-1590.
224. Ekren, O., B.Y. Ekren, and B. Ozerdem, *Break-even analysis and size optimization of a PV/wind hybrid energy conversion system with battery storage – A case study*. Applied Energy, 2009. 86(7–8): p. 1043-1054.

225. Ekren, O. and B.Y. Ekren, *Size optimization of a PV/wind hybrid energy conversion system with battery storage using response surface methodology*. Applied Energy, 2008. 85(11): p. 1086-1101.
226. Clark, J.D. and B.H. Stark. *Component sizing for multi-source renewable energy systems*. 2009.
227. del Real, A.J., A. Arce, and C. Bordons, *Optimization strategy for element sizing in hybrid power systems*. Journal of Power Sources, 2009. 193(1): p. 315-321.
228. Sinha, S. and S.S. Chandel, *Review of software tools for hybrid renewable energy systems*. Renewable and Sustainable Energy Reviews, 2014. 32(0): p. 192-205.
229. Erdinc, O. and M. Uzunoglu, *Optimum design of hybrid renewable energy systems: Overview of different approaches*. Renewable and Sustainable Energy Reviews, 2012. 16(3): p. 1412-1425.
230. Connolly, D., et al., *A review of computer tools for analysing the integration of renewable energy into various energy systems*. Applied Energy, 2010. 87(4): p. 1059-1082.
231. Belmili, H., et al., *Sizing stand-alone photovoltaic–wind hybrid system: Techno-economic analysis and optimization*. Renewable and Sustainable Energy Reviews, 2014. 30(0): p. 821-832.
232. Lambert, T., P. Gilman, and P. Lilienthal, *Micropower System Modeling with Homer*, in *Integration of Alternative Sources of Energy*. 2006, John Wiley & Sons, Inc. p. 379-418.
233. Shaahid, S.M. and M.A. Elhadidy, *Economic analysis of hybrid photovoltaic–diesel–battery power systems for residential loads in hot regions—A step to*

- clean future*. Renewable and Sustainable Energy Reviews, 2008. 12(2): p. 488-503.
234. Rehman, S. and L.M. Al-Hadhrami, *Study of a solar PV–diesel–battery hybrid power system for a remotely located population near Rafha, Saudi Arabia*. Energy, 2010. 35(12): p. 4986-4995.
235. Nfah, E.M., et al., *Simulation of off-grid generation options for remote villages in Cameroon*. Renewable Energy, 2008. 33(5): p. 1064-1072.
236. Valente, L.C.G. and S.C.A.b. de Almeida, *Economic analysis of a diesel/photovoltaic hybrid system for decentralized power generation in northern Brazil*. Energy, 1998. 23(4): p. 317-323.
237. Hrayshat, E.S., *Techno-economic analysis of autonomous hybrid photovoltaic-diesel-battery system*. Energy for Sustainable Development, 2009. 13(3): p. 143-150.
238. Al-Karaghoul, A. and L.L. Kazmerski, *Optimization and life-cycle cost of health clinic PV system for a rural area in southern Iraq using HOMER software*. Solar Energy, 2010. 84(4): p. 710-714.
239. Mark P, M., *A technical, economic, and greenhouse gas emission analysis of a homestead-scale grid-connected and stand-alone photovoltaic and diesel systems, against electricity network extension*. Renewable Energy, 2012. 38(1): p. 126-135.
240. Rehman, S., et al., *Feasibility study of hybrid retrofits to an isolated off-grid diesel power plant*. Renewable and Sustainable Energy Reviews, 2007. 11(4): p. 635-653.
241. Devine, M., et al., *Wind-diesel hybrid options for remote villages in Alaska*. Available from: U.S. Department of Energy's Wind Powering America Program

<http://www.ceere.org/rerl/publications/published/2004/AWEA%2004%20Wind%20Diesel%20in%20Remote%20Villages,%20Alaska.pdf>, 2000.

242. Nandi, S.K. and H.R. Ghosh, *Prospect of wind–PV-battery hybrid power system as an alternative to grid extension in Bangladesh*. *Energy*, 2010. 35(7): p. 3040-3047.
243. Kenfack, J., et al., *Microhydro-PV-hybrid system: Sizing a small hydro-PV-hybrid system for rural electrification in developing countries*. *Renewable Energy*, 2009. 34(10): p. 2259-2263.
244. Mills, A. and S. Al-Hallaj, *Simulation of hydrogen-based hybrid systems using Hybrid2*. *International Journal of Hydrogen Energy*, 2004. 29(10): p. 991-999.
245. Mousa, K., H. AlZu'bi, and A. Diabat. *Design of a hybrid solar-wind power plant using optimization*. in *Engineering Systems Management and Its Applications (ICESMA), 2010 Second International Conference on*. 2010.
246. El-Shimy, M., *Viability analysis of PV power plants in Egypt*. *Renewable Energy*, 2009. 34(10): p. 2187-2196.
247. Himri, Y., A. Boudghene Stambouli, and B. Draoui, *Prospects of wind farm development in Algeria*. *Desalination*, 2009. 239(1–3): p. 130-138.
248. Chen, F., et al., *Renewislands—Renewable energy solutions for islands*. *Renewable and Sustainable Energy Reviews*, 2007. 11(8): p. 1888-1902.
249. Chen, H., et al., *Progress in electrical energy storage system: A critical review*. *Progress in Natural Science*, 2009. 19(3): p. 291-312.
250. Daim, T.U., et al., *Evaluation of energy storage technologies for integration with renewable electricity: Quantifying expert opinions*. *Environmental Innovation and Societal Transitions*, 2012.

251. Connolly, D., *A Review of Energy Storage Technologies: For the integration of fluctuating renewable energy*. Version 4. University of Limerick, Limerick, 2010.
252. Glasnovic, Z. and J. Margeta, *Sustainable Electric Power System: Is It Possible? Case Study: Croatia*. *Journal of Energy Engineering*, 2010. 136(4): p. 103-113.
253. Bermúdez, J.M., et al., *New concept for energy storage: Microwave-induced carbon gasification with CO<sub>2</sub>*. *Energy Conversion and Management*, 2014. 78(0): p. 559-564.
254. Ma, T., H. Yang, and L. Lu, *Feasibility study and economic analysis of pumped hydro storage and battery storage for a renewable energy powered island*. *Energy Conversion and Management*, 2014. 79(0): p. 387-397.
255. Hadjipaschalis, I., A. Poullikkas, and V. Efthimiou, *Overview of current and future energy storage technologies for electric power applications*. *Renewable and Sustainable Energy Reviews*, 2009. 13(6-7): p. 1513-1522.
256. Rabiee, A., H. Khorramdel, and J. Aghaei, *A review of energy storage systems in microgrids with wind turbines*. *Renewable and Sustainable Energy Reviews*, 2013. 18(0): p. 316-326.
257. Rahman, F., S. Rehman, and M.A. Abdul-Majeed, *Overview of energy storage systems for storing electricity from renewable energy sources in Saudi Arabia*. *Renewable and Sustainable Energy Reviews*, 2012. 16(1): p. 274-283.
258. D áz-Gonz ález, F., et al., *A review of energy storage technologies for wind power applications*. *Renewable and Sustainable Energy Reviews*, 2012. 16(4): p. 2154-2171.
259. Kousksou, T., et al., *Energy storage: Applications and challenges*. *Solar Energy Materials and Solar Cells*, 2014. 120, Part A(0): p. 59-80.

260. Okou, R., A.B. Sebitosi, and P. Pillay, *Flywheel rotor manufacture for rural energy storage in sub-Saharan Africa*. *Energy*, 2011. 36(10): p. 6138-6145.
261. Koochi-Kamali, S., et al., *Emergence of energy storage technologies as the solution for reliable operation of smart power systems: A review*. *Renewable and Sustainable Energy Reviews*, 2013. 25(0): p. 135-165.
262. Succar, S., D.C. Denkenberger, and R.H. Williams, *Optimization of specific rating for wind turbine arrays coupled to compressed air energy storage*. *Applied Energy*, 2012. 96(0): p. 222-234.
263. Figueiredo, J. and J. Martins, *Energy Production System Management – Renewable energy power supply integration with Building Automation System*. *Energy Conversion and Management*, 2010. 51(6): p. 1120-1126.
264. Zhang, L., N. Gari, and L.V. Hmurcik, *Energy management in a microgrid with distributed energy resources*. *Energy Conversion and Management*, 2014. 78(0): p. 297-305.
265. Wang, Y., et al., *Modelling and simulation of a distributed power generation system with energy storage to meet dynamic household electricity demand*. *Applied Thermal Engineering*, 2013. 50(1): p. 523-535.
266. Etxeberria, A., et al., *Comparison of three topologies and controls of a hybrid energy storage system for microgrids*. *Energy Conversion and Management*, 2012. 54(1): p. 113-121.
267. Dhillon, J., A. Kumar, and S.K. Singal, *Optimization methods applied for Wind–PSP operation and scheduling under deregulated market: A review*. *Renewable and Sustainable Energy Reviews*, 2014. 30(0): p. 682-700.

268. Alotto, P., M. Guarnieri, and F. Moro, *Redox flow batteries for the storage of renewable energy: A review*. *Renewable and Sustainable Energy Reviews*, 2014. 29(0): p. 325-335.
269. Rydh, C.J. and B.A. Sandén, *Energy analysis of batteries in photovoltaic systems. Part I: Performance and energy requirements*. *Energy Conversion and Management*, 2005. 46(11–12): p. 1957-1979.
270. Rydh, C.J. and B.A. Sandén, *Energy analysis of batteries in photovoltaic systems. Part II: Energy return factors and overall battery efficiencies*. *Energy Conversion and Management*, 2005. 46(11–12): p. 1980-2000.
271. Divya, K.C. and J. Østergaard, *Battery energy storage technology for power systems—An overview*. *Electric Power Systems Research*, 2009. 79(4): p. 511-520.
272. Lacerda, V.G., et al., *Separation of Cd and Ni from Ni–Cd batteries by an environmentally safe methodology employing aqueous two-phase systems*. *Journal of Power Sources*, 2009. 193(2): p. 908-913.
273. Krieger, E.M., J. Cannarella, and C.B. Arnold, *A comparison of lead-acid and lithium-based battery behavior and capacity fade in off-grid renewable charging applications*. *Energy*, 2013. 60(0): p. 492-500.
274. Broussely, M. and G. Pistoia, *Industrial applications of batteries: from cars to aerospace and energy storage*. 2007: Elsevier.
275. Evans, A., V. Strezov, and T.J. Evans, *Assessment of utility energy storage options for increased renewable energy penetration*. *Renewable and Sustainable Energy Reviews*, 2012. 16(6): p. 4141-4147.

276. Gustavsson, M. and D. Mtonga, *Lead-acid battery capacity in solar home systems—Field tests and experiences in Lundazi, Zambia*. Solar Energy, 2005. 79(5): p. 551-558.
277. D áz, P. and E. Lorenzo, *Solar home system battery and charge regulator testing*. Progress in Photovoltaics: Research and Applications, 2001. 9(5): p. 363-377.
278. Baker, J., *New technology and possible advances in energy storage*. Energy Policy, 2008. 36(12): p. 4368-4373.
279. Depernet, D., O. Ba, and A. Berthon, *Online impedance spectroscopy of lead acid batteries for storage management of a standalone power plant*. Journal of Power Sources, 2012. 219(0): p. 65-74.
280. Margeta, J., *Water storage as energy storage in green power system*. Sustainable Energy Technologies and Assessments, 2014. 5(0): p. 75-83.
281. Messenger, R.A., *Photovoltaic systems engineering*. 3rd ed. 2010: CRC Press/Taylor & Francis 503.
282. Ding, H., Z. Hu, and Y. Song, *Stochastic optimization of the daily operation of wind farm and pumped-hydro-storage plant*. Renewable Energy, 2012. 48(0): p. 571-578.
283. Saini, R.P., *Large-Scale Energy Storage Systems*. Indian Institute of Technology Roorkee, 2011.
284. Rangoni, B., *A contribution on electricity storage: The case of hydro-pumped storage appraisal and commissioning in Italy and Spain*. Utilities Policy, 2012. 23(0): p. 31-39.
285. Rastler, D., *Electricity Energy Storage Technology Options: A White Paper Primer on Applications, Costs, and Benefits*. Electric Power Research Institute (EPRI), Technical Update, USA, 2010.

286. Wood, A.J. and B.F. Wollenberg, *Power generation, operation, and control*. 2012: John Wiley & Sons.
287. Iea, R., R. de Vos, and J. Sawin, *Appendix B - Renewable Energy Technologies*, in *Ready: Renewable Energy Action on Deployment*. 2012, Academic Press: Boston. p. 193-209.
288. Miller, R.R. and M. Winters, *Opportunities for Pumped Storage: Supporting Renewable Energy Goals*. <http://www.hydroworld.com/>. 2009.
289. Lise, W., et al., *Assessment of the required share for a stable EU electricity supply until 2050*. *Energy Policy*, 2013. 59(0): p. 904-913.
290. Kaldellis, J.K., M. Kapsali, and D. Tiligadas, *Presentation of a stochastic model estimating the wind energy contribution in remote island electrical networks*. *Applied Energy*, 2012. 97(0): p. 68-76.
291. Chen, N., et al., *Environmental Friendly PV Power Plant*. *Energy Procedia*, 2012. 16, Part A(0): p. 32-37.
292. Ardizzon, G., G. Cavazzini, and G. Pavesi, *A new generation of small hydro and pumped-hydro power plants: Advances and future challenges*. *Renewable and Sustainable Energy Reviews*, 2014. 31(0): p. 746-761.
293. Xydis, G., *Comparison study between a Renewable Energy Supply System and a supergrid for achieving 100% from renewable energy sources in Islands*. *International Journal of Electrical Power & Energy Systems*, 2013. 46(0): p. 198-210.
294. Duić, N., G. Krajačić, and M. da Graça Carvalho, *RenewIslands methodology for sustainable energy and resource planning for islands*. *Renewable and Sustainable Energy Reviews*, 2008. 12(4): p. 1032-1062.

295. Papaefthymiou, S.V., et al., *Dynamic analysis of island systems with wind-pumped-storage hybrid power stations*. *Renewable Energy*, 2015. 74(0): p. 544-554.
296. Caralis, G., D. Papantonis, and A. Zervos, *The role of pumped storage systems towards the large scale wind integration in the Greek power supply system*. *Renewable and Sustainable Energy Reviews*, 2012. 16(5): p. 2558-2565.
297. Anagnostopoulos, J.S. and D.E. Papantonis, *Simulation and size optimization of a pumped-storage power plant for the recovery of wind-farms rejected energy*. *Renewable Energy*, 2008. 33(7): p. 1685-1694.
298. Parastegari, M., et al., *Joint operation of wind farm, photovoltaic, pump-storage and energy storage devices in energy and reserve markets*. *International Journal of Electrical Power & Energy Systems*, 2015. 64(0): p. 275-284.
299. Zhou, Y., J.A. Ferreira, and P. Bauer. *Grid-connected and islanded operation of a hybrid power system*. in *Power Engineering Society Conference and Exposition in Africa, 2007. PowerAfrica '07. IEEE*. 2007.
300. Novosel, T., et al., *The influence of reverse osmosis desalination in a combination with pump storage on the penetration of wind and PV energy: A case study for Jordan*. *Energy*, 2014(0).
301. N.E., M.R., et al., *Optimisation of Pumped-hydro Storage System for Hybrid Power System Using Power Pinch Analysis*. *CHEMICAL ENGINEERING*, 2013. 35: p. 85-90.
302. Aihara, R., et al. *Impact of operational scheduling of pumped storage power plant considering excess energy and reduction of fuel cost on power supply reliability in a power system with a large penetration of photovoltaic*

- generations. in *Power System Technology (POWERCON), 2010 International Conference on*. 2010.
303. Glasnovic, Z. and J. Margeta, *Optimal sizing of photovoltaic-hydro power plant*. *Progress in Photovoltaics: Research and Applications*, 2009. 17(8): p. 542-553.
304. Margeta, J. and Z. Glasnovic, *Role of Water-Energy Storage in PV-PSH Power Plant Development*. *Journal of Energy Engineering*, 2011. 137(4): p. 187-197.
305. Kaldellis, J.K., et al., *Design of an Integrated PV-based Pumped Hydro and Battery Storage System Including Desalination Aspects for the Island of Tilos*, in *International Conference on CLEAN ELECTRICAL POWER*. 2013: Alghero, Sardinia, Italy.
306. Carlos, P., et al., *New high head pumped-storage power station design to increase the wind power penetration in island autonomous power systems*, in *Environmental Hydraulics - Theoretical, Experimental and Computational Solutions*. 2009, CRC Press. p. 281-284.
307. Iea, R., R. de Vos, and J. Sawin, *Chapter One - Global and Regional Trends in Renewable Energy*, in *Ready: Renewable Energy Action on Deployment*. 2012, Academic Press: Boston. p. 1-28.
308. Aihara, R., et al. *Optimal operation scheduling of pumped storage hydro power plant in power system with a large penetration of photovoltaic generation using genetic algorithm*. in *PowerTech, 2011 IEEE Trondheim*. 2011.
309. Parastegari, M., et al., *Joint operation of wind farms and pump-storage units in the electricity markets: Modeling, simulation and evaluation*. *Simulation Modelling Practice and Theory*, 2013. 37(0): p. 56-69.

310. Pálmason, Á.V., *Wind Power Pumped Storage System for Hydropower Plants*, in *Faculty of Industrial Engineering, Mechanical Engineering and Computer Science*. 2009, University of Iceland.
311. Papaefthimiou, S., et al., *Operating policies for wind-pumped storage hybrid power stations in island grids*. *Renewable Power Generation, IET*, 2009. 3(3): p. 293-307.
312. Papaefthymiou, S.V., et al., *A Wind-Hydro-Pumped Storage Station Leading to High RES Penetration in the Autonomous Island System of Ikaria*. *Sustainable Energy, IEEE Transactions on*, 2010. 1(3): p. 163-172.
313. Caralis, G. and A. Zervos, *Analysis of the combined use of wind and pumped storage systems in autonomous Greek islands*. *Renewable Power Generation, IET*, 2007. 1(1): p. 49-60.
314. Anagnostopoulos, J.S. and D.E. Papantonis, *Pumping station design for a pumped-storage wind-hydro power plant*. *Energy Conversion and Management*, 2007. 48(11): p. 3009-3017.
315. Caralis, G., K. Rados, and A. Zervos, *On the market of wind with hydro-pumped storage systems in autonomous Greek islands*. *Renewable and Sustainable Energy Reviews*, 2010. 14(8): p. 2221-2226.
316. George C, B., *Feasibility study of a hybrid wind/hydro power-system for low-cost electricity production*. *Applied Energy*, 2002. 72(3-4): p. 599-608.
317. Hatziargyriou, N., J. Stefanakis, and S. Alexandridis. *Safe increase of wind energy penetration in island systems by pumped storage units - the crete case*. in *RENES 2001*. 2001. Athens, Greece.
318. Protopapas, K. and S. Papathanasiou, *Application of pumped storage to increase wind penetration in isolated island grids*, in *EWEC 2006*. 2006: Athens, Greece.

319. Boulaxis, N. and M. Papadopoulos. *Assessment of the contribution of hybrid systems in renewable energy penetration in islands*. in *ISAP 2003 conference*. 2003. Lemnos, Greece.
320. Theodoropoulos, P., A. Zervos, and G. Betzios, *Hybrid systems using pump-storage implementation in Ikaria island*, in *OPET island international conference*. 2001: Chania, Greece.
321. Mantas, Z., et al., *Hybrid system using pump-storage for maximum wind energy penetration in Serifos island*, in *Bulletin of the Hellenic Association of Mechanical & Electrical Engineers*. 2003.
322. Kaldellis, J., K. Kavvadias, and D. Vlachou, *Electricity load management of APS using wind hydro solution*, in *MedPower 2002*. 2002: Athens, Greece.
323. Katsaprakakis, D.A., et al., *Pumped storage systems introduction in isolated power production systems*. *Renewable Energy*, 2008. 33(3): p. 467-490.
324. Krajačić, G., et al., *Analysis of financial mechanisms in support to new pumped hydropower storage projects in Croatia*. *Applied Energy*, 2013. 101(0): p. 161-171.
325. Krajačić, G., N. Duić, and M.d.G. Carvalho, *How to achieve a 100% RES electricity supply for Portugal?* *Applied Energy*, 2011. 88(2): p. 508-517.
326. Ćosić, B., et al., *Environmental and economic aspects of higher RES penetration into Macedonian power system*. *Applied Thermal Engineering*, 2012. 43(0): p. 158-162.
327. Bueno, C. and J.A. Carta, *Technical–economic analysis of wind-powered pumped hydrostorage systems. Part I: model development*. *Solar Energy*, 2005. 78(3): p. 382-395.

328. Bueno, C. and J.A. Carta, *Technical–economic analysis of wind-powered pumped hydrostorage systems. Part II: model application to the island of El Hierro*. Solar Energy, 2005. 78(3): p. 396-405.
329. Katsaprakakis, D.A. and D. Christakis. *Maximisation of RES penetration in Greek insular isolated power systems with the introduction of pumped storage systems*. in *Proc. European Wind Energy Conference and Exhibition (EWEC) 2009*. 2009.
330. Papaefthymiou, S.V. and S.A. Papathanassiou, *Optimum sizing of wind-pumped-storage hybrid power stations in island systems*. Renewable Energy, 2014. 64(0): p. 187-196.
331. Papaefthymiou, S., S. Papathanassiou, and E. Karamanou, *Application of Pumped Storage to Increase Renewable Energy Penetration in Autonomous Island Systems*, in *Wind Energy Conversion Systems*, S.M. Mueeen, Editor. 2012, Springer London. p. 295-335.
332. Dursun, B. and B. Alboyaci, *The contribution of wind-hydro pumped storage systems in meeting Turkey's electric energy demand*. Renewable and Sustainable Energy Reviews, 2010. 14(7): p. 1979-1988.
333. Reuter, W.-H., et al., *Investment in wind power & pumped storage in a real options model - a policy analysis*, in *World Renewable Energy Congress*. 2011: Linköping, Sweden. p. 2530-2537.
334. Kapsali, M., J.S. Anagnostopoulos, and J.K. Kaldellis, *Wind powered pumped-hydro storage systems for remote islands: A complete sensitivity analysis based on economic perspectives*. Applied Energy, 2012. 99(0): p. 430-444.
335. Benitez, L.E., P.C. Benitez, and G.C. van Kooten, *The economics of wind power with energy storage*. Energy Economics, 2008. 30(4): p. 1973-1989.

336. Vieira, F. and H.M. Ramos, *Hybrid solution and pump-storage optimization in water supply system efficiency: A case study*. Energy Policy, 2008. 36(11): p. 4142-4148.
337. Crettanand, N., *Small storage and pumped storage plants in Switzerland*. International Water Power and Dam Construction, 2012. 64(4): p. 22-24.
338. Ma, T., et al., *Pumped storage-based standalone photovoltaic power generation system: Modeling and techno-economic optimization*. Applied Energy, 2015. 137(0): p. 649-659.
339. Connolly, D., et al., *The technical and economic implications of integrating fluctuating renewable energy using energy storage*. Renewable Energy, 2012. 43(0): p. 47-60.
340. Padrón, S., J.F. Medina, and A. Rodríguez, *Analysis of a pumped storage system to increase the penetration level of renewable energy in isolated power systems. Gran Canaria: A case study*. Energy, 2011. 36(12): p. 6753-6762.
341. Bueno, C. and J.A. Carta, *Wind powered pumped hydro storage systems, a means of increasing the penetration of renewable energy in the Canary Islands*. Renewable and Sustainable Energy Reviews, 2006. 10(4): p. 312-340.
342. Kapsali, M. and J.K. Kaldellis, *Combining hydro and variable wind power generation by means of pumped-storage under economically viable terms*. Applied Energy, 2010. 87(11): p. 3475-3485.
343. Poullikkas, A., *Optimization analysis for pumped energy storage systems in small isolated power systems*. Journal of Power Technologies, 2013. 93(2): p. 78-89.

344. Katsaprakakis, D.A., et al., *Introduction of a wind powered pumped storage system in the isolated insular power system of Karpathos–Kasos*. Applied Energy, 2011(0).
345. Tuohy, A. and M. O'Malley, *Pumped storage in systems with very high wind penetration*. Energy Policy, 2011. 39(4): p. 1965-1974.
346. Varkani, A.K., A. Daraeepour, and H. Monsef, *A new self-scheduling strategy for integrated operation of wind and pumped-storage power plants in power markets*. Applied Energy, 2011. 88(12): p. 5002-5012.
347. Islam, S., *Increasing wind energy penetration level using pumped hydro storage in island micro-grid system*. International Journal of Energy and Environmental Engineering, 2012. 3(1): p. 9.
348. Iqbal, T., *Feasibility Study of Pumped Hydro Energy Storage for Ramea: Wind-Diesel Hybrid Power System*. 2010, Faculty of Engineering and Applied Science, Memorial University. p. 23.
349. Qian, K., Y. Jiang, and Z. Li. *Improve wind energy penetration in an isolated power system by a stand-alone wind pumped storage hydropower plant*. 2011.
350. Glasnovic, Z. and J. Margeta, *Solar hydro electric power plant*. 2009.
351. Glasnovic, Z., K. Margeta, and V. Omerbegovic, *Artificial Water Inflow Created by Solar Energy for Continuous Green Energy Production*. Water Resources Management, 2013. 27(7): p. 2303-2323.
352. Margeta, J., *Integration of Solar and Hydro Energy*. European Journal of Scientific Research, 2012. 90(3): p. 409-424.
353. Margeta, J. and Z. Glasnovic, *Theoretical settings of photovoltaic-hydro energy system for sustainable energy production*. Solar Energy, 2012. 86(3): p. 972-982.

354. Margeta, J. and Z. Glasnovic, *Exploitation of temporary water flow by hybrid PV-hydroelectric plant*. *Renewable Energy*, 2011. 36(8): p. 2268-2277.
355. Margeta, J. and Z. Glasnovic, *Hybrid RES-HEP Systems Development*. *Water Resources Management*, 2011. 25(9): p. 2219-2239.
356. Margeta, J. and Z. Glasnovic, *Introduction of PV Energy Into an Existing HEP*. *Energy Conversion, IEEE Transactions on*, 2011. 26(3): p. 717-727.
357. Margeta, J. and Z. Glasnovic, *Feasibility of the green energy production by hybrid solar + hydro power system in Europe and similar climate areas*. *Renewable and Sustainable Energy Reviews*, 2010. 14(6): p. 1580-1590.
358. Glasnovic, Z. and J. Margeta, *The features of sustainable Solar Hydroelectric Power Plant*. *Renewable Energy*, 2009. 34(7): p. 1742-1751.
359. Javanbakht, P., S. Mohagheghi, and M.G. Simoes. *Transient performance analysis of a small-scale PV-PHS power plant fed by a SVPWM drive applied for a distribution system*. in *Energy Conversion Congress and Exposition (ECCE), 2013 IEEE*. 2013.
360. Manolakos, D., et al., *A stand-alone photovoltaic power system for remote villages using pumped water energy storage*. *Energy*, 2004. 29(1): p. 57-69.
361. Junhui, Z., et al. *A hybrid electric/hydro storage solution for standalone photovoltaic applications in remote areas*. in *Power and Energy Society General Meeting, 2012 IEEE*. 2012.
362. Haque, A. and M.A. Rahman. *Study of a solar PV-powered mini-grid pumped hydroelectric storage & its comparison with battery storage*. in *Electrical & Computer Engineering (ICECE), 2012 7th International Conference on*. 2012.
363. Akbarpour, M., et al., *Optimal Utilization of a Combined System of Photovoltaic-Pumped Storage Power Plant using PSO algorithm*. 2013.

364. Kaldellis, J., et al. *Design of an integrated PV-based pumped hydro and battery storage system including desalination aspects for the Island of Tilos*. in *International Conference on CLEAN ELECTRICAL POWER*, Alghero, Sardinia, Italy. 2013.
365. Ruisheng, L., et al. *Design of wind-solar and pumped-storage hybrid power supply system*. in *Computer Science and Information Technology (ICCSIT), 2010 3rd IEEE International Conference on*. 2010.
366. Ren, Y. and Y. Li. *Simulation and optimization of hybrid wind-solar-pumped-storage power system*. in *Electric Information and Control Engineering (ICEICE), 2011 International Conference on*. 2011.
367. Yan, R., et al., *Modelling and optimization of hybrid wind/PV pumped-storage power system*. *Applied Mechanics and Materials*, 2011. 48 - 49.
368. Cristofari, C., et al. *Pumped hydroelectric storage coupling wind-solar resources: A solution for increase ren on islands electrical grid*. in *Energy and Sustainable Development: Issues and Strategies (ESD), 2010 Proceedings of the International Conference on*. 2010.
369. Yan, R. and Z. Yuan, *Optimal Design of PV/Wind/Pumped-Storage Hybrid System Based on Improved Particle Swarm Optimization*. *Advanced Science Letters*, 2012. 6(1): p. 660-663.
370. Hu, X., et al. *Multi-Objective Optimal Design of Wind/PV/Pumped-Storage System Based on GA*. in *Power and Energy Engineering Conference (APPEEC), 2012 Asia-Pacific*. 2012.
371. Chen, G.Z., et al. *Determination of installed capacity of pumped storage station in WSP hybrid power supply system*. in *Sustainable Power Generation and Supply, 2009. SUPERGEN '09. International Conference on*. 2009.

372. Heindl, E., *Hydraulic Hydro Storage System for Self-sufficient Cities*. Energy Procedia, 2014. 46(0): p. 98-103.
373. Spyrou, I.D. and J.S. Anagnostopoulos, *Design study of a stand-alone desalination system powered by renewable energy sources and a pumped storage unit*. Desalination, 2010. 257(1-3): p. 137-149.
374. Tetsuo Fujihara, H.I., Katsuhiro Oshima, *Development of pump turbine for seawater pumped-storage power plant*. Hitachi Review 1998. 47(5): p. 199-202.
375. Katsaprakakis, D.A., et al., *Technical details regarding the design, the construction and the operation of seawater pumped storage systems*. Energy, 2013(0).
376. Katsaprakakis, D.A. and D.G. Christakis, *Seawater pumped storage systems and offshore wind parks in islands with low onshore wind potential. A fundamental case study*. Energy, 2014. 66(0): p. 470-486.
377. McLean, E. and D. Kearney, *An Evaluation of Seawater Pumped Hydro Storage for Regulating the Export of Renewable Energy to the National Grid*. Energy Procedia, 2014. 46(0): p. 152-160.
378. Segurado, R., et al., *Increasing the penetration of renewable energy resources in S. Vicente, Cape Verde*. Applied Energy, 2011. 88(2): p. 466-472.
379. Li, Y., et al., *The Research of Wind-Light Complementary Based on Pumped Storage Power System*. Advanced Materials Research, 2012. 354 - 355: p. 1132-1136.
380. Schoppe, C., *Wind and pumped-hydro power storage-determining optimal commitment policies with knowledge gradient non-parametric estimation*, in *Department of Operations Research and Financial Engineering*. 2010, Princeton University. p. 128.

381. Dinglin, L., et al., *Economic evaluation of wind-powered pumped storage system*. Systems Engineering Procedia, 2012. 4(0): p. 107-115.
382. Kaldellis, J.K., M. Kapsali, and K.A. Kavadias, *Energy balance analysis of wind-based pumped hydro storage systems in remote island electrical networks*. Applied Energy, 2010. 87(8): p. 2427-2437.
383. Brown, P.D., J.A. Peas Lopes, and M.A. Matos, *Optimization of Pumped Storage Capacity in an Isolated Power System With Large Renewable Penetration*. Power Systems, IEEE Transactions on, 2008. 23(2): p. 523-531.
384. Glasnović, Z., M. Rogošić, and J. Margeta, *A model for optimal sizing of solar thermal hydroelectric power plant*. Solar Energy, 2011. 85(5): p. 794-807.
385. Bose, S., et al. *A methodology for sizing and cost optimization of wind power with pumped-hydro storage*. in *Proceedings of the International Conference—RES and RUE for Islands—Sustainable Energy Solutions*. 2004.
386. Khatibi, M. and M. Jazaeri. *An analysis for increasing the penetration of renewable energies by optimal sizing of pumped-storage power plants*. in *Electric Power Conference, 2008. EPEC 2008. IEEE Canada*. 2008.
387. Westgate, M. and D.A. Bergman, *Plans for a Demonstration Photovoltaic/Wind/Pumped Storage System Integrated on an Island in Boston Harbor*, in *Energy for Rural and Island Communities*, J. Twidell, I.A.N. Hounam, and C. Lewis, Editors. 1986, Pergamon. p. 63-70.
388. Manolakos, D., et al., *A simulation-optimisation programme for designing hybrid energy systems for supplying electricity and fresh water through desalination to remote areas: Case study: the Meressini village, Donoussa island, Aegean Sea, Greece*. Energy, 2001. 26(7): p. 679-704.

389. Papadakis, G., et al., *A hybrid renewable energy system for supplying electricity and fresh water through desalination to remote places in Mediterranean Conference on Renewable Energy Sources for Water Production*. 10-12 June 1996: Santorini, Greece. p. 265-270.
390. Sunlabob, *Compilation and Analysis of Information on Existing Rural Electrification and Renewable Energy Programmes in the Province of Oudomxay, Lao PDR*. 2007.
391. Nfah, E.M. and J.M. Ngundam, *Feasibility of pico-hydro and photovoltaic hybrid power systems for remote villages in Cameroon*. *Renewable Energy*, 2009. 34(6): p. 1445-1450.
392. Benlarbi, K., L. Mokrani, and M.S. Nait-Said, *A fuzzy global efficiency optimization of a photovoltaic water pumping system*. *Solar Energy*, 2004. 77(2): p. 203-216.
393. Blas, M.A.d., et al., *Selecting a suitable model for characterizing photovoltaic devices*. *Renewable Energy*, 2002. 25(3): p. 371-380.
394. Zhang, L., A. Al-Amoudi, and B. Yunfei. *Real-time maximum power point tracking for grid-connected photovoltaic systems*. in *Power Electronics and Variable Speed Drives, 2000. Eighth International Conference on (IEE Conf. Publ. No. 475)*. 2000.
395. Walker, G., *Evaluating MPPT converter topologies using a matlab PV model*. *Journal of Electrical & Electronics Engineering, Australia*, 2001 21(1): p. 49-55.
396. Kim, S.-K., et al., *Modeling and simulation of a grid-connected PV generation system for electromagnetic transient analysis*. *Solar Energy*, 2009. 83(5): p. 664-678.
397. PVsyst. <http://www.pvsyst.com/>.

398. King, D.L., J.A. Kratochvil, and W.E. Boyson, *Photovoltaic array performance model*. 2004, Sandia National, Laboratories; United States. Dept. of, Energy: Washington, D.C.; Oak Ridge, Tenn.
399. INSEL. <http://www.insel.eu/>.
400. Hansen, A.D., et al., *Models for a Stand-Alone PV System*. 2000, Risø National Laboratory. p. 77.
401. PVWATTS, <http://www.nrel.gov/rredc/pvwatts/>.
402. Bellini, A., et al. *Simplified model of a photovoltaic module*. in *Applied Electronics, 2009. AE 2009*. 2009.
403. Ma, T., H. Yang, and L. Lu, *Performance evaluation of a stand-alone photovoltaic system on an isolated island in Hong Kong*. *Applied Energy*, 2013(0).
404. Zhou, W., H. Yang, and Z. Fang, *A novel model for photovoltaic array performance prediction*. *Applied Energy*, 2007. 84(12): p. 1187-1198.
405. Davies, J.A. and D.C. McKay, *Evaluation of selected models for estimating solar radiation on horizontal surfaces*. *Solar Energy*, 1989. 43(3): p. 153-168.
406. Zhou, W., H. Yang, and Z. Fang, *Battery behavior prediction and battery working states analysis of a hybrid solar-wind power generation system*. *Renewable Energy*, 2008. 33(6): p. 1413-1423.
407. Manwell, J.F. and J.G. McGowan, *Lead acid battery storage model for hybrid energy systems*. *Solar Energy*, 1993. 50(5): p. 399-405.
408. LAMBERT, T., P. GILMAN, and P. LILIENTHAL, *Micropower system modeling with homer*. Available from [www.mistaya.ca/software/docs/MicropowerSystemModelingWithHOMER.pdf](http://www.mistaya.ca/software/docs/MicropowerSystemModelingWithHOMER.pdf), 2006.

409. Billinton, R. and R.N. Allan, *Reliability evaluation of power systems*. 2nd ed. 1996, New York: New York : Plenum Press, c1996.
410. Celik, A.N., *Techno-economic analysis of autonomous PV-wind hybrid energy systems using different sizing methods*. *Energy Conversion and Management*, 2003. 44(12): p. 1951-1968.
411. Protogeropoulos, C., B.J. Brinkworth, and R.H. Marshall, *SIZING AND TECHNO-ECONOMICAL OPTIMIZATION FOR HYBRID SOLAR PHOTOVOLTAIC/WIND POWER SYSTEMS WITH BATTERY STORAGE*. *International Journal of Energy Research*, 1997. 21(6): p. 465-479.
412. Dalton, G.J., D.A. Lockington, and T.E. Baldock, *Case study feasibility analysis of renewable energy supply options for small to medium-sized tourist accommodations*. *Renewable Energy*, 2009. 34(4): p. 1134-1144.
413. Bernal-Agustín, J.L. and R. Dufo-López, *Economical and environmental analysis of grid connected photovoltaic systems in Spain*. *Renewable Energy*, 2006. 31(8): p. 1107-1128.
414. Lu, L., H. Yang, and J. Burnett, *Investigation on wind power potential on Hong Kong islands—an analysis of wind power and wind turbine characteristics*. *Renewable Energy*, 2002. 27(1): p. 1-12.
415. Weisser, D., *A wind energy analysis of Grenada: an estimation using the 'Weibull' density function*. *Renewable Energy*, 2003. 28(11): p. 1803-1812.
416. Johnson, G.L., *Wind energy systems / Gary L. Johnson*. 1985, Englewood Cliffs, N.J.: Englewood Cliffs, N.J. : Prentice-Hall.
417. Justus, C.G., *Winds and wind system performance*. 1978: Philadelphia: Franklin Institute Press.

418. Katsaprakakis, D.A., et al., *Electricity supply on the island of Dia based on renewable energy sources (R.E.S.)*. Applied Energy, 2009. 86(4): p. 516-527.
419. SNL, *Stand-Alone Photovoltaic Systems: A Handbook of Recommended Design Practices* 1995, Photovoltaic Design Assistance Center, Sandia National Laboratories: Albuquerque, NM.
420. Boehm, R.F., *Minimizing peak residential electrical demand in hot climates*. 2nd Asian-US-European Thermophysics Conference: Thermal Science for Sustainable World 2012.
421. Dennis Barley, C. and C. Byron Winn, *Optimal dispatch strategy in remote hybrid power systems*. Solar Energy, 1996. 58(4–6): p. 165-179.
422. Dalton, G.J., D.A. Lockington, and T.E. Baldock, *Feasibility analysis of stand-alone renewable energy supply options for a large hotel*. Renewable Energy, 2008. 33(7): p. 1475-1490.
423. Cotrell, J., et al., *Modeling the feasibility of using fuel cells and hydrogen internal combustion engines in remote renewable energy systems*. 2003, Golden, Colo.: National Renewable Energy Laboratory.
424. Kaldellis, J.K., K. Kavadias, and E. Christinakis, *Evaluation of the wind–hydro energy solution for remote islands*. Energy Conversion and Management, 2001. 42(9): p. 1105-1120.
425. Cozorici, F., et al. *Design and simulation of a small wind-hydro power plant*. in *Clean Electrical Power (ICCEP), 2011 International Conference on*. 2011.
426. Glavin, M.E., P.K.W. Chan, and W.G. Hurley. *Optimization of autonomous hybrid energy storage system for photovoltaic applications*. in *Energy Conversion Congress and Exposition, 2009. ECCE 2009. IEEE*. 2009.

427. Erdinc, O. and M. Uzunoglu, *A new perspective in optimum sizing of hybrid renewable energy systems: Consideration of component performance degradation issue*. International Journal of Hydrogen Energy, 2012. 37(14): p. 10479-10488.
428. Campana, P.E., H. Li, and J. Yan, *Dynamic modelling of a PV pumping system with special consideration on water demand*. Applied Energy, 2013. 112(0): p. 635-645.
429. Sallem, S., M. Chaabene, and M.B.A. Kamoun, *Energy management algorithm for an optimum control of a photovoltaic water pumping system*. Applied Energy, 2009. 86(12): p. 2671-2680.
430. Holland, J.H., *Adaptation in natural and artificial systems*. 1992: MIT Press. 211.
431. Malhotra, R., N. Singh, and Y. Singh, *Genetic Algorithms: Concepts, Design for Optimization of Process Controllers*. Computer and Information Science, 2011. 4(2).
432. Das, D.C., A.K. Roy, and N. Sinha, *GA based frequency controller for solar thermal–diesel–wind hybrid energy generation/energy storage system*. International Journal of Electrical Power & Energy Systems, 2012. 43(1): p. 262-279.
433. Feroldi, D. and D. Zumoffen, *Sizing methodology for hybrid systems based on multiple renewable power sources integrated to the energy management strategy*. International Journal of Hydrogen Energy, (0).
434. Konak, A., D.W. Coit, and A.E. Smith, *Multi-objective optimization using genetic algorithms: A tutorial*. Reliability Engineering & System Safety, 2006. 91(9): p. 992-1007.

435. Menicucci, D.F., *Photovoltaic array performance simulation models*. Solar Cells, 1986. 18(3–4): p. 383-392.
436. HKSAR, *Future Fuel Mix for Electricity Generation*. 2014, Environment Bureau, Hong Kong SAR.
437. Lund, H., *Large-scale integration of optimal combinations of PV, wind and wave power into the electricity supply*. Renewable Energy, 2006. 31(4): p. 503-515.
438. Vechiu, I., et al. *Hybrid energy storage system with unique power electronic interface for microgrids*. in *Innovative Smart Grid Technologies Europe (ISGT EUROPE), 2013 4th IEEE/PES*. 2013.
439. Etxeberria, A., et al., *Control of a Vanadium Redox Battery and supercapacitor using a Three-Level Neutral Point Clamped converter*. Journal of Power Sources, 2014. 248(0): p. 1170-1176.
440. Glavin, M.E., et al. *A stand-alone photovoltaic supercapacitor battery hybrid energy storage system*. in *Power Electronics and Motion Control Conference, 2008. EPE-PEMC 2008. 13th*. 2008.
441. Glavin, M.E. and W.G. Hurley. *Ultracapacitor/ battery hybrid for solar energy storage*. in *Universities Power Engineering Conference, 2007. UPEC 2007. 42nd International*. 2007.
442. Rajagopal, A. and J.G. K, *Wind integrated battery/super capacitor combination in UPS* International Journal of Engineering and Innovative Technology, 2013. 3(2): p. 365-367.
443. Sathishkumar, R., S.K. Kollimalla, and M.K. Mishra. *Dynamic energy management of micro grids using battery super capacitor combined storage*. in *India Conference (INDICON), 2012 Annual IEEE*. 2012.

444. Glavin, M.E. and W.G. Hurley, *Optimisation of a photovoltaic battery ultracapacitor hybrid energy storage system*. Solar Energy, 2012. 86(10): p. 3009-3020.
445. Xisheng, T. and Q. Zhiping. *Economic analysis of EDLC/battery hybrid energy storage*. in *Electrical Machines and Systems, 2008. ICEMS 2008. International Conference on*. 2008.
446. Lijun, G., R.A. Dougal, and S. Liu, *Power enhancement of an actively controlled battery/ultracapacitor hybrid*. Power Electronics, IEEE Transactions on, 2005. 20(1): p. 236-243.
447. Xiaolei, H., K.J. Tseng, and M. Srinivasan. *Optimization of battery energy storage system with super-capacitor for renewable energy applications*. in *Power Electronics and ECCE Asia (ICPE & ECCE), 2011 IEEE 8th International Conference on*. 2011.
448. Kan, S.Y., M. Verwaal, and H. Broekhuizen, *The use of battery-capacitor combinations in photovoltaic powered products*. Journal of Power Sources, 2006. 162(2): p. 971-974.
449. Miller, J.R., *Battery-capacitor Power Source for Digital Communication Applications: Simulations using Advanced Electrochemical Capacitors*, in *Electrochemical Society* 1995: Chicago.
450. Xiong, L., et al. *Control of hybrid battery/ultra-capacitor energy storage for stand-alone photovoltaic system*. in *Energy Conversion Congress and Exposition (ECCE), 2010 IEEE*. 2010.
451. Tammineedi, C., *Modeling battery-ultracapacitor hybrid systems for solar and wind applications*, in *Department of Energy and Mineral Engineering*. 2011, The Pennsylvania State University.

452. Awerbuch, J.J. and C.R. Sullivan. *Control of Ultracapacitor-Battery Hybrid Power Source for Vehicular Applications*. in *Energy 2030 Conference, 2008. ENERGY 2008. IEEE*. 2008.
453. Gee, A.M. and R.W. Dunn. *Novel battery / supercapacitor hybrid energy storage control strategy for battery life extension in isolated wind energy conversion systems*. in *Universities Power Engineering Conference (UPEC), 2010 45th International*. 2010.
454. Wei, L., G. Joos, and J. Belanger, *Real-Time Simulation of a Wind Turbine Generator Coupled With a Battery Supercapacitor Energy Storage System*. *Industrial Electronics, IEEE Transactions on*, 2010. 57(4): p. 1137-1145.
455. Ribeiro, E., A.J.M. Cardoso, and C. Boccaletti. *Power conditioning supercapacitors in combination with batteries for stand-alone power systems*. in *Power Electronics, Electrical Drives, Automation and Motion (SPEEDAM), 2012 International Symposium on*. 2012.
456. Kuperman, A. and I. Aharon, *Battery-ultracapacitor hybrids for pulsed current loads: A review*. *Renewable and Sustainable Energy Reviews*, 2011. 15(2): p. 981-992.
457. Seim, L.H., *Modeling, control and experimental testing of a supercapacitor/battery hybrid system - passive and semi-active topologies*, in *Department of Mathematical Sciences and Technology*. 2011, Norwegian University of Life Sciences.
458. Dougal, R.A., S. Liu, and R.E. White, *Power and life extension of battery-ultracapacitor hybrids*. *Components and Packaging Technologies, IEEE Transactions on*, 2002. 25(1): p. 120-131.

459. *Compilation and Analysis of Information on Existing Rural Electrification and Renewable Energy Programmes in the Province of Oudomxay, Lao PDR (final report)*. October 2007, SUNLABOB RURAL ENERGY SYSTEMS LTD, Lao PDR.
460. Yunqing, P., et al. *Auto-master-slave control technique of parallel inverters in distributed AC power systems and UPS*. in *Power Electronics Specialists Conference, 2004. PESC 04. 2004 IEEE 35th Annual*. 2004.
461. Naxin, C., J. Schmid, and A. Chen. *Data and performance evaluation of a PV hybrid system in Gambia*. in *Power Electronics and Motion Control Conference, 2009. IPEMC '09. IEEE 6th International*. 2009.
462. Glasnovic, Z. and J. Margeta, *Vision of total renewable electricity scenario*. *Renewable and Sustainable Energy Reviews*, 2011. 15(4): p. 1873-1884.
463. Sasitharanuwat, A., et al., *Performance evaluation of a 10kWp PV power system prototype for isolated building in Thailand*. *Renewable Energy*, 2007. 32(8): p. 1288-1300.
464. Radziemska, E., *The effect of temperature on the power drop in crystalline silicon solar cells*. *Renewable Energy*, 2003. 28(1): p. 1-12.